THE PREDICTION AND CONTROL OF TRANSIENTS IN THYRISTOR VALVES

by

MICHAEL JOHN BARNES

Submitted for the Degree of Doctor of Philosophy

at

The University of Aston in Birmingham

May 1985

THE PREDICTION AND CONTROL OF TRANSIENTS IN THYRISTOR VALVES

SUMMMARY

This thesis describes an investigation of methods by which both repetitive and non-repetitive electrical transients in an HVDC converter station may be controlled for minimum overall cost.

Several methods of inrush control are proposed and studied. The preferred method, whose development is reported in this thesis, would utilize two magnetic materials, one of which is assumed to be lossless and the other has controlled eddy-current losses. Mathematical studies are performed to assess the optimum characteristics of these materials, such that inrush current is suitably controlled for a minimum saturation flux requirement. Subsequent evaluation of the cost of hardware and capitalized losses of the proposed inrush control, indicate that a cost reduction of approximately 50% is achieved, in comparison with the inrush control hardware for the Sellindge converter station.

Further mathematical studies are carried out to prove the adequacy of the proposed inrush control characteristics for controlling voltage and current transients during both repetitive and non-repetitive operating conditions. The results of these proving studies indicate that no change in the proposed characteristics is required to ensure that integrity of the thyristors is maintained.

KEYWORDS

i) High Voltage Direct Current (HVDC)
ii) Thyristor Valves
iii) Control of Transients
iv) Saturating Reactors
v) Mathematical Modelling

by MICHAEL JOHN BARNES

Submitted for the Degree of Doctor of Philosophy

at

The University of Aston in Birmingham

May 1985

ACKNOWLEDGEMENTS

The work described in this thesis was carried out under the industrial supervision of Mr M L Woodhouse; the author wishes to express his gratitude to Mr Woodhouse for his helpful guidance.

The author also wishes to thank the following:

Dr A L Bowden for his advice, continual encouragement and interest;

Mr N Kerruish for his advice on the mathematical aspects of the work;

Dr D J van Rest for his effective co-ordination of the supervisory team;

Miss M Ainsworth and Mrs N Evans for their careful preparation of the typescript of this thesis;

My wife for her continual support and patience.

LIST OF CONTENTS

		Page No
List of Symbols		x
CHAPTER 1.	Introduction	1
1.1	Background to Thesis	1
1.2	Outline of the Thesis	4
1.2.1	Application and Fundamental Principles of HVDC	5
1.2.2	Mathematical Techniques	6
1.2.3	Control of Inrush Current Transients	7
1.2.4	Proving Studies	9
CHAPTER 2.	HVDC Transmission	12
2.1	Introduction	12
2.2	Development of HVDC Technology	13
2.2.1	Mercury Arc Valve	14
2.2.2	Solid State Technology	15
2.3	The Role of HVDC Transmission	15
2.4	Operation of a Six-Pulse Bridge	20
2.4.1	Idealized Bridge-Rectifier Commutation	20
2.4.2	Effect of Firing Delay	21
2.4.3	Rectification and Inversion	23
2.4.4	Harmonics Generated by the Converters	25
2.4.5	Reactive Power	27
2.4.6	Individual Control Characteristics of the Rectifier and Inverter	28
2.5	Valve Arrangement	31
2.6	Converter Arrangement	32

CHAPTER 3. Transient Phenomena and their Control 35

3.1 Introduction 35

3.2 Electrical Transients within a Converter Circuit 37

3.2.1 Turn-off of the Thyristor Valves 37

3.2.2 Turn-on of the Thyristor Valves 38

3.2.3 Voltage Transients 42

3.3 Turn-on Processes in Thyristors 47

3.3.1 Gating via the Gate Electrode 49

3.3.2 Ungated Turn-on 51

3.4 Turn-off Processes in Thyristors 55

3.5 Inrush Current Control 57

3.6 Sellindge converter station 59

3.6.1 Electrical Circuit 59

3.6.2 Cost of Inrush Control 66

CHAPTER 4. Modelling Techniques 72

4.1 Introduction 72

4.2 Simulation Techniques 74

4.2.1 General 74

4.2.2 Computer Analysis: VTECAP 77

4.3 Representation of Semi-Conductor Characteristics 79

4.3.1 Thyristor Turn-on 79

4.3.2 Thyristor Turn-off 81

4.3.3 Thyristor Junction Capacitance 85

4.4 Representation of Main-Circuit, Non-linear Element, Characteristics 87

4.4.1 Surge Arrester 87

4.4.2 Saturating Reactor 89

4.5 Representation of Converter Transformer Equivalent Circuit 93
4.5.1 Electrostatic Model 93
4.5.2 Transformer High-Frequency Characteristic 95
4.5.3 Refined Model of the Converter Transformer 96
4.6 Impulse Generator 98

CHAPTER 5. Increased Transient Resistance 101
5.1 Introduction 101
5.2 Proposed Strategy 103
5.3 Background Theory 104
5.3.1 Diffusion of Electric-Current 104
5.3.2 Effect of Diffusion upon Transient Resistance 107
5.4 Application to Inrush Control 108
5.5 Solution of the Diffusion Equation 112
5.5.1 Introduction 112
5.5.2 Application of a Current Ramp 115
5.5.3 Application of a Trapezoidal Current Pulse 119
5.6 Analysis of Increased Transient Resistance 123
5.6.1 Predicted Results 123
5.6.2 Analysis of Results 126
5.7 Conclusion 130

CHAPTER 6. Control of Inrush Current Transients Occurring during Coherent Turn-on 133

6.1 Introduction 133

6.2 Proposed Inrush Control Strategy 135

6.3 Initial Design Limits for Transients 140

6.4 Sensitivity of the Inrush Current to the Characteristics of the Saturating Reactor 142

6.4.1 Introduction 142

6.4.2 Proposed Studies 143

6.4.3 Relative Value of the Inductance of part L1 to part L2 144

6.4.4 Optimization of the Value of the Reflected Parallel Resistance 146

6.4.5 Magnitude of the Incremental Inductance with Current Characteristic for the Lossy Reactor (Part L1) 146

6.4.6 Interval of Constant Incremental Inductance for Part L1 148

6.4.7 Interval of Constant Incremental Inductance for the Lossless Reactor (Part L2) 149

6.4.8 Magnitude of the Incremental Inductance with Current Characteristic for Part L2 150

6.4.9 Proposed Reactor Characteristics for Inrush Control 152

6.4.10 Removal of part L1 154

6.4.11 Refined Transformer Representation 156

6.4.12 Valve-Voltage Collapse 158

6.4.13 Normal Continuous Operation 159

6.5 Estimated cost of Proposed Inrush Control 161

6.6 Conclusions 167

CHAPTER 7. Investigation of the Sensitivity of Recovery Overvoltage and Damping Circuit Losses at Turn-off 170

7.1 Introduction 170

7.2 Basic Assumptions for these Studies 173

7.3 Thyristor Reverse Recovered Charge 178

7.3.1 Computer Predictions 178

7.3.2 Theoretical Overshoot 180

7.4 Value of Damping Capacitor/Design of Transformer Winding 181

7.5 Damping Resistor 184

7.6 Series Capacitance of Transformer Winding 185

7.7 Shunt Stray Capacitance 186

7.8 Split in Reverse Recovered Charge 187

7.9 Effect of Refining the Transformer Model 189

7.10 Magnitude of Damping Circuit Current/Energy Dissipation 190

7.11 Maximum Voltage across an Off-State Valve 198

7.12 Saturating Reactor Characteristic 199

7.13 Summary 201

CHAPTER 8 Proving Studies for Proposed Reactor Characteristics 203

8.1 Introduction 203

8.2 Surge Arrester; Effect of Pre-established Current at Valve Firing 205

8.2.1 Introduction 205

8.2.2 Basic Assumptions 207

8.2.3 Predicted Inrush Waveforms 210

8.2.4 Comments 212

8.3 Commutation Failure 212

8.3.1 Introduction 212

8.3.2 Basic Assumptions 214

8.3.3 Predicted Inrush Waveforms 216

8.3.4 Comments 218

8.4 Preliminary Study of Valve Firing Transient Interaction: 12 Pulse-Notch 219

8.4.1 Introduction 219

8.4.2 Basic Assumptions 222

8.4.3 Predicted Results 224

8.4.4 Comments 228

8.5 Preliminary Investigation of Valve Response to Impulse Test-Voltage 230

8.5.1 Introduction 230

8.5.2 Basic Assumptions 231

8.5.3 Initial Conditions; Inrush Current 236

8.5.4 Predicted Results 237

8.5.4.1 Switching-Impulse 237

8.5.4.2 Lightning-Impulse 239

8.5.4.3 Front-of-Wave Impulse 240

8.5.5 Comments 241

8.6 Summary 243

CHAPTER 9. General Conclusions and Ongoing Work 246

9.1 General Conclusions 246

9.2 Further work 249

APPENDICES

Appendix I. Converter Operation; Standard Equations 253

Appendix II. Derivation of a High-Frequency Winding Representation for a Transformer 256

Appendix III. Derivation of Component Values for an 'Impulse Generator' 263

Appendix IV. Mathematical Model of a Saturating Reactor 265

Appendix V. Volume and cost of Magnetic Material Required 274

Appendix VI. Capacitance of a Damping Capacitor 283

References 285

Tables 294

Figures 306

LIST OF SYMBOLS

SI UNITS ARE USED

A	Cross-sectional area (m^2)
a	Depth of lamination (m)
B	Flux density (T)
B_o	Peak flux density (T)
B_{SAT}	Saturation flux density (T)
b	Gradient of a ramp
b_d	Width of lamination (m)
C_B	Lumped shunt capacitance (F)
$C_{B/B}$	Lumped busbar/busbar capacitance (F)
C_{BB}	Lumped busbar and bushing shunt capacitance (F)
C_D	Value of damping capacitance referred to a valve (F)
C_d	Value of damping capacitor, per level (F)
C_{FG}	Value of fast-grading capacitance referred to a valve (F)
C_{fg}	Value of fast-grading capacitor, per level (F)
C_G	Ground capacitance - attributable to transformer winding (F)
C_I	Lumped, interturn, series capacitance (F)
C_J	Incremental junction capacitance (space-charge capacitance) of a thyristor (F)
C_m	Shunt capacitance of midpoint busbar (F)
C_N	Lumped neutral capacitance (F)
C_n	Value of incremental capacitance (F). Subscript n; nth state of non-linear capacitance
C_t	Equivalent ground capacitance (F): obtained by the series addition, per phase, of the Thevenin equivalent electrostatic model (F)
c	Specific heat capacity ($J\ kg^{-1}\ k^{-1}$)
D	Arbitary constant
d	Depth of penetration of half-wave front (m): equals ($ht^{\frac{1}{2}}$)
$\frac{di}{dt}$	Rate-of-rise of current ($A\ \mu s^{-1}$)

$\frac{di}{dt}_m$	Maximum rate-of-rise of current to first current peak ($A\ \mu s^{-1}$)
$\frac{di}{dt}_1$	Initial rate-of-rise of current ($A\ \mu s^{-1}$)
$\frac{di}{dt}_2$	Maximum rate-of-rise of current to second current peak ($A\ \mu s^{-1}$)
$\frac{dV}{dt}$	Rate-of-rise of voltage ($V\ \mu s^{-1}$)
$\frac{dV}{dt}_L$	'Maximum' rate-of-rise of voltage across an off-state thyristor level ($V\ \mu s^{-1}$); neglecting voltage-sharing errors and redundancy and assuming distributed valve inductance
$\frac{dV}{dt}_T$	'Maximum' rate-of-rise of voltage across an off-state thyristor ($V\ \mu s^{-1}$); neglecting voltage-sharing errors and redundancy
dw'	Instantaneous power dissipation (W)
$\bar{dw}'$	Average power dissipation (W)
$\underset{\sim}{E}$	Electric-field stength ($V\ m^{-1}$)
E_t	Energy dissipation (J) (Subscript 't': up to an elapsed time t)
E_I	Instantaneous value of induced e.m.f. (V)
$E_{I(rms)}$	RMS value of induced e.m.f. (V)
$E_{I(PK)}$	Peak value of induced e.m.f. (V)
f	Frequency (Hz)
g	$m^{\frac{1}{2}} = \frac{y}{2(kt)^{\frac{1}{2}}}$
$\underset{\sim}{H}$	Magnetic field strength ($A\ m^{-1}$)
h	Coefficent of velocity ($m\ s^{\frac{1}{2}}$): equals $(\rho/\mu)^{\frac{1}{2}}$
h_r	Harmonic order
H_{SF}	Length scale-factor
I	Total current (A): (subscript n; associated with n^{th} breakpoint of non-linear element)
I_A	Anode current (A)
I_a	RMS value of an alternating current (A)
I_{C1}	Collector current for p-n-p transistor (A)
I_{C2}	Collector current for n-p-n transistor (A)

I_c	Surge arrester co-ordinating current (A)
I_d	Direct-current (A)
$I_{G(n)}$	Gate-drive for p-n-p transistor (A)
$I_{G(p)}$	Gate-drive for n-p-n transistor (A)
I_{gt}	Thyristor gate current (A)
I_K	Cathode current (A)
I_o	Peak reverse current (A)
I_{rms}	RMS current (A)
I_{RD}	Damping circuit current (A)
$\hat{I}_{RD}$	Peak value of damping circuit current (A)
I_{pk}	Peak of oscillatory current (A)
i_{DK}	Displacement current in a thyristor (A)
i_n	Current flowing in valve n (A)
$i_{1(pk)}$	Magnitude of first-peak of inrush current (A)
$i_{1(tr)}$	Magnitude of first-trough of inrush current (A)
$i_{2(pk)}$	Magnitude of second current peak of inrush current (A)
i^2erfc	Twice integral of complementary error function
J	Current density (A m^{-2})
J_s	Surface current density (A m^{-2})
J'_y	Current density at normalised depth y' (A m^{-2})
k	Diffusivity (m^2 s^{-1}): equals (h^2)
k_1	Proportion of total reverse recovered charge recovered up to peak reverse current
L_c	Commutating inductance per star phase (H)
L_D	Damping circuit stray inductance referred to a valve (H)
L_{eq}	Equivalent commutating inductance (H)
l_g	Length (m)
l_m	Magnetic-path length (m)
$L_{I(t)}$	Transient inner inductance (H)
L_{LT}	Transformer 'series' inductance (high-frequency representation) (H)

L_n	Incremental inductance (H).	Subscript n; n^{th} state of non-linear inductor
L_p	Parallel inductance for hfr winding representation (H)	
L_s	Lumped stray inductance (H)	
L_{SM}	DC smoothing inductance (H)	
L_T	Leakage inductance of a transformer winding (H)	
L_w	Valve winding inductance (H)	
M_n	Avalanche multiplication coefficient (electrons)	
M_p	Avalanche multiplication coefficient (holes)	
m	$\frac{y^2}{4kt}$	
N	Number of turns	
n	Integer number	
P	Active AC power (W)	
p	Density (kg m^{-3})	
P_L	Pulse number (6, 12 ...)	
Q	Charge	subscript n; assoicated with n^{th} break-point of non-linear capacitor
Q'	'Residual' charge (C)	
Q_a	Reactive power (VAr)	
Q_{rr}	Total reverse recovered charge (C)	
q	$\frac{L_c}{R_D^2 C_D}$	
R_D	Value of damping resistance referred to a valve (Ω)	
R_d	Value of damping resistor, per level (Ω)	
R_{dc}	DC resistance (Ω)	
R_e	Reflected resistance (Ω)	
R_{fg}	Value of fast-grading resistor (Ω)	
R_n	Incremental resistance (Ω)	subscript n; associated with n^{th} break-point of non-linear resistance
R_p	Parallel resistance: hfr winding representation (Ω)	

$R(t)$	Instantaneous resistance of a thyristor as a function of elapsed time (Ω)
R_S	Effective series resistance (Ω)
R_{tr}	Transient resistance (Ω)
r_1	Inner radius (m)
r_2	Outer radius (m)
$\underset{\sim}{S}$	Poynting vector ($W\ m^{-2}$)
s	$\frac{y^2}{(4k(t-t_b))}$
$T(t)$	Surface temperature as a function of elapsed time (°C)
t	Elapsed time (s)
t_b	Elapsed time at which delayed cancellation ramp commences (s)
t_d	Delay time (s)
t^*_{gt}	Turn-on time (s)
T_J	Thyristor junction temperature (°C)
t_q	Turn-off time (s)
t_r	Rise time (s)
U	Solution to diffusion equation Subscripts used are:- E Electric-field H Magnetic-field I Current J Current density t Elapsed time
U_o	Overlap angle (electrical degrees), unless otherwise stated
V_c	Phase to phase rms voltage (V)
V_{co}	Maximum average DC voltage (no load and without firing delay) (V)
V_d	Mean direct voltage (V)
V_e	Instantaneous value of driving e.m.f. (V)
V_f	Valve firing voltage (V)
V_{LM}	Volume (m^3)
V_m	Capacitor precharge: impulse generator representation (V)

V_n	Instantaneous value of voltage across valve n (V)
V_q	Break-point voltage of non-linear capacitor (V). Subscript n; associated with n^{th} break-point
V'_q	Voltage associated with a break-point of a non-linear capacitor, due to a residual charge Q' (V). Subscript n; associated with n^{th} break-point
V_{REC}	Maximum value of recovery voltage (V)
V_r	Break-point voltage of non-linear resistor (V). Subscript n; associated with n^{th} break-point.
V'_r	Voltage source value (V). Subscript n; associated with n^{th} break-point of non-linear resistor (i.e., surge arrester)
V_{SF}	Volume scale-factor
V_T	Instantaneous thyristor voltage (V)
V_p	Velocity of penetration (m s^{-1})
V_V	Valve-voltage (V)
$V_{V(pk)}$	Peak valve-voltage (V)
W_m	Magnetic energy (W)
w'	Total power dissipation (W)
X_p	$2\pi fL_p$ (Ω)
X_c	Commutating reactance per star phase (Ω)
X_{LT}	Transformer series leakage reactance (high-frequency representation) (Ω)
X_S	Effective series reactance of a transformer winding (determined at fundamental fequency), (Ω)
X_T	Leakage reactance of a phase of a transformer (Ω)
x	Distance in the x-direction (m)
y	Distance in the y-direction (m)
y_1	Height of rib (m)
y'	Normalised height (y/y_1)
Z	Impedance
z	Distance in the z-direction (m)
α	Firing delay angle (electrical degrees), unless otherwise stated

α_n Common-base current-gain for n-p-n transistor

α_p Common-base current-gain for p-n-p transistor

β Angle of advance (electrical degrees)

γ Extinction angle (electrical degrees)

ΔQ Change in uncovered fixed charge (C)

ΔV Change in bias which results in ΔQ (V)

ξ $\text{erf}\left(\frac{y}{2(kt)^{\frac{1}{2}}}\right)$

θ wt (radians)

μ Absolute permeability of a magnetic-circuit ($\mu_o\mu_e$) (H m^{-1})

μ_e Effective permeability of a magnetic-circuit

μ_r Relative permeability of a homogeneous magnetic material

μ_o Permeability of a vacuum (H m^{-1})

ρ Resistivity (Ω.m)

σ Conductivity (mho.m^{-1})

T Time constant of damping circuit (s). ($T = C_dR_d$)

T_1, T_2 Time constants (impulse generator) (s)

ϕ Flux (Wb) subscript n: assoicated with n^{th} 'break point' of non-linear inductor

ϕ' 'Residual' flux (Wb) subscript n: associated with n^{th} 'break point' of non-linear inductor

ϕ_{SAT} Saturation flux (Wb)

Ψ Phase difference between fundamental frequency voltage and current components (electrical degrees)

w Angular frequency (rads s^{-1}) ($2\pi f$)

SUPERSCRIPTS

$\sim$ Complex conjugate

$\wedge$ Peak value

ABBREVIATIONS

AC Alternating current

BOD Breakover diode

DC	Direct current
DOV	Dynamic overvoltage
EHV	Extra high voltage
e.m.f.	electro-motive force
HV	High voltage
HVAC	High voltage alternating current
HVDC	High voltage direct current
NSC	Neutral surge capacitor
PRI	Peak reverse current
p.d.	Potential difference
p.u.	per unit
rms	Root-mean-square
SA	Surge arrester
VTECAP	Variable topology electrical circuit analysis programme

1. INTRODUCTION

1.1 BACKGROUND TO THESIS

There are prospective, and in some cases established and expanding markets for High Voltage Direct Current (HVDC) terminal equipment in every continent of the world as well as many of the smaller land masses. In the Western World, prospective suppliers of HVDC terminal equipment are presently: United Kingdom, Sweden, Switzerland, Germany, Japan (home markets only at present), the USA and their licensees. The sole UK supplier of HVDC terminal equipment is the Transmission and Distribution Projects (TDPL) Division of GEC Power Engineering Limited.

TDPL have been in the business of HVDC system engineering for over 20 years. In the 1960's mercury arc valves were designed and constructed by TDPL for several installations;

a) Sardinia - Italian mainland: 200MW (200kV, 1000A)
b) Nelson River - Winnipeg, Canada: 1620MW (±450kV, 1800A)
c) Kingsnorth - London, England: 640MW (±266kV, 1200A)

Early work by GEC contributed significantly to the development of a successful mercury arc valve. The Nelson River scheme utilizes the highest voltage and highly rated mercury arc valves to be found in the world.

However, circa 1968 GEC foresaw solid-state technology would eventually progress sufficiently to provide a real alternative to mercury arc valves, and thus embarked upon a programme of development of thyristor valves for HVDC application.

In the mid 1970's TDPL, working in close co-operation with the CEGB, replaced one of the Willesden mercury arc valves with a thyristor valve. This was carried out using the thyristor technology of the time (56mm thyristors) to prove fully the valve hardware for connection to the CEGB system in the proposed Sellindge terminal of a 2000MW, HVDC Cross-Channel link.* However, HVDC is still a rapidly developing technology and during the design and manufacture of the Sellindge converter station valves, other manufacturers were applying valve designs utilizing 75mm and in one instance 100mm thyristors.

Recognising the importance of HVDC power transmission on a world-wide basis and that TDPL is the only UK company with expertise in this specialized field, further funding was obtained from the Department of Trade and Industry (DTI) to accelerate the development programme.

The main objectives of the TDPL development programme are to utilize recent advances in thyristor technology to reduce overall costs whilst increasing converter efficiency

* For simplicity, this converter station will be referred to as the 'Sellindge converter station' throughout this thesis.

and reliability. In order to exploit the properties of available thyristors to the maximum it is essential to provide them with a safe working environment at a minimum overall cost.

The application engineering required to apply thyristors successfully for HVDC transmission is extremely detailed. Long series strings of thyristors (often as many as 100) must be provided with networks to control the distribution of voltage in an off-state valve, series inductance to limit the inrush current at turn-on, protection against ungated turn-on, and a means of triggering the thyristors on demand.

The Sellindge converter station utilized linear inductance external to the valve, and both quasi-linear and saturating inductance within the valve, to control the inrush current transients. Both the saturating and quasi-linear inductance are 'distributed' that is the total valve inductance is subdivided into blocks equal to the number of thyristors in the valve.

It is the aim of this thesis to investigate alternative means to those used in the Sellindge converter station, for controlling the inrush current transients, within all future HVDC thyristor valves, for a minimum overall cost. The existing circuit design of the Sellindge converter station was used as a basis for proposing modifications for future converter stations.

1.2 OUTLINE OF THE THESIS

This thesis may be subdivided into four distinct, but related parts:-

(i) An outline of the circumstances in which HVDC is applied; the fundamental principles of HVDC; and the limited capabilities of the thyristors employed within a valve.

(ii) A description of the main mathematical techniques employed by TDPL to predict electrical transients within a converter station.

(iii) An investigation of two suitable alternative techniques, to that of the Sellindge converter station, for controlling the inrush current transients during coherent turn-on of the thyristors within a valve. Both techniques are believed to be original in this application.

(iv) Studies to prove that the proposed technique for controlling the inrush transients is adequate for controlling other, specified electrical transients which occur within the converter station.

These will be expanded upon briefly in the following sections.

1.2.1 Application and Fundamental Principles of HVDC

In specific circumstances, HVDC can have certain technical and economic advantages over HVAC; these are discussed in Chapter 2. This is followed by a brief description of the operation of a six-pulse bridge including the effects of firing delay and a commutating reactance. Although this theory is well known it is fundamental to this thesis.

In a converter station there are unavoidable stray capacitances. These stray capacitances give rise to inrush currents at turn-on which may thermally overstress the thyristors. Since thyristors are not self-healing action must be taken to mitigate the effects of these stray capacitances.

The components included within the Sellindge converter station to control the inrush current transients, are outlined in Chapter 3. The cost of the inrush control hardware and evaluated losses associated with this hardware are calculated for the Sellindge converter station. These costs are compared in Chapter 6 with the cost of providing an alternative means of inrush control.

1.2.2 Mathematical Techniques

The electrical and thermal stresses to which the valve components are subjected are predicted using the computer programme VTECAP. In order that these predictions are accurate, the analytical studies must take into account circuit non-linearities. Chapter 4 outlines the piece-wise linear techniques, utilized by the computer programme VTECAP, for representing circuit non-linearities.

Modelling techniques employed should accurately represent the circuit elements. The converter transformer, with its associated stray capacitances, contributes significantly towards the production of circuit transients. Thus, refined techniques for representing the converter transformer have been developed and are described in Chapter 4. The refined representation models each phase of the converter transformer by distributed pi-sections. End effects of the transformer winding are allowed for within the representation. The number of pi-sections used to represent each phase has been optimized for accuracy of results and CPU time usage during an analysis.

1.2.3 Control of Inrush Current Transients

The method employed within the Sellindge converter station to control the inrush current transients provides a safe electrical environment for the thyristors, (Chapter 3.6). However, to enhance the degree of safety of the working environment and to reduce the costs associated with the control of transients, it is necessary to investigate an alternative method of achieving the required control. Thus, Chapters 5 and 6 describe two different, but related, methods investigated for achieving the control. The cost reduction aimed for was 50% of the cost of inrush control hardware of the Sellindge converter station. In addition, the evaluated losses associated with these components (Chapter 3.6) should not be increased and should preferably be decreased in comparison with the inrush limiting components of the Sellindge converter station.

The method detailed in Chapter 5 for providing resistive losses to damp the inrush current oscillations is akin to the deep-bar effect associated with induction motors. A ribbed busbar is housed in a semi-closed slot so that the transient resistance of the rib is increased.

Equations are developed, for the rib in a semi-closed slot, so that the suitability of this concept may be evaluated. The equations are based upon the assumption that the excitation may be approximated to a 'trapezoidal' current pulse. Non-linearity of the magnetic material characteristic is neglected.

The transient current distribution within the rib is calculated, and thus the transient resistance of the rib is evaluated. The transient resistance of the rib, at any given elapsed time, is shown to be dependent upon the effective relative permeability of the magnetic-circuit and the elapsed time after which the trapezoidal current pulse is assumed to level off.

The dimensions of the rib which give a specified transient resistance after a specified elapsed time are determined in Chapter 5. These dimensions are such that mechanical difficulties would be encountered in constructing, handling and housing the ribbed busbar in a semi-closed slot. Hence, Chapter 6 outlines an alternative, mechanically simpler and more robust, method of achieving the inrush control. This proposed method utilizes a two-part saturating reactor for controlling circuit transients. One part of the proposed reactor is considered to be constructed from a lossless magnetic material, whilst the other part has controlled eddy-current losses.

As the reactors are used primarily to control the inrush current transient, mathematical studies modelling coherent turn-on of the thyristors within a valve were performed. The ideal characteristics of the two-part saturating reactor are derived such that the inrush current transient is kept within the assumed capabilities of the thyristors for a minimum volume of magnetic material. The derivation of these ideal characteristics is described in Chapter 6. The preliminary costings, performed in Chapter 6, shows that the proposed reactor is likely to give a cost reduction of approximately 50% in comparison with the inrush control hardware of the Sellindge converter station. In addition, replacement of the inrush control hardware of the Sellindge converter station, by the proposed two-part saturating reactor, is shown to give a reduction in adjudicated losses, evaluated for normal full load current, of approximately $137,500 per valve.

1.2.4 Proving Studies

Turn-off of a thyristor valve excites an oscillation primarily between the commutating reactance of the converter transformer and the valve stray capacitances. This oscillation is controlled by the inclusion of a damping circuit in parallel with each thyristor. The magnitude of the losses in the damping circuit is determined to a large extent by the

capacitance value of the damping capacitor. However, other components act to damp the oscillation, e.g., the lossy saturating reactor and high-frequency losses within the converter transformer. Thus, the components of the converter station must be optimized to give the maximum performance for minimum overall cost. Chapter 7 outlines the results of predictions performed to assess the dependence of the evaluated losses, and magnitude of voltage overshoot transients, upon firstly the modelling techniques employed, and secondly upon circuit and device parameters.

It is shown in Chapter 7 that the damping circuit losses, at turn-off of a thyristor valve, are only slightly reduced by increasing the inductance of the proposed saturating reactor. In addition, an increase in the inductance value is at variance with the optimum characteristic required for coherent turn-on considerations. Thus, no change is contemplated in the proposed characteristics.

The purpose of the studies reported upon in Chapter 8 were to ensure that the characteristics of the proposed two-part reactor are adequate for controlling transients occurring during other operating conditions. All of these operating conditions, with the exception of '12-pulse notch' are non-repetitive operating conditions. Thus, provided that the proposed characteristics adequately control the transients, no

modification of the characteristics is necessary. Similarly, the '12-pulse notch' studies were performed primarily to assess the effect of firstly the proposed saturating reactor, and secondly the modelling techniques employed upon the predicted voltage transients.

The results of these analytical studies indicate that the characteristics of the proposed saturating reactor are adequate for controlling voltage and current transients during all the operating conditions studied.

2. HVDC TRANSMISSION

2.1 INTRODUCTION

Following a brief description of the history of HVDC transmission this chapter discusses the principles and application of HVDC. In specific circumstances DC transmission can have many technical and economic advantages over HVAC. Examples of such circumstances are given in this chapter.

Operation of a six-pulse bridge is described including the effects of firing delay and a commutating reactance. The voltage and current waveforms associated with rectification and inversion are presented and means by which harmonics generated by the HVDC converter, may be minimized are described. The relationship of the active and reactive powers of a converter to the firing delay angle is briefly discussed and the required control characteristics of the rectifier and inverter, for the control of mean direct voltage and current of an HVDC scheme are outlined.

The general electrical and mechanical arrangement of a valve and converter is discussed with reference to the required reliability and availability of an HVDC transmission scheme.

2.2 DEVELOPMENT OF HVDC TECHNOLOGY

When the use of AC transmission and distribution was still in its infancy, Marcel Deprez published the first theoretical examination of HVDC power transmission. This theory was put into practice by 1882, when 1.5kW was transmitted at 2kV over a distance of 56km.

Rene Thury further developed the work of Deprez, and used a number of series-connected DC generators at the sending end to attain high transmission voltages. At the receiving end there were a number of series connected motors, each driving an AC or DC generator. There were about twenty such systems installed in Europe, the most important being from Moutiers in the French Alps to Lyon. This system was increased in size by the addition of series stations and transmitted 19.3MW at 125kV over a total distance of 225km. This scheme operated at constant current and was used as a reinforcement of an existing AC system.

The use of low speed water turbines driving the generators of the Thury system, had resulted in very few problems. However, with the advent of the steam turbine as a prime mover for the generation of power, the use of steam turbines for DC generation depended on the availability of high-speed reduction gearing.[1]

The main advantage of AC over DC is the ability to vary voltage level by means of transformers in the transmission and distribution network. However, since the late 1940's direct current has again become an economic proposition for energy transmission in certain specific cases. This is due mainly to the difficulties of operating large interconnecting AC systems combined with the successful development of high voltage rectifying and inverting equipment. Early converter equipment used grid controlled mercury arc valves which were subsequently replaced by solid state technology.

2.2.1 Mercury Arc Valve

In the early days of the power electronic industry, mercury arc rectification was found to be the most successful method of switching large currents. Multi-phase, mercury-pool-cathode valves, constructed with a control electrode (or grid), have been used extensively in industry and for railway applications for over 50 years.

The mercury valve was successfully developed for high voltage applications,[1] in the late 1940's. This development paved the way for the first commercial HVDC scheme in 1954, which was rapidly followed by ten others of increased ratings. Even with some refinements in design, the mercury arc valve suffered from backfiring and commutation faults and required a relatively high degree of maintenance. However, the provision of spare valves and skilled maintenance staff resulted in a good record of availability.

2.2.2 Solid State Technology

In parallel with the rapid development of the micro-electronic technology there has been equally impressive, though less publicised, advances in macro-electronic devices for use in the power field.

In spite of the successful operation of the mercury arc schemes, voltage limitations together with the need for considerable maintenance encouraged development of solid state technology. Thyristors have now been developed for use in high voltage valves (see section 2.5) and have proved to be extremely reliable.

Advances in thyristor technology have reduced not only the valve cost (which was initially much the same as the cost of mercury arc valves), but also the cost of station plant and layout. Thus, the initial experience obtained, by manufacturers, with thyristor valves was enough to discourage any further development of mercury arc technology.

2.3 THE ROLE OF HVDC TRANSMISSION

Gavrilovic[2] points out that, "An AC transmission network provides the advantages of interconnection of previously independent systems. Security of supply is thus improved, more efficient usage of plant results to suit varying load requirements in different regions and at various times, and adequate operational control and stability are maintained".

However, in considering the method of interconnection, there are economic and technical advantages for using HVDC lines and interconnections[3]. (A simplified schematic of a DC scheme is shown in figure 2.1). Advantages of HVDC over HVAC transmission include the following:-

a) Lines or cables carrying DC do not require reactive compensation. AC lines or cables may need reactive compensation depending on length.
b) The size of a DC conductor is smaller than an AC conductor of comparable current carrying cabability.
c) Interconnections of AC systems using HVDC does not result in an increase in the fault current level of the AC system.
d) DC interconnection of AC systems provides an asynchronous link.
e) A converter bridge may be controlled rapidly, thus the stability of an AC system may be enhanced.

HVDC can compete successfully with HVAC in specific circumstances where these advantages become signficant and may even be the only feasible method; some of the situations may include a combination of the following[4]:-

a) Long sea crossings.
b) Transmission of power to large densely populated urban areas.

c) Interconnecting networks of different frequencies, or of systems with different power versus frequency dependencies in normal load and in emergency load shedding circumstances.

d) Transmission over long distances by overhead lines.

e) Interconnecting or sectionalising large AC networks.

These will be discussed in turn.

(a) Long Sea Crossings

Long sea crossings by submarine cable allows no possibility of reactive power correction at intermediate positions along the route. Consequently, at system frequency and beyond a certain length of cable, the capacitive current will exceed the rated current of the cable. HVDC is the main alternative, as there is no requirement for reactive power compensation.

(b) Transmission of Power to Large Densely Populated Urban Areas

As urban areas grow in size, the load density increases, and the possibility of installing additional overhead lines diminishes, the feasibility of installing long underground cables increases. The choice is then between the lower cable costs and higher terminal costs associated with HVDC versus the higher cable costs and lower terminal costs of HVAC. The breakeven distance for an HVDC scheme, in comparison with an HVAC scheme, is approximately 60km[4].

(c) Interconnecting Networks of Different Frequencies

HVDC is the only static method of interconnecting AC networks of different frequencies, unsynchronized AC networks of nominally the same frequency, or initially synchronized AC networks which could become unsynchronized due to loading or faults.

If the AC networks to be interconnected are close neighbours, then the DC link may be of zero length. The DC link is then referred to as a 'back-to-back' scheme.

(d) Transmission Over Long Distances by Overhead Lines

Bulk power transfer over long transmission distances typically occur in the following situations:-

i) Energy source remote from the load[5].

ii) Interconnection between two regional systems[6].

iii) Supplying moderate amounts of power from the power grid of a central region[2] to, remote, recently developing areas which have little local generation.

HVDC lines do not have a reactive power requirement, and voltage drop is due solely to line resistance. HVAC transmission lines require reactive compensation depending on the load and operating voltage[4]. The reactive compensation requirement for an AC line during an 'overload' condition will be predominantly capacitive, whilst that for no-load will be predominantly inductive.

For lines up to about 400km [(24°)* at 50 Hz], this compensation may be supplied at the terminals[4]. The additional compensation required for longer lines adds considerably to the overall cost of long AC transmission lines.

Power flow disturbances are quickly reflected in transmission angle oscillations[4] and therefore, for reasons of stability, the transmission angle is kept at relatively low values under normal operating conditions, (about 30°)[4][7]. The reactance of the line may be reduced by insertion of series capacitors and paralleling lines. For large power flows the system voltage may be necessarily set very high and thus, require shunt reactors for overvoltage control if not for improving the power capability[2]. Hence, for the same power transmitted the cost of an HVDC line can be lower than the cost of an HVAC line[4].

HVDC lines which are designed for an economic current density may be capable thermally of transmitting twice the rated operating current. Consequently, failure of one pole of a bipolar line (see figure 2.1) is not serious since the other pole can take over almost the full power rating[4][7]. The DC line is in effect a double-circuit line since earth return (see figure 2.1) may be used under fault conditions; in such circumstances the scheme is running monopolar.

* For simplicity, this notation will be used to mean 'electrical degrees' throughout this thesis, unless stated otherwise.

In addition, towers used on HVDC lines are lighter and less expensive than those utilized for HVAC lines of the same rating[4].

(e) Interconnecting or Sectionalising Large AC Networks

An advantage of HVDC is its 'non-synchronous' nature and its inherent ability to prevent the flow of fault current from one system to another[8]. The short-circuit current in either system is not increased by the introduction of an HVDC tie line and consequently circuit breakers need not be uprated[1]. In contrast to AC lines, load tapping stations for DC lines are not readily feasible, although technically possible.

2.4 OPERATION OF A SIX-PULSE BRIDGE

2.4.1 Idealized Bridge-Rectifier Commutation

In order to understand the process of 'line commutation' as opposed to 'forced commutation', it is desirable to consider the idealized case of a converter bridge, containing diodes, connected to a power system of zero source impedance. A line commutated bridge rectifier is shown in figure 2.2, together with the switching sequence of the diodes within the bridge.

With reference to figures 2.2 (a) and 2.2(b), and initially considering instant 'A', when phases R and Y are carring current through conducting diodes 1 and 6, the common cathode of the bridge is nominally at potential E_R and the common anode at

potential E_Y. This operating state continues up to point 'B' when diode 2 becomes forward biased, i.e. E_B is more negative than E_Y. Thus, at point 'B' current commutates naturally from diode 6 to diode 2.

A similar situation occurs at point 'C' when the potential E_Y becomes more positive than the potential E_R; current commutates from diode 1 into diode 3. The switching sequence continues with current commutating from diode 2 to diode 4 at point 'D', from diode 3 to diode 5 at point 'E', from diode 4 to diode 6 at point 'F' and from diode 5 to diode 1 at point 'G', completing the cycle sequence.

Figure 2.2(b) shows the voltage variation of the common cathode and common anode with respect to the transformer neutral. Figure 2.2(c) shows the common cathode voltage with respect to the common anode. The output voltage has a ripple, or harmonic frequency, of six times the supply frequency.

2.4.2 Effect of Firing Delay

If thyristors are employed instead of diodes then current will flow, normally, when the thyristors are forward biased and have a suitable pulse applied to their gates. The requirement of normally needing a gate pulse (Chapter 3.3) allows a 'controlled firing delay' after the thyristor becomes forward biased. The effect of this firing delay upon the common cathode

and common anode voltage is shown in Figure 2.3(a). The mean direct voltage is reduced in proportion with this delay, (see Appendix 1 equation 1).

For delay angles above 60°, the instantaneous bridge output voltage contains some negative voltage periods (Figure 2.3(b)). However, the provision of a large smoothing reactor maintains positive current flow during these negative periods, and energy is transferred from the magnetic-field of the reactor to the AC system. As the delay angle is further increased the periods of negative voltage also increase in duration. When the delay angle is 90° the periods of negative voltage are equal to the periods of positive voltage and the mean direct voltage is zero.

Beyond 90° the mean direct output voltage of a bridge becomes negative and bridge operation can only be maintained in the presence of a DC power supply[9][10][11]. The current continues to flow in the same direction in the bridge, i.e. anode to cathode, in opposition to the induced e.m.f. of the converter transformer[9][10][11]. Power is now being supplied to the AC system, from the DC system and the converter is said to be inverting[10][11].

The three conditions necessary to permit inversion can thus be summarised :

i) An AC voltage source to provide the commutating voltage waveforms.

ii) Firing angle control to delay the firing angle (α) beyond 90°.

iii) A DC power supply.

2.4.3 Rectification and Inversion

The above description of 'idealized bridge-rectifier commutation', considers the AC power system to have zero source impedance. Thus the current was able to transfer from one arm of the bridge, e.g. arm 6, to another, e.g. arm 2, as soon as the anode of the latter becomes positive with respect to the anode of the former and the latter receives a gate pulse.

However, due to the leakage reactance of a converter transformer, the current transfer from one arm of the bridge to another does not occur instantaneously. During this period both arms of the bridge conduct simultaneously (figure 2.4(a)), and this period is called the overlap angle, U_o. Thus, in the case of current commutating from arm 6 to arm 2, the common anode voltage approaches the average of the commutating phase voltages during the period of overlap. Figure 2.4 shows a simplified equivalent circuit of the commutation between phases of a star-secondary, converter transformer.

The voltage and current waveforms for the commutation process described above are shown in figures 2.4(b) and 2.4(c) respectively. The voltage and current waveforms of a six-pulse

bridge, during rectification, are shown in figure 2.5. The causes of these waveforms are described in standard texts. (9)(10)(11)(12)

Similarly, the voltage and current waveforms associated with inverter operation of the bridge are shown in figure 2.6. Commutation cannot be delayed beyond the point C, because the polarity of the phase to phase voltage reverses at this point. In practice the commutation has to be advanced by an 'extinction angle' (γ) to allow the valve, in the arm turning-off, to fully recover from its period of conduction (Chapter 3.4). In addition to this extinction angle an overlap angle (U_o) has to be included to allow current commutation between the phases. The sum of this overlap angle and the extinction angle, defines the angle of advance, β. Should the angle of advance be reduced such that the necessary extinction angle is not available to the recovering valve, the probability of the recovering valve failing commutation is increased. The overlap angle may be calculated from the appropriate equations of Appendix I.

In reality, the equivalent circuit of a six-pulse converter is not as simple as that shown in figure 2.2(a); the circuit also contains unavoidable stray inductances and capacitances (figure 2.7). In addition, the arms of a modern HVDC converter bridge utilize high power thyristors as the switching elements; these thyristors require intervals of time to turn-on and to turn-off.

The total effect of the above is to modify, transiently, the standard valve-voltage and valve-current waveforms (figures 2.5 and 2.6) during commutation. Thus, when a thyristor valve in the bridge turns-on the unavoidable stray capacitance, shunting the valve, will discharge through the thyristors within this valve, (Chapter 3.2.2). This displacement current is in addition to the load current transfer into the valve, (Chapter 3.2.2). The effect of valve stray capacitances is such as to prevent an instantaneous change in the valve-voltage.

Similarly, towards the end of the on-state period of the thyristors, the thyristors do not immediately turn-off (Chapter 3.2.1) but require some interval to achieve their blocking capability (Chapter 3.4). The effect of this, together with the valve stray capacitances, is to modify transiently the valve current and voltages (Chapter 3.2.1). Again the valve-current and voltages cannot change their value instantaneously.

2.4.4 Harmonics Generated by the Converters

The thyristor converter is a switching system, with a large smoothing reactor in the DC line. The effect of this smoothing reactor is to provide a, nominally, DC current from the converter bridge. Thus, the current waveshape, in each of the conducting valves in the bridge, is nominally flat topped.

The DC smoothing reactor also performs other functions,[2] namely:-

i) To limit the rate-of-rise of fault current during transmission system faults.

ii) Limitation of harmonic currents in the DC transmission system.

iii) Limiting the rate-of-rise of a surge voltage, when overvoltages travel down the DC transmission system into the converter station.

In the absence of commutating reactance, the current through each arm of the bridge is a rectangular pulse whose duration is 120°. These flat-topped currents flow through each phase of the converter transformer, and represent the current waveshape, for a six-pulse bridge, of the AC line current.

The AC current waveform can be modified to be a closer approximation to a sinewave (figure 2.8) by connecting two six-pulse bridges, with a relative phase shift of 30°, in series on the DC side and in parallel on the AC side, (figure 2.9). In this situation 12 pulse operation is obtained, i.e. the ripple voltage on the DC side has 12 equal pulses per cycle at fundamental frequency. On the AC side, currents of harmonic orders 11, 13, 23, 25 ..... are in phase from the converters and are of double amplitude[13]. The converters can produce a small amount of uncharacteristic harmonics on the AC side, (e.g., 5th and 7th) due mainly to the small unbalance in converter

transformer reactances. However, with modern control systems the unbalance due to valve firing is a second-order effect[14][15].

On the AC side of a large converter it is usually necessary to provide filters to reduce harmonic currents and voltages in the AC system. The harmonics, if unrestrained, could adversely effect the operation of other equipment, or interfere with communication circuits. Such filters are of a considerable size and represent an appreciable portion of the cost of a converter station[13]. Thus in order to minimize the cost of AC filter equipment, it is necessary to avoid the use of components, within the converter bridge, which result in the generation of excessive uncharacteristic harmonics. Uncharacteristic harmonics, with reference to the AC current, have frequencies other than those determined by the expression $P_L h_r \pm 1$, (for h_r = 0, 1 ..... n), where P_L is the pulse number, (see above).

2.4.5 Reactive Power

Due to the firing delay and commutation angles the converter current in each phase lags the corresponding voltage, (see figure 2.5): the rectifier is therefore absorbing reactive power. Similarily, during inverter operation (see figure 2.6) the current supplied to the AC system, by the inverter, lags the corresponding positive half of the phase voltage by more than 90° or lags the negative half by less than 90°. Thus, the inverter, like the rectifier, acts as an absorber of reactive power.

It can be shown [10] that the active and reactive powers of a rectifier vary with the firing delay angle (see Appendix I). In order to maximize the rated power for a given voltage and current, it is necessary to retain a high power factor (Section 2.4.6).

2.4.6 Individual Control Characteristics of the Rectifer and Inverter

Modern HVDC automatic control systems provide several desirable features of control[16]. These include:-

i) Limitation of the maximum current, thus avoiding excessive temperature rises within current-carrying devices, e.g. thyristors.

ii) Limiting the occurence of commutation failure at the inverter by predictive means. (Commutation must be completed before the commutating voltage reverses at $\gamma = 0°$).

iii) Minimization of the losses, for a given power, by retaining the sending end voltage at its rated value.

iv) Control of the power delivered.

v) Retention of a high power factor: this ensures that the rated power of the converters is as high as possible for given voltage and current ratings of the converter transformers and valves[2], (See Appendix 1). The voltage rating of the transformer and the voltage across the valves, when not conducting, are both proportional to the maximum average DC voltage (no load and zero firing

delay), V_{co}, but the power is proportional to the mean direct voltage, V_d[16]. In addition, for a high power factor, the firing delay angle is small (Appendix 1), and thus the stresses on the valves and damping circuits are reduced in comparison to operation with a low power factor. Similarily, neglecting losses in the converter, the AC power must be equal to the DC power ($P = 3^{\frac{1}{2}} V_c I_a \cos\psi = V_d I_d$). Hence, for a given DC power, the AC line losses are minimized by maximizing the power factor $\cos\psi$.[16]

The power factor can be increased by adding reactive compensators[2]. A maximum power factor may be obtained by minimizing the firing delay angle, α, and the extinction angle, γ.[16] The extinction angle is not controlled directly, but instead the angle of advance, β, is controlled. However, sufficient margin must be added to the minimum angle of advance required, to allow for AC voltage waveform distortion or fluctuations in the DC load.

The rectifier generally controls the direct current whilst the inverter controls the direct voltage.[16] Thus, if the inverter voltage is raised by any means, the rectifier voltage must be raised in proportion in order to retain a constant current. This may be achieved rapidly by electronic control of the firing delay angle. However, this angle can only be decreased to zero ($\cos\alpha = 1$); at this point, the rectifier voltage can only be further increased by tap changer action on the converter

transformer. Hence, in practice the rectifier tap changer position is controlled such as to bring α into the range 6° to 15°.[16] These values of firing delay angle represent a compromise:-

i) Keeping the power-factor high.

ii) Retaining a margin for a fast increase in rectifier voltage (by decreasing α).

Should there be a reduction in the AC system voltage at the inverter which persists for several cycles, then the tap-changer of the converter transformer at the inverter raises the secondary voltage and thus the direct voltage back to normal, or until the limit of the tap-changer is reached.[16] If the direct voltage is not restored to its original value, the direct current will increase, but may be restored to its original value by increasing the rectifier firing delay angle.

Alternatively, if the rectifier AC voltage is reduced to an extent such that operation of the rectifier tap-changer and a reduction in the firing delay angle cannot restore the direct voltage to its original value, then the direct current will decrease in value. This occurs only if the inverter is considered to be operating under the control of 'constant extinction angle': in such a situation, the rectifier and inverter characteristics do not intersect (figure 2.10) and the current and power decrease to zero.[16] Thus, to avoid the collapse of power

transfer the inverter also has a constant current control (see figure 2.10). This current control is set below that of the rectifier. Should the direct current now decrease substantially, the inverter constant current control will override the inverter 'constant extinction angle control', and thus the angle of advance is increased.[16] In such circumstances, the rectifier is controlling the direct voltage and the inverter the direct current.

2.5 VALVE ARRANGEMENT

A thyristor valve consists of a number of series connected thyristors to obtain the required voltage rating. It may also be necessary to parallel thyristors, to achieve the required current rating.

For the Sellindge converter station, each of the series connected thyristors has circuitry to protect the thyristor against current and voltage transients and overvoltages.[17] A thyristor, together with its protective circuitry, is referred to as a thyristor level.

During normal repetitive operation of a thyristor valve, each thyristor level should receive a gate-pulse identical to, and simultaneous with, each and every other level of that valve.[17] The gating 'signal' is generated in a control room and transmitted to 'interface cubicles' generally situated beneath the valve hall. From here the gating signal is re-directed to each thyristor level.

In order to retain a high degree of reliability, the gating signal is re-directed individually to each thyristor level. To achieve the required degree of electrical isolation, interference immunity and rapid propagation, it is advantageous to use fibre-optics as the link between the interface cubicle and the thyristor level.

The current flowing through each thyristor valve is measured, using a shunt, and the measurement is digitised. This information is then transmitted, via fibre-optic light guides, to the control room for processing. In the control room the thyristor junction temperature is predicted.[18] From this information, an available margin for fault current survival may be determined (see Chapter 3.3.2), thus continuously defining an overload capacity.[17]

2.6 CONVERTER ARRANGEMENT

Two six-pulse bridges are generally connected, displaced by 30° (see section 2.4.4 and figure 2.1). The four valve units of one phase are normally stacked together vertically to form a quadrivalve: three quadrivalves form a 12-pulse bridge. Two twelve-pulse bridges, one at either end of the link, are generally termed a pole. The pole is thus between positive or negative and earth (figure 2.1). This arrangement results in a compact and economic layout of the valves in the valve hall.

Two poles of opposite polarity are connected electrically in series to form a bipole, (see Figures 2.1 and 2.9). Bipoles may then be electrically paralled to achieve the required rating.

Alternatively, it is often advantageous to electrically parallel poles. However, this has the disadvantage of requiring a smoothing reactor for each 12-pulse converter and current-balancing controls must be used for the two rectifiers or inverters connected in parallel.[19] However, it is a useful technique to employ when a scheme is being developed in several, distinct, stages.[19] In addition, in the event of losing a transmission line, there may be a requirement to be able to transmit the rated power down healthy conductors, by paralleling two converters. In such circumstances, the transmission line must be capable of carrying the required overload. The temporary line losses will be increased, but there will not be a reduction of transmission capacity.

A DC transmission scheme must be designed to accept failures within the auxiliary equipment and control systems with a minimal loss of transmission capacity. Thus, failure of a single component should, as far as possible, not affect more than one thyristor level or cause loss of, or reduction in, transmission capability.[17] In addition a second component failure in any system should not give rise to risk of consequential catastrophic failure of major equipment, even though transmission may be disrupted.[17]

The Sellindge converter station[8][14][17] is due to be commissioned in October 1985. This converter station is designed such that the incidence of forced outages caused by the thyristor valves, arising from all causes, should not exceed more than 0.1 per annum, for 24 valves, averaged over the design life of 25 years[17]. To achieve this with a single annual maintenance period, which when taken with the allowance for forced outage, leads to an average annual transmission capability of not less than 98% of the rated annual transmission capability.[17]

3. TRANSIENT PHENOMENA AND THEIR CONTROL

3.1 INTRODUCTION

This Chapter outlines the causes and discusses the characteristics of both the repetitive and non-repetitive voltage and current transients which may occur in a converter station. The features of an inrush current transient, which may overstress a thyristor, are given. Means by which the severity of the transients may be reduced are described.

This chapter, in reviewing transient phenomena, provides a background to and shows a need for the investigations carried out in later chapters. References are therefore made, thoughout this chapter, to later sections in the thesis where there is a more detailed discussion.

Various gate structures are presented, in this chapter, since the gate structure influences greatly a thyristors' ability to survive a given inrush current and thus the characteristics of components required to control the inrush current.

Reference is made to the two-transistor analogue of the thyristor whilst discussing the events which may lead to a catastrophic, 'ungated' turn-on of a thyristor.

The recovery process within a thyristor is outlined with reference to the thyristors increased vunerability to an ungated turn-on during this interval.

The existing circuit design of the Sellindge converter station is used as a basis for the development work, reported on in Chapter 6, 7 and 8. Hence, the electrical circuit of the Sellindge converter station is described in this chapter with particular reference to the hardware used to control the inrush transients. The function of the major components, associated with each thyristor level, are described.

The cost of the inrush control hardware and evaluated losses of this hardware are calculated for the Sellindge converter station. These costs, for both the hardware and evaluated losses, are to be compared in a later chapter with the cost of providing an alternative means of inrush control; thus the losses are calculated for an operating condition and valve firing voltage which is common to both circuits.

3.2 ELECTRICAL TRANSIENTS WITHIN A CONVERTER CIRCUIT

3.2.1 Turn-off of the Thyristor Valves

If initially the thyristor is considered to be a switch, which opens at current zero crossing within the main-circuit, then a very simplified equivalent circuit of a thyristor valve, at turn-off, can be drawn (figure 3.1). Whilst the thyristor valve is in its on-state the shunt stray capacitances (C_B) are effectively short-circuited. At current zero crossing within the main-circuit, the switch is considered to open. Neglecting losses the voltage across the stray capacitances and the off-state thyristors will rise to a maximum value of 2 p.u., where the instantaneous value of the driving e.m.f. (V_e) behind the equivalent leakage inductance (L_{eq}) of the converter transformer is considered to be 1 p.u. The maximum value to which the voltage rises during this interval is known as the recovery overvoltage (V_{REC}). The degree to which the recovery overvoltage overshoots the driving e.m.f. is the overshoot factor. The overshoot factor is normally expressed as a percentage of the instantaneous driving e.m.f.

As a result of the interaction between the transformer leakage inductance and the stray capacitances the recovery overvoltage will be of an oscillatory nature. The normal method of damping the oscillation is to connect a series connected

capacitor (C_d) and resistor (R_d) in parallel with each thyristor. The damping capacitance value per valve (C_D) [figure 3.2] is chosen, typically, to be two to three times greater than the shunt stray capacitances. As the ratio of the value of damping capacitance to stray capacitance is increased, for a given value of damping resistance (R_D) per valve, the degree of damping of the recovery overvoltage is increased. This is, however, achieved at the expense of losses within each damping resistor, (Chapter 7).

During the turn-off period the thyristors carry current in the reverse direction for a short period of time (figure 3.3). The peak reverse current (I_o) results in a stored magnetic energy ($\frac{1}{2} L_{eq} I_o^2$), in the commutating inductance, at the instant of snap-off. This magnetic energy is redistributed, throughout the circuit, as the peak reverse current decays. A proportion of this energy is redistributed to the shunt stray capacitances (C_B) and thus tends to increase the magnitude of the recovery overvoltage (figure 3.3). The remainder of the magnetic energy is mainly dissipated within the damping resistors. The turn-off characteristics of a thyristor are discussed in detail later in this chapter, (section 3.4).

3.2.2 Turn-on of the thyristor valve

A simplified, single-phase equivalent circuit of a thyristor valve is shown in Figure 3.4. Both the shunt stray capacitance and the damping circuit capacitor associated with

each thyristor, discharge at thyristor turn-on. The discharge path of the damping capacitor is via its associated damping resistor and thyristor. The displacement current from the shunt stray capacitance, flows in the main circuit through all the series connected thyristors within the valve.

The physical design of a thyristor valve is, normally, such that the main busbar through the valve is arranged in the form of a rectangular spiral, thus inserting a linear 'winding inductance' (L_w) within the valve in series with the thyristors, (see figure 3.4).

If the thyristors are considered to be perfect switches, a high-frequency oscillation is excited, at turn-on, between the valve winding inductance and the shunt stray capacitances. Referring to figure 3.4 and considering static initial conditions (i.e., zero initial current in an off-state valve) the initial rate-of-rise and magnitude of the displacement current [figure 3.5(a)] from the shunt stray capacitance, for a given valve firing voltage (V_f), are given by :

$$\frac{di_1}{dt} = \frac{V_f}{L_w} \qquad (1)$$

$$I_{pk} = V_f \left(\frac{C_B}{L_w}\right)^{\frac{1}{2}} \qquad (2)$$

respectively. These quantities, di_1/dt and I_{pk}, are superimposed upon the load current transfer into the commutating valve, (see chapter 2.4.3).

Also, local current flows as a result of the pre-charged damping capacitor associated with each thyristor [figure 3.5(b)]. If stray inductance within the discharge loop is neglected and the series connected thyristors are considered to be perfect switches too, then the discharge current from the damping circuit is given by :

$$I_{RD} = \hat{I}_{RD} e^{-t/T} \qquad (3)$$

where,
$$\hat{I}_{RD} = \left(\frac{V_f}{R_D} \right) \qquad (4)$$

and
$$T = C_D R_D \qquad (5)$$

Thus, the total current through the thyristor [Figure 3.5(c)], in this simplified equivalent circuit (figure 3.4), is given by the sum of the displacement current from the shunt stray capacitances, the discharge current from the damping circuit and a commutation current. It should be noted that all of these occur as a result of the collapse of anode voltage.

Thyristors are not self-healing, so must not be overstressed if the integrity of the thyristor is to be ascertained with a good degree of confidence. For turn-on of

thyristors, overstressing can result from any one or a combination of the following features of the inrush transient [see figure 3.5(c)]:

i) The magnitude of the 'step' discharge, $\hat{I}_{RD}$, from the damping network.

ii) The maximum rate-of-rise of thyristor current (di_m/dt), together with its time of occurrence, resulting mainly from the discharge of stray capacitances.

iii) The magnitude of the first peak of thyristor current [$i_{1(pk)}$], which is approximately equal to the sum of the displacement current from the shunt stray capacitances and the discharge current from the damping network.

iv) The magnitude of the first trough of the thyristor current [$i_{1(tr)}$]. The first current trough results from the oscillation excited between the shunt stray capacitances and the valve winding inductance [see figure 3.5(c)]. If the main-circuit is considered to be lossless, the oscillation is undamped. The magnitude and rate of decay of the discharge current from the damping network influences the magnitude of the first-current trough (see figures 3.5).

3.2.3 Voltage transients

Thyristor valves contain semi-conductors, hence unlike conventional equipment, they have a voltage withstand capability only slightly dependent upon the waveshape of an impulse. Thus, it is necessary to provide a suitable protective level which is largely independent of the impulse waveshape. Gapless arresters, using semi-conductor material such as zinc oxide non-linear resistor blocks, are most suitable for this duty. The protection level of the valve arresters should be kept as low as possible for an economic valve design[20].

A thyristor in the off-state, at voltages not approaching its breakover voltage, exhibits a characteristic of a polarity sensitive, temperature-dependent resistor shunted by a voltage and temperature dependent capacitor. The equivalent capacitance of the thyristor is maximum at zero voltage, and decreases with increasing applied voltage of either polarity (section 3.3.2). The equivalent resistance of the thyristor falls with increasing temperature, thus increasing the leakage current (section 3.3.2). Excessive leakage current through the thyristor will result in permanent thermally induced damage.

A rapidly changing thyristor voltage may result in a significant displacement current within the thyristor junction (section 3.3.2). When the quantity of charge injected into the junction is sufficient to dislodge further charge carriers, avalanche breakdown occurs (section 3.3.2). The consequential,

'ungated' turn-on of the thyristor will lead to localised overheating (section 3.3). In addition, the magnitude of the thyristor voltage must be limited if ungated turn-on is to be avoided (section 3.3.2). A valve design must therefore, include protection from overvoltage, excessive forward dV/dt and overtemperature [17].

Voltage transients may originate either from within, or external to, the converter bridge. Repetitive voltage transients occur as a result of commutations within the bridge. Non-repetitive voltage transients occur as a result of non-continuous, external influences.

a) Non-repetitive Voltage Transients

Overvoltages on the AC terminals of a system may result from a lightning-impulse, AC system fault clearance, switching operations, or load rejection. For HVDC schemes situated within countries where the occurrence of atmospheric disturbances are infrequent, and this applies to Britain, the presence of high pass filters, on the AC terminals, ensures that the wavefront of remote strikes is elongated, and their magnitude reduced to an acceptable level for the equipment [20].

The suppression of non-characteristic harmonics, on the AC line, is achieved by connecting frequency selective damped filters on the AC terminals, (chapter 2.4.4). These filters also act to limit overvoltages caused by switching, fault clearance, or load rejection [20].

The waveshape of the impulse generated in the AC system can be quite different from that on the secondary terminals of the converter transformer; due mainly to valve firing and commutation, which has the effect of continuously changing the electrical configuration of the converter.

A switching-impulse may be inductively transferred through the converter transformer. The relatively long rise time associated with the wavefront of a 'standard test' (as defined in IEC 60) switching-impulse (250/2500μs) will not, generally, cause an excessive rate- of-rise of voltage across the off-state thyristors, (Chapter 8.5).

A front-of-wave impulse may be generated by an insulation breakdown within the converter station. The high rate-of-rise of voltage associated with a 'standard test' (as defined in IEC 60) front-of-wave impulse (0.25/5μs), can result in an excessive rate-of-rise of voltage across an off-state thyristor, (chapter 8.5). The

rate-of-rise of thyristor voltage will depend upon the distribution and magnitude of inductances, resistances and capacitances within the off-state valve.

Each thyristor, within a valve, is normally provided with protection which issues a gate pulse to the thyristor in the event of an excessive rate-of-rise of forward voltage or magnitude of forward voltage (see section 3.6). Thus, in the face of a switching-impulse or front-of-wave impulse, a thyristor valve may be expected to be gated by overvoltage and dV/dt protection respectively, (Chapter 8.5). The action of a valve turning-on is to collapse its anode voltage; this results in a corresponding rate-of-rise of voltage across the series connected, off-state, valve (see figure 2.7). If the series connected valve experiences an excessive rate-of-rise of voltage it too would be protectively turned-on.

Overvoltages originating from the DC cable are limited in magnitude by a, DC line, surge arrester. This arrester is connected from line to ground.

b) Repetitive Voltage Transients

Repetitive voltage transients are generated by normal converter operation. These repetitive transients must be allowed for at the design stage of a converter bridge, so

that their presence does not degrade the operation of a converter bridge. There are several causes of these transients:-

i) When a thyristor valve turns-on, a high-frequency oscillation is excited between the shunt stray capacitances and valve inductance, (section 3.2.2). The degree of damping of this oscillation depends upon the circuit configuration and component values, (Chapter 6.4). The initial rate of collapse of the voltage across the valve turning-on results in a corresponding rate-of-rise of voltage across the series connected, off-state, valve (see figure 2.7); this should be prevented from triggering the off-state thryristors into conduction.

ii) Non-coherent turn-on of the thyristors within a valve is generally caused by a thyristor not receiving a firing pulse coherently with the others in the same valve. In such circumstances, the potential difference across the 'late' thyristor level will rise rapidly and may exceed the forward breakover voltage unless protective action is taken, (see section 3.6).

iii) Turn-off of the thyristor valve (Chapter 7), excites an oscillation between the converter transformer leakage reactance and the shunt stray capacitances, (section 3.2.1). The negative voltage across the recovering thyristors initially increases in magnitude and may result

in a corresponding increase in magnitude of positive voltage across several off-state valves (see figure 2.7). The magnitude of positive voltage should not activate the overvoltage protection of the off-state valves.

iv) Turn-on of a thyristor valve should not result in a positive going voltage across a recovering valve, such that the recovering valve fails commutation (Chapter 8.4).

3.3 TURN-ON PROCESSES IN THYRISTORS

It is necessary to control di/dt to within certain values, until the area of the thyristor junction in conduction has spread sufficiently, if the performance of the thyristor is not to be degraded. During turn-on, current transfer takes place from the auxiliary cathode to the main current carrying area of the thyristor[21]. The main current carrying area spreads radially from the emitter periphery at an approximate rate of 0.1mm per microsecond. Current density must be restricted to prevent excessive, localised, energy dissipation. Thus, due to the limited area of silicon initially in conduction, the intial rate-of-rise of current must be controlled.

However, it is possible to design the gate structure of a thyristor such that its initial di/dt capability is enhanced[22]. This is, however, often attainable only at the expense of other, important, characteristics[22]:-

i) Conventional centre gate and conventional side gate (or point-gate thyristors), (figure 3.6 and 3.7 respectivley), have a limited di/dt rating. The area intially turned-on, and hence the di/dt capability, is dependent greatly upon the gate current drive.

ii) The field initiated gate (figure 3.8) is designed to turn-on a definite length of thyristor emitter periphery, even with a soft gate drive. This is achieved by utilising a small pilot thyristor to gate the 'main' thyristor into conduction. With this type of structure delay time (see chapter 4.3) is dependent greatly upon the gate drive.

iii) The N^+ gate (figure 3.9) is designed to turn-on a definite length of thyristor emitter periphery, but requires a stiff gate drive. A short delay time is achieved with this structure.

iv) The amplifying-gate thyristor (figure 3.10) employs a pilot thyristor. The anode current of the pilot thyristor initiates the turn-on in the main current-carrying portion of the device. Only a relatively small magnitude of conventional gate current is required to turn the device on. The area of immediate turn-on, in an amplifying-gate thyristor, is shown in figure 3.11.

In order to increase the di/dt rating of a thyristor, the cathode-area initially in conduction could be increased. This can be achieved by employing an interdigitated gate structure. Fingers, extending radially into the cathode area, increase the length of the perimeter of the gate and decrease the radial distance over which the current can spread; this decreases the interval up to the time when the whole of the cathode area is in conduction. However, the major disadvantage of an interdigitated structure, is that the fingers reduce the cathode area available for conduction. Thus, the on-state losses increase in magnitude, relative to a non-interdigitated structure.

In general, amplifying-gate thyristors are used for HVDC applications; this ensures that a power supply of limited energy storage capability is adequate for gating the thyristors.

3.3.1 Gating via the Gate Electrode

A conventional thyristor consists of a p-n-p-n structure. This structure can be visualised as consisting of two transistors, a p-n-p and an n-p-n interconnected to form a regenerative feedback pair, (see figure 3.12) The collector of the n-p-n transistor, together with the gate drive for the p-n-p transistor, provides base drive to the p-n-p transistor. Similarly, the collector of the p-n-p transistor together with any gate current for the n-p-n

transistor supplies the base drive for the n-p-n transistor. When the positive feedback gain between the transistors exceeds unity, a regenerative situation exists. Conventional transistor theory can be used to analyse this transistor analogue of a thyristor[22].

The two transistor analogy may be analysed in terms of its common base current gains (α_p and α_n for the p-n-p and n-p-n respectively), and the avalanche multiplication coefficients, M_p and M_n [22], where $(\alpha_p M_p + \alpha_n M_n)$ is the loop gain.

When the thyristor is biased such that its anode is positive with respect to its cathode, and in the absence of any gate signal, the avalanche multiplication coefficients are approximately unity, and the transistor base gains are very low [23]. Under these conditions the p-n-p-n structure is said to be in its forward blocking or high impedance 'off' state.

The thyristor assumes a low impedance or 'on' state if the loop gain is raised to unity. The transistors, in the analogy, are driven into saturation by their own regenerative action. Once in saturation, all junctions assume a forward bias, and the potential drop across the device approximates to that of a single p-n junction[22].

3.3.2 Ungated turn-on

During normal or 'gated' turn-on, a gate current is temporarily injected into the thyristor providing current carriers. Anode to cathode current increases, and results in the regenerative action in the two-transistor analogy.

However, 'ungated' turn-on can result from any other means which increases the loop gain to unity. Some of these mechanisms are:-

a) Voltage

As the anode to cathode voltage of a thyristor is increased, a point is reached when the quantity of charge injected into the device (leakage-current flow), is sufficient to dislodge additional carriers. These additional carriers dislodge further carriers and the junction can go into avalanche breakdown, characterised by a sharp increase in anode current.

b) Rate of Change of Voltage

Any p-n junction has space-charge capacitance; the larger the junction area, the larger the capacitance. The magnitude of the incremental, space-charge capacitance is dependent upon the change in fixed charge ΔQ (fixed acceptors and fixed donors)

covered or uncovered [figure 3.13(b)], as the bias is changed by a magnitude ΔV. Thus, the incremental, space-charge, capacitance of a junction is given by $\Delta Q / \Delta V$.

The manner in which the space-charge capacitance changes as the applied voltage across a junction, is altered, is derived by Millman and Halkias [24]. The magnitude of the space-charge capacitance is inversely proportional to the width of the depletion layer.

As forward bias is applied to a p-n junction, the zero bias p.d. across the boundary [see figure 3.13(a)] is overcome. Charge-carriers of both signs move and recombine at the junction, [figure 3.13(b)] and the width of the depletion layer is reduced, thus covering up a fixed charge, ΔQ. This represents an increase in the value of the incremental capacitance.

As reverse bias is applied to a p-n junction the zero bias p.d. across the boundary increases, [figure 3.13(b)] preventing the further diffusion of charge carriers. Thus, the depletion layer increases in width, uncovering some fixed charge. This represents a decrease in the value of the incremental capacitance.

A thyristor consists of p-n-p-n junctions; thus, when an off-state thyristor is forward biased, two of the junctions become forward biased (covering up fixed charge), whilst one junction becomes reverse biased (uncovering further fixed charge). Figure 3.14 shows a typical plot of equivalent incremental, space-charge, capacitance (C_J) versus thyristor voltage for a 56mm thyristor.

The thermal diffusion of holes and electrons causes a nett migration of charge across the boundary, with zero bias applied to the thyristor. The resulting p.d. at a junction presents the depletion layer as a barrier of a fraction of a volt [figure 3.13(a)].

Thus, as the junction temperature is increased further charge is able to migrate and recombine at the junction, decreasing the width of the depletion layer, thus covering up fixed charge. Hence, there is a nett increase in the incremental space-charge capacitance, (figure 3.14).

If a fast-rising voltage is impressed across the anode-cathode terminals of a thyristor, a charging current (i_{LK}) will result. The magnitude of this

charging current is dependent upon the instantaneous value of incremental space-charge capacitance (C_J) of a thyristor and the applied dV/dt:-

$$i_{LK} = C_J \left(\frac{dV}{dt}\right)$$

When the quantity of charge injected into a junction is sufficient to dislodge additional carriers, the junctions can go into avalanche breakdown.

c) Temperature

At high temperatures there is a significant, thermally-induced leakage current. If this leakage current is of sufficient magnitude to dislodge additional carriers, the junctions can go into avalanche.

During an 'ungated' turn-on, the area initially in conduction is an 'uncontrolled region' within the device. Thus, the di/dt capability of the thyristor is significantly reduced in comparison to a 'gated' turn-on. Similarily, during the on-state, a succession of fault current loops must not cause excessive heating of the thyristor junction, otherwise the device may not recovery safely [18].

3.4 TURN-OFF PROCESSES IN THYRISTORS

When a HVDC thyristor is in its conducting state, the two base regions (B_p, B_n) (see figure 3.15) are heavily saturated with holes and electrons respectively, (stored charge)[22].

During the turn-off process, holes and electrons in the vicinity of the two end junctions, J_1 and J_3, will diffuse to these junctions and this results in a reverse current in the external circuit. The voltage across the thyristor remains small whilst this reverse current increases in magnitude, (figure 3.3)[17]. As soon as sufficient holes and electrons have been swept out of the end junctions, J_1 and J_3, these junctions assume a blocking state. The reverse recovery voltage can then increase across the thyristors[22]. In an HVDC scheme, the line commutated thyristors may recover to a voltage significantly greater than the driving e.m.f., (section 3.2.1).

Recovery is not yet complete, as a high concentration of holes and electrons exist in the region of the centre junction, J_2[17]. This concentration decreases by the process of recombination[17]. Diffusion of electrons into the p-region and holes into the n-region leaves the region near the junction depleted of majority and minority carriers[22]. As the charges of the fixed donor and acceptor ions near the junction are no longer balanced by the charges of the mobile carriers, so an electric-field builds up (figure 3.16). The direction of the

electric-field is such as to oppose the flow of majority carriers to the other side of the junction. The field would normally build up until it completely counteracts any nett flow of majority carriers.

A dynamic equilibrium can thus be achieved, in which the region near the junction is depleted of majority carriers and in which space-charge layers (or depletion layers), containing high electric-fields, are formed[22]. A forward voltage (less than the thyristors forward breakover voltage) may be applied to the thyristor without causing it to turn-on. [22] The time that elapses after the cessation of forward current flow, and before forward voltage may be safely re-applied is called the thyristor 'turn-off time', t_q, (Chapter 8.4).

The forward recovery capability of the thyristor is strongly dependent upon the lifetime of the electron-hole plasma trapped in the B_n region of the thyristor [17]. Partially recovered thyristors are vunerable to catastrophic failure, unless they are properly protected against an ungated turn-on occurring. The probability of an uncontrolled turn-on occurring is dependent upon the electron-hole plasma density, the magnitude of re-applied dV/dt and the characteristic of the saturating reactor[17]. In order to shorten the 'turn-off time' recombination may be accelerated by the provision of recombination centres (defects in the crystal lattice).

However, a disadvantage of doing this is that during normal conduction the rate of recombination of holes and electrons will increase, thus increasing the forward volt-drop and losses associated with the thyristor.

3.5 INRUSH CURRENT CONTROL

A thyristor has a limited ability to accept current during the turn-on period, (section 3.3). In order to control the current density (and hence, limit the heating of the slice), it is necessary to limit the rate-of-rise of current during this interval. All HVDC schemes require inductance to limit, to within safe levels, the inrush current when the thyristor valve turns on. It is uneconomical to utilize linear inductance, within the valve, as this increases the size of the valve and the reactive power requirements of the converter station, (Chapter 2.4.5).

Saturating reactors (non-linear inductance), are normally used to limit the intial rate-of-rise of thyristor valve current, and hence the rate of dissipation of energy in the silicon-slice, during turn-on. During this interval, the thyristor is exhibiting a characteristic analogous to a non-linear resistor whose value is dependent upon the quantity of charge passed through the resistor.

The switching action of the thyristors excites an oscillation between the shunt stray capacitances and the valve inductance (section 3.2.2). This oscillation can be detrimental to the safe operation of the thyristors (section 3.2.2). The displacement current from the stray capacitances, together with the damping circuit discharge current, mainly contribute to the magnitude of the first peak of inrush current [figure 3.5(c)]. Following the first peak of displacement current, from the shunt stray capacitance, the current will decrease in magnitude and if undamped reverse significantly. Any reversal of the displacement current will reduce the magnitude of the thyristor current (first current trough), [Figure 3.5(c)]. If the thyristor current falls below a certain value the area of silicon in conduction may decrease reducing the capability of the device to survive subsequent high rates-of-rise of forward current. In addition, reversal of thyristor current during turn-on may extinguish the device. The main source of damping of the oscillation may be by thyristor switching and on-state losses.

It is advantageous to provide additional means of damping the oscillation, so as to reduce the magnitude of the reverse displacement current [figure 3.5(a)], and hence increase the magnitude of the first current trough. The total energy dissipated within the silicon-slice can thus be reduced (a proportion being dissipated elsewhere in the circuit) thus

reducing the thermal stresses imposed upon the thyristor. In the Sellindge converter station this is achieved by including several inrush control components with parallel connected damping networks (section 3.6).

However, when a tender for an HVDC link is adjudicated, the losses in the circuit are evaluated, against the tenderer, at a rate of approximately five US dollars per watt. Thus, it may be disadvantageous, economically, to increase the circuit losses within the additional components provided to control the inrush.

3.6 SELLINDGE CONVERTER STATION

3.6.1 Electrical Circuit

The 2000MW HVDC Cross-Channel link consists of two bipoles, each rated at 1000MW; each bipole is constructed from two poles (chapter 2.6). Twelve thyristor valves form two six-pulse bridges, the outer bridge has a converter transformer with a star secondary, the inner bridge has a delta secondary (chapter 8.3).

Each thyristor valve consists of 125 series connected thyristor modules. Within this, there are 3 redundant modules to allow for possible failures of thyristors or associated electronic equipment. This redundancy allows

the design to meet a specified requirement of not more than 0.05 forced outages per annum for 12 valves of one pole, averaged over the design life of 25 years (chapter 2.6).

The HVDC air-cooled module contains two, parallel connected, 56mm diameter, amplifying-gate thyristors (THY1, THY2 figure 3.17). These together with a ferrite saturating reactor (L1a) and a quasi-linear reactor (L1b) form the main high current path through the module.

The saturating reactor (L1a) consists of 26 toroidal ferrites mounted on a central copper conductor. The initial rate of change of flux density with magnetic-field strength of the ferrite is high, resulting in a high initial incremental inductance (approximately 38 mH per valve). The high initial incremental inductance, under repetitive operating conditions, results in a low initial rate-of-rise of main-circuit current at thyristor turn-on; allowing a time of about one microsecond, during worst-case repetitive operation, whilst the discharge current from the damping circuit transfers from the auxiliary cathode to the main current-carrying area.

The ferrite begins to saturate at a level of magnetic-field corresponding to a main circuit current of approximately 40A. Due to the early saturation of the ferrite reactor, after an elapsed time of about 1μs during worst-case repetitive operation, an additional inductance

in the form of a six-turn spiral (L1b) is necessary to control the subsequent inrush current. The windings of the six-turn spirals are, electrically insulated copper-strands, built up to a height of three strands. Subdivision of the winding reduces the magnitude of the eddy-currents induced in the spiral.

In addition to the six-turn spiral it was also necessary to include a connection reactor on the secondary of the converter transformer, per AC phase (figure 3.18). This helps to reduce the severity of the inrush current, at valve turn-on, which would otherwise result from the shunt stray capacitances of the converter transformer. A 500pF capacitor is connected in parallel with each valve; the purpose of this capacitor is primarily to control the transient voltage distribution throughout the twelve-pulse bridge.

The AC connection reactor, together with the 500 pF valve capacitor, also act to control the rate-of-rise of voltage across an off-state thyristor valve, provided that any impulse emanates from the converter transformer side of the AC connection reactor, (see figure 3.18).

There is also a DC connection reactor (figure 3.18) which acts to buffer the stray capacitances of the smoothing reactor and the DC line (or cable) from the

thyristor valves. There is a resistor connected in parallel with both the AC and DC connection reactors; this acts to damp oscillations excited between the connection reactors and stray capacitances.

The saturation of the ferrite reactor is abrupt and results in a sudden change in di/dt. Although the resulting di/dt has been shown to be safe, by test, it is also known to be stressful to the thyristors.

A damping network, R_d and C_d, (see figure 3.17) is connected in parallel with each thyristor. The damping network may provide four main functions:-

i) Control of the recovery voltage at thyristor turn-off (section 3.2.1 and chapter 7).

ii) A 'priming-current', I_{RD}, (section 3.2.2) to aid turn-on of the thyristor.

iii) Control of the AC voltage distribution between thyristor levels in a valve. Differences in power frequency voltage distribution between thyristor levels may result from either or both of the following:-

   a) Differences between the capacitance values of the damping capacitors, due to tolerances.

   b) Differences in reverse recovered charge between thyristors (see Appendix VI).

iv) Charging of the power supply for the gate electronics (see figure 3.17). An energy storage capacitor, within the power supply, provides rapid charge storage during positive excursions of thyristor voltage; also enabling the gate electronics to fire the thyristors immediately following energisation of the converter bridge, should circumstances require such action.

A fuse is provided within the damping circuit to protect against failure of the damping capacitor to short-circuit. In such circumstances operation of the fuse will, very shortly afterwards, result in failure of the thyristor(s), of the same level, to short-circuit; using up redundancy in the valve but not interrupting the operation of the converter station.

A fast grading network, R_{fg} and C_{fg}, (see figure 3.17) is connected in parallel with each thyristor level to control the voltage distribution, between levels, during conditons of fast transient voltage impulses, (e.g., lightning or front-of-wave impulses). Without the fast-grading circuit the voltage distribution, during fast voltage transients, would be mainly dependent upon the magnitude and distribution of circuit inductances, resistances and stray capacitances. The fast-grading resistor, which is also designed to act as a fuse in case

of the fast-grading capacitor failing to short-circuit, damps voltage oscillations which are excited between the capacitor and circuit inductance by fast voltage transients.

A current transformer, coupled into the fast-grading circuit (see figure 3.17), is used to indicate the dV/dt across the thyristor level. The change in thyristor voltage lags the change in voltage across the level due mainly to the ferrite (L1a) and the six-turn sprial (L1b). Thus, the dV/dt seen by the protection is phase advanced in comparison with the thyristor dV/dt. This allows the gate electronics to issue a protective firing-pulse to the thyristors in advance of a high dV/dt exceeding the thyristors capability; which could otherwise result in an ungated turn-on of the thyristor.

In the event of a thyristor not receiving a gate-pulse from the gate-electronics, overvoltage protection of the thyristor is provided by a Breakover Diode (BOD), (see figure 3.17). The BOD acts to limit the magnitude of positive voltage excursion across a thyristor whilst also providing a supplementry means of gating off-state thyristors.

A short-term, repetitive, overvoltage may activiate the overvoltage protection of a complete valve: the resulting inrush current results in thermal stresses,

within the thyristor, which are more severe than during normal repetitive duty. These stresses should be controlled to within the thyristors capability if the thyristors integrity is to be maintained, (Chapter 6).

Figure 3.18 shows a simplified equivalent circuit used for the prediction of inrush current transients occurring within the Sellindge converter station[25]. The resulting worst-case repetitive inrush current, when the valves turn-on from maximum forward overvoltage, is shown in figure 3.19[25].

The nominally lossless ferrite together with the, high conductivity copper, six-turn spiral (DC resistance is approximately 150μΩ), control the main circuit di/dt and the magnitude of the first current peak of the inrush current.

To damp the inrush current oscillation a bypass diode and series resistor are connected in parallel with the six-turn spiral (figure 3.18). The diode conducts, electrically introducing the bypass resistor, when the main circuit current is reducing in magnitude. Electrically in parallel with the AC connection reactor (see figure 3.18) there is a resistor to aid damping of the parasitic oscillations of the inrush current, excited between the converter transformer stray capacitances and valve inductance (section 3.2.2).

In summary, the components used in the Sellindge converter station of the 2000MW Cross-Channel link to provide inrush control are:-

a) DC connection reactor together with a shunt resistor.
b) AC connection reactor, per phase, together with a shunt resistor.
c) Ferrite reactor per thyristor level.
d) Quasi-linear reactor (six-turn spiral), together with a bypass diode and resistor, per thyristor level.

3.6.2 Cost of Inrush Control

i) Hardware

The cost of inrush control may be estimated from the total cost of the necessary hardware together with a relevant loss-evaluation figure. The cost of hardware includes a figure for any assembly procedures, and testing of the component.

At the tender stage of a contract the estimated, converter station, losses must be specified to the customer. The losses are normally adjudicated at a rate of about $5 per watt and the resulting figure, for the loss evaluation, often exceeds the cost of the hardware in question. The following hardware costs for the inrush control components of the Sellindge

converter station are the equivalent costs, per level, at January 1984 prices. The loss evaluation assumes a rate of $5 per watt and an exchange rate of $1.5 to the pound.

a)	Connection reactors (AC and DC)	£168.58 per level
b)	Bypass diode and resistor	£25.87 per level
c)	Ferrite reactor and quasi-linear reactor	£328.28 per level
Total cost of hardware for inrush control -		£522.73 per level

ii) Evaluated Losses

Losses are normally adjudicated for a scheme under worst-case, full load current, inverter operation. However, to aid comparison, the following loss evaluation is performed for 'worst-case' repetitive inrush conditions; the sum of the individual BOD levels within a valve, have been chosen to be identical for the Sellindge converter station and a future scheme, the development of which is the subject of later chapters. However, future schemes will take advantage of an asymmetrical voltage characteristic of a thyristor by co-ordinating the arrester level with the reverse capability of the valve (see chapter 8.2). Hence, the p.u. insulation level is greatly reduced in comparison with the Sellindge converter station (see chapter 8.2). As a

result, a future scheme considered to have the same 'sum of BOD protective levels' will be designed to operate at an increased amplitude of line-to-line voltage. Hence, the firing voltage, at a given firing angle, will be different for the two schemes. However, the magnitude of the evaluated losses is dependant upon the firing voltage: thus, a comparison of losses must be made at the same firing voltage, (i.e., the sum of the BOD protective levels in this case).

The following estimates of energy dissipation, within the inrush control hardware, during 'commutation in' and 'commutation out' are based upon a constant rate of change of current during this time interval. This rate of change of current is assumed to be given by the valve overvoltage protective level (400kV) divided by the commutating inductance, (59.69mH).

$$\text{Thus, } di/dt = \left(\frac{400 \times 10^{3}}{59.69 \times 10^{-3}} \right) = 6.7A\ \mu s^{-1}$$

Hence, the following estimates (per valve) can be made for the dissipation:-

a) AC connection reactors (500Ω shunt resistor)

Inrush transient:

Computer prediction	204J	(t = 45μs)
Commutation in	25.6J	
Commutation out	25.6J	
Total =	255.2J	

b) Bypass resistance, 150Ω, (in parallel with Quasi-linear inductance)

Inrush transient:

Computer prediction	169.3J	(t = 45μs)
Commutation out	85.4J	
Total =	254.7J	

c) Hence, the energy dissipated as a result of the 500Ω shunt resistor associated with each connection reactor and the bypass resistance associated with the quasi-linear inductance is given by (a + b); 509.9J per valve

Thus, for 50Hz application: 25.5kW per valve

d) In addition to this, the six-turn spiral has a DC resistance of approximately 150μΩ per level. The load current is approximately 1103A rms, hence for a 125 level valve, the losses are given by:-

$150 \times 10^{-6} \times 125 \times 1103^2 =$ <u>22.8kW per valve</u>

e) The AC connection reactors have a DC resistance of approximately 3.174mΩ. The load current, per AC phase, is approximately 1560A rms, therefore, the losses are given by:-

$3.174 \times 10^{-3} \times 1560^2 =$ <u>7.724kW</u> (per two valves)

f) The DC connection reactor has a DC resistance of approximately 2.888mΩ. Full load DC current is approximately 1911A, hence, the losses are given by:-

$2.888 \times 10^{-3} \times 1911^2 =$ <u>10.547kW</u> (per 12-pulse bridge)

g) Therefore, the total losses, per valve, as a result of quasi-linear reactors within the valve and connection reactors in the scheme, for full load current (1911A) are given by:-

$(d + {}^{e}/2 + {}^{f}/12)$ =

(22.8 + 7.72/2 + 10.55/12)kW = 27.5kW per valve

h) Therefore the total estimated power loss, per Sellindge converter station valve, attributable to inrush control components, is given by (c + g):-

(25.5 + 27.5)kW = 53kW per valve

i) Hence, evaluating these losses at a rate of $5 per watt and an exchange rate of $1.5 to the pound:-

Adjudicated loss = $265,000 per valve

or Adjudicated loss = £1413 per level

Hardware cost = £522.73 per level

Total cost (attributable to inrush control) = £1935 per level

or

Total cost (attributable to inrush control) = £242,000 per valve

4. MODELLING TECHNIQUES

4.1 INTRODUCTION

Thyristor valves for HVDC and AC applications are normally designed for a minimum life of 25 years. In addition, the degree of availability required is high. Thus, the electrical and thermal stresses to which the valve components are subjected must be within their transient and continuous performance capabilities. Hence there is a need for careful analysis of the transient system behaviour during both normal and abnormal conditions of operation.

So that the design predictions are accurate the studies must take into account circuit non-linearities. A powerful computer programme (VTECAP) has been developed at GEC over the last 15 years, which is used in conjunction with real time (analogue) models and an AC-DC simulator to investigate various aspects of valve design. VTECAP was employed by the author in undertaking the studies reported in this thesis. Thus, this chapter contains a description of the piece-wise linear techniques used by VTECAP for representation of non-linear capacitances, inductors and resistances.

In addition, the chapter contains a description of various modelling techniques employed for valve design studies. Some of these technqiues are well established within the company, e.g., the transformer electrostatic model. Other techniques have been

developed by the author and are now regularly used during the process of valve design (e.g., a refined representation of the converter transformer).

All the techniques described in this chapter are utilised during one or more of the studies described in Chapters six, seven and eight.

4.2 SIMULATION TECHNIQUES

4.2.1 General

In order to achieve a high degree of reliability and availability, the original valve design must ensure that the electrical and thermal stresses to which the valve components (in particular the thyristors) are subject, are within their transient and continuous performance capabilities. Thus, there is a requirement for careful and accurate analysis of the transient system behaviour during both normal and abnormal modes of operation.

So that the results of these analyses are accurate, the studies must take account of circuit non-linearities. The non-linearities of the thyristor, such as the device dynamic impedance during the transition from 'off-state' to 'on-state', reverse recovered charge at turn-off (Chapter 3.4), leakage current (Chapter 3.3.2) and displacement current (Chapter 3.3.2), and the inevitable diversity of characteristics between thyristors in the same valve must all be considered. All these characteristics of the thyristor interact in a complex manner with the main converter station circuit, which itself may contain non-linear elements such as saturating reactors and surge arresters.

The converter transformer, with its associated stray capacitances, contributes significantly towards the production and magnitude of circuit transients. The converter transformer

stray capacitances comprises both shunt and series winding capacitances together with bushing stray capacitance. In addition to these, busbar and valve stray capacitances shunt the valve. The valve also has a winding inductance (Chapter 3.2.2) which affects the nature of the transients.

In order to analyse the resulting complex circuit, under various operating conditions, a powerful and versatile computer programme has been developed at GEC, over the last 15 years. The 'Variable Topology Electrical Circuit Analysis Program' (VTECAP), is used in conjunction with real time analogue models and an AC-DC simulator to investigate various valve design aspects[26].

An AC simulator consisting essentially of resistors, inductors and capacitors can be used to model complete converter stations, including the control systems and the non-linear characteristics of the converter transformers.[27] The stray capacitances of the real system are not normally modelled, as the simulator is used primarily to assess the behaviour of the control system and overvoltages of fundamental frequency or generally, for frequencies below that of 17th harmonic.[20] In order to simulate the behaviour of a real system above that of 17th harmonic, accurate modelling of stray capacitances and system non-linearities would be required [e.g., thyristor recovery characteristic (chapter 3.4)].

The simulator is an invaluable tool for assessing the magnitude and waveshape of temporary overvoltages occurring, for example, during AC system fault conditions or load rejection[20].

The flexibility of the simulator, together with the ease of adjustment of parameters, is an advantage in surveying a wide variety of transient overvoltage conditions. The most onerous condition identified can then be further investigated by use of a real time, analogue, model or by digital computer analysis[20].

Real Time, analogue, models of systems need only incorporate the components of significance to the transient response being considered. These circuit components are simulated by readily available electronic components. Non-linear elements, such as saturating reactors and surge arresters may be simulated by an appropriate combination of electronic components and magnetic materials. Voltages and currents are scaled equally by factors between 500 and 20,000.[20]

As a result of the difficulties associated with accurately simulating non-linear elements, the real time analogue model is limited in accuracy. However, it is able to represent complex systems together with all known stray components distributed throughout the model. Thus, the likely transient duty imposed

on individual items (arresters, valves and transformers), may be predicted at an early stage in the design.

By means of mathematical analysis, using a computer program, the valve components are more precisely sized, rated and toleranced to protect the thyristors from being overstressed under the most adverse conditions during system disturbances and valve commutation. However, it is important that the results of predictions are checked against experimentally observed behaviour. When this is done, a close correlation has been found to exist between the computed transient results from VTECAP, and both the real time analogue waveform and the waveforms associated with a valve under test[26]. This has, over the years, established confidence in the analytical techniques employed.

4.2.2 Computer Analysis : VTECAP

The Variable Topology Electrical Circuit Analysis Program (VTECAP), is a general transient analysis programme for linear and non-linear electrical circuits.[26] The basic circuit topology (i.e. connections within the network) and circuit parameters may be changed during the transient study.[26] These changes may be due to switch action, representing for instance a valve, or due to non-linear elements, representing for instance saturating reactors or surge arresters[20].

A generalised mesh analysis method converts the electrical network data into the form of a set of linear or step-wise

linear differential and algebraic mesh circuit equations.[26] The equations are solved simultaneously by the Kutta-Merson method [28] of step-by-step numerical integration to obtain the complete transient solution[26].

The integration routine has built-in control of the step length, which is continually adjusted by the program, in order to achieve the required accuracy.[26] The routine also has a supplementary facility to reduce any integration step in order to achieve a required network or parameter change at any required instant, with user-specified accuracy, in accordance with the 'controls' of the non-linear element or the switch concerned in the change.[26]

The output calculated by the program, e.g. branch voltage, current, power and energy are user specified. Approximate graphical output may also be obtained to ease visualization of the results.

Data can be made available in order to permit a continuation of a study. Specific data may also be written to a file to allow subsequent plotting using a graphics package. From the wide variety of facilities available only those of particular importance in the application of the program to valve design have been mentioned.

4.3 REPRESENTATION OF SEMI-CONDUCTOR CHARACTERISTICS

4.3.1 Thyristor Turn-on

The normal transition from the off-state to the on-state, which is initiated by a gate pulse, may be subdivided into three regions[29] :

a) Delay Time

Delay time (t_d) varies from thyristor to thyristor and is the time taken to respond to a gate pulse, (figure 4.1). The delay time is generally defined from 10% of gate current to 90% of firing voltage. Thyristors exhibiting longer delay times are exposed to overvoltages arising from the earlier collapse of voltage across the rest of the valve, and the valve design must allow for this[29].

b) Rise Time

Rise time (t_r) is the initial period during which thyristor current rises as the anode voltage collapses, (figure 4.1).

c) Turn-on time

Turn-on time (t^*_{gt}) is the period of time following the application of gate current to the collapse of anode voltage. The elapsed time is measured from 10% of gate current to 36.5% of firing voltage, (Figure 4.1).

d) Spreading Time

Spreading time is the interval during which the conducting area spreads to occupy the whole of the silicon slice.

During rise time and the early stages of spreading time, the current carrying capability of a thyristor is severely limited, thus the initial rate-of-rise of current must be restricted (Chapter 3.3). The turn-on time (t^*_{gt}) is dependent upon the immediate history of the device, i.e., the quantity of charged passed through the thyristor. Thus, the turn-on time is greatly dependent upon the initial anode voltage and junction temperature.[30] The delay time is also dependent upon the anode voltage and, to a lesser extent, the junction temperature.[30] The delay time and turn-on time are also both greatly dependent upon the magnitude of gate-current drive.[31] Hence, the rate of transition from the off-state to the on-state consistent with the initial anode voltage, junction temperature and gate drive of interest must be represented in each study.

In order to represent, with any degree of accuracy, the transition of the thyristor from the off-state to the on-state laboratory measurements are required showing the anode voltage collapse and rise of thyristor current (figure 4.1), for a particular junction temperature and gate drive.

The coherent turn-on of thyristors may be modelled as a time dependent resistance, R(t). The instantaneous value of the resistance is obtained from the laboratory measurements and is taken to be the ratio of the instantaneous value of the anode voltage (V_T) to the instantaneous value of the anode current (I_A). Thus:

$$R(t) = \frac{V_T\ (t)}{I_A\ (t)} \qquad (1)$$

The thyristor model is revised to coincide with the firing voltage, junction temperature and gate drive of interest.

4.3.2 Thyristor turn-off

Following current zero, the turn-off process of a thyristor is a complicated one, normally characterised by a short period of increasing reverse current as carriers are swept out of the reverse biased junctions (Chapter 3.4). This is followed by a longer period of decaying reverse current (figure 3.3) as the carriers recombine in the vicinity of the forward biased junction, (Chapter 3.4). The period of reverse current is usually expressed in terms of the total reverse recovered charge, Q_{rr}. Any variation in reverse recovered charge, between thyristors, will cause a voltage distribution unbalance which must be catered for in the valve design (Chapter 8.4 and Appendix VI)). During the few hundred microseconds that recovery lasts, the thyristor progressively recovers its capability to withstand forward voltage and forward dV/dt

(Chapter 3.4). However, economics dictate that thyristors for HVDC should be stressed before recovery is complete[29]. This is necessary to retain a high power factor (chapter 2.4.5) and also to minimize the stresses on the valves and damping circuits (chapter 2.4.6).

The total reverse recovered charge increases with both the commutation di/dt and junction temperature, T_J. Thus, the total reverse recovered charge is circuit dependent as well as device dependent. The thyristors are subject to turn-off experiments, in laboratories, in order to assess the total reverse recovered charge at given junction temperatures and commutation di/dt's.

In order to limit the magnitude of the reverse recovery voltage across a thyristor, at turn-off, an R-C damping network is normally connected in parallel with each thyristor, (chapter 3.2.1). In order that the damping network components are adequately sized and rated, the reverse recovered charge of the thyristors must be modelled.

The behaviour of the thyristors, during the recovery interval, can be represented by the total reverse recovered charge (Q_{rr}) and a proportion, k_1, which is recovered before the thyristor begins to support reverse voltage (Chapter 3.4), (i.e., during the interval of increasing reverse current), (see figure 3.3). A proportion ($1-k_1$) of the total reverse recovered charge is recovered during a period of decaying reverse current, (see figure 3.3).

The reversed recovered charge and the proportion before peak reverse current is obtained, for the mathematical model, by interpolation between the laboratory measurements approximately appropriate to the circuit conditions of interest.

The di/dt during commutation is dependent upon the peak line-to-line voltage, the firing angle of the valve turning-on and the inductance around the commutation loop. However, due to the influence of saturating reactors (chapter 3.5), the inductance around the commutation loop is not constant. Thus, the reverse recovered charge estimated, and modelled, for the thyristor should take into account, where possible, the saturating reactor characteristic.

Normally the non-linearity of the saturating reactor characteristic is such that the consequent reduction in reverse recovered charge is difficult to estimate accurately. Thus, no allowance is made, in the mathematical model of the thyristor, for a reduction in total reverse recovered charge resulting from short intervals (generally less than 100A) of high incremental inductance; hence, the prediction will be pessimistic.

For a thyristor turning-off, the reverse biased junctions do not achieve a blocking state until their depletion layers have formed, (chapter 3.4). The di/dt during increasing reverse current (see figure 3.3) is, for a given driving e.m.f., mainly dependent upon the inductance around the commutation loop. The

magnitude of the peak reverse current is thus determined by the di/dt, the total reverse recovered charge and the proportion, k_1, of the total charge recovered upto peak reverse current.

The 'conventional' turn-off model of a thyristor is shown in figure 4.2. Prior to zero current crossing, the switches in parallel with resistance (R), inductance (L), and capacitance (C) are all considered to be closed. At the time of current zero crossing, in the commutating phase, the switch in parallel with the capacitance (chosen to be 1 Farad in the model) opens. Thus the integral of the reverse current with respect to time (Q), is directly proportional to the capacitance voltage, (Q = capacitance voltage).

At the instant the capacitance voltage is equal to $k_1 Q_{rr}$ the reverse current, in the model of a recovering thyristor, is transferred, mathematically, into the inductance and resistance, whose values are large compared with those of the main circuit (e.g., 30H and 1MΩ respectively, are typical values). This results in a 'snap-off' characteristic being modelled for the thyristor at the time of peak reverse current. The inductance, in series with the resistance, gives a time constant of decay ($^L/R$) representing the recombination of carriers within the forward biased thyristor junction, (Chapter 3.4).

The peak reverse current (I_o) is calculated from an estimated di/dt and a Q_{rr} interpolated from laboratory measurements for the appropriate rate of current commutation;

$$I_o = (2k_1 Q_{rr} \cdot di/dt)^{\frac{1}{2}} \quad (2)$$

Thus, the time constant of decay is given by ;

$$L_{/R} = (1-k_1)(Q_{rr}/I_o) \quad (3)$$

4.3.3 Thyristor Junction Capacitance

The displacement current of thyristors during fast-varying voltages depends on the applied voltage, its polarity, and the thyristor junction temperature, (Chapter 3.3.2). The thyristor has an effective incremental capacitance which is large at low voltage and approaches a low value asymptotically as the voltage increases, (chapter 3.3.2). For modelling purposes, this characteristic is approximated by a stepped function suitable for representing the thyristors as piece-wise linear, voltage-dependent capacitors, (figure 4.3). The incremental capacitance is given by :

$$C_1 = \frac{\Delta Q_1}{\Delta V_{q1}} = \frac{Q_1 - 0}{V_{q1} - 0} = \frac{Q_1}{V_{q1}} \quad (4)$$

and

$$C_2 = \frac{\Delta Q_2}{\Delta V_{q2}} = \frac{Q_2 - Q_1}{V_{q2} - V_{q1}} \quad (5)$$

To avoid step changes in voltage across the voltage dependent capacitance when it changes state, it is necessary to calculate a pre-charge to insert with the revised state of the non-linear capacitance. With reference to figure 4.3, the value

of this 'pre-charge', whilst the voltage is increasing (e.g., the non-linear capacitance is changing from state C_1 to C_2) is given by:-

$$Q_2' = Q_2 - \left(\frac{Q_2 - Q_1}{V_{q2} - V_{q1}} \right) \cdot V_{q2} \qquad (6)$$

where, Q_2' is the 'pre-charge' at voltage zero, necessary on capacitance C_2, to avoid a step change in voltage during the transition from capacitance value C_1 to C_2 at voltage V_{q1}.

$$\text{Hence,} \quad Q_2' + C_2 V_{q1} = C_1 V_{q1} \qquad (7)$$

$$\text{Generally ;} \quad Q_n' + C_n V_{q(n-1)} = C_{(n-1)} V_{q(n-1)} = Q_{(n-1)} \qquad (8)$$

Similarily, whilst the voltage is decreasing in magnitude, e.g., the non-linear capacitance is changing from state C_2 to C_1, the 'initial' charge (Q_1') on capacitance C_1, to avoid a step change in voltage during this transition, has the value:-

$$Q_1' = Q_1 - \frac{Q_1 - Q_0}{V_{q1} - V_{q0}} \cdot V_{q1} \qquad (9)$$

Thus at a 'break' voltage (i.e., voltage at which the non-linear capacitance changes state) the charge is conserved, (see figure 4.3).

The energy stored within the non-linear capacitance is calculated by integrating the volt-current product with respect to time.

4.4 REPRESENTATION OF MAIN-CIRCUIT, NON-LINEAR ELEMENT, CHARACTERISTICS

4.4.1 Surge Arrester

Insulation co-ordination forms an important part of the design of AC and DC schemes; excessive system cost or unacceptable fault probability can arise if the protective arrangement and the equipment withstand have not been co-ordinated adequately[20]. The interaction between the surge arresters and the system may be determined by studies. Both analogue and digital models can be used as tools for the insulation co-ordination.[20]

As HVDC schemes increase in transmission capacity the higher transmission voltages and currents result in an increase in stored energy in the AC harmonic filters and DC line[20]. Thus, the surge arresters must have a high energy-absorption capability. It is possible to achieve this capability by proper matching of the electrical characteristics of several parallel columns of varistor blocks[20].

The manufacturers of surge arresters are, generally, willing to divulge relevant, unpublished, test data regarding their arresters. All the relevant information must then be

mathematically modelled in order to assess its effect upon the integrity of the thyristor valves.

The voltage-current characteristic for a surge arrester will be modified according to the wavefront applied. A switching-impulse will result in a certain co-ordinating current at a given voltage, but a lightning-impulse may result in a reduced co-ordinating current at the same voltage thus having a reduced effect in limiting the voltage excursion. A voltage-current characteristic appropriate to the wavefront under consideration must therefore be selected and represented, (figure 4.4).

The method of representing the required characteristic is to use a piece-wise, linear, current dependent resistance. Each value of incremental resistance is given by the ratio of a change in the voltage characteristic to the corresponding change in the current characteristic, (figure 4.5).

$$\text{Thus, } R_1 = \frac{\Delta V_{r1}}{\Delta I_1} = \left(\frac{V_{r1} - 0}{I_1 - 0} \right) = \frac{V_{r1}}{I_1} \qquad (10)$$

$$\text{and, } R_2 = \frac{\Delta V_{r2}}{\Delta I_2} = \left(\frac{V_{r2} - V_{r1}}{I_2 - I_1} \right) \qquad (11)$$

Hence, to avoid step changes in the predicted voltage or current, when the resistance changes state, it is necessary to calculate the magnitude of a voltage source to insert with the revised state of the non-linear resistance.

Thus, for an increasing voltage, from figure 4.5, the magnitude of the voltage source may be calculated:-

$$V_{r2}' = V_{r2} - \left(\frac{V_{r2} - V_{r1}}{I_2 - I_1} \right) . I_2 \qquad (12)$$

Where, V_{r2}' is the initial voltage, at current zero, which must be modelled in series with R_2 to avoid a step change in voltage or current during the transition from resistance value R_1 to R_2 at voltage V_{r1}.

$$\text{Hence, } V_{r2}' + I_1 R_2 = I_1 R_1 = V_{r1} \qquad (13)$$

$$\text{Generally, } V_{rn}' + I_{(n-1)} R_n = I_{(n-1)} R_{(n-1)} = V_{r(n-1)} \qquad (14)$$

Similarily, whilst the voltage is decreasing in magnitude, e.g., the non-linear resistance is changing from state R_2 to R_1, the series voltage source inserted will have a value given by:-

$$V_{r1}' = V_{r1} - \frac{V_{r1} - V_{r0}}{I_1 - I_0} . I_1 \qquad (15)$$

The energy dissipated within the arrester is calculated by integrating the volt-current product with respect to time.

4.4.2 Saturating Reactor

All HVDC schemes utilise saturating reactors primarily to protect the thyristors from excessive rates-of-rise of inrush current when a valve turns-on (chapter 3.5). This inrush current is a result of unavoidable shunt stray capacitances discharging as the thyristor anode voltage collapses (chapter

3.2.2). The saturating reactor may also be used to control the inrush current oscillations (Chapter 6), which are excited between the shunt stray capacitances and valve inductance (Chapter 3.2.2). If uncontrolled, the peak of an oscillation may result in excessive current density within the junction of the thyristor, thus overheating the junction and degrading or permanently damaging the device. The trough of an oscillation could result in the thyristor current being decreased near to zero and the thyristor extinguished, or its subsequent current carrying capability severely degraded, (chapter 3.5).

In addition to controlling the inrush current, the saturating reactor influences the rate of valve-voltage collapse at valve turn-on. This voltage collapse is important as it is capacitively coupled to other valves in the bridge, and may affect their performance (chapters 8.4 and 8.5). The voltage collapse also affects the level of radio interference generated by the converter.

In the event of an impulse being impressed across a thyristor valve (chapter 8.5) the saturating reactor interacts electrically with the damping circuit, thyristor junction capacitance, the fast grading circuit (depending upon its position of connection) and both stray inductance and stray capacitance to control the dV/dt across off-state thyristors, (figure 4.6).

The saturating reactor forms an important part of the design. Excessive magnetic material results in a large valve structure and thus requires a large valve hall. The net effect of excessive material is an escalation of system cost. However, there must be sufficient magnetic material, displaying an adequate inductance versus current characteristic, to protect the thyristors electrically. Hence the saturating reactor characteristics are selected to keep the predicted transients within experimentally ascertained safe operating limits for the thyristors. The interactions between the system and the saturating reactors are determined by digital computational methods. These interactions are then confirmed, experimentally, to be safe for the thyristors.

The saturating reactor, generally designed by GEC TDPL, consists of toroidal magnetic material mounted on, but insulated from, a central copper conductor (chapter 3.6). To limit the copper losses, the conductor is designed to be of a large diameter (e.g., 50mm). Thus, it is convenient to utilize reactors with a single-turn, as opposed to a multi-turn reactors requiring stranded conductors connected in parallel.

The saturating reactor is represented as a piece-wise linear, current controlled inductance. Each value of incremental inductance is given by the ratio of a change in the flux characteristic to the corresponding change in the current, (figure 4.7).

$$\text{Thus, } L_1 = \frac{\Delta \phi_1}{\Delta I_1} = \left(\frac{\phi_1 - 0}{I_1 - 0}\right) = \left(\frac{\phi_1}{I_1}\right) \qquad (16)$$

$$\text{and, } L_2 = \frac{\Delta \phi_2}{\Delta I_2} = \left(\frac{\phi_2 - \phi_1}{I_2 - I_1}\right) \qquad (17)$$

Thus, in order to avoid step changes in the calculated flux, when the piece-wise linear current dependent inductance changes state, it is necessary to calculate an appropriate 'residual flux' at current zero, associated with the revised state of the non-linear inductance.

Thus, for an increasing current, from figure 4.7 the magnitude of the 'residual flux', ϕ'_2, may be calculated:-

$$\phi_2' = \phi_2 - \left(\frac{\phi_2 - \phi_1}{I_2 - I_1}\right) \cdot I_2 \qquad (18)$$

or

$$\phi_2' + L_2 I_1 = L_1 I_1 = \phi_1 \qquad (19)$$

In general:

$$\phi'_n + L_n I_{(n-1)} = L_{(n-1)} I_{(n-1)} = \phi_{(n-1)} \qquad (20)$$

Similarily, whilst the current is decreasing in magnitude, e.g., the non-linear inductance is changing from state L_2 to L_1, the 'residual flux' (ϕ'_1) inserted will have a value given by:-

$$\phi'_1 = \phi_1 - \frac{\phi_1 - \phi_0}{I_1 - I_0} \cdot I_1 = \phi_1 - L_1 I_1 \qquad (21)$$

Where, in this example, $\phi_1 = L_1 I_1$ (see equation 16), thus the residual flux ϕ'_1 has a value of zero.

Since no 'back e.m.f.' is inserted with the revised state of the piece-wise linear inductance, there will inevitably be step changes in voltage across and di/dt through, the mathematical representation of the non-linear inductance, when it changes state.

The magnetic-energy stored within the reactor is calculated by integrating the volt-current product with respect to time.

4.5 REPRESENTATION OF CONVERTER TRANSFORMER EQUIVALENT CIRCUIT

4.5.1 Electrostatic Model

All HVDC schemes and Thyristor Controlled Reactors contain unavoidable stray capacitance. These stray capacitances are mainly within the converter transformer but are also associated with busbars and bushings, and the thyristor valve itself.

Within a thyristor valve, the stray capacitances are from each level to ground and between each and every level. Thus, the equivalent electrostatic model of a multilevel valve would be extremely complex. It is usual, for the majority of studies, to estimate the shunt stray capacitance associated with the valve, and to model it as a lumped parameter. The interlevel capacitances may, depending upon the study undertaken, be neglected. If the distribution and magnitude of the interlevel capacitances are also important, e.g. transient voltage distribution within an off-state thyristor valve, a real time analogue model may be constructed from electronic components. All components considered to be of significance to the transient response are included.

The busbars between the converter transformer and valves also have stray capacitance to ground and between busbars. Although this is a 'distributed' capacitance (i.e., transmission line) it may be possible to consider it to be 'lumped' (figure 4.8), depending upon the study to be undertaken.

The converter transformer has a complex distribution of stray capacitances, between windings of the same and different phases, and between windings and earth. However, it is convenient during the early stages of a valve design, to derive a lumped capacitance model, (figure 4.8). This lumped model consists of lumped interturn (series) (C_I), lumped shunt (C_G), and lumped neutral (C_N), capacitances.

Whilst performing certain analyses, numerically, the equivalent circuit simulated on the VTECAP program cannot contain capacitance meshes. Such circumstances include ;

i) Operation of a switch in a capacitance mesh;

ii) Operation of a switch that alters the number of meshes in the circuit;

iii) Operation of a parallel switch which alters the format of a mesh (e.g. an inductive mesh becoming a resistive mesh).

Hence, if any of the above switch operations are required, in a circuit representation containing capacitance meshes, the capacitances must be manipulated into an equivalent circuit which does not contain capacitance meshes. Thus, for a converter transformer (figure 4.8), the behaviour of the

transformer, as viewed from its terminals, must be the same in both mathematical models, (figure 4.9). The inter-phase and phase to earth displacement currents must be equivalent. This may be achieved by equating the effective shunt and series capacitances for both models, as seen from the transformer terminals[32]. The leakage inductances of the transformer remain unchanged (see figures 4.8 and 4.9).

4.5.2 Transformer High-Frequency Characteristic

A converter transformer winding exhibits a high-frequency resistance (hfr) characteristic. This characteristic is the result of two phenomena; namely proximity-effect and skin-effect. At the lower frequencies the apparent increase in resistance is approximately proportional to the square of the frequency which indicates that the phenomenon is that due to the proximity-effect.[33] This effect arises from the fact that the distribution of current across the conductor cross-section is affected by the magnetic-field of the rest of the conductors comprising the winding.[34] The apparent resistance of the winding also tends to increase as the conductor thickness increases.[32]

At higher frequencies, the apparent resistance is approximately proportional to the square-root of the frequency, which indicates that the phenomenon is that due to skin-effect.[35] This phenomenon is due to the tendency of the currents to confine themselves to a surface layer as a consequence of the magnetic-field of the conductor itself. The

apparent resistance of the winding decreases as the thickness of the conductors comprising the winding increases[32]. The derivation of the, single-section, high-frequency transformer winding model[32] is given in Appendix II.

Whilst considering turn-on it is unnecessary to include high-frequency resistance within the model of the transformer, [36][37] (figures 4.9 and 4.10). It is, however, important to include high-frequency resistance within the model (figure 4.11), whilst the valve is considered to be recovering[32].

4.5.3 Refined Model of the Converter Transformer

a) Modelling Technique

The transient interaction between the valve and converter transformer greatly influences valve design and cost (Chapters 6, 7 and 8). It is thus desirable to ensure that the modelling techniques employed to simulate the transformer and valves are optimised to be both accurate and efficient. The resultant valve/transformer design should be such as to give a minimum overall equipment cost.

During the initial stages of a design, a 'lumped' transformer model is normally utilised, (figure 4.9). However, a more accurate representation of the transformer is obtained if each phase is sub-divided into many sections, thus obtaining an approximate 'distributed' converter transformer model (figures 4.10 and 4.11). The optimum number of sections for each phase of the transformer winding model has been found to be

five. [36][37] Although an 'evenly' distributed model would be acceptable for infinitely long transmission lines, transformers require the consideration of end-effects. [36][37][38]

Rudenberg[38] has shown that end-effects can be taken into account by allowing the ground capacitance, C_G, to rise to twice its value at the end of a coil. Similarly, the interturn capacitance, C_I, and leakage inductance, L_T, decrease at the end of a finite coil to half the value at the centre, (figure 4.10). Thus, the three central sections of a five-section model are identical to one another and the end-sections represent end-effects. The derivation of this model is described in reference 36.

b) High-frequency resistance

The reduction in the inductance at the end of a finite winding is due to leakage flux effects. Due to the reduced flux linking the end-section of a coil, and hence a reduced rate of change of flux with respect to time, the effective driving e.m.f. (considered to be 'behind' the commutating inductance) is reduced in comparison with the centre of the winding. Similarily the magnitude of the induced eddy-currents, resulting from the field of the conductor itself, is also reduced. Howeyer, the frequency of the driving flux is unaltered; thus the depth of penetration of the eddy-currents is unchanged throughout the winding. Thus, the reduced magnitude of eddy-currents flow in an unaltered cross-sectional area, in

comparison with the centre of the winding. Hence, the eddy-current losses, at the end of the winding, are reduced in comparison with those at the centre of the winding (Appendix II).

Similarly, the proximity-effect is basically frequency dependent. Again, the frequency of the exciting flux at the end of the winding is unaltered in comparison to the centre of the winding, although its magnitude is decreased; hence, the magnitude of eddy-currents induced at the end of a winding is reduced in comparison with the centre of the winding. The eddy-currents are conducted in an unaltered cross-sectional area in comparison with the centre of the winding: hence, the eddy-current losses are reduced at the end of the winding compared to the centre.

Thus, in deriving the high-frequency resistance transformer model (section 4.5.2) coincidently with a refined transformer model (with end-effects), the high frequency resistance is considered to be distributed equally throughout each section of the model (Appendix II), (see figure 4.11).

4.6 IMPULSE GENERATOR

Thyristors can be impropely triggered into conduction by displacement currents arising from application of an excessive forward dV/dt[17]. This, ungated, turn-on is characterised by a very limited ability to cope with any ensuing di/dt (Chapter 3.3.2).

Similarly, an excessive magnitude of forward or reverse voltage will also result in an undesirable magnitude of leakage current. This leakage current will cause localised heating of the junction. A point will be reached where sufficient charge has been injected into the junction such that the current carriers arriving at the junction dislodge many further carriers. Further carriers are dislodged by these carriers and the junction goes into a form of avalanche breakdown characterised by a rapid increase in anode current, (Chapter 3.3.2). Overvoltage protection may be employed to protect the thyristor from a forward overvoltage (Chapter 8.5).

HVDC thyristors have an asymmetrical voltage characteristic, and the reverse voltage capability exceeds the forward voltage capability. In order to take economic advantage of the asymmetry, it is standard practice to co-ordinate the reverse capability of the thyristors with the surge arrester protective level[17], (chapter 8.2).

By international convention (IEC 700), the thyristor valves are tested at voltages 15% above the protective level of the arrester for switching-impulses, (as defined in IEC 60) (250/2500 μs), and lightning-impulses, (as defined in IEC 60) (1.2/50 μs). This test voltage is increased to 20% above the protective level for front-of-wave impulses (as defined in IEC 60) (0.25/5μs). The thyristor valve must be demonstrated to survive these voltages and associated rates-of-rise of voltage, (chapter 8.5).

In order to model an impulse applied to an off-state valve it is necessary to mathematically describe an impulse 'generator'. The techniques employed assume that the applied impulse can be subdivided into two exponentially decaying waveforms of opposite polarity. Thus, the sum of these exponentials gives the required impulse waveshape (figure 4.12);

$$V_V = V_m (e^{-t/T_1} - e^{-t/T_2}) \qquad (22)$$

This equation can be electrically reproduced by a circuit such as that shown in figure 4.13.

An approximate methodology for calculating the required circuit component values is given in Appendix III, together with component values for switching (250/2500μs), lightning (1.2/50μs) and front-of-wave (0.25/5μs) impulses.

Due to the inherent difficulties in defining a representative high-frequency source impedance for the impulse generator, the component values can be chosen such that the high-frequency output impedance is very low compared to the high-frequency impedance of the load. Thus, the load will not, noticeably, modify the output of the generator and will result in a pessimistic prediction.

5. INCREASED TRANSIENT RESISTANCE

5.1 INTRODUCTION

The major circuit transients which may occur within the electrical circuit of a converter station are described in Chapter 3. One of the most significant of these transients is that associated with turn-on of a thyristor valve, (Chapter 3.2.2).

The method presently employed to control these transients does provide a safe working environment, (Chapter 3.6). However, in order to enhance the safety of the working environment and to reduce the cost associated with the control of transients, it is necessary to investigate other means of achieving the required control.

A method of damping the inrush current oscillation without incurring excessive evaluated losses, is to transiently increase the resistive dissipation within the main-current path through the valve. However, the overall losses associated with inrush control components should be unaltered or preferably reduced in comparison with those of the Sellindge converter station.

The method considered in this chapter for increasing the transient resistance is akin to the deep-bar effect associated

with induction motors. A 'thin-ribbed' busbar is considered to be housed within a magnetic material which forms a semi-closed slot around the busbar*. The current distribution within the rib, is calculated firstly for a current ramp and then for a trapezoidal current pulse. Hence, the transient resistance of the busbar is determined.

The ratio of a change in flux density to the corresponding change in magnetic-field strength is assumed to be constant throughout the cross-sectional area of the magnetic material and during the analysis. The dimensions of the rib and slot are calculated for this ratio to obtain a transient resistance value of 1 ohm per thyristor level at an elapsed time of 1μs from the start of rise time (Chapter 4.3.1). The mechanical difficulties associated with the construction of such a reactor are briefly discussed.

---

* For simplicity, the semi-closed slot formed by the magnetic material will be referred to throughout this chapter as a 'semi-closed slot'.

5.2 PROPOSED STRATEGY

The method initially considered for achieving an increased transient resistance is similar to that used in induction motors. This method utilizes conductors placed within a semi-closed slot (see figure 5.1). Induction motors require an increased transient resistance when the motor is first energised to prevent the armature winding drawing excessive current (and burning out as a consequence). At energisation there is no induced e.m.f. in the rotor winding and only the armature winding resistance limits the magnitude of current drawn from a supply of zero source impedance.

Swann and Salmon[39] have analysed the performance of a rectangular conductor housed in a semi-closed slot, based upon AC conditions of excitation. Silvester[40] has presented a solution for deep-bar effect which he claims is capable of finding "any desired steady-state or transient performance characteristics or field distributions within the conductor with ease".

In the present investigations, studies have been performed to assess the feasibility of utilizing a thin-ribbed conductor, housed within a semi-closed slot, to increase the transient resistance of the main-circuit busbar of the valve. These preliminary studies did not utilize Silvesters' method[40] but instead, are based upon a solution of the Diffusion Equation; this allows rapid computation of the required parameters, by a

digital computer. In addition, the effect of assuming values for various physical parameters (e.g., geometry of the busbar, resistivity of the conductor or effective relative permeability of the magnetic-circuit) may be readily assessed.

Figure 5.1 shows a conductor within a semi-closed slot; the conductor is assumed to be non-magnetic, solid and homogeneous. The magnetic material is also assumed to be solid and homogeneous. Thus, the effective relative permeability of the magnetic-circuit surrounding the conductor is dependent upon the relative permeability of the magnetic material and the length of the air-gap.

The effective relative permeability of the magnetic-circuit is utilized throughout the analysis, to allow the effects of both changes in the geometry of the magnetic-circuit and/or conductor to be considered.

5.3 BACKGROUND THEORY

5.3.1 Diffusion of electric-current

A transient electromagnetic field penetrates into a conductor according to whether it is excited by the application of a fixed but time-varying H or B-field.[41][42]. The concept of 'applying a current' may be imagined as a voltage applied to a circuit dominated by pure resistance of a large value compared to the impedance of the conductors which form the busbars. The resulting current may be considered as 'applied' to the busbars[43]. Thus, if the saturating inductance of the valve is

neglected, and the thyristors are considered to be resistive switching elements, then the discharge current from the stray capacitances may be considered to be a 'current applied to the main circuit busbar of the valve'.

When electric current is caused suddenly to flow in a conductor, initially, it is entirely at the surface of the conductor[43]. The current density diffuses into the conductor, the direction of the 'diffusion-wave' of current penetration being transverse to the direction of flow of the electric current[43].

The penetration of current density into a conductor, over the time-period of interest in this thesis, is analogous to thermal diffusion and transient heat flow[42][43][44][45], (i.e., displacement current may be neglected); the penetration is described by the classic diffusion equation[46]:

$$\nabla^2 E - \mu\sigma \cdot \frac{\partial E}{\partial t} = 0 \qquad (1)$$

K.W. Miller[43], points out the following for a conductor in free-space: "The velocity of penetration of the wavefront of this 'diffusion wave' decreases inversely as the square-root of time, and the distance penetrated increases as the square-root of time, that is, the 'velocity' of current

density penetration is not constant. However, the velocity of penetration is unaffected by geometrical configuration and is independent of whether it is 'parallel diffusion' or 'convergent diffusion' or 'divergent diffusion'. The crest-value of a diffusing-wave (which remains fixed at the initiating surface, line or point), has its rate of decay altered by the degree of geometrical convergence or divergence encountered by the advancing wave".

A changing magnetic-flux induces eddy-currents within the conductor which oppose the uniform distribution of current density and delays the growth of current. At the instant of excitation by a fixed H or B-field the transient resistance is infinite and decreases in inverse proportion to the square-root of time[41]. Similarly, at the instant of excitation the transient inner inductance is zero and increases in proportion to the square-root of time [41].

With reference to figure 5.1, the Poynting-vector ($\underset{\sim}{S}$) denotes the power (per unit area) as given by the cross product of the electric-field ($\underset{\sim}{E}$) and magnetic-field ($\underset{\sim}{H}$). For a busbar in a semi-closed slot, excited by a current ramp (figure 5.2) the Poynting-vector is normal to the top surface of the rib. Thus the current density penetrates, by diffusion, from the top surface of the rib into the conductor, normal to the direction of flow of the current.

The velocity of penetration (V_p) is given by[43]

$$V_p = h/(t)^{\frac{1}{2}} \tag{2}$$

where, h is the coefficient of velocity, and is given by,

$$h = (\rho/\mu)^{\frac{1}{2}} \tag{3}$$

where, $$\mu = \mu_o \mu_e \tag{4}$$

and μ_e is the effective permeability of the magnetic-circuit.

5.3.2 Effect of Diffusion upon Transient Resistance

The cross-sectional area of the conductor effectively in conduction, at various instants in time, increases as the current density diffuses into the conductor. The difference between transient resistance and DC resistance is caused entirely by the difference in current distribution[45]. Thus, the effective resistance of the conductor is dependent upon the elapsed time following the application of a fixed H or B-field. When the current density is uniform, the DC resistance is defined as ;

$$R_{dc} = \frac{l_g}{\sigma A} \tag{5}$$

When the current density is not uniform, the resistance is usually defined in terms of power loss;[45]

$$\frac{R_{tr}}{R_{dc}} = \frac{\text{watts}}{I^2 R_{dc}} \tag{6}$$

Thus, $$R_{tr} = \frac{\text{watts}}{I^2} \tag{7}$$

Hence, the transient resistance ratio (the ratio of the transient resistance to the DC resistance) can be calculated by integrating the square of the current density over the cross-sectional area of the conductor and dividing by the square of the integral of the current density over the cross-sectional area[45].

5.4 APPLICATION TO INRUSH CONTROL

It is possible to control, to some degree, the transient resistance with time characteristic of a conductor. To achieve a relatively high transient resistance, followed by a relatively low steady-state resistance suggests that, transiently, the current should be forced to flow in a thin rib (small cross-sectional area) of busbar (figure 5.1). Under steady-state conditions the current should have a large cross-sectional area of high conductivity material in which to flow (figure 5.1), thus, minimising the steady-state losses.

The geometry of the rib can be altered to give various transient resistance with time characteristics. The height of the rib controls the time for which the increased transient resistance is maintained, whereas the width controls the magnitude of the resistance (for a given resistivity of the conductor, effective relative permeability of the magnetic-circuit and applied waveform).

To minimize steady-state losses, the main body of the conductor should be a high conductivity material such as copper. However, it is not considered feasible to utilize different materials for the rib and main busbar for the following reasons:-

a) Construction of the rib from a high resistivity material would increase the rate of diffusion of the current density (see equations 2 and 3). Thus, the height of the rib may have to be increased to achieve a certain resistance value at a given elapsed time (say 1 ohm per level after an elapsed time of 1μs), measured from the start of rise time.

b) The joint between the two materials would have to be of a very low resistance. If there were to be a significant resistance present, at the joint, a high current would produce excessive losses and heating. The two materials may have very different coefficients of thermal expansion. Thus the localised heating could cause degradation, and the possibility of eventual failure of the joint.

The analysis of the performance of the 'ribbed busbar in a semi-closed slot', assumes that the mode of excitation is by a fixed H-field. The reasoning behind this assumption is that the thyristor resistance, during switching, is large compared to the ability of the busbar, within the semi-closed slot, to restrict current flow. This is not necessarily the case at every instant of time and is dependent upon the instantaneous value of the

incremental inductance of the ribbed busbar in a semi-closed slot, and the instantaneous value of the incremental resistance of the thyristor. Hence, if the inductance is of such a value that it has, transiently, a greater effect in restricting current flow than does the dynamic resistance of the thyristor, then the predominant mode of excitation would be that of a fixed B-field[42].

The instantaneous value of incremental inductance, of the ribbed busbar in a semi-closed slot, for a given magnetic material (e.g. ferrite), is dependent upon the length of the air-gap and effective cross-sectional area of magnetic material. Both of these dimensions are themselves dependent upon the required width and height of the 'rib' to achieve a specified transient resistance-time characteristic.

In order to assess the feasibility of a 'ribbed busbar in a semi-closed slot', it is necessary to make an assumption regarding the shape of the wavefront of current excitation; this is assumed to be of a trapezoidal nature. Thus, the inrush current from the shunt stray capacitances is approximated to be a constant gradient up to first current peak, (Figure 5.2). The rate-of-rise of this inrush current and the time at which the trapezoid is considered to level-off are, however, two variables within the equations developed, whose effect can be assesed.

The product of the rate-of-rise of current associated with the wavefront of a trapezoid and the incremental inductance of the busbar within the semi-closed slot, results in an 'induced e.m.f', E_I:-

$$E_I = L_n \, di/dt \tag{8}$$

The magnitude of flux associated with the magnetic material, for a single-turn winding, is assumed to be given by the integral of the instantaneous voltage (E_I) with respect to time.

$$\emptyset = \int_0^t E_I \, . \, dt \tag{9}$$

The time varying magnetic-field gives rise to an electric-field ($\underset{\sim}{E}$), within the rib of the busbar and within the magnetic material (see Appendix IV.I). This electric-field results in eddy-currents within the busbar and also within the magnetic material. The eddy-currents result in a reaction H-field which opposes the applied H-field. The eddy-current density ($\underset{\sim}{J}$) is given by,

$$\underset{\sim}{J} = \text{curl } \underset{\sim}{H} \tag{10}$$

In a conductor the electric-field strength is linked to the current density by Ohms law[42]:

$$\underset{\sim}{J} = \sigma \underset{\sim}{E} \tag{11}$$

The transient resistance is dependent upon the cross-sectional area of the busbar effectively in conduction, at any instant in time. An increase in the effective relative permeability of the magnetic-circuit and/or in the conductivity of the conductor results in a reduced rate of diffusion of the magnetic-field (see equations 2, 3 and 4). Thus, for a given busbar, the transient resistance may be controlled by suitable specification of the flux density versus magnetic-field characteristic of the magnetic material surrounding the busbar.

5.5 SOLUTION OF THE DIFFUSION EQUATION

5.5.1 Introduction

The process of current density penetration into a conductor, starting from the surface during current transients, is analogous to thermal diffusion and transient heat flow [42][43][44][45]. Both are governed by the same basic 'diffusion equation' (when displacement current may be neglected). The basic diffusion equation which governs the linear flow of heat is[46]:

$$\frac{\partial^2 U_t}{\partial y^2} - \frac{1}{k}\frac{\partial U_t}{\partial t} = 0 \qquad (12)$$

The totality of solutions of a partial differential equation is very large [47]. For example:-

a) Consider the following expression which satisfies equation (12)

$$U_t = t^{-\frac{1}{2}} \cdot e^{-m} \qquad (13)$$

where, $$m = \left(\frac{y^2}{4kt}\right) \tag{14}$$

$$\frac{\partial U_t}{\partial t} = -\tfrac{1}{2}t^{-3/2} \cdot e^{-m} + \frac{y^2}{4k} \cdot t^{-5/2} \cdot e^{-m} \tag{15}$$

and $$\frac{\partial^2 U_t}{\partial y^2} = -\frac{1}{2k} t^{-3/2} \cdot e^{-m} + \frac{y^2}{4k^2} \cdot t^{-5/2} \cdot e^{-m} \tag{16}$$

Equations (13) and (14) have the properties ;

$U_t \to 0$ as $t \to 0$ for fixed $y \neq 0$

$U_t \to$ infinity as $t \to 0$ for $y = 0$

and $$\int_{-\infty}^{\infty} U_t \cdot dy = 2(\pi k)^{\frac{1}{2}} \text{ for all } t > 0$$

U_t, as given by equation (13) may be regarded physically as the solution corresponding to the release of a quantity of heat energy $[2pc(\pi k)^{\frac{1}{2}}]$, per unit area over the plane $y = 0$, at $t = 0$[46].

b) The most usual form of the solution to the basic diffusion equation, equation (12), is that using error functions:-

$$U_t = \int_0^y t^{-\frac{1}{2}} \cdot e^{-m} \cdot dy \tag{17}$$

or $$U_t = 2k^{\frac{1}{2}} \int_0^{(y/2)(kt)^{-\frac{1}{2}}} e^{-\xi^2} \, d\xi \tag{18}$$

Therefore, using the notation:

$$\text{erf } y = 2\pi^{-\frac{1}{2}} \int_0^y e^{-\xi^2} \, d\xi \qquad (19)$$

Then, $U_c = D.\text{erf}[(y/2)(kt)^{-\frac{1}{2}}]$ is a solution to equation (12) where;

D is an arbitrary constant

Hence, for a known excitation and conductor arrangement, the basic diffusion equation may be solved to enable calculation of the magnetic or electric-field distribution within the conductor. The mode of excitation to be considered here, is that due to a magnetic-field (section 5.4) and the distribution of the current density, within the conductor, is of interest. The transient resistance of the conductor (see equations 6 and 7), may then be calculated by integrating the square of the current density over the cross-sectional area of the conductor and dividing by the square of the integral of the current density over the cross-sectional area, (section 5.3.2).

The main circuit current, when a thyristor valve turns on, is for the purposes of this analysis approximated to a trapezoid (figure 5.2). Hence, the initial surface excitation is a ramp which is considered to level off abruptly after several microseconds. This assumption simplifies the analysis considerably.

5.5.2 Application of a current ramp

Carslaw and Jaeger[46] derive the following solution to equation (12) for the application of a ramp of heat energy to the surface of a thermal conductor;

$$U_t = bt\left[(1 + \frac{y^2}{2kt})\ \mathrm{erfc}(\frac{y}{2(kt)^{\frac{1}{2}}}) - \frac{y}{(\pi kt)^{\frac{1}{2}}} e^{-(\frac{y^2}{4kt})}\right] \quad (20)$$

$$\therefore\ U_t = 4bt\ i^2\ \mathrm{erfc}(\frac{y}{2(kt)^{\frac{1}{2}}}) \quad (21)$$

where the surface-temperature $T(t) = bt$

i^2 erfc is the 'twice integral' of the complementary error function

The equivalent solution to equation (12) for the application of a ramp of current, $I(t) = bt$, may thus be derived, giving:

$$U_I = 4bt\ i^2\ \mathrm{erfc}(\frac{y}{2(kt)^{\frac{1}{2}}}) \quad (22)$$

where $k = h^2 = (\rho/\mu)$

The magnetic-field is assumed to be in the x-direction, and is a spatial function of y, (figure 5.3). Thus, the eddy-currents will be induced, in this simplified approach, entirely in the z-direction. Hence, omitting the displacement current which is negligible in conductors, Maxwell's equations reduce to[48]:

$$\frac{\partial H_x}{\partial y} = -J_z \quad (23)$$

The mode of excitation is assumed to be a current of trapezoidal nature, whose initial gradient and whose peak

magnitude are known. Thus, if the simplifying assumption is made that the relationship between the applied current and magnetic field is constant, i.e.

$$H = NI/l_m \tag{24}$$

then equation (22), for a ramp of current, may be combined with equation (24) and rewritten;

$$U_{H(y,t)} = 4bt \frac{N}{l_m} i^2 \operatorname{erfc}\left(\frac{y}{2(kt)^{\frac{1}{2}}} \right) = 4bt \frac{N}{l_m} i^2 \operatorname{erfc}(m^{\frac{1}{2}}) \tag{25}$$

and from equation (23),

$$J_z = - \frac{\partial H_x}{\partial y}$$

$$\text{Hence, } U_J = - \frac{\partial U_H}{\partial y} \tag{26}$$

Where U_J and U_H are solutions to the diffusion equation (equation 12), and are functions of both y and t.

$$\text{Thus, } U_J = - \frac{N}{l_m} \left[\frac{bty}{kt} \operatorname{erfc}(m^{\frac{1}{2}}) - \frac{2bt}{(\pi kt)^{\frac{1}{2}}} e^{-m} \right] \tag{27}$$

Thus, the solution of the basic diffusion equation for the electric-field may be derived:-

$$\text{Let } U_J = \sigma U_E \tag{28}$$

Where U_E is a function of both y and t.

Then combining equations (27) and (28)

$$U_E = \left[\frac{U_J}{\sigma} \right] = \frac{N}{l_m} \left[\frac{bty}{\sigma kt} \operatorname{erfc}\ (m^{\frac{1}{2}}) - \frac{2bt}{\sigma(\pi kt)^{\frac{1}{2}}} e^{-m} \right] \tag{29}$$

If the magnetic material, together with its air-gap, are assumed to have a constant effective relative permeability then

the time varying magnetic energy, W_m (t), (in a section of unit area), is given by :

$$W_{m(t)} = (\mu/2) \int_0^\infty U_H^2 \, dy \qquad (30)$$

Combining equations (25) and (30):

$$W_{m(t)} = (\mu/2) \int_0^\infty [\frac{4bt}{l_m} Ni^2 \, erfc(m^{\frac{1}{2}})]^2 \, dy \qquad (31)$$

Where:

$$W_{m(t)} = \tfrac{1}{2} L_{I(t)} I(t)^2 \qquad (32)$$

In order to evaluate the integral of equation (31), let $m^{\frac{1}{2}}$ be equal to g. Hence;

$$dg/dy = \tfrac{1}{2}(kt)^{-\frac{1}{2}} \qquad (33)$$

Substituting (33) into (31) gives;

$$W_{m(t)} = (\mu/2) \int_0^\infty [4bt \, (N/l_m) \, i^2 \, erfc(g)]^2 \, dg \times 2(kt)^{\frac{1}{2}}$$

Therefore:

$$W_{m(t)} = \frac{\mu \times 16b^2t^2N^2 \times 2(kt)^{\frac{1}{2}}}{2l_m^2} \int_0^\infty [i^2 \, erfc(g)]^2 \, dg \qquad (34)$$

The limits of integration are in practice from 0 to ∞. However, for $g>2$ $[i^2\text{erfc}(g)]^2$ approaches zero rapidly. Thus, to aid numerical integration, the limits of the integral (equation (34)) are rewritten as from 0 to 2.

Hence:-

$$W_{m(t)} = \frac{16\mu b^2 t^{5/2} N^2 (k^{\frac{1}{2}})}{l_m^2} \int_0^2 [i^2 \text{erfc}(g)]^2 \, dg \qquad (35)$$

The term $\int_0^2 [i^2\text{erfc}(g)]^2 dg$ in equation (35) was evaluated using the Trapezoidal rule of integration. The interval of the integral was subdivided into 20 steps. This gave

$$\int_0^2 [i^2\text{erfc}(g)]^2 dg = 0.0129$$

Hence, $$W_{m(t)} = \frac{16\mu b^2 t^{5/2} N^2 (k^{\frac{1}{2}})}{l_m^2} \times 0.0129$$

$$W_{m(t)} = \frac{0.2064 \, \mu b^2 N^2 t^{5/2} k^{\frac{1}{2}}}{l_m^2} \qquad (36)$$

Thus, from equations (32) and (36) the transient inner inductance($L_{I(t)}$) of the conductor may be determined:

$$L_{I(t)} = \frac{0.413 \, \mu b^2 N^2 t^{5/2} k^{\frac{1}{2}}}{l_m^2 \times (I(t))^2} \qquad (37)$$

and substituting $I(t) = bt$ gives:-

$$L_{I(t)} = \frac{0.413 \, \mu b^2 N^2 t^{5/2} k^{\frac{1}{2}}}{l_m^2 b^2 t^2} = \frac{0.413 \, \mu N^2 (kt)^{\frac{1}{2}}}{l_m^2} \qquad (38)$$

From equation (38), the transient inner inductance of the conductor at the instant of excitation is zero, and increases in proportion to the square-root of elapsed time, following the application of a current-ramp.

5.5.3 Application of a Trapezoidal Current Pulse

A trapezoidal surface excitation may be formulated from two ramps, (figure 5.4). The second ramp (cancellation ramp) is delayed in time by an interval t_b, and has a negative gradient, with respect to the first current ramp. The solution of the basic diffusion equation for the flat portion of the trapezium, is similar to that carried out above (section 5.5.2). However, there are two ramps of opposite gradient but identical magnitude of the gradient (figure 5.4), to consider.

From equation (25), the magnetic-field resulting from a current ramp surface-excitation (figure 5.4), starting at t = 0, is given by:

$$U_{H(1)} = 4bt \frac{N}{l_m} i^2 \operatorname{erfc}\left(\frac{y}{2(kt)^{\frac{1}{2}}} \right) \qquad (39)$$

Similarily the magnetic-field resulting from a negative ramp (cancellation ramp) surface excitation (Figure 5.4), starting at an elapsed time t_b, is given by:

$$U_{H(2)} = -4b(t-t_b) \frac{N}{l_m} i^2 \operatorname{erfc}\left(\frac{y}{2[k(t-t_b)]^{\frac{1}{2}}} \right) \qquad (40)$$

Thus, the total magnetic-field, for $t > t_b$, is given by the sum of the fields resulting from the ramps, (equations 39 and 40):

$$U_H = U_{H(1)} + U_{H(2)} \tag{41}$$

$$U_H = \frac{4bN}{l_m}\left[ti^2\ \mathrm{erfc}\left(\frac{y}{2(kt)^{\frac{1}{2}}}\right) - (t-t_b)i^2\ \mathrm{erfc}\left(\frac{y}{2[k(t-t_b)]^{\frac{1}{2}}}\right)\right] \tag{42}$$

let $m = y^2(4kt)^{-1}$

and, $s = y^2[4k(t-t_b)]^{-1}$

Equation (42) may be rewritten:-

$$U_H = 4b\frac{N}{l_m}\left[ti^2\ \mathrm{erfc}(m^{\frac{1}{2}}) - (t-t_b)i^2\ \mathrm{erfc}(s^{\frac{1}{2}})\right] \tag{43}$$

Substituting equation (43) into equation (26)

$$U_J = \frac{-N}{l_m}\left[\frac{-2bt}{(\pi kt)^{\frac{1}{2}}}e^{-m} + \frac{bty}{kt}\ \mathrm{erfc}(m^{\frac{1}{2}}) - \frac{by(t-t_b)}{k(t-t_b)}\ \mathrm{erfc}(s^{\frac{1}{2}}) + \frac{2b\ (t-t_b)}{(\pi k(t-t_b))^{\frac{1}{2}}}e^{-s}\right] \quad \text{for } t > t_b \tag{44}$$

If a magnetic-circuit of constant effective relative permeability is considered, then the time-varying magnetic energy, $W_{m(t)}$, (in a section of unit area of the conductor) is given by equation (30):

$$W_{m(t)} = \frac{\mu}{2}\int_0^\infty U^2_H dy$$

From equation (41),

$$U_H^2 = U_H^2(1) + U_H^2(2) + 2U_{H(1)}\ U_{H(2)} \tag{45}$$

Substituting equations (39) and (40) into equation (45) and the resultant into equation (30) with reference to equation (36):-

$$W_{m(t)} = \frac{0.2064\ \mu b^2 N^2 k^{\frac{1}{2}}}{l_m^2}\left[t^{5/2} - (t-t_b)^{5/2}\right] + 2(\mu/2)\int_0^\infty U_{H(1)}\ U_{H(2)}\ dy \tag{46}$$

when, $t = t_b$; $U_{H(2)} = 0$, and hence, from equation (46):

$$W_{m(t)} = \frac{0.2064\ \mu b^2\ N^2\ k^{\frac{1}{2}}}{l_m^{\ 2}} (t_b^{\ 5/2}) \qquad (47)$$

At this elapsed time, t_b, the inner inductance is given by equation (38):

$$L_{I(t)} = \frac{0.413\ \mu^2\ N^2\ (kt_b)^{\frac{1}{2}}}{l_m^{\ 2}}$$

The presence of the cancellation ramp for $t>t_b$, complicates the analysis considerably, and makes the evaluation of the transient inner inductance extremely complex. Thus, for the purposes of this preliminary analysis, the assumption is made, for $t>>t_b$ that the trapezoid can be approximated to a simple step (figure 5.5). In addition, the effective relative permeability of the magnetic-circuit is considered constant, hence the transient inner inductance may be calculated.

From Carslaw and Jaeger[46], for a step surface excitation of current (I):

$$U_H = (N/l_m)\ I\ \mathrm{erfc}\left(\frac{y}{2}(kt)^{-\frac{1}{2}}\right) \qquad (48)$$

Substituting equation (48) into equation (26) gives:-

$$U_J = \frac{-NI}{l_m} (\pi kt)^{-\frac{1}{2}} \cdot e^{-m} \qquad (49)$$

Thus substituting equation (49) into equation (28) gives:-

$$U_E = \frac{-NI}{\sigma l_m} (\pi kt)^{-\frac{1}{2}} \cdot e^{-m} \qquad (50)$$

The time-varying magnetic energy (in a section of conductor of unit area) is given by equation (30).

$$W_{m(t)} = \left[\frac{\mu}{2}\right]\int_0^\infty U^2_H \, dy$$

Thus, substituting equation (48) into equation (30) gives:-

$$W_{m(t)} = \frac{\mu N^2 I^2}{2l_m^2} \int_0^\infty [\text{erfc}(\frac{y}{2(kt)^{\frac{1}{2}}})]^2 \, dy \qquad (51)$$

Now let $g = \frac{y}{2}(kt)^{-\frac{1}{2}} = m^{\frac{1}{2}}$

$$W_{m(t)} = \frac{\mu N^2 I^2 2(kt)^{\frac{1}{2}}}{2l_m^2} \int_0^\infty [\text{erfc}\ (g)]^2 \, dg \qquad (52)$$

The limits of integration are in practice from 0 to ∞. However, for $g>2$, $[\text{erfc}(g)]^2$ approaches zero rapidly. Thus, to aid numerical integration, the limits of the integral (equation 52) may be rewritten as from 0 to 2.

$$W_{m(t)} = \frac{\mu N^2 I^2 (kt)^{\frac{1}{2}}}{l_m^2} \int_0^2 [\text{erfc}(g)]^2 \, dg \qquad (53)$$

The term, $\int_0^2 [\text{erfc}(g)]^2 dg$, in equation (53) was evaluated using the Trapezoidal rule of integration. The interval of the integration was subdivided into 20 steps. This gave $\int_0^2 [\text{erfc}(g)]^2 dg = 0.331$.

$$\text{Hence,} \quad W_{m(t)} = \frac{\mu N^2 I^2 (kt)^{\frac{1}{2}}}{l_m^2} \times 0.331 \quad \text{for } t>>t_b \qquad (54)$$

Thus, substituting equation (54) into equation (32) the transient inner inductance may be derived.

$$L_{I(t)} = \frac{0.662 \mu (kt)^{\frac{1}{2}} N^2}{l_m^2} \qquad (55)$$

for t>>tb

Comparing equations (38) and (55), it can be seen that the magnitude of the transient inner inductance at a given time (for a system considered to be of a constant relative permeability), is dependent upon the waveshape of surface excitation.

The transient resistance, of the rib, of the conductor may be evaluated (section 5.3.2) from the following expression[45];

$$\frac{R_{tr}}{R_{dc}} = \frac{\text{watts}}{I^2 R_{dc}} = \frac{\int_0^1 (J_y'/J_s)^2 \, y' \, dy'}{[\int_0^1 (J_y'/J_s) y' \, dy']^2} \qquad (56)$$

where, $J_s = U_J$ at the surface, $y = 0$

and $J_y' = U_J$

For $0 < t < t_b$, J_s and J_y' are evaluated from equation (27), for a rising ramp.

For $t > t_b$, J_s and J_y' are evaluated from equation (44), for the sum of a rising and falling ramp displaced in time, of equal magnitude, but opposite gradients.

The DC resistance, R_{dc} (equation 56), is that referred to the rib only, and hence care must be taken that, over the time scale of interest, negligible current density penetrates into the main body of the conductor.

5.6 ANALYSIS OF INCREASED TRANSIENT RESISTANCE

5.6.1 Predicted Results

In order to assess the concept of increased transient resistance for inrush current control, preliminary mathematical studies have been carried out. An initial design parameter was

to achieve a transient resistance of 1 ohm per thyristor level after an elapsed time of 1μs, measured from the start of rise time. The waveform of excitation was considered to be a trapezoidal current pulse, (section 5.4).

For the interval of elapsed time $0 < t < t_b$ equation (27) was used to determine the transient distribution of the current density. Similarily, for $t > t_b$ equation (44) was used to calculate the transient distribution of the current density. In both cases equation (56) was then used to evaluate the transient resistance ratio. The predicted results of this mathematical assessment are shown in figures 5.6, 5.7, 5.8 and 5.9 together with Table 1.

Figure 5.6 shows a plot of the transient resistance ratio, R_{tr}/R_{dc}, versus dimensionless time[44][45] $[t/(\mu y_1^2\sigma)]$ for a ramp, surface excitation of current. Choosing the dimensionless time $[t/(\mu y_1^2\sigma)]$ as an axis on the graph ensures that, for a linear waveform of excitation (e.g. a ramp), only one curve is required to plot the variation of R_{tr}/R_{dc}, (for a range of values of resistivities and effective relative permeabilities).

The transient resistance ratio at a given dimensionless time is unaffected by the absolute gradient of the ramp, provided that the gradient of the applied ramp is assumed constant throughout an analysis. If the gradient is assumed to change during an analysis, e.g. a rising ramp is abruptly added to a 'cancellation ramp' (section 5.5.3), there is an abrupt

change in the transient resistance ratio, (figure 5.7). The difference between transient resistance and DC resistance is caused entirely by the difference in current distribution, (section 5.3.2). Thus, by levelling the ramp off, i.e. applying a cancellation ramp, a more uniform current distribution is obtained within the rib (figure 5.8) and hence a reduced transient resistance ratio is achieved (figure 5.7).

The current distribution, within the rib, at the instant of levelling-off of the ramp (t_b) affects the magnitude of the 'abrupt change' in the transient resistance ratio. If the rib of the conductor is considered to be part of a magnetic-circuit which has a high effective relative permeability then, transiently, the current density is confined near to the top surface of the rib, $y = 0$. Hence, if the elapsed time at which the trapezoid 'levels off' (t_b) is assumed to be constant and the effective relative permeability is assumed to be increased, then at this instant, the dimensionless time $[t_b/(\sigma\mu y_1^2)]$ is reduced. Hence, the non-uniform nature of the current distribution is exagerated by the increased effective relative permeability (figure 5.9). Thus, a plot of transient resistance ratio versus dimensionless time $[t/(\mu y_1^2\sigma)]$ for a non-linear waveform of excitation, does not result in identical curves for magnetic-circuits of different effective relative permeabilities, (figure 5.7).

5.6.2 Analysis of Results

The results of the preliminary studies have been interpreted to assess the dependence of the dimensions of the rib upon both the effective relative permeability of the magnetic-circuit and the conductivity of the rib. However, in order to analyse the results, several assumptions must be made:-

i) The length of the magnetic-path is approximately 0.3m.

ii) Length of air-gap is approximately 4mm, (to house the rib and insulation).

iii) Length of conductor, through the magnetic material, is about 0.2m per thyristor level.

a) Initially, copper was considered for the rib, ($\rho = 17.24 \times 10^{-9}$ ohm. metres): calculations were performed to assess the influence of different, constant, effective relative permeabilities of the magnetic-circuit, upon the 'width' of rib required. (Table 1).

The maximum required width of the rib increases in proportion to the square-root of the increase in effective relative permeability, (Table 1). Similarily, the depth of penetration of the current density, at a given elapsed time, decreases in proportion to the square-root of the increase in the effective relative permeability, (Table 1).

b) The relative permeability of the magnetic material, with no air-gap, is assumed to be infinite: the effective relative permeability of the magnetic-circuit is approximately

50, and assumed to be constant. The effective relative permeability is dependent, to a small degree, upon the flux distribution within the rib of the busbar; the flux distribution effects the length of the magnetic-path. The distribution of flux is itself dependent upon the eddy-currents which are opposing the penetration of the magnetic-field.

Assuming a constant effective relative permeability of say 50, the influence of the conductivity, upon the dimensions of the rib, may be assessed:-

i) If (R_{tr}/R_{dc}) is assumed to be 500 at an elapsed time (t) of 1μs, then from figure 5.7:

$$[t/(\sigma\mu y_1^2)] = 1.6 \times 10^{-6} \qquad (57)$$

Hence, if $\mu_e = 50$

$$\sigma y_1^2 = 9947$$

Thus, if the height of the rib (y_1) is assumed to be 1mm, then the conductivity of the conductor which gives a transient resistance ratio of 500, at t = 1μs, is equal to $9.947 \times 10^9 \text{mho.m}^{-1}$.

Therefore, the maximum desirable cross-sectional area to achieve a DC resistance of 2milli-ohms (i.e. R_{tr} = 1ohm) is $\underline{10 \times 10^{-9} \text{m}^2}$. Hence, the maximum allowable width of rib is $\underline{10\mu\text{m}}$ which is considered too 'thin' from the point of view of mechanical handling.

ii) Alternatively, assuming the width of the rib is 2mm and the height of the rib (y_1) 1mm (to aid mechanical handling), then the cross-sectional area of rib is $2 \times 10^{-6} m^2$. Thus, for a conductor in a semi-closed slot, for a length of 0.2m per thyristor level, the transient resistance ratio is:

$$R_{tr}/R_{dc} = 1 \times 10^{-5} \sigma R_{tr}$$

The required transient resistance (R_{tr}) is 1 ohm at an elpased time of 1μs, hence;

$$R_{tr}/R_{dc} = 1 \times 10^{-5} \sigma \qquad (58)$$

Similarily, the dimensionless time is given by

$$[t/(\sigma \mu y_1^2)] = \frac{15915}{\sigma} \qquad (59)$$

Therefore, extrapolating the curves of figure 5.7, the above two equations (58) and (59), are satisfied when $R_{tr}/R_{dc} = 20$, giving:-

$\sigma = 2 \times 10^6$ mho.m^{-1}, ($\rho = 0.5 \times 16^{-6}$ ohm.m)

To limit steady-state losses to an acceptable level the resistivity ($\rho = 0.5 \times 10^{-6}$ ohm.m) which results in a mechanically manageable width of rib, would result in an unacceptably large cross-sectional area and mass of conductor. A composite conductor, comprising a relatively high resistivity (low conductivity) rib and high conductivity main body, would

result in an acceptable level of steady-state losses. There would, however, be mechanical disadvantages associated with a composite conductor. These disadvantages include :

i) Ensuring that the 'joint' between the conductors is both electrically and mechanically sound. The joint must allow the efficient transfer of current density from the rib to the main body of the busbar. Excessive heat generation at the joint must be avoided in order to prevent unacceptable localised temperature excursions.

ii) The different materials, forming the rib and main-body, should have the same coefficient of thermal expansion in order to prevent mechanical stressing and consequent breaking of the joint.

iii) Mechanical construction of the composite busbar, with a controlled thickness and height of material for the rib, should be possible with suitable spraying techniques. However, the assembly of the magnetic material onto the busbar is likely to result in a high proportion of breakages, or 'chipping' of the rib.

iv) The required nature of the busbar, in a semi-closed slot, makes the mechanical handling and housing of the reactor more complex than the lossless saturating reactor presently employed, (Chapter 3.6).

5.7 CONCLUSION

The results of the preliminary analysis, performed to assess the feasibility of increasing the transient resistance of a busbar (excited by a magnetic-field), suggest that technically the proposed transient resistance of 1ohm at an elapsed time of 1μs (measured from the start of rise time) could be achieved. A method of achieving this transient resistance could be to place a ribbed conductor in a semi-closed slot which is surrounded by magnetic material of high relative permeability. To maximize the effective relative permeability of the magnetic-circuit, for a given magnetic material, the length of the air-gap must be minimized. However, the minimum length of the air-gap is constrained by the width of the rib together with that of insulating material; the minimum width of the rib of the busbar is fixed by mechanical handling and manufacturing considerations. Thus, an effective relative permeability of approximately 50 appears to be achievable in practice.

The calculated transient resistance ratios show that, in order to achieve the proposed resistance at an elapsed time of 1μs, the resistivity of the rib of the busbar should be approximately 30 times that of copper (when μ_e is assumed to be 50). Thus, in order that the cross-sectional area of the main body need not be increased greatly, to limit the magnitude

of the steady-state losses, it is necessary to consider a busbar constructed from two or more materials. The main current-carrying area of the busbar should be a high conductivity material such as copper, whilst the rib is a low conductivity material (resistivity of approximately 500 x 10^{-9} ohm.m).

There would be mechanical problems associated with the construction, handling and housing of such a reactor. These include ensuring that the coefficients of thermal expansion of the two conductors (the rib and main body) are similar, so that thermal cycling does not mechanically stress the joint between the conductors.

The maximum effective relative permeability of the magnetic-circuit, with a 4mm air-gap, is approximately 50. Thus, considering realistic dimensions for the magnetic material; l_g = 0.2m, A = 0.01m^2 and l_m = 0.3m, the incremental inductance would be approximately 2.1μH per level, for a single-turn reactor. This incremental inductance would result in an initial rate-of-rise of current, at thyristor valve turn-on, of about 2380A μs^{-1}, (5kV per level assumed). The initial maximum design limit of 200A μs^{-1} (see Chapter 6.3) is thus significantly exceeded, unless additional magnetic material were employed for di/dt control. The incremental inductance may be increased by decreasing the length of the air-gap. However, this would require a thinner rib, reduced thickness of insulation, and consequent mechanical handling problems.

Increasing the transient resistance of the busbar was therefore not taken any further: in its place a more mechanically 'robust' and simpler method of achieving transient resistive losses was sought, (Chapter 6).

6. CONTROL OF INRUSH CURRENT TRANSIENTS DURING COHERENT TURN-ON

6.1 INTRODUCTION

Chapter 3 described some of the major circuit transients which may occur within the electrical circuit of a converter station. This chapter reports the results of investigations into a means of controlling these transients using a mechanically simpler and more robust method than that described in Chapter 5. The investigations were carried out using the computer programme VTECAP; the modelling techniques utilized to represent the converter transformer and most non-linear elements are described in Chapter 4.

The reasons for investigating alternative means to those currently utilized for controlling transients are both technical and economic. It is advantageous, if possible, to provide the thyristor with a safer working environment at a reduced cost. The main aim of this chapter is to investigate the replacement, by a single passive component, of the inrush control components associated with the Sellindge converter station. The existing circuit design of the Sellindge converter station was used as a basis for proposing modifications for future converter stations.

The method investigated in this chapter for controlling transients within all future thyristor valves, involves the utilization of a two-part saturating reactor. One-part of the reactor is 'lossless', and the other part has controlled eddy-current losses.

Ideal reactor characteristics are derived for controlling worst-case repetitive inrush*, such that a minimum of magnetic material is required to achieve the control of inrush transients. [The reactor characteristics derived are those pertaining too a valves' worth of inductance (100 levels per valve assumed)].

The hardware cost and evaluated losses, associated with magnetic materials having the proposed characteristics, are compared with the cost of hardware and evaluated losses of the inrush control components utilized in the Sellindge converter station.

Using the proposed saturating reactor characteristics, together with a refined transformer model (Chapter 4.5.3),a study is performed for worst-case repetitive conditions to confirm that the predicted inrush current and rate of valve-voltage collapse are acceptable.

In addition, inrush studies utilizing a single-section representation of the transformer and a mathematical model of the proposed saturating reactor characteristics are performed to ensure that the predictions for normal repetitive turn-on ($\alpha = 90°$ + DOV, $\alpha = 90°$, $\alpha = 12°$ and $\gamma = 15°$), are acceptable.

---

* Worst-case repetitive inrush is assumed to arise from firing the valve from a voltage given by the highest voltage for which BOD firing will just occur.

6.2 PROPOSED INRUSH CONTROL STRATEGY

The inrush control components associated with the Sellindge converter station provide a safe working environment for the thyristors. However, it is necessary to adopt alternative means of inrush control in order to enhance the level of safety associated with the operating environment, whilst also reducing the total hardware and capitalized costs associated with inrush control (Chapter 3.6).

The Sellindge converter station contains several different components for the control of both inrush current and dV/dt across off-state thyristors (see figure 3.18) namely:-

a) AC connection reactor together with a parallel connected resistor.

b) DC connection reactor together with a parallel connected resistor.

c) Valve capacitor

d) Six-turn-spiral (L1b) together with bypass diode and resistor, (per thyristor level).

e) Ferrite cored saturating reactor (L1a) (per thyristor level).

The main aim of the studies reported in this chapter were to investigate the replacement, for all future schemes, of the above mentioned inrush and dV/dt control components by a single passive item.

Saturating reactors [which for the Sellindge converter station is item (e) above] are considered to be essential components of an HVDC scheme in controlling the inrush current to within safe limits, for the following reasons:-

i) Inductance is required to limit the magnitude of the step current into a thyristor, (Chapter 3.2.2).

ii) Inductance is required to limit the di/dt during turn-on, (Chapter 3.2.2).

iii) Inductance is required to limit the dV/dt and magnitude of voltage across an off-state thyristor, (Chapters 3.3.2 and 8.5).

iv) It is necessary to retain inductance <u>within</u> the valve in order to protect the thyristors, at turn-on, from the effects of stray capacitances immediately shunting the valve, (Chapter 3.5).

v) It is uneconomical to utilize linear inductance within the valve as this adversely effects the size of the valve and the reactive power requirements of the converter station, (Chapter 2.4.5).

As the saturating reactor is an essential component it must be retained. It is however, necessary to re-design the magnetic characteristics of the saturating reactor such that it limits the above effects (i to iii) and in addition the following:-

a) Magnitude of first peak of inrush current, (Chapter 3.2.2).

b) Magnitude of first trough of inrush current, (Chapter 3.2.2).

c) Rate of collapse of valve-voltage at turn-on, (section 6.4.10 and 6.4.12).

An initial consideration of the conflicting technical and economic requirements indicates that a 'two-part' saturating reactor is required:-

i) Lossy-portion of the reactor (L1)

It is desirable to introduce some resistive losses to damp the inrush current oscillation, (Chapter 3.5). This may be achieved by means of eddy-current losses within a magnetic material.

Insufficient resistive dissipation, during inrush, will result in a low degree of damping and hence a current trough of low magnitude, (Chapter 3.2.2). The consequent valve-voltage oscillations may also be underdamped (section 6.4.10), and could result in radio-interference problems.

Thus, relying upon eddy-currents within a portion of the saturating reactor, to damp the inrush oscillation, removes the requirement for the following inrush control components utilized in the Sellindge converter station (see figure 3.18);

a) Parallel connected resistor associated with each AC connection reactor.

b) Parallel connected resistor associated with each DC connection reactor.

c) Bypass diode and resistor connected in parallel with each six-turn spiral.

In addition, the lossy-portion of the reactor (L1) provides a delay in the growth of the inrush current. Thus, L1 also replaces a proportion of the linear and saturating inductance, required for the Sellindge converter station to limit the inrush current to within safe-limits.

During the interval of time associated with load current commutation (figure 6.1), no damping-function is required of the saturating reactor. Thus, any eddy-current losses which occur during this interval are unnecessary and contribute towards increased capitalized losses at adjudication. In addition, an increase in the rating of cooling plant may be necessary to cope with these losses. Hence, it is desirable that any eddy-current losses are minimised during load current commutation, without unduly effecting the damping of the inrush current transients.

ii) Lossless-portion of the reactor (L2)

The lossy-portion of the reactor (L1) has associated with it a significant loss component of current (section 6.4.4). Thus, if this current is unrestrained it will be superimposed upon the step discharge of current from the damping circuit (Chapter 3.2.2), which may overstress the thyristors (Chapters 3.2.2 and 3.5) even during normal repetitive duty.

In addition, a reactor with a significant loss component of current (section 6.4.4), has a limited effect in controlling a rate-of-rise of voltage across an off-state thyristor. Thus, it is desirable to incorporate a portion of lossless inductance (L2) in the design of the saturating reactor.

If achievable inductance L2 removes the requirement, in future schemes, for the following inrush limiting components of the Sellindge converter station (see figure 3.18);

a) AC connection reactors;

b) DC connection reactors;

c) Ferrite-reactor;

d) Quasi-linear reactor, (six-turn spiral).

The valve capacitor, together with an AC connection reactor, acts to control the rate-of-rise of voltage across an off-state thyristor valve, provided that the impulse emanates from the converter transformer side of the connection reactor (Chapter 3.6). Thus, the valve capacitor would also be redundant as all the inductance for future schemes is assumed to be housed within the valve.

iii) Complete saturating reactor

It appears from the above considerations that the two-part saturating reactor would fulfil the, often conflicting, technical requirements. One part of the

reactor is considered to be lossless (L2) whilst the other part (L1) is considered to have controlled eddy-current losses.

Each part of this saturating reactor must be designed so that its characteristics control circuit-transients to within the specified design limits, (section 6.3). This should be achieved for a minimum overall cost.

The overall cost is assumed to be minimized by:-

a) Minimizing the eddy-current losses during load current commutation (figure 6.1) without unduly degrading the damping of the inrush current oscillation, (Chapter 3.5).

b) Minimizing the total volume of magnetic materials employed. This is achieved by specifying 'optimum' inductance with current characteristics for the magnetic materials.

6.3 INITIAL DESIGN LIMITS FOR TRANSIENTS

The design of the saturating reactor must be such as to keep the inrush current within 'safe limits' for the next-generation thyristors; these are based upon the limits (derived by test) for 56mm, DCR 1278 thyristors, utilized within the Sellindge converter station. As the next-generation thyristors (75mm) were still being constructed at this stage, whilst the 100mm thyristors were still at the design stage,

the calculated volume of magnetic material (section 6.4.9), for a given scheme, may be revised when the actual design-limits are known.

The assumed limits, for turn-on under worst-case repetitive conditions, are:

a) Initial 'step' current ($\hat{I}_{RD}$) into thyristor to be less than 200A. This 'step' current (see figure 3.5) is the sum of the damping circuit discharge current and a loss component of current associated with the saturating reactor.

b) Maximum rate-of-rise of current (di_m/dt) to first current peak to be less than 200A μs^{-1}.

c) First current peak ($i_{1(pk)}$) to be less than 1000A (see figure 3.5).

d) First current trough ($i_{1(tr)}$) to be greater than 200A (see figure 3.5).

e) A dV/dt greater than 1kV μs^{-1} across an off-state thyristor level, will result in protective turn-on action of that level*.

f) No assumptions were made regarding the delay time that may be necessary for the current to transfer from the auxiliary cathode to the main current carrying area.

---

* A 'maximum' dV/dt across a thyristor or thyristor level, quoted as a result of one of the studies reported in this thesis, neglects voltage sharing errors and redundancy and assumes distributed inductance.

The actual capabilities of next generation thyristors were yet to be determined at this stage, but the above assumed capabilities were believed to be realistic. Subsequent evaluation of representative 75mm thyristors has shown that a maximum repetitive rate-of-rise of current (di_m/dt), (see (b) above), of 600A μs^{-1} to first current peak produces a situation which is marginal from the point of view of the integrity of the thyristor.[49][50]

6.4 SENSITIVITY OF THE INRUSH CURRENT TO THE CHARACTERISTICS OF THE SATURATING REACTOR

6.4.1 Introduction

As shown in Appendix IV.2, the characteristics of the saturating reactors are presumed to be capable of being modelled as shown in figure 6.2, throughout every future study reported in this thesis. The general form of the incremental inductance with inductive current characteristic, for each part of the saturating reactor (section 6.2), is as shown in figure 6.3. Each of the two parts (L1 and L2) composing a saturating reactor have initial incremental inductances considered to be constant, (i.e., constant rate of change of flux density with magnetic-field strength). The value of the incremental inductance is then considered to decrease at a constant rate as the current increases, (figure 6.3).

6.4.2 Proposed Studies

The studies undertaken[51] examined the sensitivity of the inrush current predictions, and the volume of magnetic material required, to variations in the following :

1) The initial relative values of the incremental inductances for each part of the reactor (L1 and L2), respectively.

2) The magnitude of the reflected resistance (R_e) representing eddy-current losses within part L1.

3) The magnitude of the negative rate of change of incremental inductance with current for part L1.

4) The magnitude of current up to which the incremental inductance is considered constant for part L1.

5) The magnitude of current up to which the incremental inductance is considered constant for part L2.

6) The magnitude of the negative rate of change of incremental inductance with current for part L2.

7) The accuracy of the converter transformer representation, (see chapter 4.5.3).

Figure 6.4 shows the simplified equivalent circuit of a converter station, utilized for the coherent turn-on studies; where applicable, the studies within this thesis assume the equivalent circuit to be cf a 50Hz scheme.

6.4.3 Relative Value of the Inductance of part L1 to part L2

The ratio of 'lossy' saturating inductance to 'lossless' saturating inductance effects the degree of damping of the inrush current, (section 6.4.10). The magnitude of the first current trough increases as the ratio of damped inductance increases. However, this is achieved at the expense of the total eddy-current losses.

To assess the sensitivity of the inrush current to the ratio of 'lossy' saturating inductance to 'lossless' saturating inductance, several studies were performed where the sum of the initial incremental inductances were 5 mH, (figure 6.5). The modelled ratio of an inductance value of part L1 to a corresponding inductance value of part L2 is maintained constant over the complete range of inductive current. The magnitude of the incremental inductances were considered to be constant up to a current of 150A, decreasing at a linear rate from this current, such as to completely saturate both parts of the reactor at a current of 2320A. The constant value of the reflected parallel resistance (see Appendix IV), is in each study chosen to maximize the first current trough.

The sensitivity of both the magnitude of the maximum rate-of-rise of current to first current peak and the magnitude of the first current trough are shown in figure 6.6. As the ratio of an inductance value of part L1 to a corresponding value of part L2 is increased the first current trough increases in magnitude. However, the maximum rate-of-rise of current to first current peak also increases. This increased di/dt would have the undesirable effect of increasing the current density within the silicon slice (Chapter 3.3).

Figure 6.7 shows that the magnitude of the first current peak is virtually independent of the ratio of an inductance value of part L1 to a corresponding value of part L2. However, for each additional percentage point of lossy inductance the eddy-current losses increase at the approximate rate of 310W per valve, during worst-case repetitive turn-on.

A ratio, of an inductance value of part L1 to the corresponding value of part L2, of unity results in a rate-of-rise of current to first current peak of 144A μs^{-1} (less than the 200A μs^{-1} limit), and a first current trough of 196A. The first current trough is marginally below the initial design limit of 200A. However, as it is only marginal, an initial ratio of inductance values of unity is to be used as the basis for further studies.

6.4.4 Optimization of the value of the reflected parallel resistance

The magnetic material characteristics shown in figure 6.8 were represented for these studies. The singular value of the reflected parallel resistance is changed between studies in order to find an optimum value. The value of the resistance which maximizes the magnitude of the first current trough (figure 6.9) is approximately 440Ωper valve. Further increasing the value of this resistance results in a negligible improvement in the magnitude of the trough.

The first current peak reduces in magnitude at the rate of about 20A per 100Ω increase in the value of the parallel resistance, over the range of values studied, (Figures 6.9). Similarly the maximum di/dt to first current peak decreases in magnitude at the rate of approximately 1.2A μs^{-1} per 100Ω increase in the value of the parallel resistance, over the range studied.

6.4.5 Magnitude of the Incremental Inductance with current Characteristic for the Lossy Reactor (Part L1)

The reactor characteristics used for this set of studies are shown in figure 6.10. Increasing the rate of decrease of the inductance with current for reactor L1 reduces the flux swing required, hence, the total eddy-current losses within reactor L1 are reduced (see Appendix IV, equation 27). However, as the initial incremental inductance is assumed to be unaltered, the eddy-current losses are unchanged during this initial interval.

The results of the studies indicate that neither the maximum rate-of-rise of current to first current peak nor the magnitude of first current peak are altered by a change in the rate of decrease of incremental inductance, over the range studied. However, as the saturation flux of reactor L1 is reduced, so the eddy-current losses and damping are decreased (figure 6.11). Hence, the effect upon the first current trough is to reduce it in magnitude (figure 6.11).

In order to minimize the total eddy-current losses, and the saturation flux requirement it is advantageous to saturate reactor L1 at as low a current as feasible. However, the inrush performance must not be unduly degraded. A rate of change of incremental inductance of $-5.0\mu H\ A^{-1}$, from a current of 150A, appears to result in acceptable damping of the inrush current (first current trough of approximately 184A compared with the 200A initially set as a lower-limit), without incurring unnecessary eddy-current losses, (figure 6.11).

The collapse of the valve-voltage across the commutating valve causes a corresponding rise in voltage across a series connected off-state valve. The consequent 'maximum' rate-of-rise of voltage across each level of the series valve, and each thyristor within that valve, is $520V\ \mu s^{-1}$ and $474V\ \mu s^{-1}$ respectively. These rates-of-rise are not influenced, over the range studied, by the rate of decrease of the incremental inductance with current characteristic of part L1.

6.4.6 Interval of Constant Incremental Inductance for Part L1

Both the saturation flux requirement and the total eddy-current losses may be reduced by decreasing the interval of constant incremental inductance of reactor L1 (figure 6.12). However, a reduction in the interval of constant incremental inductance increases both the maximum rate-of-rise of current to first current peak (figure 6.13), and the magnitude of the first current peak (figure 6.14).

If the incremental inductance is kept constant for a current greater than 75A, little reduction is obtained in either the maximum rate-of-rise of current to first current peak (figure 6.13) or in the magnitude of the first-current peak (figure 6.14).

Decreasing the interval of constant inductance, from 150A, results in a reduction in the magnitude of the first current trough together with an increase in the maximum rate-of-rise of current to second current peak, (see figures 6.14 and 6.13 respectively).

An interval of constant incremental inductance of approximately 75A, as opposed to 150A, results in acceptable inrush predictions whilst limiting the magnitude of the eddy-current losses. There is a consequent reduction in the saturation flux requirement by 0.187Wb per valve.

6.4.7 Interval of Constant Incremental Inductance for the Lossless Reactor (Part L2)

Figure 6.15 shows the saturating reactor characteristics modelled for this set of studies. By decreasing the interval of constant incremental inductance for reactor L2, the total saturation flux requirement is reduced. There is, therefore, a consequent saving in the volume of the magnetic material required, (for a given saturation flux density).

The effect upon the inrush transient of completely removing the interval of constant incremental inductance is negligible[51]; the rate-of-rise of current to first current peak is increased from 141A μs^{-1} by 2A μs^{-1}, (1.4%). Similarly, the first current peak is increased in magnitude by 11A from 649A (1.7%), (figure 6.16). There is a corresponding decrease in the magnitude of the first current trough from 194A to 192A. This is accompanied by an increase in eddy-current losses of 3.7% (figure 6.16), up to an elapsed time of 45μs, during worst-case repetitive turn-on.

Complete removal of the interval of constant incremental inductance from the characteristic of reactor L2, results in a consequent reduction in the saturation flux requirement of 0.375Wb per valve. In addition, the increase in the severity of the inrush current is negligible.

6.4.8 Magnitude of the Incremental Inductance with current Characteristic for Part L2

The reactor characteristics modelled for this set of studies are shown in figure 6.17. As the rate of decrease of the incremental inductance with current of reactor L2 is increased, the total saturation flux requirement is reduced. Thus, for a given saturation flux density, the volume of magnetic material required is reduced.

The results of the studies indicate that as the rate of change of the incremental inductance, is increased from $-1.15\mu H\ A^{-1}$ to $-5\mu H\ A^{-1}$ there is a corresponding increase in the magnitude of the first current peak from 660A to 886A, (figure 6.18). In addition, because the ratio of the saturation flux of part L1 to the saturation flux of part L2 is increased, the first-current trough increases in magnitude (figure 6.18).

Similarly, as the rate of change of the slope inductance is increased from about $-1.15\mu H\ A^{-1}$ to $-3.75\mu H\ A^{-1}$ the maximum rate-of-rise of current to first current peak increases from $142A\ \mu s^{-1}$ to $165A\ \mu s^{-1}$. A further increase in the rate of change of the slope inductance with current results in an abrupt increase in the maximum rate-of-rise of current to first peak. This di/dt, together with its time of occurrence, are shown in figure 6.19.

As the rate of change of incremental inductance with current increases, the eddy-current losses increase at the rate of approximately 29.6J H^{-1} A^{-1} per valve (figure 6.19). For a 50Hz application, this represents an increase in dissipation of about 1500W per valve, per Henry per Amp increase in gradient, (calculated for worst-case repetitive inrush).

As the rate of change of inductance increases, the saturation flux required for part L2 decreases, thus;

Rate of decrease of inductance with current, per valve, for part L2 ($\mu H\ A^{-1}$)	Saturation flux required per valve, for part L2 (Wb)
1	3.125
2	1.562
3	1.042
4	0.781
5	0.625

This information is presented graphically in figure 6.20.

There is an optimum relationship between capitalized losses, performance, and the minimum acceptable quantity of magnetic material. However, in order to minimize the size of the valve, the valve hall, the weight of the valve and the valve hall foundations, it is desirable to use the minimum quantity of magnetic material determined by performance criteria. Hence,

with reference to figures 6.18 and 6.19, the following studies utilize a rate of change of inductance with current of 3.8μH A^{-1} for reactor L2.

6.4.9 Proposed Reactor Characteristics for Inrush Control

In the preceding sections, the following recommendations have been made for the saturating reactor characteristics (see figures 6.21):

Lossy reactor, L1;

a) Constant interval of incremental inductance of 2.5mH, per valve, (section 6.4.3) up to 75A (section 6.4.6);
b) Thereafter, rate of decrease of the incremental inductance is -5μH A^{-1} (section 6.4.5);
c) Effective reflected parallel resistance of approximately 443 ohms per valve (section 6.4.4).

Lossless reactor, L2;

a) No interval of constant incremental inductance (section 6.4.7);
b) 'Slope' of the incremental inductance is -3.8μH A^{-1} (section 6.4.8), from 2.5mH per valve (section 6.4.3).

Within this section all the above proposed characteristics (figure 6.21) are modelled to ensure that the resulting inrush prediction, for worst-case repetitive turn-on, is acceptable.

Figure 6.22 shows the predicted inrush current when these reactor characteristics are represented. The maximum di/dt, up to first current peak (166A μs^{-1}), and the magnitude of first current peak (826A) are both within the initial maximum design limits of 200A μs^{-1} and 1000A, respectively. The first current trough (163A) is below the initial minimum design limit of 200A, but this was felt to be acceptable as the predicted first current trough is known to increase in magnitude (section 6.4.11), as the representation of the transformer is refined (Chapter 4.5.3).

The mathematical model of the six-pulse bridge included non-linear elements within the valve connected electrically in series with the commutating valve (figure 6.4). The voltage across the series connected valve and the voltage across the thyristors within that valve, together with the voltage across the commutating valve, is shown in figure 6.23.

The 'maximum' rate-of-rise of voltage across a level of the series valve is 791V μs^{-1}, (662V μs^{-1} per level for the Sellindge converter station). The corresponding 'maximum' rate-of-rise of voltage across a thyristor within the series valve is 684V μs^{-1}, (1070V μs^{-1} per level for the Sellindge converter station).

The eddy-current losses up to first current peak and up to an elapsed time of 45μs after valve turn-on, as a proportion of the 626 Joules of energy initially stored in the stray capacitances of the phases involved in the commutation are 29.9% and 57.8% respectively. The approximate saturation fluxes for parts L1 and L2 are 0.812Wb and 0.822Wb respectively. Thus the total saturation flux requirement for the valve saturating reactors is about 1.635Wb

The ideal flux with current curves for these particular reactor characteristics (figure 6.21) derived under pulse conditions, are shown in figures 6.24 and 6.25. Figure 6.24 shows the flux-current curve for reactor L2 when a 4kV step, per level, is applied across 100 levels of part L2. This is identical to the DC flux-current curve for a truly lossless reactor.

Figure 6.25 shows the flux-current curve when a 4kV step, per level, is applied across 100 levels of part L1. There is a 'let-through' current (loss component of current), of about 903A attributable to the eddy-current losses.

6.4.10 Removal of part L1

Part L1 of the reactor is included to damp oscillations, but will lead to unwanted losses during load current commutation (section 6.5). Part L1 requires approximately 50% of the total flux for the proposed saturating reactor design (section 6.4.9).

Thus, to demonstrate the necessity of part L1, a study was performed with the lossy reactor (L1) removed and only the lossless portion of the proposed reactor (section 6.4.9) was represented.

The effect upon the inrush prediction of removing part L1, is apparent when figures 6.22 and 6.26 are compared. The initial rate-of-rise of current is approximately 160A μs^{-1}. However, at an elapsed time of about 2.5μs after valve turn-on, reactor L2 saturates and the di/dt increases to about 1650A μs^{-1} (166A μs^{-1} with part L1 present) up to a first current peak of about 2360A (826A with part L1 present). This may not necessarily threaten the integrity of the thyristors.

As the main-circuit current oscillation is only lightly damped (by the damping circuits of off-state valves), the main-circuit current in the commutating valve passes through zero, and goes negative. The predicted magnitude of an 'unrestrained' negative current oscillation would be -232A. However, the thyristor may start to recover during this period of negative current, and this is unacceptable.

Comparing figures 6.23 and 6.27, the effect upon the valve-voltage of removing reactor L1 is apparent. The 'maximum' rate-of-rise of voltage across each level of a series connected valve and each thyristor within that valve are 2635V μs^{-1} and 2248V μs^{-1} respectively, (791V μs^{-1} and 684V μs^{-1} respectively,

are predicted when reactor L1 is included in the mathematical model). These rates-of-rise of voltage are likely to lead to protective firing of the series valve (1kV μs^{-1} per level assumed for the setting of the dV/dt protection). The lightly damped nature of the valve-voltage oscillation (figure 6.27), could result in radio interference problems too.

Although removal of reactor L1 allows a halving of the flux required, and also a reduction in the losses during normal load current commutation, the resultant duty on the thyristors is much more severe than initially assumed to be safe. It is possible that future work may show that these predictions are acceptable; however, for the present part L1 will continue to be considered to be an essential feature of the saturating reactor design.

6.4.11 Refined Transformer Representation

The single-section representation of the transformer used for the previous studies was subdivided into five sections per phase and together with end effects included in the mathematical model (Chapter 4.5.3). The proposed reactor characteristics were represented (figure 6.21) together with a constant value of reflected parallel resistance for L1 of 443Ω per valve, (section 6.4.4). The consequent inrush current prediction is shown in figure 6.28, together with the inrush current predicted with the single-section transformer model.

The frequency of the inrush current oscillation increases as a result of the refined transformer representation. The maximum rate-of-rise of current up to first current peak has decreased from 166A μs^{-1} to 151A μs^{-1}, (9% decrease). However, the initial rate-of-rise of current is unchanged at 151A μs^{-1}.

The first current peak is reduced, substantially, in magnitude from 826A to 697A, (15.6% decrease). Similarly the first current trough has increased in magnitude from 163A to 325A, (99.4% increase); however, there is a second current trough of 250A in magnitude. This second current trough occurs 16 microseconds later in time than the first trough; hence, the main-circuit current will have increased in magnitude, reducing the thyristors dependency upon the magnitude of the damping circuit pre-charge to provide a current during the trough.

The refined transformer representation results in a less onerous inrush current prediction than the single-section representation and, thus, in the possibility of reducing further the total volume of magnetic material specified for a valve (see Table 2). This would correspond to a reduction in the predicted saturation flux requirement of 10% and thus a consequent decrease in the calculated volume of magnetic material. However, it is not considered worthwhile, at this stage, to refine any further the proposed saturating reactor characteristics based on the results of this set of studies alone. There are several 'proving studies' to be performed (Chapters 7 and 8), to show

the adequacy of the proposed reactor characteristics, during other operating conditions.

The total energy initially stored within the stray capacitances of the 3-phase system model is 683.8 Joules, prior to valve turn-on. Twenty-two percent of this energy is dissipated in the reflected parallel resistance (representing eddy-current losses) of part L1 by first current peak. The energy dissipated by the end of the study (elapsed time of 45 μs after valve turn-on) is approximately 36.5% of the total, initially stored energy.

6.4.12 Valve-Voltage Collapse

The design of the saturating reactor influences the rate of valve-voltage collapse at valve turn-on (section 6.4.10). This voltage collapse is capacitively coupled to other valves in the bridge, and may effect their performance, (Chapter 8.4). The valve-voltage collapse also effects the level of radio interference generated by the converter, (section 6.4.10).

However, the result of refining the transformer model is to increase the maximum predicted rate-of-rise of voltage across the series connected valve and thyristors within that valve. The 'maximum' predicted rate-of-rise of voltage across a level in the series valve is increased from 791V μs^{-1} to 838V μs^{-1}, (5.94% increase). Similarly the 'maximum' rate-of-rise of voltage predicted across a thyristor in the series valve increases from 684V μs^{-1} to 714V μs^{-1}, (4.38% increase).

Figure 6.29 shows the predicted valve-voltage collapse for a valve in the Sellindge converter station. Superimposed on this figure is the predicted valve-voltage collapse when the inrush-control hardware is replaced by saturating reactors with the proposed characteristics (figure 6.21). The rate of valve-voltage collapse is similar to that predicted for a Sellindge converter station valve, and thus the level of radio interference would be expected to be of a comparable magnitude.

6.4.13 Normal Continuous Operation

All the foregoing studies have been performed for the 'worst-case' repetitive duty, a duty which in practice is limited to a few seconds duration at the most.

Thus, turn-on studies have also been carried out for normal continuous operation, using the proposed reactor characteristics of figure 6.21. These studies utilized a single-section transformer representation.

The mathematical model of the converter circuit was identical to that used for the worst-case repetitive studies (figure 6.4), except for the initial circuit precharges and driving e.m.f.'s.

The initial circuit pre-charges were calculated from the following assumptions:-

1) For a scheme with a sum of BOD protective levels of 400kV, the switching-impulse test level (co-ordinating current level) is anticipated to be 20% above this figure, i.e. 480kV. (The reverse voltage capability of the thyristors is expected to be about 20% above their forward voltage capability).

2) Insulation co-ordination level is 1.7 p.u. (see Chapter 8.2)

3) Dynamic overvoltage is assumed to be 1.3 p.u. (see Chapter 7.2)

4) Normal rectifier operation is given by $\alpha = 12°$ (see Chapter 2.4.6)

5) Normal inverter operation is given by $\gamma = 15°$ (see Chapter 2.4.6), and hence from the equations of Appendix I,

   $U_o = 20.5°$

   a) Peak line-to-line voltage ($2^{\frac{1}{2}}V_c$), [$\alpha = 90°$ operation] is given by:

      $2^{\frac{1}{2}}V_c = (480/(1.15 \times 1.7))\times10^3 = \underline{245.5kV}$ peak

   b) $\alpha = 90° + DOV \Rightarrow \underline{319.1kV}$

   c) $\alpha = 12° \Rightarrow 51.04kV$

   d) $\gamma = 15°$, $U_o = 20.5°$, $\beta = 35.5° \Rightarrow \underline{142.5kV}$

The results of the above studies are given in Table 3.

In all these studies, the initial di/dt at valve turn-on is equal to the maximum di/dt upto first current peak. These studies modelled non-linear elements in the valve connected in series with the commutating valve (figure 6.4). The 'maximum' predicted dV/dt across a level, and across a thyristor within

the series valve are shown in Table 3. The energy dissipated ($E_{(45)}$) in the 'parallel reflected resistance' of part L1, up to an elapsed time of 45μs after valve turn-on is also given.

Inrush predictions for cases (a) to (d) above are shown in figure sheets 6.30 through to 6.33. The predictions do not reveal any features of the inrush current which would give rise to concern for the integrity of the thyristors.

6.5 ESTIMATED COST OF PROPOSED INRUSH CONTROL

The cost of inrush control may be estimated from the total cost of the necessary hardware together with a relevant loss-evaluation figure, (Chapter 3.6):

i) Hardware

The initial, worst-case repetitive, coherent turn-on studies indicate a saturation flux requirement of approximately 1.6Wb per valve, (section 6.4.11). Magnetic materials with saturation flux densities of above 1.5T are available, (e.g. Cobalt/Iron amorphous alloy has a saturation flux density of 2.3T). However, as many of these materials are not produced in large volumes they are relatively expensive e.g., £40 per kg for the Cobalt/Iron amorphous alloy[51]. It is assumed, in the following estimate, that a magnetic material with a 1.5T saturation flux density will be used to provide inrush control. However, an allowance of 0.3T is made for remanent flux density. Thus, the usable, unipolar, flux density swing available for use is 1.2T.

The magnetic material is to be driven into saturation, i.e., the whole cross-sectional area is to be utilized. Hence, the calculation of the volume of magnetic-material, required per valve, is based upon the actual cross-sectional area, as opposed to its effective cross-sectional area as defined by IEC 205.

Thus, the cross-sectional area (A) is given by:-

$$A = (1.6/1.2)m^2 = 1.333m^2 \text{ per valve}$$

Allowing for an 85% space-factor, the actual cross-sectional area required is $1.568m^2$. The volume and length of magnetic material are dependent upon the inner radius and outer radius of the toroid of magnetic material, (see Appendix V). Hence, basing the initial reactor design upon toroidal rings of similar dimensions to those used for a ferrite reactor in the Sellindge converter station;

$$r_1 = 21mm$$

$$r_2 = 63mm$$

The total length of magnetic material, l_g, per valve is given by:-

$$l_g = 1.568/(63 \times 10^{-3} - 21 \times 10^{-3})$$

Therefore, $l_g = 37.3m$ per valve

Thus, the total volume of magnetic material required, per valve, is $0.414m^3$. Hence, if the magnetic material is assumed to have a density of 7.1g per cc^3 and a finished cost of £6 per kg[51], then the total weight of magnetic material, per valve, is approximately 2940kg. The cost of this quantity of material is approximately £17,640 (based on £6 per kg). For comparison with the cost of inrush control hardware for the Sellindge converter station (Chapter 3.6), the inrush control hardware cost should

include a figure for any assembly procedures and testing of the component. Thus, allowing a further £100 per level for assembly and testing of the reactor, the estimated hardware cost for the proposed reactor is approximately £277 per level (£27,700 per valve).

The inrush control for the Sellindge converter station utilizes approximately 0.54m^3 of ferrite, per valve, and a total length of 48.7m per valve. This inrush control was achieved for a hardware cost of £522.73 per level, (£65341 per valve) at January 1984 prices, (Chapter 3.6). Thus, the estimated saving in hardware costs, in comparison with the Sellindge converter station, is approximately £37,640 per valve.

ii) Evaluated Losses

The evaluated losses for the proposed two-part reactor (figure 6.21) are calculated for worst-case repetitive operation. This is also the operating condition for which the losses, associated with the inrush control hardware, were evaluated for a valve of the Sellindge converter station in chapter 3.6.

Basing the estimate of the losses, over the interval associated with load current commutation, upon a constant rate of change of current, given by the valve overvoltage protective level divided by the commutating inductance;

$$\frac{di}{dt} = \frac{4 \times 10^5}{59.69 \times 10^{-3}} = 6.7A\ \mu s^{-1}$$

Part L1 is considered to be 2.5mH, per valve, upto a current of 75A and completely saturated at 575A (figure 6.21). The induced e.m.f. in reactor L1, upto an inductive current of 75A, is assumed to be given by the product of the di/dt and instantaneous inductance which gives 16750V per valve. This results in a loss component of current of 37.8A, attributable to the eddy-current losses (assuming a constant value of reflected resistance of 443Ω per valve).

Similarly, when part L1 is saturated, there is assumed to be no induced e.m.f. in this part of the reactor; thus, there would be no eddy-current losses either.

The rms current (I_{rms}) through the parallel reflected resistance (of the representation of reactor L1), during commutation of load current, is given by[52]:-

$$I_{rms} = 3^{-\frac{1}{2}} \left(i_r^2(0) + i_r^2(1) + i_{r(0)}\, i_{r(1)}\right)^{\frac{1}{2}} \qquad (1)$$

Where $i_{r(0)}$ and $i_{r(1)}$ are the loss components of current at the start and end of the interval of interest, respectively.

If $i_{r(0)} = 37.8A$ and $i_{r(1)} = 0A$ then $I_{rms} = 21.8A$

The approximate period of time (Δt) taken for the commutation of load current from 75A to 575A is given by:-

$$\Delta I / \frac{\Delta I}{\Delta t} = \left(\frac{575-75}{6.7}\right) \mu s = 74.63 \mu s \qquad (2)$$

Hence, the energy dissipated over this interval is given by:-

$$I^2_{rms} \times R_e \times \Delta t \qquad (3)$$

$$= \underline{15.7J \text{ per valve}}$$

Similarly, the energy dissipated during the first 75A of the characteristic of part L1 is also given by equation (3) :-

$$\left(\frac{2.5 \times 10^{-3} \times 6.7 \times 10^{6}}{443} \right)^2 \times \left(\frac{75}{6.7 \times 10^{6}} \right) \times 443$$

$$= \underline{7.1J \text{ per valve}}$$

Hence, the total dissipation resulting from a commutation is 22.8J per valve. The total estimated energy dissipation, resulting from eddy-current losses, for part L1 is given by:-

Inrush transient (computer prediction)	= 363J (t = 45μs)
Commutation in	= 22.8J
Commutation out	= 22.8J
TOTAL	= 408.6J per valve
Thus for a 50Hz application	= 20.4kW per valve

The penalty at adjudication, of these losses, at a rate of $5 per watt, would have been approximately :

$102,000 per valve (£68,000 per valve at $1.5 to the pound).

During worst-case repetitive operation approximately 25.5kW per valve is dissipated, as a result of the inrush limiting components of the Sellindge converter station, during the inrush transient and commutation in and out of the load current (Chapter 3.6). The corresponding figure for the proposed two-part reactor is 20.4kW per valve.

Neglecting the above saving in the inrush and commutation losses (5.1kW per valve), and approximating the total saving to the reduction in losses during full load current: by removing the quasi-linear reactors, the AC connection reactors and the DC connection reactor: there is a decrease in losses of approximately 27.5kW per valve, (Chapter 3.6).

The penalty at adjudication of these losses (27.5kW), at a rate of $5 per watt, would have been approximately:-

$137,500 per valve (£91,600 per valve at $1.5 to the pound)

Losses are normally adjudicated for worst-case, full load current, inverter operation. The above losses, resulting from the inrush current transient and load current commutation, would be reduced in both cases if the evaluation were performed for worst-case, full load current, inverter operation. However, the losses associated with full load current (27.5kW) are independent of the firing voltage; thus, the saving in evaluated losses due to the removal, from future designs, of the connection reactors and quasi-linear reactors would be at least $137,500.

For the Sellindge converter station 97.9J (14.7% of the 666J of energy initially stored in the stray capacitances of the commutating phases, prior to valve turn-on), is dissipated up to first current peak. For the proposed reactor design 187J (29.9% of the 626J of energy initially stored in the stray capacitances of the commutating phases, prior to valve turn-on), is dissipated up

to first current peak. Thus, the proposed two-part reactor has the advantage that a higher proportion of the energy is dissipated up to first current peak, thus damping the circuit oscillations more effectively.

The estimated savings in comparison with the Sellindge converter station are :

Hardware	= £37640 per valve
Evaluated losses (neglecting saving in inrush and commutation losses)	= £91600 per valve
Total (neglecting saving in inrush and commutation losses)	= £129,240 per valve

6.6 CONCLUSIONS

The inrush control components associated with the Sellindge converter station provided a safe working environment for the thyristors. However, the inrush control was achieved for a total hardware cost and capitalized losses (calculated under worst-case repetitive operating conditions (Chapter 3.6)), of approximately £242,000 per valve.

This chapter has investigated the possibility of replacing, for all future HVDC schemes, the inrush control components of the Sellindge converter station (section 6.2) by a single, passive, device. Consideration of the transient effects to be controlled (section 6.2), resulted in a two-part saturating reactor. One part of the reactor was considered to be lossless (L2) whilst the other part (L1) has controlled eddy-current losses.

The design of the two-part saturating-reactor should be such as to result in a minimum overall cost, whilst retaining or enhancing the safety of the thyristors' operating environment. The overall cost is minimized by reducing, as far as possible, the eddy-current losses during normal load current commutation without degrading, unduly, the damping of the inrush current oscillation, (sections 6.4.5 and 6.4.6). In addition, the total volume of magnetic material is minimized by specifying 'optimum' inductance with current characteristics.

The proposed characteristics for parts L1 and L2 (section 6.4.9), result in acceptable inrush current predictions for turn-on during worst-case repetitive operation; this is achieved for a total flux requirement of approximately 1.6Wb per valve. When a refined model of the converter transformer is utilized (Chapter 4.5.3), the inrush current prediction is known to be less onerous, (section 6.4.11); hence, the total flux requirement of the two-part saturating reactor could be reduced from 1.6Wb by approximately 10%. However, no additional studies were performed to refine further the proposed characteristics. This was not considered worthwhile, at this stage, as there are several proving studies to be carried out, to show the adequacy of the proposed characteristics during other operating conditions (Chapters 7 and 8).

Studies performed, with a representation of the proposed reactor characteristics, for normal repetitive operation did not indicate that any changes in these characteristics were required.

Thus, these characteristics will be modelled for the proving studies, (Chapters 7 and 8).

A preliminary estimate of the cost of both hardware and capitalized losses (assuming $5 per watt and $1.5 to the pound), for the proposed saturating reactor, indicate costs of £27,700 per valve and £68,000 per valve respectively (evaluated under worst-case repetitive operating conditions). The corresponding figures for the Sellindge converter station, inrush control hardware and capitalized losses, were £65,300 and £176,700 respectively. This indicates a total saving on hardware and capitalized costs of approximately £146,300 per valve during worst case repetitive operation, achieved by adopting the proposed saturating reactor in place of the inrush control hardware utilized for the Sellindge converter station.

Losses are normally adjudicated for a scheme for worst-case, full load current, inverter operation. Thus, approximating the reduction in evaluated losses, by adopting the proposed reactor in place of the inrush control hardware utilized in the Sellindge converter station, to the difference in losses during full load current there is a saving of approximately £91,600 per valve. This is in addition to the saving in inrush control hardware of approximately £37,640 per valve. Thus, the total saving (on inrush control hardware and evaluated losses), would be approximately £129,240 per valve adjudicated for full load current, inverter operation.

7. INVESTIGATION OF THE SENSIVITITY OF RECOVERY OVERVOLTAGE AND DAMPING CIRCUIT LOSSES AT TURN-OFF

7.1 INTRODUCTION

Turn-off of a thyristor valve excites an oscillation between predominantly the transformer leakage inductance and stray capacitance shunting the thyristor valve. This oscillation is damped, mainly, by the damping network associated with each thyristor level, (Chapter 3.2.1).

It is not practical to critically damp the recovery oscillation; thus, the valve-voltage will swing beyond the prospective, point-on-wave, recovery voltage. The magnitude of the recovery overvoltage and damping circuit losses are further exaggerated by the reverse recovered charge of the thyristors, (Chapter 3.4).

The recovery overvoltage and damping circuit losses can be controlled by:[32][53]

i) Judicious choice of damping circuit capacitor and resistor values.

ii) Selecting a transformer with specific effective resistance characteristics at the recovery frequency, (Chapter 4.5.2).

iii) Minimizing the reverse-recovered charge of the thyristors used.

Increasing the transformer resistance at a frequency appropriate to the recovery oscillation would permit either or both of the following:[32][53]

i) reduction of the capacitance value of the damping capacitor and, thus, an associated decrease in the damping circuit losses;
ii) reduction of the recovery overvoltage allowing, in some situations, the use of fewer series-connected thyristors per valve.

A transformer winding design which increases the resistance at recovery oscillation frequency generally also has increased fundamental frequency losses; hence, capitalized costs associated with these losses will be higher.[32][53] The effect of selecting one of three alternative transformer winding configurations, on the total capitalized losses associated with the transformer and the valve damping circuits, has been assessed. The assessment is based on one of the converter transformers for the 2000MW Sellindge converter station with the following alternative windings:[32]

i) Design A (980kW, 50Hz loss), conductor thickness = 1.5mm
ii) Design B (1030kW, 50Hz loss), conductor thickness = 2.7mm
iii) Design C (1190kW, 50Hz loss), conductor thickness = 4.8mm

The high frequency resistance, for the above windings, is shown as a function of frequency in figure 7.1.

It is standard practice to include surge arresters, connected in parallel with each valve, whose protective level is co-ordinated with the reverse capability of the valve, (Chapter 8.2). The interaction of the arrester, during the recovery interval, with the electrical circuit influences the magnitude of the recovery overshoot, the damping circuit losses and the rating of the arrester.

This chapter considers the sensitivity of recovery overvoltage and damping circuit losses, at turn-off, to the following:-

a) The capacitance value of the damping capacitor.

b) The magnitude of the shunt stray capacitances and of the series stray capacitance associated with the transformer winding.

c) Thyristor characteristics:

   i) The magnitude of the reverse recovered charge, (Chapter 3.4).

   ii) Proportion of total reverse recovered charge recovered up to peak reverse current, (Chapter 4.3.2).

   iii) The effect upon the prediction of modelling a sharp 'snap-off'.

d) i) The presence of surge arresters.

   ii) The protective level of the surge arresters (Chapter 8.2).

e) The inductance with current characteristic of the saturating reactors, (Chapter 6.4).

7.2 BASIC ASSUMPTIONS FOR THESE STUDIES

(a) Studies were performed with an electrical circuit based upon the existing design of the Sellindge converter station circuit (e.g. 50Hz operation). This equivalent circuit has the basic configuration shown in figure 7.2. The proposed saturating reactor characteristics (Chapter 6.4.9) were modelled.

(b) A converter transformer with a star secondary was modelled, as used for the recovery overvoltage predictions performed for the Sellindge converter station.[32]

(c) The transformer electrostatic model (Chapter 4.5.1), was derived in accordance with reference (32).

(d) Fast-grading capacitance was not included in the equivalent circuit of the converter station (the time constant of a fast-grading circuit is fast in comparison with the circuit transients, at turn-off).

(e) The star connected converter transformer is assumed to be in the upper six-pulse bridge.[54] The lower six-pulse bridge is represented by a shunt capacitance of 8.589nF (see below), and an on-state commutating inductance of 60.04mH behind this capacitance (figure 7.2).

A value of 8.589nF was arrived at for the shunt capacitance as follows:

i) 0.873nF mid-point to ground capacitance (C_m), (see figure 6.4)

ii) 0.2nF valve stray capacitance

iii) 7.516nF 'equivalent' ground capacitance results from the series addition, per phase, of the Thevenin equivalent electrostatic model[32] of the delta winding. The transformer busbar and bushing stray capacitances (Chapter 4.5.1), are all included within the Thevenin equivalent circuit.

The equivalent commutating inductance of 60.04mH is obtained by summing the transformer commutating inductance, (59.69mH taken) with the winding inductance associated with two on-state valves, (175μH per valve).

(f) The converter station is assumed to be in the emergency connection mode, running monopolar, with a neutral cable return (see Chapter 2.3). This emergency connection mode was studied for the Sellindge converter station during the recovery overshoot studies.[32] However, its influence upon the results requires verification.

In this mode of connection, both DC neutral surge capacitors are inserted (figure 7.2). The nominal capacitance value of these capacitors are:

i) surge capacitor in valve hall 1.2μF

ii) surge capacitor outside valve hall 100μF

(g) The peak line-to-line voltage ($\alpha = 90°$), during normal operation is 245.5kV, (see Chapter 6.4.13).

(h) Load rejection results in a dynamic overvoltage (DOV), of 1.3p.u.

(i) The maximum recovery voltage occurs when the valve turning-off is recovering to a voltage consistent with $\alpha = 90° +$ DOV operation, (i.e. 319.15kV without overshoot).

(j) The transformer high-frequency resistance winding model (Chapters 4.5.2 and 4.5.3), is derived in accordance with Appendix II. All the predictions presented in this chapter, unless otherwise stated, represent the converter transformer winding B (see section 7.1), by a single-section model.

(k) A refined transformer model, with end-effects, is represented in the manner described in chapter 4.5 and Appendix II.

(l) Unless otherwise stated, the winding assumed for the converter transformer is of an interleaved construction.

(m) Unless otherwise stated, the model of the thyristor, during recovery, is as described in Chapter 4.3.2, and produces a 'snap-off' characteristic.

(n) Unless otherwise stated, the thyristor reverse recovered charge used, for the 75mm thyristors considered, was 6400μC per thyristor. This magnitude of reverse recovered charge was extrapolated from laboratory measurements[55], reproduced in figure 7.3. The junction temperature of interest was 117°C, (i.e. consistent with the laboratory measurements of maximum reverse recovered charge). The rate of change of current, in order to maximise the reverse recovered charge Q_{rr}, is that appropriate to $\alpha = 90° +$ DOV operation, (i.e. 5.3A μs^{-1}).

(o) The computer analyses were performed using a 'Variable Topology Electrical Circuit Analysis Programme' (VTECAP), (Chapter 4). The refined converter transformer model (Chapter 4.5), introduces capacitive meshes into the equivalent circuit. Thus, care must be taken that operation of the parallel switches, in the representation of reverse recovery of the thyristor, does not alter the format of a mesh, (Chapter 4.5.1).

(p) To establish realistic initial conditions, a mathematical study was set up with initial currents of sufficient magnitude to saturate the reactors within the commutating valves. The duration of the study was arranged such that the study would finish prior to current zero crossing within the representation of the recovering valve. The results of this study, written to a file, can then be used as the basis for comparable further studies.

(q) Many of the studies represent an equivalent damping resistance value of 3,281Ω per valve and an equivalent damping capacitance value of 22.8nF per valve. These values correspond to the maximum tolerance damping resistance and minimum tolerance capacitance for a valve in the Sellindge converter station.

(r) Surge Arresters :

i) Co-ordinating current of 1kA is drawn at the switching-impulse protective level.

ii) The forward withstand capability of the valve is given by the sum of the individual, thyristor, forward withstand capabilities and is 400kV.

iii) The reverse withstand capability of the thyristors is 15% above their forward withstand capability.

iv) The switching-impulse protective level of the surge arrester is 15% below the thyristor valve reverse withstand. This level is thus:

$$\frac{400 \times 1.15}{1.15} = \underline{400 \text{ kV}} \quad \text{(1p.u say)}$$

v) The 'maximum design' protective level of the surge arrester is 2.5% below the required protective level, (i.e. 0.975p.u.).

The 'nominal design' protective level of the arrester is 2.5% below the 'maximum design' protective level, (i.e. 0.975^2 p.u.).

The 'minimum design' protective level of the arrester is 2.5% below the 'nominal design' protective level, (i.e. $0.\dot{9}75^3$ p.u.).

Included within these tolerances is an allowance for temperature and ageing effects.

vi) The energy dissipation capability of the arrester is approximately 5MJ. Recovery from a 3 phase AC fault is estimated to inject energy of about 4MJ into a valve arrester. Thus, if a valve design were to consider recovery from a 3 phase AC fault to be immediately followed by a period of DOV 1MJ could be dissipated in the arrester, during DOV, without endangering its integrity. Typically, a period of DOV lasts between 2 to 5 seconds. Similarly, a period of operation at $\alpha = 90$, is assumed to last for a maximum of 1 minute;

thus, the consequent 1MJ dissipation capabilities are:

2 to 5 seconds for operation at $\alpha = 90 + DOV$ of 30%

1 minute of operation at $\alpha = 90$, with normal voltage.

vii) The dissipation capability of the arrester during continuous operation is 100W.

viii) The leakage current through the surge arrester is 100μA at peak line-to-line voltage.

A typical surge arrester characteristic is shown in figure 4.4.

7.3 THYRISTOR REVERSE RECOVERED CHARGE

7.3.1 Computer Predictions

In order to assess the effect of thyristor reverse recovered charge upon the magnitude of recovery voltage and damping circuit losses, a study was first performed in which no reverse recovered charge was modelled. The study was then repeated for a G.E.thyristor,1644, using the 'conventional' turn-off model, (Chapter 4.3.2). In order to assess the effect of 'snap-off', upon the magnitude of recovery overvoltage and damping circuit losses, it was desirable to model the reverse current more accurately, i.e. with a rounded peak (Figure 7.4).

In order to achieve this, the assumption was made that the thyristor, during recovery, could be represented as a non-linear resistance whose instantaneous value is dependent upon the quantity of charge passed. The resistance versus charge passed characteristic (figure 7.5) was derived, from an oscillogram

(reproduced as figure 7.4), by dividing the instantaneous value of thyristor voltage by the instantaneous value of reverse current. Figure 7.6, shows a refined 'conventional' model of the thyristor which produces the 'rounded' peak of the current.

The operation of this refined model is as follows:

i) Switches in parallel with the capacitance (C), inductance (L) and resistance (R) are initially closed. The initial value of the non-linear resistance (R_n) is zero ohms.

ii) At current zero crossing (negative gradient) in the thyristor, the switch in parallel with the one Farad capacitance opens, allowing it to charge. The magnitude of reverse charge passed is directly proportional to the voltage associated with the one Farad capacitance.

iii) The value of the non-linear resistance is controlled by the voltage associated with the one Farad capacitance.

iv) When the required proportion, k_1, of the total reverse recovered charge (Q_{rr}) has been recovered (voltage across capacitance = $k_1 Q_{rr}$) the switches in parallel with the inductance and linear resistance can be opened to give the required current tail, (Chapter 4.3.2). However, it is not necessary to re-insert these elements at all, provided that sufficient values of the non-linear resistance are defined. [Note. The 'conventional' method of modelling turn-off (Chapter 4.3.2), switches the capacitance out of the circuit when the capacitance voltage = $k_1 Q_r$; this should not be attempted with this refined method of modelling.]

The results of the above studies are given in Table 4. The refined model of the thyristor reduces the recovery overvoltage by 1.5 percentage points compared to the 'conventional' model, and similarly reduces the predicted energy dissipation in the damping resistors by 42kW per six-pulse bridge, during recovery.

The effect of not modelling reverse recovered charge is to reduce the predicted overshoot by 22.5 percentage points, in comparison with the conventional thyristor model, to 16.3%. The predicted energy dissipation, due to recovery transients, in the damping circuits of the six-pulse bridge is reduced by 265kW (30.8%).

7.3.2 Theoretical Overshoot

The theoretical overshoot factor, in a six-pulse bridge, may be obtained using the equation[56].

$$q = \frac{L_c}{R_D^2 C_D}$$

Thus if:

$L_c = 30.02\text{mH}$, $R_D = 3280\Omega$, and $C_D = 22.28\text{nF}$

$$\underline{q = 0.122}$$

Hence, from figure 7.7[56], which shows the dependence of the overshoot factor upon q, the theoretical overshoot is 18% (c.f. 16.3% predicted).

The theoretical overshoot factor exceeds the predicted value by less than two percentage points when reverse recovered charge is neglected. The stray capacitances and saturating reactors act to exacerbate the overshoot. However, the transformer high frequency resistance (chapter 4.5) and the eddy-current losses of the proposed reactor (chapter 6.4.9), have a moderating effect upon the overshoot.

7.4 VALUE OF DAMPING CAPACITOR/DESIGN OF TRANSFORMER WINDING

As shown in Appendix VI, it is advantageous to choose a large capacitance value for the damping capacitor to minimize the effects of differences in reverse recovered charge between thyristors.

Such a requirement is, however, at variance with the need to choose a low capacitance value in order to minimize damping circuit losses. The low frequency component of these losses is proportional to the square of the damping capacitance[32][56]. For a 50Hz application, with a peak line-to-line voltage of 245.5kV (Chapter 6.4.13), and considering $\alpha = 90°$ operation with a DOV of 30%, the approximate overlap angle (U_o) is 7.166°. Assuming a damping capacitor value of 3μF per level and a damping resistor value of 27.5Ω per level, then the low frequency damping circuit loss is approximately 66W per level for a valve of 100 levels. The high-frequency losses (1750W) which are dominant, are directly related to the sum of the valve stray and damping capacitances[32][56]. It is necessary to

minimize both the total losses (excluding transformer high-frequency losses) and the recovery overvoltage for each of the three transformer winding designs, (section 7.1). Thus, studies have been performed to assess the sensitivity of the overshoot, during $\alpha = 90 + DOV$ operation, to both the winding design and the value of the damping capacitance.

The results of the predictions are summarized in figure 7.8. All results are displayed as increases in recovery overshoot factor during $\alpha = 90 + DOV$ operation. The total damping circuit losses are evaluated for $\alpha = 15°$ operation, for several values of damping capacitance. These losses are added to the fundamental frequency transformer losses; the variation, in comparison with a hypothetical scheme, of the sum of these damping circuit and fundamental frequency transformer losses, is plotted in figure 7.8. This hypothetical scheme is considered to consist of transformer winding design B and damping circuit consisting of $C_d = 2.28\mu F$ and $R_d = 35\Omega$ per level. The high-frequency mathematical model of the transformer represented the high-frequency resistance to be equal to the theoretical value (i.e., no allowance is made for possible inaccuracies in the derivation of the theoretical value).

Figure 7.8 shows that, for a given damping capacitor, design C of the transformer winding results in the least recovery overvoltage: the largest overshoot results with winding design A. The curve of recovery overshoot for winding design B, shows a decrease in the overshoot factor at the rate

of approximately 5.5 percentage points per microfarad increase in damping capacitor, (above a value of approximately 2μF). As the damping capacitor is decreased below a value of approximately 2μF, the overshoot factor increases rapidly.

The losses are normally adjudicated under worst-case continuous operating conditions, (Chapter 3.6). The following comparison of the 6-pulse bridge losses, is carried out for rectifier operation with a firing angle of 15°.

The six-pulse bridge, high-frequency (recovery and turn-on transients), damping circuit losses together with fundamental frequency damping circuit and transformer losses, increase as the value of the damping capacitor is increased. The evaluated losses of the six-pulse bridge increase at a rate of approximately 83kW per microfarad increase in the value of the damping capacitors within a bridge, (above a value of damping capacitor of 2μF per level).

Figure 7.8 shows that, in order to achieve the same overshoot factor (35.1%), during $\alpha = 90°$ + DOV operation, as predicted when transformer winding design C is modelled, with C_d = 2.28μF), winding designs B and A require damping capacitors of about 2.85μF, per level, and 3.65μF, per level, respectively. As a consequence, the six pulse-bridge damping circuit losses for design C, during $\alpha = 15°$ operation, are larger than those for design B by 106kW to achieve the same overshoot.

Coincidentally, for design A, the 3.65μF damping capacitor produces the same overshoot factor as winding design B (with 2.85μF damping capacitor), but results in an increase of approximately 26kW in the six-pulse bridge losses.

7.5 DAMPING RESISTOR

The dependence of the overshoot factor, for three different values of damping capacitor (1μF, 2.28μF and 4μF), upon the value of the damping resistor is shown in figure 7.9. Similarly, the damping circuit losses per valve, as a result of recovery transients throughout the six-pulse bridge, are plotted in figure 7.10, for $\alpha = 90 + DOV$ operation.

For a damping capacitor value of 1μF the minimum overshoot factor (approximately 60%) is obtained with a damping resistor of about 40Ω per level. With a 4μF damping capacitor, per level, the minimum overshoot factor (approximately 25.5%), is obtained with a damping resistor of 29Ω per level. However, the evaluated losses ($\alpha = 15°$) in the damping circuits of the six-pulse bridge increase at the approximate rate of 83kW per microforad increase in the value of the damping capacitors (section 7.4).

In order to minimize the difference in recovery voltages between levels, at turn-off (Appendix VI), it is desirable to have a large value of damping capacitor. This is at variance with the requirement to minimize evaluated losses. Thus, the minimum acceptable value of capacitance is also dependent upon

the difference in reverse recovered charge between thyristors. The minimum acceptable damping resistor value is dependent upon the thyristors capability at turn-on.

7.6 SERIES CAPACITANCE OF TRANSFORMER WINDING

The design of the Sellindge converter transformers, is based upon an interleaved winding with a relatively high value of series capacitance (e.g., 935pF and 285pF for the star and delta transformer respectively). For the Sellindge converter station, Transformer Design (Power) indicated that an alternative winding based on intershielded windings may be possible. The intershielded windings exhibit a relatively low value of series capacitance (typically one tenth of the corresponding values for an interleaved winding).

The dependence of the overshoot factor upon the damping resistor value (when C_d = 2.28μF), for both an interleaved and intershielded winding, are shown in figure 7.11. The minimum overshoot factor is decreased by about 2.4 percentage points by adopting an intershielded transformer winding. Similarly, the six-pulse bridge damping circuit losses, with damping resistors selected to obtain the minimum overshoot, decrease by about 37.5kW from approximately 837kW, (during α = 90 + DOV operation).

Thus, an intershielded disc wound transformer design allows either, or a combination of, the following:-

i) A reduction in the recovery overshoot factor by 2.4 percentage points.

ii) A reduction in the value of the damping capacitor, to retain the same overshoot, and thus a consequential decrease in evaluated losses. From figure 7.8, the damping capacitor could be reduced in value by approximately 0.43μF per level, reducing the evaluated six-pulse bridge losses by about 36kW during $\alpha = 15°$ operation.

7.7 SHUNT STRAY CAPACITANCE

In future schemes, it may be desirable to house the thyristor valves in 'transformer tank structures'. The provision of such tanks will increase the shunt stray capacitances associated with the valve. The effect of increasing the valve shunt stray capacitance by a factor of approximately twenty (200pF to 4.2nF) has been examined.

Figure 7.11 shows the overshoot factor as a function of damping resistor value (with $C_d = 2.28\mu F$), with and without the increased shunt stray capacitance. For values of damping resistor greater than that which results in minimum overshoot factor, the curves diverge. A damping resistor of about 30Ω per level results in a minimum overshoot factor in both cases. However, increasing the shunt stray capacitance has exacerbated the minimum overshoot by about 3 percentage points. The total losses in the six-pulse bridge also increase, by approximately 16kW, from about 837kW during $\alpha = 90°$ + DOV operation.

From Figure 7.8, it is expected that in order to retain the same overshoot factor, when the valve shunt stray capacitance is increased twenty-fold, requires an increase in damping capacitor from 2.28μF by about 0.5μF per level. This would be expected to increase the total evaluated (α = 15°), six-pulse bridge damping circuit losses by approximately 42kW.

7.8 SPLIT IN REVERSE RECOVERED CHARGE

A mean reverse recovered charge for the 75mm MEDL thyristors has been derived from measurements performed on a limited number of thyristors[55]. These measurement have been extrapolated to obtain the Q_{rr} at a junction temperature of 117°C for a di/dt at recovery of approximately 5.3A μs^{-1}, (α = 90 + DOV operation). Thus, from figure 7.3 the Q_{rr} for these operating conditions is approximatley 6400μC. Studies have been performed to find the sensitivity of the overshoot factor and six-pulse bridge damping circuit losses, resulting from the recovery transients, to the percentage of the charge recovered prior to the instant the thyristors begin to support voltage. This instant, throughout the recovery studies, coincided with peak reverse current (PRI).

The damping circuit losses increase linearly with PRI over the range studied (figure 7.12). The rate of increase is approximately 2.34kW per Amp, per six-pulse bridge (C_d = 4μF and R_d = 30Ω). However, the overshoot factor does not increase linearly with the PRI over the range studied. At the bottom end of the range (125A PRI), the overshoot factor increases at the

rate of 0.08 percentage-points per amp. Near the top end of the range studied (220A PRI), the overshoot factor increases at the rate of 0.27 percentage points per amp, (See figures 7.12 and 7.13).

If the thyristors within a recovering valve are considered to have zero reverse recovered charge then, with a 4μF damping capacitor and 30Ω damping resistor, the high-frequency damping circuit losses, resulting from recovery transients throughout the six-pulse bridge, are approximatley 968kW per bridge. This is increased to 1200kW per bridge (an increase of 24.3%), by including a total reverse recovered charge of 6400μC, split in the proportions 37/63%. Figure 7.13 shows the recovery overshoot and the high-frequency, damping circuit losses, versus the proportion of charge recovered upto the instant the thyristor supports reverse voltage, (Q_{rr} maintained at 6400μC). The losses increase at the approximate rate of 6.2kW per percentage point of charge recovered prior to snap-off.

The magnitude of charge recovered prior to the instant the thyristors support reverse voltage was then held constant (i.e. peak-reverse current held constant), and the total Q_{rr} varied, (i.e. time-constant of recombination altered).

The effect of decreasing this time-constant from 375μs (Q_{rr} = 49.387mC split 3.3%/96.7%), to 36.4μs (Q_{rr} = 6.4mC split 25%/75%), is to reduce the overshoot factor from 23% by 3.4 percentage points and the total six-pulse bridge damping circuit

losses by 146kW, (during α = 90 + DOV operation). Thus, the overshoot factor is not very sensitive to the assumed rate of recombination.

Hence, for a given reverse recovered charge, it is advantageous to minimise the proportion of charge recovered before 'snap-off'. This has the effect of reducing the magnitude of PRI and consequently the recovery overshoot and high-frequency damping circuit losses, resulting from recovery transients throughout the six-pulse bridge.

7.9 EFFECT OF REFINING THE TRANSFORMER MODEL

The single-section star transformer representation, which was used for the aforementioned studies, was subdivided into five sections per phase, and end effects were included in the model (see Chapter 4.5.3 and Appendix II). To compare the effect of refining the transformer model, a comparative study was performed with a damping capacitor of 2.28μF per level and a damping resistor of 32.8Ω per level. The total reverse recovered charge modelled was 6400μC, split 37/63%.

The results of this study, together with those for the equivalent study utilising a single-section transformer model, are tabulated in table 5. The effect of refining the transformer model is to reduce the overshoot factor from 37.6% by 2.2 percentage points (i.e. 5.85% of the overshoot factor). Similarly, the six-pulse bridge damping circuit losses, resulting from recovery transients, decrease by 36kW (during α = 90 + DOV operation).

Decreasing the value of the damping capacitor, by approximately 0.4μF per level, to retain the overshoot factor as predicted with a single-section transformer model, would reduce the evaluated (α = 15° say) losses by about 33kW, per six-pulse bridge.

7.10 MAGNITUDE OF DAMPING CIRCUIT CURRENT/ENERGY DISSIPATION

A damping capacitor of 2.28μF and a damping resistor of 30Ω, together with a reverse recovered charge aggregate of 6400μC (split 37/63%), results in an overshoot factor of 37.8% (obtained with a single-section transformer representation). At the time of this overshoot the voltage across the damping resistors in the recovering valve is 221.7kV: the charge on the damping capacitors results in 218.1kV. The voltage across the damping resistors is as a result of 73.9A of current flowing in the damping circuit.

The magnitude of damping circuit current may, in future schemes, be reduced by virtue of a surge arrester, connected in parallel with each valve, conducting current during recovery to maximum system voltage. Thus, it may be possible to 'clip' the magnitude of the recovery overshoot, by utilising the surge arrester, during α = 90° + DOV operation. A maximum tolerance arrester will be less effective than a minimum tolerance arrester in limiting the magnitude of the overshoot. Hence, a study has been performed for α = 90 + DOV operation with a maximum tolerance arrester represented to find its effect upon the overshoot. The surge arrester must not dissipate excessive

energy such that its integrity is endangered, (section 7.2). The predicted energy in the arrester is maximized, during all operating conditions, when a minimum tolerance arrester is represented. Hence, studies have been carried out to predict the energy dissipation in the arrester, during the following operating conditions;

a) $\alpha = 90 + DOV$

b) $\alpha = 90$

c) Normal continuous operation

a) $\alpha = 90 + DOV$

Including maximum tolerance surge arresters (section 7.2), in the model of a six-pulse bridge, during $\alpha = 90° + DOV$ operation, decreases the predicted recovery overshoot from 37.8% to 16.54%. Similarly, the energy dissipation in a valve damping circuit, as a result of recovery transients throughout the six-pulse bridge, is decreased by 28kW per valve (per second), (for a 50Hz application). The predicted energy dissipation within a line-to-line surge arrester is approximately 0.205MW (per second), resulting from the recovery transients throughout the six-pulse bridge.

Similarly, when minimum tolerance surge arresters (section 7.2) are represented, the recovery overshoot, during $\alpha = 90 + DOV$ operation, is reduced to about 9% (figure 7.14). The predicted energy dissipation within the damping resistors is

reduced by about 42.4kW per valve (per second), in comparison to arresters not being modelled; however, arrester dissipation is approximately 445kW per valve (per second). This energy dissipation, within the surge arresters, is an order of magnitude greater than the consequent reduction in damping circuit, high-frequency, losses during recovery.

Figure 7.15 shows the current flowing within the (Y-phase) recovering valve and also that in the Y-phase of the, star secondary, converter transformer when no surge arresters are modelled during recovery. Figure 7.16 shows the current flowing within the Y-phase of the star secondary converter transformer with surge arresters modelled. The consequent current flow in the surge arrester, during a recovery transient, is plotted in figure 7.17.

The magnitude of surge arrester energy dissipation (445kW) results from the arrester providing a low impedance path in parallel with the recovering valve. The presence of the surge arrester decreases the magnitude of the maximum reverse voltage across the recovering valve. Thus, the reverse current flowing in the commutating inductance of the converter transformer, during the recovery interval, decays at a reduced rate in comparison with no surge arresters being present. Thus, the surge arrester conducts a significant current for several hundred microseconds, (Figure 7.17).

The value of the damping capacitor influences the surge arrester and damping circuit losses at recovery. When a minimum tolerance surge arrester is considered, the effect of increasing the value of the damping capacitance results in the following:

a) The energy dissipation in the valve surge arrester during the recovery transient decreases at the rate of approximately 1000J per cycle, per microfarad (per level) increase in the value of the damping capacitor, during α = 90° + DOV operation (figure 7.18).

b) The energy dissipation in the valve damping circuit during recovery, increases at the rate of 900J per cycle, per microfarad (per level) increase in the value of the damping capacitor, during α = 90° + DOV operation (figure 7.18).

c) A decrease of the recovery overshoot factor by 0.25 percentage points per microfarad, (figure 7.19).

However, increasing the value of the damping capacitor exacerbates the six-pulse bridge, damping circuit, high-frequency losses (recovery and turn-on). The fundamental frequency evaluated losses associated with the damping circuit increase too. The damping circuit losses are evaluated during worst-case continuous operation, and increase at the approximate rate of 83kW per six-pulse bridge, per microfarad increase in the value of the damping capacitor, (section 7.4).

The energy absorption capability of the arresters is assumed to be 5MJ each, (Section 7.2). It is estimated

that recovery from a 3 phase AC fault would result in the injection of 4MJ into each arrester, (section 7.2). However, recovery from a 3 phase-fault can result in a period of dynamic overvoltage. A duration of dynamic overvoltage greater than 2 seconds may endanger the integrity of the valve arresters, under such conditions of operation.

b) $\alpha = 90°$

Operation at $\alpha = 90°$ is assumed to continue for a maximum of 1 minute, (section 7.2). During this interval, the energy dissipation per valve arrester must not exceed 1MJ.

In order to predict the maximum magnitude of the dissipation, minimum tolerance surge arresters were represented. The predicted dissipation was approximately 298kJ (per minute) and is thus within the assumed surge arrester dissipation capability.

c) Continuous operation

i) Surge arrester

During normal continuous rectifier operation ($\alpha = 6°$ minimum, through to $\alpha = 15°$ maximum) and inverter operation ($\gamma = 14°$ minimum, through to $\gamma = 16°$ maximum), valve-voltages do not reach a magnitude such as to cause significant arrester current. However, the power dissipation within the arrester

must be limited to below, say, 100 watts (section 7.2). Maximum energy dissipation, within the arrester, is achieved if the arrester is of a minimum tolerance.

In order to predict realistic arrester power dissipations, under continuous operating conditions, it is necessary to model the arrester as accurately as possible at representative, continuous, operating voltages. The characteristic of a maximum tolerance arrester was chosen such that it gave 1kA co-ordinating current at 400kV. In addition, the leakage current was assumed to be 100μA at peak line-to-line voltage (section 7.2), (245.5kV). This represents a 'maximum tolerance' arrester and the characteristic must be scaled to give a 'minimum tolerance' arrester.

Table 6 shows the predicted energy dissipation, in the arresters, during normal continuous operation. The total energy dissipation, associated with each surge arrester in a six-pulse bridge, is higher for rectifier operation than inverter operation. For normal rectifier operation, when valve 6 (figure 7.2) is recovering, maximum surge arrester energy dissipation is associated with off-state valves 4 and 5. The maximum surge arrester power dissipation, associated with continuous rectifier operation, occurs at minimum firing-angle ($\alpha = 6°$) and is predicted to be about 17.7 watts per arrester.

For normal inverter operation maximum surge arrester energy dissipation is associated with the valve in series with the recovering valve. The maximum surge arrester power dissipation, associated with continuous inverter operation, occurs at maximum extinction angle and is predicted to be about 6.7 watts per arrester.

ii) Damping resistors

Table 6 also shows the predicted energy dissipations within the damping resistors of the commutating and off-state valves, as a result of the recovery transient, (C_d = 2.28μF and R_d = 30 Ω). The sum of these dissipations, at any particular firing angle, gives the total high-frequency losses in the damping resistors of a valve, due to the six-pulse bridge recovery transients. For a 50Hz application, and a valve considered to consist of 100 levels, the high-frequency losses attributable to recovery transients are:-

Firing/Extinction angle	High-frequency losses in a damping resistor during recovery
	Watts per level
α = 6	278.7
α = 12	303.2
α = 15	321.7
γ = 14	53.6
γ = 15	61
γ = 16	68.8

The above, relevant, high frequency dissipation together with that associated with coherent turn-on many be summed with the, damping resistor, low-frequency losses to obtain the resistors' continuous rating.

The results of turn-on studies for normal continuous operating conditions were presented in chapter 6.4.13. A further study has been carried out, nominally on the same circuit considered in the aforementioned chapter (figure 6.4), but with a representation of a 30Ω damping resistor and 2.28μF capacitor, per level. Valve V2 was considered to be turning-on and Valve V1 was in full conduction, (see figure 6.4).

The predicted high-frequency losses in the damping resistance (R_D) (up to an elapsed time of 45μs for all valves), for turn-on during $\alpha = 12°$ operation were;

Valve V4 2.2J per valve

Valve V5 11.74J per valve

Valve V3 2.154J per valve

The calculated energy dissipation in the damping resistors of the valve turning-on is:-

Valve V2 $\frac{1}{2}C_D V_f^2 = \frac{1}{2} \times 2.28 \times 10^{-8} \times (51040)^2 = 29.70J$

Total 45.8 Joules per valve

Thus, the total high-frequency losses predicted (turn-on and recovery), during $\alpha = 12°$ operation, are 32.61kW per valve damping circuit, (for 50Hz operation).

The equivalent high-frequency loss predicted using conventional formula[56], which necessarily ignores reverse recovered charge, and simplifies the voltage jumps resulting from commutations to 'step-changes', is 28.3kW per valve.

7.11 MAXIMUM VOLTAGE ACROSS AN OFF-STATE VALVE

During recovery of a thyristor valve the consequent, negative, voltage excursion is reflected as a positive voltage excursion across off-state valves, and is superimposed upon the 'normal' valve-voltage. This voltage excursion must not result in a magnitude of positive voltage such that the overvoltage protection, of the off-state valve, may be activated. Thus, studies have been performed in order to identify the condition which results in a peak positive voltage across an off-state valve.

The maximum voltage occured across the valve connected, electrically, in series with the recovering valve; during inverter operation, with an extinction angle of 28.5°. The voltage is greater than that occurring during $\alpha = 90° + DOV$ operation because of the magnitude of the pre-charge on the damping capacitors of the series connected, off-state, valve.

A damping capacitor value of 2.28μF per level and a damping resistor of 30Ω per level, for a valve of 100 levels, were assumed. Allowing for a dynamic overvoltage of 30% the voltage across the series connected, off-state, valve increased to a maximum of 370.2kV, (50% overshoot factor).

Thus, for a scheme where the sum of the maximum overvoltage protective levels is 400kV, if the minimum protective firing level is considered to be 10% below the protective level (i.e., 360kV), the series connected, off-state, valve may have been turned on by its overvoltage-firing protection (neglecting the influence of surge arresters). The effect of surge arresters would be to decrease the magnitude of the overvoltage. Similarly, an increase in the value of the damping capacitor (which is desirable for minimizing the differences in recovery voltages between recovering levels), would decrease the maximum voltage across an off-state valve.

7.12 SATURATING REACTOR CHARACTERISTIC

In order to keep the magnitude of the recovery overshoot and total six-pulse damping circuit losses to a minimum, it is advantageous to minimize the reverse recovered charge, associated with a thyristor (section 7.8). For a given thyristor, the reverse recovered charge can be decreased by reducing the di/dt at commutation out, (figure 7.3).

The di/dt at commutation out may be significantly reduced by including a substantial magnitude of saturating inductance (say 20% of commutating inductance, i.e. 12mH), within the valve. Assuming this inductance remains constant upto peak reverse current (figure 7.20), the decrease in reverse recovered charge and peak reverse current may be estimated (see figure 7.3).

Considering α = 90 + DOV, without this saturating inductance, the di/dt at commutation out is about 5.3A μs^{-1}. Thus, with the 12mH saturating inductance, the di/dt at commutation out, near current zero, is likely to be 4.4A μs^{-1}. From figure 7.3, the resultant reverse recovered charge, at a junction temperature of 117°C, is estimated to be 5830 μC, (c.f. 6400μC).

When the saturating reactor characteristic of figure 7.20 is represented in place of the 'proposed two-part reactor' the magnitude of the recovery overshoot is reduced from 37.8% by one percentage point (when C_d = 2.28μF and R_d = 30Ω). The predicted high-frequency losses, as a result of the six-pulse bridge recovery transients during α = 90 + DOV operation, are reduced from 140.3kW to 133kW, a saving in losses of 7.3kW per valve damping circuit.

Similarly, from figure 7.8, in order to retain the same overshoot (during α = 90 + DOV operation), the value of the damping capacitor could be reduced by approximately 0.18μF, per level; this would reduce the damping circuit evaluated losses (α = 15° say) by approximately 15kW per six-pulse bridge (section 7.4).

The inclusion of a large value of incremental-inductance (figure 7.20) is at variance with coherent turn-on requirements. For efficient use of the reactor, during coherent turn-on, the value of the incremental-inductance must be as low as possible whilst still constraining the di/dt to within safe limits.

7.13 SUMMARY

This chapter has reported the results of studies which were performed to assess the sensitivity of both the predicted recovery overshoot and damping circuit losses, at thyristor recovery, to refined modelling techniques and circuit and device parameters.

The sensitivity of the recovery overshoot is studied for $\alpha = 90 + DOV$ operation. Refined modelling techniques decrease, slightly, the magnitude of the predicted recovery overshoot transient. Similarly, device parameters (e.g. the value of the converter transformer interturn capacitance) effect the magnitude of the recovery transient.

The reverse recovered charge of a thyristor contributes significantly to the magnitude of the recovery transient and the damping circuit losses. Although the magnitude of the reverse recovered charge can be reduced by adopting a saturating reactor with a large value of incremental inductance up to peak reverse current, the decrease in the overshoot and damping circuit losses is a second order effect. In addition, a large value of incremental inductance, to control the recovery transient, is at variance with the optimum characteristic for controlling the inrush current at turn-on. Thus, based on the predictions to date, no change is contemplated for the proposed characteristics of the 'two-part' reactor.

Where a refined modelling technique or a change in a device parameter effects the overshoot, the transient can be returned to its original value by altering the value of the damping capacitor; this will also effect the magnitude of the damping circuit evaluated losses. Hence, where applicable, this chapter reports the effects of such changes upon the evaluated losses, (for $\alpha = 15°$). However, the minimum value of the damping capacitor is constrained by the requirement to control the effects of a difference in reverse recovered charge between thyristors.

A major reduction in the overshoot factor may be achieved by utlizing surge arresters to 'clip' the overvoltages. However, to ensure that the integrity of a minimum tolerance arrester is not endangered, when recovery from a three phase AC fault is immediately followed by a period of DOV, the assumed rating of the arresters should be increased. Normal continuous operation of the thyristor bridge does not result in an excessive dissipation in the arresters.

8. PROVING STUDIES FOR PROPOSED REACTOR CHARACTERISTICS

8.1 INTRODUCTION

In chapter 6 the optimum inductance versus current characteristics were developed for a two-part reactor, for worst-case repetitive inrush considerations. The characteristics were developed such that the inrush current was controlled to within specified limits for a minimum total cost.

Chapter 7 examined the sensitivity of the magnitude of the recovery overshoot voltage transient, and the energy dissipation within the damping resistors to various circuit parameters. It was concluded, within chapter 7, that it is not economically viable to modify the proposed reactor characteristics by including additional magnetic material to control either the magnitude of this transient or the damping circuit losses at recovery.

The reactor characteristics developed in chapter 6 must be shown to control, adequately, circuit transients during other operating conditions. Thus, the studies reported upon in this chapter were concerned with proving that the characteristics of the proposed reactor, are suitable and adequate for the most significant repetitive and non-repetitive operating conditions.

Several of the possible 'worst-case' situations which were studied did not arise in the Sellindge converter station; thus, there are no comparative predictions, in these cases, with the Sellindge converter station studies. One such situation is a large current pre-established in a surge arrester at valve firing; this current may occur concurrently with overvoltage firing of the valve and is as a result of future valve designs taking economic advantage of thyristor asymmetry.

For the Sellindge converter station, it was possible to apply negative gate bias to aid recovery of a thyristor, thus reducing the possibility of a commutation failure as a result of repetitive voltage transients occurring during the recovery interval. However, future schemes will not be able to make use of this technique; hence, the converter station electrical circuit should adequately control circuit transients during this recovery interval, (see Chapter 9).

The integrity of the thyristors must not be endangered by any of the current and voltage waveforms predicted in this chapter. Laboratory tests, reproducing some of the predicted results, are required to confirm that this is the case.

8.2 SURGE ARRESTER; EFFECT OF PRE-ESTABLISHED CURRENT AT VALVE FIRING

8.2.1 Introduction

All HVDC schemes utilize surge arresters to protect the thyristor valves from excessive voltages. A surge arrester is, generally, sited in close proximity to, and electrically in parallel with, each thyristor valve; this limits the magnitude of overvoltages across the valve. In addition, a DC line arrester is generally connected from the DC line to earth; this limits the magnitude of overvoltages from the DC cable. Similarly, AC line arresters (from phase to earth) are often included to limit the magnitude of transient overvoltages across the inductors and resistors within the AC filters.

Due to the asymmetrical voltage capability of thyristors, the reverse withstand voltage of a valve exceeds the forward voltage capability. In taking economic advantage of this asymmetry, it is standard practice to co-ordinate the arrester protective level with the reverse capability of the valve. Protective overvoltage firing of the thyristors is utilized to relieve the valve of forward overvoltage stress.

By international convention (IEC 700) the reverse capability of a valve (i.e., the test level) is 15% above the switching-impulse protective level of the arrester (figure 8.1). Because of tolerances, actual protective levels of

practical arresters may allow a larger margin than this, i.e. an arrester may limit an impressed overvoltage by drawing its co-ordinating current at a voltage below 85% of the valve reverse withstand voltage.

In designing valves with respect to their forward protective overvoltage firing level, account has to be taken of the increased turn-on stresses if, as a result of an impulse, significant arrester current is present when the overvoltage firing level is reached. This is because the pre-established arrester current is available for immediate commutation into the valve as the valve anode voltage falls.

In the past, a high pre-established current in the arrester, coincident with the overvoltage firing level, has been avoided. This was achieved by lowering the forward overvoltage firing level of the thyristors and connecting sufficient thyristors in series to give the required minimum magnitude of forward overvoltage firing of the valve. Thus, the arrester protective level could be co-ordinated with the high reverse withstand of the thyristor valve; hence full advantage was not taken of thyristor asymmetry.

In future schemes, economics dictate that only the minimum number of thyristor levels required will be used. Therefore, either the overvoltage protective level of the valve must be reduced or the valve must be designed to accept

a large pre-established current, in the arrester, at the overvoltage firing level. In the former case the overvoltage firing level would have to be set below 1.4 p.u. for an arrester protective level of 1.75 p.u. Such a low level cannot be tolerated from a system performance point of view, as repetitive voltage transients within the converter bridge would trigger the overvoltage protection.

8.2.2. Basic Assumptions

Recognising that commutation of arrester current into a valve at turn-on, will be a reality in future schemes, has led to a preliminary investigation of the likely consequences. Studies have been performed based on the following assumptions:

(a) The reverse withstand capability of the thyristor exceeds the forward withstand capability by 20%.

(b) The switching-impulse co-ordinating level for the surge arrester is 15% below the sum of the thyristor reverse withstand levels.

(c) The tolerance of the surge arrester, over its life, including temperature and ageing effects is ±5% of a nominal value.

(d) The design of the converter electrical circuit is based upon the existing circuit design of the Sellindge converter station (Chapter 3.6), with the following modifications:

i) AC connection reactors, together with their parallel connected resistors, removed:

ii) DC connection reactor, together with the parallel connected resistor, removed:

iii) Valve-capacitor removed:

iv) Module six-turn spiral, bypass resistor and diode dispensed with:

v) Module ferrite-reactors replaced by magnetic materials whose characteristics are as shown in figure 6.21.

(e) The maximum forward overvoltage firing level of the valve is 400kV.

Thus, from (a), the sum of the reverse withstand capabilities of the thyristors within the valve is assumed to be given by;

$$400 \times 1.2 = 480\text{kV}.$$

From (b), the maximum 'switching-impulse' protective level of the arrester is obtained;

$$\frac{(480\text{kV})}{(1.15)} = 417.4\text{kV}$$

Hence, from (c), the nominal 'switching-impulse' voltage of the arrester when conducting its co-ordinating current is given by;

$$\frac{417.4}{1.05} = 397.5\text{kV} \pm 19.9\text{kV}$$

Therefore, in the event of a switching-impulse being impressed upon the valve, when the forward voltage on the valve reaches 400kV the surge arrester may be conducting

its full co-ordinating current (I_c). The consequent firing of the valve e.g., by its overvoltage protection, will result in the co-ordinating current transferring into the valve, as the valve anode voltage falls.

In order to predict the severity of this current transfer, studies have been carried out on a simplified equivalent circuit (figure 8.2) of a six-pulse bridge[57]. In setting up the initial conditions for these studies the following assumptions were made:

(1) The valve turning-on will do so from a voltage given by the highest voltage for which BOD firing will just occur i.e., 400kV

(2) The valve damping circuit is pre-charged to the overvoltage protective level, and thus there is no current pre-established in this valve, (i.e. the reactors are not pre-saturated).

(3) Due to the complex nature of correctly modelling a switching-impulse behind a representative source impedance, the co-ordinating current was modelled as being supplied by the DC link (i.e. an infinite source of energy).

Three different magnitudes of co-ordinating current were studied; these magnitudes were 3kA, 2kA and 1kA.

8.2.3. Predicted Inrush Waveforms

Figure 8.3 shows the voltage-current characteristics for a surge arrester such that the co-ordinating currents are 3kA, 2kA and 1kA at 400kV. Figures 8.4 and 8.5 show the resulting, predicted, thyristor inrush current and current transfer from the surge arrester when there is 3kA pre-established in the arrester.

Similarly, figure 8.6 shows the resulting, predicted, thyristor inrush current and current transfer from the surge arrester when there is 1kA pre-established in the arrester. The results of the above studies are given in Table 7.

When a current of 1kA is considered to be pre-established in the arrester, the current troughs of all the oscillations, up to an elapsed time of 45μs, de-saturate both the lossless reactor (L2) and the lossy reactor (L1). This has the effect of increasing the magnitude of the eddy-current losses which act to damp the high-frequency oscillation.

As can be seen from Table 7, which gives the salient features of the inrush predictions, up to an elapsed time of approximately 2.5μs the predicted rate-of-rise of current is below 200A μs^{-1} in all three studies. Up to an elapsed time of 4μs the predicted rates-of-rise of current, for each of the three studies, are very similar in magnitude, increasing steadily to approximately 500A μs^{-1}.

Saturation of reactor L2 occurs at an elapsed time of about 3μs after valve turn-on; reactor L1 saturates about 2μs later. Immediately following saturation of reactor L1, only the winding inductance of the valve limits the rate-of-rise of current through the thyristors [circa 2kA μs^{-1}] and the magnitude of the first current peak in that valve (over 5kA in the worst-case). Table 8 shows the magnitude of the first peak of inrush current for each of the three studies. In each case the first current peak occurs at an elapsed time of approximately 7μs, after valve turn-on.

The overvoltage firing of the valve causes a fast voltage transient on the adjacent valve connected to the same AC phase. The predicted rate-of-rise of voltage is virtually independent of the magnitude of the pre-established co-ordinating current, represented as flowing in the surge arrester, and is;

Thyristor level	2880V μs^{-1}
Thyristor	2280V μs^{-1}

Thus, with a nominal dV/dt limit of 1kV us^{-1} per level (see Chapter 6.3) the series valve would have been fired by dV/dt protection. The effect of this consequential action has not been studied.

8.2.4 Comments

The method of modelling the co-ordinating current at 400kV, as a current supplied by the DC link, results in a pessimistic prediction. However, the fact that no damping circuit charging current is modelled at the start of the study, will err the prediction on the optimistic side. It is expected that, taking the above into account together with the nature of the reactor characteristics, these predictions are likely to be more onerous (particularly at longer times) than that which would be produced by a set of studies modelling the source of the arrester current as a limited energy, voltage impulse, behind a representative impedance.

The predicted current transients, though severe, are not obviously damaging to the thyristors; the initial few microseconds of modest di/dt are likely to be adequate to allow sufficient conducting area to be established. Laboratory tests will determine whether this is the case.

For the present, the duty is being presumed safe for the thyristors and, therefore, no modification to the proposed reactor characteristics is required.

8.3. COMMUTATION FAILURE

8.3.1 Introduction

For the Sellindge converter station, worst-case non-repetitive inrush current arose for a complex commutation

failure and overvoltage firing sequence of events, within a 12-pulse bridge, from maximum valve-overvoltage firing level[25]. The studies have been repeated, including the proposed valve reactor characteristic instead of the inrush control hardware of the Sellindge converter station.

Non-repetitive inrush current arises from discharge of all capacitances to ground of the 12-pulse converter station (figure 8.7). To minimize the impedance between these capacitances and a valve (adjacent to the neutral DC busbar) whose turn-on is delayed, it is assumed that firing is preceded by commutation failure in the lower six-pulse bridge followed by overvoltage firing of the only non-conducting valve in the quadrivalve (figure 8.7). In addition, the reactors within the valves conducting load current are assumed to be carrying sufficient current to be saturated. Therefore, a low impedance path for discharging capacitances remote from the valve being fired will be available. For example, referring to figure 8.7;

(a) Valve V11 in the lower six-pulse bridge is conducting full load current. Valve V9 has failed commutation and thus current is commutating out of valve V1 into valve V9. Valves V1, V9 and V11 are each assumed to be conducting sufficient current to saturate their module reactors.

(b) Valve V12 in the upper six-pulse bridge is conducting full load current. Valve V2 has just turned-on and is picking up load current from valve V10. Valves V2, V10 and V12 are each assumed to be conducting sufficient current to saturate their module reactors.

(c) Valve V4 is assumed to be turned on by its overvoltage firing protection.

(d) Valve V3 experiences a rising voltage and is also turned on by its overvoltage firing protection. A 2μs delay is assumed in the turn-on of this valve, with respect to valve V4, to simulate the delay time of the BOD's and thyristors in valve V3.

8.3.2 Basic Assumptions

The equivalent circuit used to predict inrush current for non-repetitive operating conditions, is given in figure 8.7. The mathematical model is based upon the Sellindge converter station design, but with the modifications referred to in section 8.2.2(d). The valve which is exposed to the most severe inrush duty when it turns-on has been chosen to be the 'delayed' valve (V3). This valve is the one adjacent to the neutral DC busbar, such that the transformer and stray capacitances of the lower bridge discharge directly through the valve to the neutral DC busbar. Further, the energy initially trapped in the electrostatic field of a delta connected transformer is greater than that trapped in the electrostatic field of a

star connected transformer.[25] The delta connected secondary is, historically, associated with the lower six-pulse bridge[54].

It is assumed that the converter is operating at a load current of 1911A, which is equivalent to full load current for the Cross-Channel scheme. The module reactors of all the conducting valves are considered to be saturated: therefore a low impedance path for discharging capacitances, remote from the valve being fired, will be available.

The non-repetitive inrush is assumed to arise from protectively turning-on valve V4, in the upper six-pulse bridge from a voltage given by the highest voltage for which BOD firing will just occur. A valve-voltage of 400kV has been used as for the Sellindge converter valves (viz 3.2kV x 125); the initial voltage across the delayed valve (V3) is also 400kV. However, the turn-on of valve V3 is assumed to be delayed by 2μs with respect to valve V4, thus, the stray capacitances in the lower six-pulse bridge charge to a higher voltage by the instant valve V3 turns-on: this exacerbates the resulting inrush current for the delayed valve.

The damping component tolerances are chosen such that there is maximum stored energy at the instant of firing (i.e. maximum C_d = 2.728 μF per level for a valve of 100

levels) and the initial step of current injected into the thyristor at turn-on is maximized (i.e. minimum R_d = 27.5Ω per level for a valve of 100 levels). These damping component values are scaled from those appropriate to the Sellindge converter valves, (i.e. C_d = 3.4μF per level maximum, and R_d = 22Ω per level minimum, for a valve of 125 levels). This gives the same magnitude of the 'step' of current from the damping network, at turn-on, and the same time constant of decay of the damping circuit current.

8.3.3 Predicted Inrush Waveforms

The resulting inrush prediction is shown in Figure 8.8. An equivalent prediction for the Sellindge converter is shown in figure 8.9. The salient features of these predictions are given in Table 9.

For the Sellindge converter following the turn-on of valve V3, there was a delay of approximately 1.5μs, in the growth of the main-circuit of this valve (figure 8.9). This delay was provided by the ferrite reactor (L1a) (figure 3.18) and allowed time for the transfer of current from the auxiliary cathode to the main current-carrying area. However, due to the low current (say 40A) at which the ferrite saturates, a damping circuit charging current could saturate the, series connected, ferrite reactors removing the period of low di/dt at valve turn-on. The quasi-linear inductor (L1b) present within each thyristor

module of the Sellindge converter limits the resulting rate-of-rise of current and magnitude of first current peak to acceptable values.

The incremental inductance of the proposed reactors (figure 6.21) is of significant value up to relatively large magnitudes of current. Hence, the damping circuit charging current would not be expected to make a significant difference to the predicted non-repetitive inrush current, (figure 8.8).

The circumstances resulting in the non-repetitive inrush include commutation failure of valve V9 (figure 8.7). At the time of commutation failure, the current in valve V9 may have decreased to a low value, allowing the area of the thyristor junction in conduction to decrease. A worst-case for the thyristors in valve V9 is when the thyristor current is assumed to be nearly zero at the instant when commutation failure occurs; thus, the thyristors in this valve may have to 'respread' as the current in the valve increases. In these circumstances, in order to achieve an initial current of sufficient magnitude to saturate the proposed reactors, approximately 100μs must have elapsed since valve V9 failed commutation. Figure 8.8 shows the current through valve V9 approximately 100μs after V9 failed commutation. A peak of current (4754A) occurs in valve V9 9μs after the delayed valve (V3)

turns-on. This peak of current exceeds the magnitude of the peak inrush current in the delayed valve (V3). However, the predicted rate-of-rise of current, in valve V9, is less onerous than that through valve V3.

The turn-on of valve V3 is delayed with respect to valve V4: hence, the stray capacitances shunting valve V3 conduct a proportion of the displacement current from the stray capacitances of the upper six-pulse bridge. Thus, the magnitude of voltage across valve V3 will increase and reaches a maximum value of 417.9kV, 0.94μs after valve V3 turns-on (i.e. 2.94μs after valve V4 turns-on).

The inrush current prediction for valve V4 (figure 8.8), which is modelled as having no turn-on delay, shows there to be a maximum di/dt of about 179A μs^{-1} up to an elapsed time of 6μs, after V4 turns-on. The module reactors in the delayed valve (V3) then saturate, and this results in a low-impedance discharge path for the capacitances of the upper six-pulse bridge. Hence, when this occurs the rate-of-rise of current through valve V4 increases to 672A μs^{-1}. The peak current in valve V4 is 2227A and occurs at an elapsed time of approximately 11μs after V4 turns-on.

8.3.4 Comments

The predicted inrush currents are of a very similar nature to those predicted when a co-ordinating current is

pre-established in the surge arrester, (see section 8.2). Absolute magnitudes of salient points, of the inrush prediction, compare well with that obtained with 2kA co-ordinating current, at valve overvoltage protective level.

The predicted current transients would not obviously be damaging to the thyristors, although this requires experimental confirmation; thus, no change is recommended to the proposed characteristics of the two-part reactor. Due to the similar nature of these predictions with those obtained for the pre-established co-ordinating current in the surge arrester (section 8.2), it is recommended that a single laboratory test reproducing the inrush current prediction for 3kA co-ordinating current, at valve overvoltage protective level, be carried out. This magnitude of co-ordinating current gave a 'worst-case' prediction.

8.4 PRELIMINARY STUDY OF VALVE FIRING TRANSIENT INTERACTION: 12-PULSE NOTCH

8.4.1 Introduction

When a valve turns-on, the collapse of the valve-voltage is coupled electrostatically to other valves within the 12-pulse bridge. During 12-pulse operation, the phase-orientation of the voltages in the two six-pulse bridges is such that conditions will inevitably arise when the firing transient of one valve is transferred onto a

closely coupled adjacent valve while it is in its recovery phase (Chapter 3.4), (figure 8.10). If the voltage transient (termed a voltage 'notch') is too severe it may either trigger forward recovery protection or reduce a design margin allowed for AC voltage waveform distortion.

Referring to figure 8.11, when valves in firing positions 1, 5 or 9 turn-on, the collapse of voltage will be transferred onto valves 8, 12 and 4 respectively, at the time when the latter are recovering. Each pair of valves are closely coupled electrostatically.

The magnitude and rate-of-rise of the voltage 'notch' depend upon:-

(i) The voltage from which the valve is fired and the rate at which the valve-voltage collapses;[58]

(ii) The distribution of stray and component capacitances across the entire 12-pulse converter pole[58] (in particular the relative effective capacitances to earth at the midpoint busbar, the DC busbar and the transformer valve winding terminals);

(iii) Overlap angle[58], this is load current dependent.

The ability of a recovering thyristor to withstand a positive notch of voltage, without turning-on, depends largely upon:

(i) The position of the voltage notch relative to valve current zero[58] (nominally at $\gamma = 15°$), (see figure 8.10).

(ii) The rate-of-rise of positive going thyristor voltage, at voltage zero crossing, across the recovering valve.[58]

(iii) The time and magnitude of any ensuing increased rate-of-rise of positive going voltage.[58]

(iv) The time and magnitude of the peak positive value of the thyristor voltage as a result of the voltage notch.[58]

For the Sellindge converter valves, negative gate bias was applied, during recovery, to remove surplus charge carriers from the thyristor. This assisted the ability of the thyristor to withstand a positive going voltage notch without turning-on. This technique is not suitable for future thyristors, thus, the converter electrical circuit must effectively control the degree of electrostatic coupling to within safe limits.

The overlap angle determines the position of the voltage notch relative to the instant at which current zero occurs. The recovery voltage on which the voltage notch is superimposed is dependent upon the AC sinewave voltage condition and the nominal values of the valve damping components. In addition, the differences in recovered

charge and component tolerances will influence the distribution of the transient and steady-state portions of the recovery voltage between the levels of the valve (see Appendix VI). This can, for some levels, degrade the conditions required to ensure safe forward recovery.

The preliminary 12-pulse notch investigation[59] is confined to the operating condition where the extinction angle (γ) is controlled to a nominal 15°. In practical schemes, sudden and unforeseen variation in bridge current or transformer voltage prior to, or during, commutation can cause variation in the overlap angle and/or the timing of the positive going sinewave voltage. Consequently, the actual γ at recovery may differ from the desired value. In cases of gross disturbance, actual γ can be reduced to, or near to, zero leading to inevitable commutation failure. The existence of the 12-pulse notch will erode the margin between valve recovery time and actual γ at recovery. No studies have been performed to assess the significance of this effect when γ, at recovery, is less than 15°.

8.4.2 Basic Assumptions

(a) The transformer secondary windings are assumed to be connected as for the Sellindge converter station: for a Yy0 and Yd11 connected transformer, the phase displacement of the windings in the bridges is such that outer valves in the lower six-pulse bridge are fired at the instant when inner valves in the upper

six-pulse bridge, in the same stack, are undergoing recovery. It can be seen from the equivalent circuit (figure 8.11) that if valve V9 is fired when valve V4 is in its recovery phase, the collapse of voltage across valve V9 is coupled, electrostatically, onto valve V4.

(2) The electrical circuit studied is based upon the design of the Sellindge converter station, with the modifications referred to in 8.2.2(d), and together with the following modifications and assumptions;

(i) A 25nF fast-grading capacitor (C_{fg}) is connected in parallel with each thyristor level. No fast-grading resistance is represented.

(ii) 0.2nF valve stray capacitance (C_B) is lumped, in the representation, with the fast-grading capacitance (see figure 8.11).

(iii) The damping component tolerances are chosen such that there is maximum stored energy at the instant of firing (i.e. maximum C_d = 2.728μF per level for a valve of 100 levels). The minimum resistance value of the damping resistor is 27.5Ω per level for a valve of 100 levels. These damping component values are scaled from the values appropriate to a Sellindge converter valve (i.e. C_d = 3.4μF per level maximum, R_d = 22Ω per level minimum for a valve of 125 levels).

(c) The peak line-to-line valve winding voltage is 245.5kV peak (see Chapter 6.4.13). Normal full load inverter operation is given by $\gamma = 15°$ and $U_o = 20.47°$, (calculated from the equations of Appendix I). This yields a valve firing voltage (V_f) of 142.5kV.

(d) Studies have been performed firstly with single-section transformer representations. The stray capacitance of the busbars and bushings of valves V3, V7 and V11 were included within the electrostatic model of the delta connected transformer.

(e) The study was then repeated with refined (five-section including end-effects) transformer representations[36][37]. The busbar and bushing capacitances are included in the shunt capacitance at the termination of the valve winding connections of the transformer model.

8.4.3 Predicted Results

(a) Single-section and refined transformer representation

Figure 8.12 shows the predicted voltage notch, obtained with a single-section transformer representation, across the recovering valve (V4) and also across the thyristors within valve V4, when valve V9 turns-on. Similarly, figure 8.13 shows the predicted voltage notches

obtained with a refined transformer representation. In both cases, the predicted voltage notch reverses the voltage both across valve V4 and the thyristors within valve V4.

The salient features of the voltage notches are tabulated in Table 10. The magnitude of the predicted voltage notches across the thyristors within the recovering valve (V4), for the single-section and refined transformer representations are 20% and 21.26% of the firing voltage of valve V9, respectively.

The Sellindge converter station studies [58] utilized a single-section transformer model; the predicted magnitude of the voltage notch was 25% of the firing voltage, with a 25nF per level fast-grading capacitor and a 12.5Ω per level fast-grading resistor, at 1p.u. load current. However, the predicted voltage notch[58] did not result in a voltage zero crossing in the voltage of the recovering valve; this is attributable to the larger overlap angle resulting from a lower peak line-to-line voltage (see Appendix I). Hence, the initial value of the reverse voltage on the recovering valve was larger in magnitude, by about 41.5%, whilst the valve firing voltage is lower by about 21.6%, in comparison with the 'development' circuit.

The, positive going, voltage zero crossing associated with the thyrsitors of valve V4 occurs at an elapsed time of approximately 530μs after current zero in valve V4. The predicted dV/dt's, immediately following the positive going voltage zero crossing, are approximately 51V μs^{-1} per thyristor and 41.5V μs^{-1} per thyristor for the single-section and refined transformer representations, respectively.

For the study which utilized single-section representations of the transformers, the predicted dV/dt immediately following, positive going, thyristor voltage zero crossing was the maximum dV/dt across the thyristor during the period of positive voltage. However, for the study which used refined representations of the transformers, the maximum dV/dt during the period of positive voltage, across the recovering thyristors, was 46.3V μs^{-1} per thyristor and occurred approximately 0.5μs after, positive going, thyristor voltage zero.

Figure 8.14 shows the Sellindge converter station module forward recovery protection characteristic, without negative gate bias, for a junction temperature of 75°C. An equivalent, estimated characteristic for the next generation of thyristors is also shown in figure 8.14.

Figure 8.14 indicates that if the recovering thyristors are not to be protectively fired when they

experience a forward dV/dt of 51V μs^{-1}, obtained with a single-section transformer representation, a minimum elapsed time of 490μs, measured from current zero in the recovering valve, is required. Alternatively, figure 8.14 also indicates that for the less onerous prediction of 46.5V μs^{-1}, obtained with the refined transformer representation, a minimum elapsed time of about 475μs since current zero crossing is required, if the recovering valve is not to be protectively turned-on. The overlap angle modelled is 20.47°, therefore, the voltage notch is 9.53°(530μs) after current zero crossing in the recovering valve (assuming an undistorted sinewave recovery voltage). Thus, basing the forward recovery capability of the thyristors upon the estimated characteristic, the thyristors in the recovering valve (V4) would have successfully recovered under the modelled operating condition. However, the margin is not great and leaves little margin for voltage distortion of the AC sinewave.

The predicted voltage notch, across the recovering valve, is mainly due to a voltage developed across the damping resistors in that valve. For the refined transformer representation the magnitude of the voltage notch, across the thyristors within the recovering valve, is 30.28kV, of which 1577 volts (5.2%) is as a result of a positive change in the damping capacitor voltage. Thus, 10.44A of current flowing through the damping resistors of the recovering valve, results in 94.8% of the magnitude of

the predicted voltage notch. Damping circuit stray inductance was not represented, however, its influence upon the severity of the voltage notch is expected to be small in comparison to that of the damping resistor.

8.4.4 Comments

The main cause of the voltage notch, across the recovering thyristors, is the voltage developed across the damping resistors. Thus, worst-case damping resistor tolerances, assuming tolerances of ±5% of a nominal value, may exacerbate the predicted dV/dt by approximately 10% on several levels within the recovering valve.

A spread in reverse recovered charge, between thyristors, will also increase the likelihood of turn-on by forward recovery protection. Figure 8.15 shows the notch superimposed upon several undistorted sinewave recovery voltages such that the positive magnitude of the notch, and dV/dt at positive voltage zero crossing, is dependent upon the spread in reverse recovered charge and value of damping capacitor, ($\Delta V = \Delta Q_{rr}/C_d$).

The absolute magnitude of the voltage notch and the forward dV/dt across a recovering thyristor at, positive going, voltage zero crossing is dependent upon the load current[58]. As the load current is reduced the overlap angle is decreased; the initial voltage from which the valve is fired is reduced too, thereby reducing the

absolute magnitude of the voltage notch. However, the magnitude of the sinusoidal voltage across the recovering valve, at the instant of valve firing, is also reduced. Thus, the voltage notch, superimposed upon the sinewave recovery voltage, may take the voltage of the recovering valve significantly positive, though later in time.[58] As the voltage zero crossing is later in time the thyristors are capable of withstanding an increased dV/dt, during recovery, without requiring protective firing (figure 8.14).

The preliminary results show that, with the proposed reactor characteristics, the magnitude of the voltage notch, as a proportion of the firing voltage, is slightly less onerous than for the Sellindge converter station. However, unlike the Sellindge converter station, the technique of applying a negative gate bias to assist thyristor turn-off is unsuitable for future thyristors. Thus, other techniques for mitigating the effect of the voltage notch will be required[59] (see Chapter 9).

The magnitude of acceptable dV/dt across a recovering thyristor, as a function of elapsed time following current zero in the recovering valve, at a specified junction temperature, must be determined in order to assess the acceptability of these predictions. However, at present the duty is presumed safe for the thyristors and, therefore, no modification to the proposed reactor characteristics is required.

8.5 PRELIMINARY INVESTIGATION OF VALVE RESPONSE TO IMPULSE TEST-VOLTAGE

8.5.1 Introduction

By international convention (IEC 700) thyristor valves must be capable of being tested at voltages 15% above the protective level of the arrester for switching and lightning-impulses (section 8.2), and 20% above for front-of-wave impulses. The thyristor valve must be demonstrated to survive the rates-of-rise of forward voltage and the magnitude of voltage associated with the wavefronts, (Chapter 3.2.3).

The valve must withstand the voltage in the reverse direction for all wavefronts. In the forward direction, the thyristors may be relieved of excessive voltage stress by overvoltage firing protection. During the application of a lightning-impulse or front-of-wave impulse, the valve may also be protectively fired by dV/dt protection. Irrespective of the mode of protection, the thyristors must be adequately protected against the ensuing inrush current, (Chapter 3.3.2).

The preliminary studies consider the voltage stresses on a valve which has only sufficient thyristors such that the sum of the reverse withstand voltages are equal to the switching impulse test level (section 8.2). Thus, the saturating reactors are utilized to hold-off the extra voltage associated with the lightning-impulse and front-of-wave impulse test voltages.

8.5.2 Basic Assumptions

Studies have been performed with an electrical circuit based upon the existing design of the Sellindge converter circuit but with the modifications detailed in section 8.2.2(d). The studies modelled the proposed valve reactor characteristics (Chapter 6.4.9).

In addition to the above, the following assumptions were made during the derivation of the model;

a) The fast-grading circuit was omitted from the model; thus, appropriate connection of the fast-grading capacitor could be used to reduce the severity of the predicted dV/dt. For very fast wavefronts, e.g. lightning-impulse and front-of-wave impulse, the stray capacitances within a valve and from the valve to earth, will influence the voltage distribution. Hence, the mode of connection of the fast-grading circuit is important in order that it adequately controls the voltage distribution within an off-state valve.

b) The off-state thyristors were modelled as open-circuits; the non-linear capacitance of the thyristor junction was not modelled. Thus, the severity of the predicted dV/dt across each thyristor may be reduced by appropriate modelling of the voltage-dependent, junction capacitance.

c) Damping circuit stray inductance was not represented: hence, the severity of the predicted dV/dt and the magnitude of the voltage across each thyristor, would be increased if the damping circuit stray inductance were to be modelled.

d) The predicted thyristor dV/dt is obtained from a simplified mathematical model of a thyristor valve (figure 8.16). Represented in parallel with the thyristor valve there is an 'impulse generator' (Chapter 4.6) of negligible source impedance. Thus, the presence of the valve and stray capacitances does not modify, to any degree, the impressed voltage waveform.

e) The initial design limit for the maximum allowable, forward, dV/dt across a thyristor is 1kV μs^{-1}, as for the Sellindge converter station design. The MEDL 75mm thyristors have a proposed capability of 1.5kV μs^{-1}.

f) The current and voltage associated with the thyristor valve, as a result of an impressed impulse, can be input directly into a 'service-condition' representation of the valve turning-on (figure 8.17). No surge arresters are modelled within the six-pulse bridge; thus, the results of these inrush studies are not fully representative of a 'service-condition' turn-on. However, the results of these predictions are required to formulate an impulse generator with an appropriate source impedance, for test purposes, which results in both the appropriate test-voltage impulses across the valve and the inrush current (without surge arresters) following valve turn-on.

In the case of a 'standard test' switching-impulse (as defined in IEC 60) (250/2500 μs), the pre-established current is modelled as flowing through the on-state valve

in the lower-half of the six-pulse bridge, via the leakage inductance of the transformer, and back through the damping circuits within the valve about to turn-on, (figure 8.17).

In the cases of a lightning-impulse and front-of-wave impulse the pre-established current through the off-state valve, is modelled as flowing through the stray capacitances associated with the transformer, busbars and bushings, (figure 8.18).

g) The valve considered to be subject to the impulse may turn on due to excessive dV/dt or by overvoltage firing. This valve is chosen to be adjacent to the neutral DC busbar because the energy initially trapped in the electrostatic field of the delta winding is greater than that of the star transformer[25]; the delta winding has historically been associated with the lower six-pulse bridge[54].

h) To maximize both the initial step current injected into the thyristor at turn-on, and the magnitude of pre-established valve current, the damping capacitor is chosen to be of maximum value (i.e. C_d maximum = 2.728μF per level for a valve of 100 levels), and the damping resistor is chosen to be of minimum value (i.e. R_d minimum = 27.5Ω per level for a valve of 100 levels). These damping component values are scaled from those appropriate to a Sellindge converter valve (i.e. C_d = 3.4μF maximum, per level, and R_d = 22Ω minimum, per level for a 125 level valve).

However, the most onerous dV/dt and magnitude of voltage across a thyristor, would be obtained when one of these levels has a maximum tolerance damping resistor and a minimum tolerance damping capacitor.

i) The study representing turn-on of the thyristor valve, with a pre-established valve current, was performed with a single-section transformer model. The busbar and valve stray capacitances were included within the transformer electrostatic model, (see Chapter 4.5).

j) With reference to the 'typical valve insulation co-ordination diagram' shown in figure 8.1, the studies performed[60] are based upon the following assumptions;

   i) The thyristor reverse withstand capability exceeds the forward withstand capability by 15%. Thus the reverse withstand is given by:

$$(400 \times 1.15)\text{kV} = 460\text{kV}$$

   ii) The switching-impulse protective level of the surge arrester is 15% below the sum of the thyristor reverse withstands and is thus given by:

$$\frac{460}{1.15}\ \text{kV} = 400\text{kV}$$

   iii) The arrester protective level, for a lightning-impulse, is 4% above that for a switching-impulse.

   iv) The arrester protective level, for a front-of-wave impulse, is 8% above that for a lightning-impulse.

1) By international convention (IEC 700) the thyristor valves must be capable of being tested at voltages 15% above the protective level of the arrester for a switching-impulse and lightning-impulse and 20% for a front-of-wave. The magnitude of the test impulses are thus;

i) Switching-impulse;

$$400 \times \frac{1.15}{1.15} \times 1.15 = 460\text{kV}$$

ii) Lightning-impulse;

$$400 \times \frac{1.15}{1.15} \times 1.04 \times 1.15 = 478.4\text{kV}$$

iii) Front-of-wave;

$$400 \times \frac{1.15}{1.15} \times (1.04 \times 1.08) \times 1.20 = 539.7\text{kV}$$

m) Several of the inrush studies are performed with a pre-established current represented as flowing in the electrostatic-field of the converter transformer (i.e. lightning-impulse and front-of-wave impulse studies) and are, thus, equivalent to the test-conditions. (Test-conditions would normally include a capacitor to represent the scheme 'lumped' stray capacitances). The switching-impulse inrush studies represented the pre-established valve-current as flowing through the leakage inductance of the converter transformer. Thus, these studies are not truly representative of a turn-on during test. However, these inrush current predictions are

more onerous than those experienced during test; this is attributable to the magnetic energy associated, initially, with the commutating inductance of the converter transformer.

8.5.3 Initial Conditions; Inrush Current

During the application of a switching, lightning or front-of-wave impulse, a thyristor valve must be relieved of excessive voltage stress in the forward direction, by dV/dt or overvoltage protection. Irrespective of the mode of protection, the thyristors must be adequately protected against the ensuing inrush current. The impulse will act to pre-saturate, to a degree, the inrush limiting reactors. Thus, it is necessary to perform studies to ensure that this pre-saturation does not degrade unduly the inrush current limiting function of the reactors.

The initial conditions for the 'inrush studies', were selected from the following (where appropriate);

i) Thyristor valve protectively turning-on from 400kV (sum of individual overvoltage protection levels) across the thyristors, with the corresponding initial current in the valve.

ii) Thyristor valve turning-on from maximum valve-current (reactors saturated to the greatest degree) - but only if this occurs before the sum of the, individual, overvoltage protection levels is 400kV.

iii) An instant in time between the occurrence of maximum valve-current (ii) and the sum of thyristor voltages reaching 400kV (i).

iv) The thyristors within the valve are assumed to be protectively turned-on when the level dV/dt exceeds 1kV μs^{-1}. An elapsed time of 1μs is then assumed necessary for the protection to gate the thyristors into conduction. The currents and voltages appropriate to this 'delayed' time are used as initial conditions.

8.5.4 Predicted Results

8.5.4.1 Switching-impulse

Figure 8.19 shows a switching-impulse, whose prospective peak voltage is 460kV at an elapsed time of 250μs after the start of the study. The rise time of this impulse is 250μs from 0% to 100% of peak voltage. The wavetail decays to approximately 50% of peak voltage 2500μs after the occurrence of the peak. The resulting sum of thyristor voltages, within the off-state valve, is also shown in figure 8.19. The 'maximum' predicted dV/dt across a thyristor, within the off-state valve, is 71.8V μs^{-1}. This dV/dt occurs at an elapsed time of 10μs after the start of the study.

The prospective maximum reverse voltage across the off-state thyristors is 461.2kV, which exceeds the assumed reverse withstand capability by 1.2kV per valve.

Table 11 contains the three sets of initial conditions obtained for the, six-pulse bridge, inrush studies. These initial conditions correspond to i), ii), and iii) in section 8.5.3. The most onerous of the inrush predictions (figure 8.20) is that obtained when the sum of the thyristor voltages is 400kV [corresponding to (i)]. This prediction gives the highest rate-of-rise of current to first current peak [638A μs^{-1}, 4.6μs after valve turn-on], the highest peak inrush current [1346A, 5.6μs after valve turn-on] and the lowest first current trough [117.5A, 15μs after valve turn-on].

The 'maximum', 'service-condition', dV/dt predicted across a thyristor within the series connected off-state valve and across a level of the valve, are 1.16kV μs^{-1} per thyristor and 1.35kV μs^{-1} per level respectively. These maximum dV/dt's occurs, during turn-on, when the sum of thyristor voltages within the valve is equal to 400kV. For the Sellindge converter station a dV/dt greater than approximately 1kV μs^{-1}, across a thyristor level, would result in the thyristor being protectively fired. The consequences of protectively firing the thyristors within the series connected valve have not been examined. Table 12 gives the salient results of the above studies, together with those obtained for turn-on from 400kV valve-voltage with static initial conditions, (see chapter 6.4.9).

The effect of considering the dynamic initial conditions is to increase the severity of the predicted inrush current. It is not expected that the increased severity would endanger the integrity of the thyristors within the commutating valve. However, the more onerous 'service-condition' dV/dt, occurring across the thyristors within the series connected valve, may result in protective turn-on of the series valve.

8.5.4.2 Lightning-Impulse

Figure 8.21 shows a lightning-impulse whose prospective peak voltage is 478.4kV at an elapsed time of 1.2μs after the start of the study. The rise time of this impulse is 1.2μs from 0% to 100% of peak voltage. The wavetail decays to approximately 50% of peak voltage 50μs after the occurrence of the peak. The resulting sum of thyristor voltages, within the off-state valve, is also shown in figure 8.21. The 'maximum' dV/dt across a thyristor within this valve is 3.14kV μs^{-1}. This dV/dt occurs at an elapsed time of 0.6μs after the start of the study. The level dV/dt exceeds 1kV μs^{-1} thus, the thyristors are assumed to be protectively fired.

The maximum reverse voltage across the off-state thyristors is 424.8kV, which is below the assumed reverse withstand capability of 460kV. The saturating reactors are acting to 'hold-off' the difference in applied valve-voltage and actual voltage across the thyristors.

Table 13 contains the two sets of initial conditions obtained, from the above, for the turn-on studies. These initial conditions correspond to cases i) and iv), described in section 8.5.3. The pre-established valve current is represented as flowing in the electrostatic-field of the transformer (figure 8.18).

Table 15 contains the salient results of the two sets of inrush predictions. The most onerous of the two predictions (figure 8.22), is that obtained with a sum of thyristor voltages equal to 400kV.

8.5.4.3 Front-of-wave Impulse

Figure 8.23 shows a front-of-wave impulse whose prospective peak voltage is 540.3kV at a time of 0.25μs after the start of the study. The rise time of this wavefront is 0.25μs from 0% to 100% of peak voltage. The wavetail decays to approximately 50% of peak voltage, 5μs after the occurrence of the peak. The sum of thyristor voltages, within the off-state valve, is also shown in figure 8.23. The peak voltage across the off-state thyristors is 381kV, and is thus below the assumed reverse withstand capability of 460kV. The 'maximum' dV/dt across a thyristor, within the off-state valve, is 5.02kV μs^{-1}; this dV/dt occurs at an elapsed time of 0.15μs after the start of the study. The level dV/dt exceeds 1kV μs^{-1}, and thus the thyristors are assumed to be protectively fired.

The initial conditions obtained for the six-pulse bridge turn-on studies are shown in Table 14. These initial conditions correspond to case iv), described in section 8.5.3. The pre-established valve current is modelled as flowing in the electrostatic field of the transformer (figure 8.18). The consequent inrush current is shown in figure 8.24.

Table 15 gives the salient features of the inrush prediction. This prediction, is slightly more onerous than the most severe prediction obtained for the lightning-impulse turn-on studies.

8.5.5 Comments

In order to assess the effect of a 'genuine' insulation failure upon the operation of the converter bridge, the equivalent electrical circuit of the converter station must include surge arresters, and more accurately modelled valve stray capacitances.

The majority of the inrush predictions indicate that the dV/dt across the thyristors within the series connected, off-state, valve exceeds 1kV μs^{-1}. The consequences of this series connected valve being protectively fired have not been studied. However the assumed setting of the dV/dt protection of 1kV μs^{-1} per level and assumed thyristor capability of 1.5kV μs^{-1} are both low. Hence, thyristor capabilities of at least 2kV μs^{-1} and preferably 3kV μs^{-1} should be specified.

Subsequent laboratory evaluation of the 75 mm MEDL thyristors,[61] revealed that the thyristors would turn-on, non-destructively, when dV/dt rates of 4kV μs^{-1} and 7kV μs^{-1} were impressed across a thyristor for voltage excursions of 2.7kV and 1.7kV respectively.

Recent laboratory evaluation [49][50] of the MEDL thyristors have shown that a maximum, repetitive, di/dt of 600A μs^{-1} to first current peak produces a situation which is marginal from the point of view of the thyristors integrity. Hence, the predicted inrush transients, though severe, are not obviously damaging to the thyristors; the inital few microseconds of modest di/dt are likely to be adequate to allow sufficient conducting area to be established. Thus, at present the duties are presumed safe for the thyristors; hence, no modification of the characteristics of the two-part reactor is required.

The severity of the predicted forward dV/dt may be reduced by accurate modelling of the off-state thyristors, and appropriate connection of the fast-grading circuit. However, this gain will be somewhat offset by the modelling of damping circuit stray inductance.

8.6 SUMMARY

This chapter has reported the results of studies which were performed to prove that the characteristics of the proposed reactor are suitable and adequate for controlling both repetitive and non-repetitive voltage and current transients.

In taking economic advantage of the asymmetrical voltage capability of thyristors the surge arrester protective level is co-ordinated with the reverse capability of the valve. Consequently, a significant co-ordinating current may be pre-established in the arrester when the valve overvoltage protective level is reached. The arrester current is available for immediate commutation into the valve as the valve anode voltage falls.

Non-repetitive inrush current may arise as a result of a commutation failure and overvoltage firing sequence of events. All the capacitances of the 12-pulse bridge may then discharge to ground via a valve turning-on.

The inrush predictions for the above mentioned situations do not appear damaging to the integrity of the thyristors; the proposed, reactor characteristics limit the initial di/dt to within safe limits for several microseconds. This should allow sufficient time for adequate spreading of the area in conduction, prior to reactor saturation.

During 12-pulse operation, the phase-orientation of the voltages in the two six-pulse bridges is such that the firing transient of a valve is transferred to a closely coupled recovering valve, during inverter operation. This may lead to repetitive commutation failure of a recovering valve.

The proposed reactor characteristics result in a magnitude of voltage notch which, as a proportion of the firing voltage, is slightly less onerous than the notch which occurs in the Sellindge converter station. Similarly, refined modelling techniques decrease, slightly the severity of the predicted voltage notch. However, the technique of applying negative gate bias to aid recovery of the thyristors is not suitable for future thyristors: thus, other techniques for mitigating the effect of the voltage notch are required (Chapter 9).

By international convention thyristor valves must be demonstrated to survive the rates-of-rise of forward voltage and the magnitude of voltage associated with switching, lightning and front-of-wave impulses. The valve may be protectively turned-on by forward dV/dt or overvoltage protection. Irrespective of the mode of protection the thyristors must survive the subsequent inrush current.

The preliminary studies considered the voltage stresses on a valve which has only sufficient thyristors such that the sum of the reverse withstand voltages are equal to the

switching-impulse test level. Thus, the proposed reactors are utilized to hold-off the additional voltage associated with lightning and front-of-wave impulses.

The reactors are pre-saturated to a degree, at valve turn-on, by the flow of charging current through the damping circuit of the off-state valve. This charging current is as a result of the test-impulse impressed across the valve. The consequent inrush current, at valve turn-on, appear to be acceptable and is not expected to endanger the integrity of the thyristors; thus, no modification is required in the proposed 'two-part' reactor characteristics.

9. GENERAL CONCLUSIONS AND ONGOING WORK

9.1 GENERAL CONCLUSIONS

Ideal characteristics have been developed for inrush control components; these characteristics are designed to achieve the required inrush control for a minimum overall cost. The existing circuit design of the Sellindge converter station was used as a basis for proposing modifications for future converter stations.

Initial costings show that the likely saving in the cost of inrush control hardware should be approximately £37,600 per valve; giving a reduction of about 50% in comparison with the cost of inrush control hardware associated with a valve of the Sellindge converter station. In addition, the initial investigations show a significant reduction in evaluated losses associated with the inrush control hardware estimated to be worth more than $137,500 per valve at adjudication.

The investigations were divided into two main parts; firstly, a suitable method of providing inrush control for a minimum overall cost was developed. Subsequently, proving studies were performed to show the suitability of the proposed reactor for controlling both voltage and current transients during repetitive, abnormal and non-repetitive operating conditions.

The proposed method of inrush control utilizes a two-part saturating reactor: one-part of the reactor provides controlled eddy-current losses, the second part is assumed to be lossless. The eddy-current losses are specified such that the inrush current transient is adequately damped without incurring excessive losses during normal load-current commutation. The inductance with current characteristics of the reactors retain the pertinent features of the inrush current to within initially specified limits, for a minimum total flux requirement. This is assumed to result in a minimum volume and hence a minimum cost of magnetic material.

The second part of the thesis reports the results of studies which utilized the proposed characteristics.

Investigations were performed to find the sensitivity of the magnitude of the voltage transient and adjudicated losses, during thyristor recovery, to the characteristics of the reactor. The results indicate that it is not cost-effective to modify the proposed inductance with current characteristics of the reactor to reduce the adjudicated losses associated with the recovery transient.

To prove the adequacy of the proposed reactor for controlling both voltage and current transients, the following operating conditions were also studied:-

a) Co-ordinating current pre-established in an arrester.

b) Commutation failure in a 12-pulse bridge.

c) 12-pulse inverter operation.

d) Voltage impulse across an off-state valve and consequent turn-on of the valve by dV/dt or overvoltage protection.

A study of the repetitive voltage transients occurring during 12-pulse inverter operation shows that the magnitude of the predicted transients, as a proportion of the firing voltage are less than those predicted for the Sellindge converter station. However, for the Sellindge converter station, negative gate bias was applied to the thyristors during recovery, which assisted their ability to withstand a positive going voltage notch. This technique is, however, not suitable for future thyristors, thus the electrical circuit of the converter station must effectively control the degree of electrostatic coupling to within safe limits. Hence, for future schemes, other techniques for reducing the severity of the voltage notch need to be developed.

The transients predicted for the other operating conditions (see a, b and d above) are not obviously detrimental to the integrity of the thyristors. Thus, no modification to the proposed characteristics is required.

The objectives of the work described in this thesis were to develop a method of controlling circuit transients for a minimum overall cost and to gain an understanding of the complex interactions of the electrical circuit; it is believed that these objectives have been achieved, and it is hoped that the results of this work will be useful in producing economic designs for future HVDC converter stations.

9.2 FURTHER WORK

Magnetic Material

The results of the theoretical investigations reported in this thesis have been discussed with several potential suppliers of magnetic materials. Some of these manufacturers are to provide 'representative' samples in the near future, whilst others are willing to invest capital into developing suitable magnetic materials. GEC TDPL have invested capital to facilitate the design and procurement of equipment for testing the performance of magnetic materials under pulsed conditions of excitation.

Further work should include the testing of samples of magnetic materials and the analysis of results. These results will indicate whether the characteristics of the ideal reactor have been attained and also verify, or otherwise, the validity of the mathematical model of the reactor.

Once a representative magnetic material is identified the proposed reactor may be built and evaluated. However, it is extremely unlikely that the exact characteristics of the ideal reactor will be obtained. Thus, the characteristics which are achieved should be mathematically modelled and the acceptability or otherwise, of the characteristics confirmed.

Non-coherent turn-on

Studies are required to prove the adequacy of the proposed characteristics for controlling circuit-transients which occur during non-coherent valve turn-on. These studies should be performed for a range of valve firing voltages to identify the worst-case for the last thyristor to turn-on.

12-pulse Inverter Operation

The results of the 12-pulse notch studies indicate that, for future schemes, a technique is required to reduce the severity of the voltage notch across a recovering valve. 94.8% of the magnitude of the predicted voltage notch is due to voltage developed across the damping resistors in a recovering valve. Thus, the magnitude of the voltage notch may be reduced by decreasing the resistance value of the damping resistor. However, to control the magnitude of the step current into the thyristor, at turn-on, the damping network could be connected from thyristor cathode and to shunt part of the proposed reactor (figure 9.1). Thus, further work is required to investigate this proposal and, if necessary, to identify an optimum 'split' in the reactor.

Fast-grading Circuit

Fast-grading capacitors are required primarily to control the distribution of voltage throughout a valve during fast voltage impulses. However, the fast-grading capacitors value and

electrical connection will influence other voltage transients, e.g., maximum rate-of-rise of voltage across an off-state thyristor. Thus, investigations are required to identify the optimum value and electrical connection of the fast-grading capacitor.

Converter Transformer

The transient interaction between the valve and converter transformer greatly influence valve design and cost. Thus, utilizing a converter transformer with an intershielded winding (instead of the interleaved winding assumed for most of the studies reported in this thesis) would, thus influence the magnitude of the circuit transients.

For future schemes it may no longer be economically advantageous to select a 'damping capacitor value'/'transformer, high-frequency resistance, winding design' in the manner described in Chapter 7.4. Instead, the transformer winding design may be selected for minimum fundamental frequency losses; a surge arrester may be used to control the magnitude of the recovery voltage during $\alpha = 90 + DOV$ operation. Similarly, it may be possible to reduce the value of the damping capacitor: however, its capacitance value must be sufficient to control the effects of differences in reverse recovered charge between thyristors.

The star-secondary converter transformer has historically been connected in the upper six-pulse bridge. However, the proposed reactor negates the original reasons behind this

connection; thus it may be advantageous for future schemes to connect the star-secondary in the lower six-pulse bridge. The energy initially trapped in the electrostatic-field associated with the star winding is less than that associated with the delta winding; hence, during normal continuous operation it should be advantageous to have the delta secondary remote from the neutral DC busbar. However, during conditions of commutation failure the duty on a valve, adjacent to the neutral DC busbar, is likely to be more severe than with the present position of connection of the transformers.

Thyristors

The predicted transients must be shown, experimentally, not to endanger the integrity of the thyristors. Experiments may show that the transients are well within the capability of next generation thyristors, thus allowing further magnetic material to be removed from the design, and reducing the overall cost of inrush control. Alternatively, additional magnetic material may be required to reduce further the severity of circuit transients.

General Comments

This thesis has reported the results of studies which are part of the development work on HVDC thyristor valves, presently being carried out at GEC TDPL, Stafford. In the future it is possible that, due to mechanical or electrical constraints, one or more of the initially assumed design parameters will be altered, necessitating a change in the electrical configuration of the circuit and further proving studies.

APPENDIX 1

CONVERTER OPERATION; STANDARD FOUATIONS

This Appendix gives, for the sake of completeness, the relationships which exist between various parameters during steady-state operation (see Chapter 2.4) of a converter station. These relations are used, where appropriate, to establish 'initial conditions' for a mathematical model, (Chapters 6.4.13, 7 and 8.4).

All of the following relations[10] consider the commutating reactance of a converter transformer.

1) Rectifier Operation

a) Voltage

$$V_d = \frac{1}{2} V_{co} [\cos\alpha + \cos(\alpha + U_o)] \quad (1)$$

or

$$V_d = V_{co} (\cos\alpha) - \frac{3X_c}{\pi} I_d \quad (2)$$

where,

$$V_{co} = \left[\frac{3(2)^{\frac{1}{2}}}{\pi} \right] V_c \quad (3)$$

b) Current

i) Incoming valve current is

$$i_n = \frac{I_d (\cos\alpha - \cos wt)}{\cos\alpha - \cos(\alpha + U_o)} \quad \text{for } \alpha < wt < \alpha + U_o \quad (4)$$

ii) Outgoing valve current is

$$i_n = I_d - I_d \frac{(\cos\alpha - \cos(wt - 2\pi/3))}{\cos\alpha - \cos(\alpha + U_o)} \quad (5)$$

$$\text{for } \alpha + \frac{2\pi}{3} < wt < \alpha + \frac{2\pi}{3} + U_o$$

iii) In between commutations the valve current is

$$i_n = I_d \text{ for } \alpha + U_o < wt < \frac{2\pi}{3} + \alpha \qquad (6)$$

iv) Direct current

$$I_d = \frac{V_c}{2^{\frac{1}{2}} X_c} [\cos \alpha - \cos (\alpha + U_o) \qquad (7)$$

2) Inverter Operation

a) Voltage

$$V_d = V_{co} \cos \gamma - \frac{3X_c}{\pi} I_d \qquad (8)$$

$$\text{or} \quad V_d = V_{co} \cos \beta + \frac{3X_c}{\pi} I_d \qquad (9)$$

$$\text{or} \quad V_d = \frac{V_{co}}{2} (\cos \beta + \cos \gamma) \qquad (10)$$

$$\text{where} \quad \beta = (\pi - \alpha) = (\gamma + U_o) \qquad (11)$$

b) Direct Current

$$I_d = \frac{V_c}{(2)^{\frac{1}{2}} X_c} (\cos \gamma - \cos \beta) \qquad (12)$$

3) Power Factor and Reactive Power

In the presence of perfect filters no distorting current flows beyond the filtering point, and the power factor can be approximated by the displacement factor[10], $\cos \psi$, where ψ is the phase difference between the fundamental frequency voltage and current components.

Under these idealised conditions, with losses neglected, the active fundamental AC power (P), is the same as the DC power[10], i.e. :

$$P = 3^{\frac{1}{2}} V_c I_a \cos\psi = V_d I_d \tag{13}$$

$$\text{and } \cos\psi = V_d I_d \, (3^{\frac{1}{2}} V_c I_a)^{-1} \tag{14}$$

$$\text{For rectifier operation: } \cos\psi \simeq \tfrac{1}{2} [\cos\alpha + \cos(\alpha + U_o)] \tag{15}$$

$$\text{and for inverter operation: } \cos\psi \simeq \tfrac{1}{2} [\cos\gamma + \cos\beta] \tag{16}$$

The reactive power (Q_a) is often expressed in terms of the active power[9], P:-

$$Q_a = P. \tan\psi \tag{17}$$

$$\text{and } \tan\psi = \frac{\sin 2\alpha + 2U_o - \sin(2\alpha + 2U_o)}{\cos(2\alpha) - \cos(2\alpha + 2U_o)} \tag{18}$$

Where U_o and α are expressed in radians.

From equations (18), (13) and (17), the active and reactive powers of a rectifier vary with the firing delay angle.

APPENDIX II

DERIVATION OF A HIGH-FREQUENCY WINDING REPRESENTATION FOR A TRANSFORMER

A transformer high-frequency winding representation allows the effects of high-frequency resistance (hfr), (Chapter 4.5), upon the operation and rating of components within a converter valve, to be considered[32][36][37]. This Appendix considers the manner in which the high-frequency resistance is included firstly in a single-section (lumped) representation of the transformer[32] and then secondly, in a refined representation of the transformer (Chapters 4.5 and 7.9).

Manufacturers of converter transformers can supply calculated information regarding the hfr of the winding[32], (figure 7.1). Thus, the hfr of a particular winding, may be determined for the extremes of a frequency range of interest.

a) Single-section representation of the transformer[32]

The hfr of the winding may be represented by a parallel combination of a resistance (R_p) and inductance (L_p)[32] (see figure A.II.1).

$$\text{Let } R_S\ (f_1) = R_1 \tag{1}$$

$$\text{and } R_S\ (f_2) = R_2 \tag{2}$$

where $R_S(f_1)$ and $R_S(f_2)$ are the values of the hfr at the lower and upper frequencies, respectively, of interest. The impedance (Z) of the L_p/R_p network is given by:-

$$Z = \frac{R_p X_p (X_p + jR_p)}{R_p^2 + X_p^2} \qquad (3)$$

where $X_p = 2\pi f L_p$

Neglecting the frequency dependence of an inductance then,

$$X_p(f_1) = 2\pi f_1 L_p \qquad (4)$$

and $$X_p(f_2) = 2\pi f_2 L_p \qquad (5)$$

Hence, equating the real part of impedance Z to the value of the hfr;

$$R_S = \frac{R_p X_p^2}{R_p^2 + X_p^2} \qquad (6)$$

Substituting firstly equations (1) and (4) into equation (6) and secondly equations (2) and (5) into equation (6) and re-arranging the resultant equations gives:-

$$R_p = \frac{R_1 R_2 (f_2^2 - f_1^2)}{R_1 f_2^2 - R_2 f_1^2} \qquad (7)$$

and rearranging equations (6) gives;

$$L_p = \frac{1}{2\pi f_2} \left[\frac{R_2 R_p^2}{R_p - R_2} \right]^{\frac{1}{2}} \qquad (8)$$

To calculate the transformer 'series' reactance (X_{LT}) (where $X_{LT} = 2\pi f L_{LT}$) (see figure A.II.1), the imaginary part of impedance Z is subtracted from the leakage reactance of a phase of the transformer (X_T).

Therefore, from equation (3)

$$X_S = \frac{R_p^2 X_p}{(R_p^2 + X_p^2)} \qquad (9)$$

where X_S is the imaginary part of impedance Z, determined at fundamental frequency.

Hence, at fundamental frequency;

$$X_{LT} = X_T - X_S \qquad (10)$$

b) Refined representation of the transformer

End-effects (Chapter 4.5.3), are taken into account by allowing the following (figure 4.10);

a) Ground Capacitance (C_G) at the end of a coil to rise to twice its value compared with the centre.

b) Interturn capacitance (C_I) and leakage inductance (L_T) decrease at the end to half their values at the centre of a finite coil.

At the end-sections, of a refined n-section representation of a transformer, the value of high-frequency resistance $[(R_p)/n]$ is considered to be identical to that at the centre of a finite winding [frequency of excitation is considered to be unaltered (see Chapter 4.5.3)]. However, the eddy-current losses are reduced by virtue of a decreased induced e.m.f. Thus, the value of L_p is considered to be reduced to half the value at the end compared with the centre of a finite winding, (see figure 4.11).

$$L_{p(end)} = \frac{L_{p(central)}}{2} \qquad (11)$$

The hfr of the winding is represented, for an n-section model, by n series-connected sections of a parallel combination of a resistance and inductance (see figure 4.11).

To determine the values of R_p and L_p, the central sections of the winding are lumped together as are the two-end sections (see figure A.II.2). Figure A.II.2 is drawn showing only the L_p/R_p networks as only these are pertinent in obtaining the values of R_p and L_p to represent the hfr ($R_S(f)$) of the winding.

In figure A.II.2, the series combination of the sections representing the hfr of the 'central sections' of a winding is designated section 'a', similarily the series combination of the sections representing the hfr of the 'two-end sections' of a winding is designated section 'b'.

The impedance (Z_a) of the central-sections is given by:-

$$Z_a = \frac{R_p X_p (n-2)[nX_p + jR_p(n-1)]}{R_p^2(n-1)^2 + n^2X_p^2} \qquad (12)$$

The hfr of these central sections ($R_{S(a)}$) is given by the real part of Z_a:

$$R_{S(a)} = \frac{R_p X_p^2 n(n-2)}{R_p^2(n-1)^2 + n^2X_p^2} \qquad (13)$$

The series-reactance of these central sections ($X_{S(a)}$) is given by the imaginary part of Z_a:

$$X_{S(a)} = \frac{R_p^2 X_p (n-1)(n-2)}{R_p^2(n-1)^2 + n^2X_p^2} \qquad (14)$$

Similarly, the impedance (Z_b) of the end-sections is given by:

$$Z_b = \frac{2R_p X_p [nX_p + 2jR_p (n - 1)]}{4R_p^2 (n - 1)^2 + n^2 X_p^2} \tag{15}$$

The hfr of these end-sections ($R_{S(b)}$) is given by the real part of Z_b:

$$R_{S(b)} = \frac{2nR_p X_p^2}{4R_p^2 (n - 1)^2 + n^2 X_p^2} \tag{16}$$

The series-reactance of these end-sections ($X_{S(b)}$) is given by the imaginary part of Z_b:

$$X_{S(b)} = \frac{4R_p^2 X_p^2 (n - 1)}{4R_p^2 (n - 1)^2 + n^2 X_p^2} \tag{17}$$

Summing the hfr of sections (a) and (b);

$$R_S = R_{S(a)} + R_{S(b)} \tag{18}$$

Substituting equations (13) and (16) into (18) gives:

$$R_S = \frac{2R_p^3 X_p^2 n(n - 1)^2 (2n - 3) + R_p X_p^4 n^4}{4R_p^4 (n - 1)^4 + 5R_p^2 X_p^2 (n - 1)^2 n^2 + n^4 X_p^4} \tag{19}$$

The optimum number of sections, for each phase of a converter transformer model, has been found to be five (Chapter 4.5.3). Thus when n = 5 :

$$R_S = \frac{X_p^2 R_p [1120R_p^2 + 625X_p^2]}{1024R_p^4 + 2000R_p^2 X_p^2 + 625X_p^4} \tag{20}$$

and

$$R_S(f_1) = \frac{(2\pi f_1 L_p)^2 R_p [1120R_p^2 + 625 (2\pi f_1 L_p)^2]}{1024R_p^4 + 2000R_p^2 (2\pi f_1 L_p)^2 + 625 (2\pi f_1 L_p)^4} \tag{21}$$

$$R_S(f_2) = \frac{(2\pi f_2 L_p)^2 R_p [1120R_p^2 + 625(2\pi f_2 L_p)^2]}{1024R_p^4 + 2000R_p^2 (2\pi f_2 L_p)^2 + 625 (2\pi f_2 L_p)^4} \tag{22}$$

Equations (21) and (22) contain a total of 2 variables (R_p and L_p): thus, these equations may be solved by 'Itterative Techniques' : a digital computer could rapidly solve these equations;

a) Choose a value for R_p and substitute this value in equation (21);

b) Determine the value of L_p which satisfies equation (21) for $R_S(f_1)$;

c) Substitute these values for R_p and L_p into equation (22) to ensure that $R_S(f_2)$ is satisfied by these values;

d) If the equation for $R_S(f_2)$ is not satisfied, choose a revised value of R_p and recalculate the value of L_p which satisfies equation (21).

e) Repeat steps (c) and (d) until equations (21) and (22) are satisfied.

NOTE: Experience has shown that a good initial value for R_p is that determined for a single-section winding representation (equation 7).

To calculate the 'series' reactance of the (n - 2) central sections [$(n - 2)X_{LT(c)}$ where $(n - 2)X_{LT(c)} = (n - 2)2\pi fL_{LT(c)}$ (see figure 4.11)], the imaginary part of impedance Z_a (given by equation (14)) is subtracted from the leakage reactance of the (n - 2) central sections [$(n - 2)X_T/(n - 1)$].

Hence,

$$X_{LT(c)} = X_T/(n-1) - \frac{R_p^2 X_p (n-1)}{R_p^2 (n-1)^2 + n^2 X_p^2} \qquad (23)$$

Where, $X_{LT(c)}$ is determined at fundamental frequency.

Similarly, to calculate the 'series' reactance of the two end-sections [$2X_{LT(e)}$ where $2X_{LT(e)} = 2(2\pi f)L_{LT(e)}$, (see figure 4.11)], the imaginary part of Z_b (given by equation (17)) is subtracted from the leakage reactance of the two end-sections [$\frac{1}{2}$ $(2X_T/(n-1))$].

Hence,

$$X_{LT(e)} = \frac{X_T}{2(n-1)} - \frac{2R_p^2 X_p^2 (n-1)}{4R_p^2 (n-1)^2 + n^2 X_p^2} \qquad (24)$$

APPENDIX III

DERIVATION OF COMPONENT VALUES FOR AN 'IMPULSE GENERATOR'

In order to mathematically model an impulse applied to an off-state valve, it is necessary to mathematically describe an 'impulse generator', (see Chapters 4.6 and 8.5). The techniques employed assume that the impulse can be described by two exponentially decaying waveforms of opposite polarity, (figure 4.12).

$$V_V = V_m \left[e^{-(t/T_1)} - e^{-(t/T_2)} \right] \qquad (1)$$

With reference to figure 4.13, the capacitor C_1 is initially charged to a value V_m and capacitor C_2 is uncharged. If capacitor C_1 is chosen to be much greater than C_2 and resistor R_2 much greater than R_1, then;

The wavefront for $R_2 >> R_1$ is given by:-

$$V_{rise} = V_m \cdot \frac{C_1}{C_1 + C_2} \left(1 - e^{-\left[\frac{C_1 + C_2}{C_1 C_2 R_1}\right] t_{rise}}\right) \qquad (2)$$

The wavetail for $C_1 >> C_2$ is given by the rate of discharge of C_1 via R_2 from a voltage equal to the peak impulse voltage, $V_{V(pk)}$

$$V_{tail} = V_{V(pk)} \; e^{-\left[\frac{t_{tail}}{C_1 R_2}\right]}$$

The value of C_2 may be chosen such that the high frequency output impedance of the impulse generator is low compared to both the impedance of the valve and the shunt stray capacitances, (i.e. $C_2 >> C_B$) (see figure 8.16).

For the purposes of modelling, the rise times are from 0% to 100% of the peak impulse voltage, whereas decay time quoted are from 100% to 50% of

the peak impulse voltage, $V_{V(pk)}$. This definition results in a higher value of dV/dt, acros an off-state valve, than taking the rise time between 10% and 90% of peak impulse voltage.

Component values are derived and then 'trimmed' using the computer programme VTECAP to analyse the circuit. These values are tabulated below for three different impulses, (as defined by IEC 60);

Switching-Impulse (250/2500μs)

$V_m = 1.159V_{V(pk)}$

$C_1 = 33.482mF$

$C_2 = 2.708mF$

$R_1 = 23.7m\Omega$

$R_2 = 0.1\Omega$

Lightning-Impulse (1.2/50μs)

$V_m = 1.043V_{V(pk)}$

$C_1 = 6.739mF$

$C_2 = 121.9\mu F$

$R_1 = 1.9m\Omega$

$R_2 = 10m\Omega$

Front-of-Wave Impulse (0.25/5μs)

$V_m = 1.073V_{V(pk)}$

$C_1 = 6.896mF$

$C_2 = 251.2\mu F$

$R_1 = 193\mu\Omega$

$R_2 = 1m\Omega$

APPENDIX IV

MATHEMATICAL MODEL OF A SATURATING REACTOR

A consideration of the conflicting technical and economic requirements for inrush control, (Chapter 6.2), resulted in the proposal for a two-part saturating reactor. One-part of this reactor was considered to have controlled eddy-current losses: the other part was considered to be lossless, (Chapter 6.2).

In order to mathematically describe the eddy-current losses within a part of the reactor, the predominant mode of excitation must be defined. The predominant mode of excitation of the lossy part (L1) (Chapter 6.2), is dependent upon the instantaneous value of inductance of part L1 (Chapters 6.4.5 and 6.4.6), part L2 (Chapters 6.4.7 and 6.4.8), and the instantaneous incremental resistance of the thyristor (Chapter 4.3.1). Thus, the predominant mode of excitation (fixed H or B-field), may change during the several microseconds following the application of a gate pulse.

This Appendix shows the derivation of the mathematical model of the lossy part of the saturating reactor (L1); this is dependent upon the predominant mode of excitation. The general form of the mathematical model is derived assuming sinusoidal conditions of excitation.

1. Excitation by a fixed H-Field

Excitation by a fixed H-field results when a load is considered to be of low-impedance compared with the source (e.g. initially part L1 does not restrict the flow of current; the inrush current is controlled by the thyristors and part L2).

A time changing magnetic-field in the magnetic core material of an AC power device results in an electric-field in the magnetic core; the electric-field results in circulating eddy-currents. These eddy-currents, within the lossy magnetic material, result in a reaction H-field which oppose, but do not significantly effect, the applied H-field.

Thus, let the excitation be, $I = I_{pk} \sin(wt)$

$$\text{If} \qquad H = \frac{NI}{l_m} \tag{1}$$

and assuming l_m is constant;

$$H = \frac{NI_{pk}}{l_m} \sin(wt) \tag{2}$$

The magnetic-field is assumed to be entirely in the x-direction (current is in the z-direction), and to be a spatial function of y; the eddy-currents in this simplified approach, will be induced entirely in the z-direction (see figure A.IV.1), thus:-

$$\frac{\partial H_x}{\partial y} = -J_z \tag{3}$$

Let $l_m = (b_d + y)$

Hence, from equation (2),

$$H = \frac{NI_{pk} \sin(wt)}{(b_d + y)} \tag{4}$$

Substituting equation (4) into (3):-

$$J = -\frac{\partial H}{\partial y} = -\frac{I_{pk}\, N}{(b_d + y)^2} \sin(wt) \qquad (5)$$

$$E = J/\sigma = -\frac{I_{pk}\, N}{(b_d + y)^2 \sigma} \sin(wt) \qquad (6)$$

By Faraday's law, the induced e.m.f. (E_I) is of a mangitude ;

$$E_I = E.l_g = \frac{-I_{pk}\, N l_g}{(b_d + y)^2 \sigma} \sin(wt) \qquad (7)$$

Where, $I_{Pk} \sin(wt)$ is the instantaneous main-circuit current. From equation (5), if both width b_d and depth y are considered to be constant then:-

$$\frac{N}{(b_d + y)^2} = \text{a constant} \qquad (8)$$

Hence, the magnitudes of the induced eddy-currents are dependent upon the instantaneous value of the sinusoidal main-circuit current.

Considering a unit length in the z-direction the induced e.m.f drives a current, I, around a loop of resistance, R_{tr}.

Where:-

$$R_{tr} = \frac{2\rho b_d}{dy} \qquad (9)$$

so that the instantaneous power, dw' is given by:-

$$dw' = (E_I^2/R_{tr}) \qquad (10)$$

$$\text{therefore, } dw' = \frac{I_{pk}^2\, N^2}{\sigma^2 (b_d + y)^4 R_{tr}} \sin^2(wt) \qquad (11)$$

The average power dissipation ($\overline{dw'}$) is given by the integral, with respect to time, of equation (11) over a power frequency cycle. Substituting euation (9) into the resultant integral gives ;

$$\overline{dw'} = \frac{1}{2} \frac{I_{pk}^2\, N^2\, dy}{(b_d + y)^4\, 2\rho\, b_d\, \sigma^2} \qquad (12)$$

This may be integrated between the limits y = 0 and y = a/2 to give a total power;

$$w' = \frac{1}{4} \int_0^{a/2} \frac{(I_{pk}^2 N^2)}{(b_d + y)^4 b_d \sigma} dy \tag{13}$$

Hence,

$$w' = \frac{1}{4} \frac{I_{pk}^2 N^2}{b_d \sigma} \left[\frac{-1}{3 (b_d + y)^3} \right]_0^{a/2} \tag{14}$$

Therefore,

$$w' = \frac{1}{12 b_d} I_{pk}^2 \frac{N^2}{\sigma} \left[\frac{1}{b_d^3} - \frac{1}{(b_d + a/2)^3} \right] \tag{15}$$

Now, if $I_{pk} = (2)^{\frac{1}{2}} I_{rms}$

$$w' = \frac{1}{6 b_d} I^2_{rms} \frac{N^2}{\sigma} \left[\frac{1}{b_d^3} - \frac{1}{(b_d + a/2)^3} \right] \tag{16}$$

This equation is comparable to

$$w' = I^2_{rms} R_S \tag{17}$$

Where,

$$R_S = \frac{1}{6 b_d} \frac{N^2}{\sigma} \left[\frac{1}{b_d^3} - \frac{1}{(b_d + a/2)^3} \right] \tag{18}$$

Hence the reflected resistance is behaving as an equivalent series resistance.

If a fixed H-field impulse is applied to the magnetic material, the resulting flux and eddy-currents diffuse into the lamination. At t = 0, the flux will be confined to the surface of the lamination, (a = 0). Thus, from equation (18), at t = 0, $R_S = 0$. As time proceeds, the effective series resistance will increase in value and approach a final value given by equation (18).

The relative permeability of the magnetic material will decrease as the material is driven into saturation. However, provided that the source of the fixed H-field is a large impedance in comparison with the reactor, saturation of the reactor will not alter the magnitude of the main-circuit current. Thus, from equation (5), the magnitude of induced eddy-currents is unaltered by a change in the relative permeability of the magnetic material (assuming uniform flux distribution). However, a reduction in the relative permeability of part L1 will result in an increased rate of diffusion of the magnetic-field. Thus, the effective series resistance, R_S (equation 18), will obtain its final value in a shorter interval of time. Similarly, introduction of an air-gap in the magnetic-circuit would reduce the initial effective relative permeability of the magnetic-circuit, allowing the initial rate of diffusion of the flux to increase.

During normal load-current commutation or during fault current conditions, the lossy-reactor (L1) will be predominantly excited by a fixed H-field. Thus, the eddy-current losses are dependent, during this interval, upon the instantaneous value of main-circuit current.

2. Excitation by a B-Field

Excitation by a fixed B-field results from a load which is considered to significantly restrict the flow of current in comparison with the other circuit elements. The reactors have a significant effect in controlling the inrush current, and are thus considered to be predominantly B-field excited during the interval of time associated with an inrush transient.

Time-changing magnetic flux in the magnetic core material of an AC power device induces e.m.f's, resulting in circulating eddy-currents: power is dissipated as a result of these eddy-currents. Calculation invoking Faradays law enables the loss under these circumstances to be determined[62]. A thin-plate geometry of figure A.IV.1 is considered: the time-changing magnetic flux is assumed to be entirely in the z-direction;

$$B_z = B_o \sin wt \tag{19}$$

where B_o is the peak flux density.

Assuming uniform flux distribution, the area enclosed by the shaded path is $2b_d y$, so that the flux, $\emptyset$ through it is:-

$$\emptyset = 2b_d y\, B_o \sin(wt) \tag{20}$$

Thus, by Faraday's law the induced e.m.f. is of magnitude

$$E_I = 2wb_d y\, B_o \cos(wt) \tag{21}$$

Taking unit length in the z-direction, this voltage drives a current, I, around a loop of resistance:-

$$R_{tr} = (2\rho b_d/dy) \tag{22}$$

so that the instantaneous power is:-

$$dw' = (E_I^2/R_{tr}) \tag{23}$$

Therefore:

$$dw' = \left(\frac{4w^2 b_d^2 y^2 B_o^2 \cos^2(wt)\sigma\, dy}{2b_d} \right) \tag{24}$$

The average power dissipation is given by the integral, with respect to time, of equation (24) over a power frequency cycle:-

$$\overline{dw}' = w^2 b_d B_o^2 y^2\, \sigma\, dy \tag{25}$$

This may be integrated between the limits y = 0 and y = a/2 to give a total power:-

$$w' = \left[w^2 b_d B_o^2 \frac{y^3}{3} \sigma \right]_0^{a/2} = \left(\frac{w^2 b_d B_o^2 a^3 \sigma}{24} \right) \tag{26}$$

Equivalent circuit representing eddy-current losses[63]

The cross-sectional area of the lamination (figure A.IV.1) is equal to ab_d. Thus, assuming uniform flux distribution, the peak value of induced e.m.f. is given by :

$$E_{I(pk)} = jwB_o b_d a \tag{27}$$

Rearranging equation (27) and substituting the resultant into equation (26);

$$w' = \frac{w^2 b_d a^3 \sigma}{24} \cdot \frac{E^2_{I(pk)}}{w^2 b_d{}^2 a^2}$$

$$\therefore \quad w' = E^2_{I(pk)} \left(\frac{a^3\sigma}{24 b_d (a)^2} \right) = E^2_{I(pk)} \frac{1}{2} \left(\frac{a\sigma}{12 b_d} \right) \tag{28}$$

This equation is comparable to:-

$$w' = \frac{E^2_{I\ (rms)}}{R_e} \tag{29}$$

Where

$$E_{I(pk)} = (2)^{\frac{1}{2}} E_{I(rms)} \tag{30}$$

Substituting (30) into (28)

$$w' = \frac{2E^2_{I(rms)}}{2} \left(\frac{a\sigma}{12 b_d}\right) = E^2_{I(rms)} \left(\frac{a\sigma}{12 b_d}\right) \tag{31}$$

Comparing equations (29) and (31), the 'lossy' magnetic material can be modelled by an inductance with a parallel resistance (figure 6.2). From equation (31), the parallel resistance (R_e) has a value;

$$R_e = \frac{12 b_d}{a\sigma} \tag{32}$$

Thus, for a given width b_d and conductivity σ, the reflected resistance (R_e) is inversely proportional to the depth of the lamination (a).

The depth of penetration (d) of the half-wave front is given by

$$d = h\ (t)^{\frac{1}{2}} \tag{33}$$

Hence

$$d = [(\rho/\mu)\ t]^{\frac{1}{2}} \tag{34}$$

Now let $(\frac{a}{2}) = d$, hence equation (34) may be substituted into equation (32);

$$R_e = 6b_d \left[\frac{\mu}{t\sigma}\right]^{\frac{1}{2}} \tag{35}$$

Thus, during the interval when there is non-uniform flux distribution throughout a lamination, the reflected resistance decreases as :

1) Relative permeability decreases (i.e. due to saturation effects). Similarly, introduction of an air-gap in the magnetic-circuit will result in a reduced initial effective relative permeability. Hence, the initial rate of diffusion of the flux will increase.

2) Elapsed time increases.

From equation (35), at $t = 0$ R_e approaches infinity. When the flux can be considered to occupy the whole lamination, uniformly, R_e approaches $\frac{12b_d}{a\sigma}$.

Comments

The mathematical model used to represent the lossy reactor (L1) is dependent upon the predominant mode of excitation. It has been shown that for a fixed, sinusoidal, H-field excitation the reactor should be represented by a non-linear inductance together with a series resistance. Similarly for a fixed, sinusoidal, B-field

excitation the reactor should be represented by a non-linear inductance with a parallel resistance.

If the reactor is the predominant, high-frequency, component restricting the flow of current then it will be B-field dependent. Thus, where the source of the current and voltage transients is energy stored within stray capacitances (e.g. at turn-on of a valve), then part L1 will be B-field dependent. Hence, it is assumed that, for the majority of investigations of circuit transients, part L1 may be represented, mathematically, as a non-linear inductance with a parallel resistance.

Due to diffusion effects, the value of this resistance will, in reality, be non-linear. However, for the preliminary studies (Chapters 6, 7 and 8), the resistance is assumed to be of a constant value.

APPENDIX V

VOLUME AND COST OF MAGNETIC MATERIAL REQUIRED

A consideration of the conflicting technical and economic requirements for inrush control (Chapter 6.2), resulted in the proposal for a two-part saturating reactor. This two-part reactor was optimized (Chapter 6.4), such that the assumed design limits (Chapter 6.3), were achieved for reduced hardware and capitalized costs in comparison with the inrush control components utilized in the Sellindge converter station. The saturating reactors in the Sellindge converter station utilize toroids of magnetic material as, magnetically, a toroid is an efficient shape. Similarly, the proposed reactor is considered to be constructed from toroids of magnetic material.

It has been shown (Chapter 6.4.11) that, for the converter station rating considered (Chapter 6), the inrush control can be achieved with a two-part reactor whose saturation flux is 1.6Wb per valve. For a given saturation flux requirement and a certain usable unipolar flux density swing (see Chapter 6.5), it is possible to choose the dimensions of a toriod of magnetic material such that an optimum relationship is obtained between the length of magnetic material, l_g, (figure A.V.1), and the total volume of magnetic material (V_{LM}) required for the reactor. The cost of the hardware necessary for inrush control is dependent upon the volume of magnetic material required.

It may be desirable in future schemes to utilize the general form of the proposed characteristics (Chapter 6.4.9) and to scale the volume of magnetic material accordingly (e.g. with the overvoltage firing level of the valve). However, if it is necessary to alter the radial dimensions of the toroids of magnetic material, care should be taken that the nature of the incremental inductance with current characteristics is not altered.

a) Volume and Length Considerations

The initial coherent turn-on studies indicate that a saturation flux requirement of approximately 1.6Wb per valve may be required, (for the converter station rating considered). Magnetic materials with saturation flux densities exceeding 1.5T are available. However, the usable unipolar flux density swing will be reduced by virtue of any remanent flux density. It is assumed in this Appendix, that the remanent flux density is 20% of the saturation flux density giving a usable unipolar flux density swing of 1.2T.

Magnetic materials are available which have saturation flux densities of up to 2.3T, e.g. Cobalt/Iron amorphous alloy[51]. However, these magnetic materials are not produced in large volumes and are, thus, expensive, (e.g. £40 per kg)[51].

The inrush transient associated with coherent turn-on of a thyristor valve, during worst-case repetitive operation [i.e. turn-on from maximum overvoltage protective level (Chapters 6.4.9, 6.4.11, 8.2, 8.3 and 8.5)], is assumed to drive both parts of the saturating reactor into saturation. Therefore, the calculation of the volume of magnetic material, required per valve, is based upon the actual cross-sectional area of the magnetic material, rather than its effective cross-sectional area as defined by IEC 205.

The ratio of outside radius (r_2) to inside radius (r_1) (ratio of radii), of a toroid affects the required volume of magnetic material for a given saturation flux requirement. For a given inside radius

the volume of magnetic material required increases linearly with increasing ratios of radii. Thus, it is advantageous to decrease the ratio of radii to minimize the required volume. However, as the ratio of the radii are reduced the required length of magnetic material, per valve, increases rapidly (figure A.V.2).

It is convenient at this point to introduce volume and length scale-factors. These factors allow the effect of a change in radial dimensions to be readily visualized. The volume scale-factors (V_{SF}) and length scale-factors (H_{SF}) versus the ratio of radii, for a given inside radius, are graphed in figure A.V.2. The units of these axes are arbitrary.

An outside to inside radius ratio of 1.5 was chosen, arbitrarily, to have a volume scale-factor of unity (see figure A.V.2). Similarly, an outside to inside radius ratio of 4.5 was chosen, arbitrarily, to have a length scale-factor of unity (see figure A.V.2).

Thus, for a given inner radius the effect of altering the outer radius of the toroid is readily calculable, for example;

i) If $(r_2/r_1) = 2.5$, then from figure A.V.2, $V_{SF} = 1.4$ and $H_{SF} = 2.35$

ii) If the outer radius is decreased, but the inner radius is kept constant, e.g. $(r_2/r_1) = 2$, then from Figure A.V.2;

$V_{SF} = 1.2$ and $H_{SF} = 3.5$

Hence,

New volume = $V_{2.5} \times 1.2/1.4 = \underline{0.857} \times$ original volume

New length = $H_{2.5} \times 3.5/2.35 = \underline{1.489} \times$ original length

Therefore, decreasing the ratio of the radii from 2.5 to 2.0, by reducing the outer radius, has decreased the required volume (and hence the mass and thus the cost of the material), by 14.3% but has increased the required length by 48.9%.

From Figure A.V.2, it appears that if both volume and length are to be optimized, a ratio of radii of about 2.875 is desirable. Figure A.V.3 is derived based upon this ratio of radii of 2.875. The volume required, to achieve a saturation flux of 1.6Wb, increases linearly as the inside radius increases. The effect of an increased inner radius upon the required mass, and hence cost of magnetic material is graphed in figure A.V.4. Figure A.V.4 is derived assuming a laminated core of 85% space-factor and a price of £6 per kilogram finished cost for the magnetic material[51]. The cost of magnetic material, per valve, increases in proportion to the inner radius of the toroid. However, figure A.V.3 shows that an advantage of an increased inner radius, for a fixed ratio of radii (thus an increased volume and cost of magnetic material), is a reduction in the length of magnetic material required.

Thus, figures A.V.2 and A.V.3 and A.V.4 can be used in conjunction with one another to estimate the dependence of the length, volume and hardware cost upon both the inside and outside radii;

1) Change of Outer Radius

a) Select the required inner radius (r_1) for the toroid. Determine the necessary volume, $V_{LM(a)}$, and length, $l_{g(a)}$, from figure A.V.3 (for a ratio of radii of 2.875).

b) Select the required outside radius (r_2) for the toroid. Determine $V_{SF(b)}$ and $H_{SF(b)}$ from figure A.V.2 [for the ratio (r_2/r_1)].

c) Scale the volume [$V_{LM(a)}$] and length [$l_{g(a)}$] according to the volume and length scale factors $V_{SF(b)}$ and $H_{SF(b)}$;

$$V_{LM(b)} = V_{LM(a)} \times \frac{V_{SF(b)}}{V_{SF(2.875)}} = \frac{V_{LM(a)} \times V_{SF(b)}}{1.55} \qquad (1)$$

$$l_{g(b)} = l_{g(a)} \times \frac{H_{SF(b)}}{H_{SF(2.875)}} = \frac{l_{g(a)} \times H_{SF(b)}}{1.825} \qquad (2)$$

Using figure A.V.4, the calculated volume [$V_{LM(b)}$] may be converted into a hardware cost per valve (assuming an 85% space-factor, density of 7.1gm cc^{-3} and a price of £6 per kg).

d) The effect of further changes in the outer radius are assessed, for a constant value of inner radius, by repeating step 'b' with the revised ratio of radii.

Step 'c' is then repeated, with the volume [$V_{LM(a)}$] and length [$l_{g(a)}$] originally determined in step 'a' but with the revised volume and length scale-factors [derived from figure A.V.2, for the new ratio of radii of interest (step b)].

2. Change of Inner Radius

Repeat steps 1(a), 1(b) above.

Using equations (1) and (2), (step 1(c)), determine the revised volume $[V_{LM(b)}]$ and length $[l_{g(b)}]$.

Using figure A.V.4 the calculated volume $[V_{LM(b)}]$ may be converted into a hardware cost per valve (assuming an 85% space-factor, density of 7.1gm cc^{-3} and a price of £6 per kg).

The effect of further changes in the inner radius (r_1) are assessed by repeating steps 1(a), 1(b) and 1(c).

3. Saturation Flux

Any increase or decrease in the required saturation flux will scale the necessary length and volume (figure A.V.3) of the reactor in proportion to this increase or decrease. However, the scale-factors (figure A.V.2) are unaltered.

4. Available Saturation Flux Density

Any increase or decrease in the available saturation flux density will scale the required length and volume of the reactor (figure A.V.3) in inverse proportion to this increase or decrease. However, the scale-factors (figure A.V.2) are unaltered.

5. Mass and Price

Any modification to the space-factor or density (i.e. different material being considered), will scale the mass and hence price axes of figure A.V.4 in direct proportion to the change. Similarly, any change in the price will scale the price axis (figure A.V.4), in proportion to this change.

6. Incremental Inductance with Current Characteristic

Chapter 6 considered the optimum characteristics of the proposed two-part reactor for control of the inrush transient, during coherent turn-on from maximum overvoltage protective level (400kV). However, it would be uneconomic for manufacturers of magnetic materials to develop materials, with appropriate characteristics, for each HVDC scheme.

Thus, it is advantageous to specify magnetic material characteristics which are suitable for all future HVDC contracts. The volume of material may be revised, between contracts, to achieve the required control of transients.

Similarly, it may be desirable to alter the radial dimensions of the magnetic material and scale the length of material, without altering the inductance with current characteristic. Thus, any change in the radial dimensions should not alter the mean magnetic-path length.

Thus, if the inside radius (r_1) is increased by a value x, then the outside radius (r_2) should be decreased by a similar amount, x;

$$l_m = \pi[(r_1 + x) + (r_2 - x)] = \pi(r_1 + r_2) \quad (3)$$

Toroids of magnetic material are added to, or removed from, the reactor to achieve the required saturation flux (figure A.V.2). Thus, considering the length of the reactor to be l_g, the cross-sectional area is given by:-

$$A = l_g(r_2 - r_1) \quad (4)$$

If the radial dimensions of the ring are altered whilst the mean magnetic path is kept constant (equation (3)), then to retain the same cross-sectional area (same saturation flux), the length of the reactor is modified to l'_g;

$$(r_2 - r_1)\, l_g = [(r_2 - x) - (r_1 + x)]\, l'_g$$

Hence,

$$l'_g = \frac{(r_2 - r_1)\, l_g}{(r_2 - r_1 - 2x)}$$

(The volume of the reactor is maintained constant).

7. Conclusions

In order to minimize the volume of magnetic material required to achieve a given saturation flux, it is necessary to keep to a minimum the inside radius of the toroid and also the ratio of outside radius to inside radius. However, in reducing the inner radius the size of busbar capable of being passed through the centre of the toroid is reduced. In addition, it may be necessary to indirectly cool the magnetic material by passing an appropriate cooling medium up the centre of the busbar. This would reduce further the cross-sectional area of the busbar available to carry current and thus increase the

resistance of the busbar. The capitalized losses associated with the busbar may thus be increased to an unacceptable level.

A penalty of reducing either the inside radius or the ratio of radii is the additional length of magnetic material necessary to achieve the same saturation flux. To optimize the volume and length required, it is recommended that a ratio of radii of approximately 2.875 be used (see page 277), irrespective of the inner radius of the toroid.

APPENDIX VI

CAPACITANCE OF DAMPING CAPACITOR

In order to damp the recovery oscillation effectively, it is desirable to select a damping capacitor which is large enough to swamp the stray capacitance shunting a valve, such that a greater amount of energy is dissipated in the damping resistor (Chapter 7).

Choice of a large value of damping capacitor also reduces the difference in recovery voltages between thyristors within a valve (Chapter 7.4) (see figure 8.15), thus reducing the likelihood of commutation failure during 12 pulse-operation, (Chapter 8.4). The dependence of a difference in recovery times, between thyristors in a valve, upon both a spread in reverse recovered charge and the capacitance of the damping capacitor may be evaluated. However, the evaluation is approximate as it neglects the effects of distortion of the AC sine-wave.

For a 50Hz scheme, with a peak line-to-line voltage of 245.5kV (Chapter 6.4.13) and thyristors with a reverse recovered charge band assumed to be ±500μC of a nominal value:

$$V_V = 2^{\frac{1}{2}} V_c \sin(wt) \qquad (1)$$

$$\frac{dV_V}{dt} = 2^{\frac{1}{2}} V_c w.\cos(wt) \qquad (2)$$

From equation (1), $t = 0, \pi, 2\pi$, etc at voltage zero crossing $[V_{V(0)}]$. Hence, equation (2) gives

$$\frac{dV_{V(0)}}{dt} = 2^{\frac{1}{2}} V_c w = 2^{3/2} V_c \pi f \qquad (3)$$

Therefore, $\frac{dV_{V(0)}}{dt} = 77.1V\ \mu s^{-1}$ per valve

and hence for a 100 level valve,

$$\frac{dV_{V(0)}}{dt} = 0.771V\ \mu s^{-1} \text{ per level}$$

For a scheme utilizing, nominally, 3μF damping capacitors, per level, and a reverse recovered charge band of ± 500μC of a nominal value, the possible difference in recovery voltage (neglecting tolerances of the capacitance value) from a nominal is:-

$$\Delta V = \frac{\pm 500 \times 10^{-6}}{3 \times 10^{-6}} = \underline{\pm 166.6V}$$

Thus, the difference in recovery time from a nominal, due to a spread in reverse recovered charge between thyristors, is given by:

$$\Delta t = \frac{\pm 166.6 \times 10^{-6}}{0.771} = \underline{\pm 216\mu s} \qquad = \underline{\pm 3.888°}$$

Increasing the damping capacitor to 4μF per level would decrease the 'spread' in recovery time from a nominal, to ±162μs, i.e. ±2.916°, but would increase the damping circuit, evaluated, losses (Chapter 7.4).

(Note: the level dV/dt is assumed to be approximately equal to the dV/dt across an off-state thyristor during the recovery transient).

REFERENCES

1. Arrillaga J : 'High Voltage Direct Current Transmission', Peter Peregrinus Ltd, 1983, Chapter 1.

2. Gavrilovic A, Ainsworth J D, Goodrich F G, Thanawala H L, Williams W P : 'The role of HVDC and Static Compensators in Electrical Power System Interconnection and Long Distance Transmission'. BEAMA Conference, Singapore, November 1979.

3. Gavrilovic A :'Some views on the choice between AC and DC alternatives' IEE Conf. Publ. no. 107, Nov. 1973, pp. 298-301.

4. Farrell J J : 'High Voltage Direct Current Transmission' IEI Trans. 1979, vol. 103, pp. 65-76.

5. Goodwin C J : 'HVDC for long distance transmission in the Nelson System' IEE Conf. Publ. no. 107, Nov. 1973, HVDC and AC Power Transmission pp. 124-128.

6. Natale M, Lane F J, Calverley T E : 'The Sardinia Italian mainland HVDC Interconnection' IEE Publ. 22, HVDC Conf. 1966.

7 Kimbark E W : 'Direct Current Transmission' (Vol. 1) John Wiley, 1971, pp. 25-28.

8. Yates J B : 'Power Engineering for the New Cross-Channel Link' Electronics and Power, January 1982, pp. 77-81.

9. Kimbark E W : 'Direct Current Transmission' (Vol. 1) John Wiley 1971, Chapter 3.

10. Arrillaga J : 'High Voltage Direct Current Transmission' Peter Peregrinus Ltd, 1983, Chapter 2.

11. Adamson C, Hingorani G : 'High Voltage Direct Current Transmission' Garraway Ltd. 1960, Chapter 3.

12. Cory B J : 'HVDC Convertors and Systems' Macdonald and Co. Ltd, 1965, Chapter 4.

13. Cory B J : 'HVDC Convertors and Systems' Macdonald and Co. Ltd, 1965, Chapter 7.

14. Abramovich B J, Brewer G L, Welch I M : 'Harmonic Filters for the Sellindge Converter Station' IEE Conf, Publ. no. 205. "Thyristors and Variable Static Equipment for AC and DC Transmission," 1981, pp. 121-125.

15. Ainsworth J D : 'The Phase-Locked Oscillator - A New Control System for Controlled Static Converters' IEEE Trans on PA and S, Vol. 87, pp. 859-865, March 1968.

16. Kimbark E W : 'Direct Current Transmission' (Vol. 1) John Wiley 1971, Chapter 5.

17. Woodhouse M L, Haddock J L, Rowe B A, Ballad J P : 'The Control and Protection of Thyristors in the English Terminal Valves, Particularly during Forward Recovery' IEE Conf, Publ. no. 205, 1981, pp. 158-163.

18. Chester J K : 'A New Technique for Deriving Self-Consistent Electrical and Thermal Models of Thyristors, during surge-loops from Experimental Data' IEE Conf, Proc, Power Electronics. 'Power Semiconductor and their Applications', London, 1977.

19. Arrillaga J : 'High Voltage Direct Current Transmission' Peter Peregrinus Ltd, 1983, Chapter 6.

20. Andersen B R, Robinson A A, Diseko N L : 'Insulation Co-ordination for the UK Terminal' IEE Conf, Publ. no 205. "Thyristors and Variable Static Equipment for AC and DC Transmission". pp. 199-203.

21. Ballad J P, Hoban P : 'Turn-on Studies on Initial Samples of the DCR1478 Thyristor' Internal Report NG u 936, Section 7, 18/5/84.

22. General Electric : 'SCR Manual including Triacs and Other Thyristors' (Sixth Edition), Chapter 1.

23. Millman J, Halkias C C : 'Integrated Electronics, analog and digital circuits and systems' McGraw Hill Kogakusha Ltd, 1972, pp. 121-124.

24. Millman J, Kalkias C C : 'Integrated Electronics, analog and digital circuits and systems' McGraw Hill Kogakusha Ltd, 1972, pp. 63-66.

25. Diseko N L : 'Inrush Current Predictions' Internal Report J87/421, 10/12/1980.

26. Diseko N L, Woodhouse M L, Thanawala H L, Crawshaw A M, Rowe J E, Andersen B R : 'Transient Analysis and Design of HVDC and AC Thyristor Valves' IEE Conf, Publ. no. 205, 1981, pp. 167-170.

27. Ainsworth J D, Bowles J P, : 'An HVDC Transmission Simulator suitable for both Steady-State and Transient Studies' IEE Conf, Publ. no. 22, 1966.

28. Fox L : 'Numerical Solution of Ordinary and Partial Differential Equations' - Based on a summer school held in Oxford, August-September 1961, Permagon Press (1962), pp. 3-27.

29. Woodhouse M L, Rout K : 'The Design and Testing of an Air-Insulated Air-Cooled Thyristor Valve for use in High Voltage Schemes' IEE Conf, Publ. no. 154, "Power Electronics - Power Semiconductors and their Applications," London, 1977, pp. 162-165.

30. Ballad J P, Hoban P : 'HVDC Development Programme: Turn-on (inrush) tests on the MEDL Thyristor Type DCR1478: Basic units and Batch 2 Encapsulated Samples', Internal Report NG u 945, 20/9/84, Section 5.1.1.

31. Ballad J P, Hoban P : 'Turn-on Studies on Initial Samples of the DCR1478 Thyristor' Internal Report NG u 936, 18/5/84, Section 4.2.

32. Diseko N L : 'Optimisation of Convercer Transformer Winding Design and Grading Network Impedance at Recovery Frequency' Internal Report J87/390, 24/9/1979.

33. Carter G W : 'The Electromagnetic Field in its Engineering Aspects' Longmans Green and Co. Ltd. (1954), pp. 256-258.

34. Hammond P : 'Applied Electromagnetism' Permagon Press (1979), pp. 220-222.

35. Hammond P : 'Applied Electromagnetism' Permagon Press (1979), pp. 205-209.

36. Barnes M J : 'A Model of Transformer High-Frequency Behaviour for use in Thyristor Valve Inrush Current Calculations' Internal Report J87/467, 23/6/1982.

37. Barnes M J, Woodhouse M L, Bowden A L : 'High-Frequency Modelling of an HVDC Converter' Proc. UPEC 19,1984, Technical Session 10.9.

38. Rudenberg R : 'Electrical Shock Waves in Power Systems' Harvard University Press, 1968, Chapters 17, 18 and 20.

39. Swann S A, Salmon J W : 'Effective Resistance and Reactance of a Rectangular Conductor placed in a Semi-Closed Slot' Proc. IEE 110, (1963), pp. 1656-1660.

40. Silvester P : 'Dynamic Resistance and Inductance of Slot-Embedded Conductors' IEEE Trans on Power Apparatus and Systems, vol. PAS-87, no. 1, Jan. 1968, pp. 250-256.

41. Mocanu C I : 'Transient Penetration of the Electromagnetic-Field Into a Conductor Excited by a Constant Electric-Field', Rev. Roum, Sci. Techn. - Électrotechn. et Énerg., 19, 4, pp. 531-546, Bucharest, 1974.

42. Stoll R J : 'The Analysis of Eddy-Currents' Clarendon Press, Oxford, 1974, Chapter 2.

43. Miller K W : 'Diffusion of Electric Current Into Rods, Tubes and Flat Surfaces' AIEE Trans, 1947, vol. 66, pp. 1496-1502.

44. Grumet A : 'Penetration of Transient Electromagnetic Fields into a Conductor' Journal of Applied Physics, vol. 30, no. 5, May 1959, pp. 682-686.

45. Tuohy E J, Lee T H, Fullerton H P : 'Transient Resistance of Conductors' IEE Trans on PA and S, vol. PAS-87, no. 2, February 1968, pp. 455-462.

46. Carslaw H S, Jaeger J C : 'Conduction of Heat in Solids' Oxford University Press, 1959, Chapter 2.

47. Kreyszig E : 'Advanced Engineering Mathematics' John Wiley and Sons, 1979, pp. 509-510.

48. Stoll R J : 'The Analysis of Eddy-Currents' Clarendon Press, Oxford, 1974, Chapter 1.

49. Ballad J P, Hoban P : 'Turn-on Studies on Initial Samples of the DCR1478 Thyristor' Internal Report NG u 936, 18/5/84, Sections 5.3 and 6.

50. Ballad J P, Hoban P : 'HVDC Development Programme: Turn-on (inrush) tests on the MEDL Thyristor Type DCR1478: Basic units and Batch 2 Encapsulated Samples' Internal Report NG u 945, 20/9/1984, Section 5.2.

51. Barnes M J : 'Inrush Current Predictions and Saturating-Reactor Optimisation for Thyristor Valve Coherent Turn-on' Internal Report 334/512, 14/3/1984.

52. Barnes M J : 'Evaluation of Magnetic Piece-Part Pulse-Test Results' Internal Report 334/511.

53. Barnes M J : 'Investigation of the Sensitivity of Recovery Overvoltage and Damping-Circuit Losses at Commutation Out' Internal Repcrt 334/538, 23/8/84.

54. Barnes M J : 'Inrush Current Predictions: Worst-Case Commutation Failure' Internal Report 334/522, 2/4/1984.

55. Ballad J P, Hoban P : HVDC Development Programme: Turn-off, Forward Drop and Reverse Avalanche Measurements on Preliminary Samples of Distributed-Gate Type DCR1478 Thyristors'. Internal Report NG u 930, 31/1/84.

56. Cory B : 'HVDC Convertors and Systems' Macdonald and Co. Ltd, 1965, pp. 165-172.

57. Barnes M J : 'Inrush Current Predictions: Co-ordinating Current Pre-established in Surge-Arrester' Internal Report 334/521, 14/4/84.

58. Diseko N L : 'Valve Firing Transient Interaction Between Converter Pole 12-Pulse Valve Groups' Internal Report J87/420, 12/12/1980.

59. Barnes M J : 'Preliminary Study of Valve-Firing Transient Interaction Between Converter Pole 12-Pulse Valve Groups' Internal Report 334/523, 25/4/1984.

60. Barnes M J : 'Preliminary Investigation of Valve-Response to Impulse Test-Voltages' Internal Report 334/579, 6/6/1984.

61. Shammas N : 'HVDC Development Programme: Impulse Tests with Forward Voltage near Linear Ramps on MEDL Thyristors Type DCR1478' Internal Report W33/0092, 1/11/84.

62. Ferrari R L : 'An introduction to Electromagnetic-Fields' Van Nostrand Reinhold Co. Ltd. 1975, pp. 142 - 143.

63. Coulson M : 'Magnetic Non-Linearity' Phd. Thesis, University of Strathclyde, 1981, pp. 123 - 124.

TABLE 1

INCREASED TRANSIENT RESISTANCE

Dependence of the maximum width of the rib upon the effective relative permeability of the magnetic-circuit

Effective Relative Permeability (μ_e) of magnetic-circuit	Predicted transient resistance ratio at t = 1μs	DC resistance of 'rib' to give a transient resistance of one ohm at t = 1μs	Maximum cross-sectional area of rib required to achieve specified transient resistance	Depth of penetration at an elapsed time of 1μs ($J'_y/J_s < 1 \times 10^{-5}$) (equivalent to minimum height of rib required)	Maximum width of rib to give required 'effective' cross-sectional area
		(m Ω)	(m^2)	(μm)	(μm)
1	5.32	188	1.83×10^{-8}	685	18.3
100	53.2	18.8	1.83×10^{-7}	68.5	183
1000	168.3	3.94	5.8×10^{-7}	21.8	580

Assumptions:- i) Excitation is due to a current-ramp (Chapter 5.4).

ii) Length of busbar housed in semi-closed slot is 0.2m, per thyristor level.

iii) Height of rib (y_1) is 1mm.

iv) Conductor is homogeneous, non-magnetic and has a resistivity of 17.24×10^{-9} ohm.m.

v) Transient resistance required is 1 ohm per level at an elapsed time (t) of 1μs, measured from the start of rise time (t_r).

TABLE 2

WORST-CASE REPETITIVE INRUSH

Predicted Saturation Flux Requirement

	Single-section transformer model (Wb)	Refined transformer model (with end-effects) (Wb)
Part L1	0.813	0.687
Part L2	0.822	0.784
Total	1.635	1.471

TABLE 3

WORST-CASE REPETITIVE INRUSH

Inrush Predictions Obtained with Proposed Reactor Characteristics
(Single-section transformer model)

	di_m/dt ($A\ \mu s^{-1}$)	$i_{1(pk)}$ (A)	$i_{1(tr)}$ (A)	di_2/dt ($A\ \mu s^{-1}$)	$i_{2(pk)}$ (A)	$\frac{dV}{dt}T$ ($V\ \mu s^{-1}$)	$\frac{dV}{dt}L$ ($V\ \mu s^{-1}$)	E_{45} (J)
$\alpha = 90°$ (Fig 6.30)	89.5	430	117	10	278	330	371	126.4
$\alpha = 90°$ +DOV (Fig 6.31)	117.6	589	144	18.4	365	477	522	219.9
$\alpha = 12°$ (Fig 6.32)	18	82.1	26	2.4	57.6	60.5	135	5.0
$\gamma = 15°$ $U_\theta = 20.5°$ (Fig 6.33)	48.3	237	72.2	7.5	160.5	180	197	51
Worst case repetitive (Fig 6.22)	166	826	163	28.1	465	684	791	362.2

TABLE 4

REVERSE RECOVERY

Effect of thyristor model upon Recovery Overshoot and Damping Circuit Energy Dissipation during recovery.

	Recovery overshoot (%)	Damping circuit energy Dissipation during recovery (Joules)					Transformer (Total hfr Losses) (Joules)
		Valve 3	Valve 4	Valve 5	Valve 6 (recovering)	Total	
No Reverse-Recovered Charge	16.3	363.9 (18.5%)	197.1 (9.97%)	194.4 (9.83%)	1221.1 (61.8%)	1976.5	178.8
Non-linear resistor (refined model) (Q_{rr} = 4811μC)	37.37	535.5 (19.7%)	279.2 (10.3%)	275.6 (10.1%)	1626.8 (59.8%)	2718.1	273.6
'Conventional' thyristor model (Q_{rr} = 4811μC)	38.85	572 (20%)	290.3 (10.15%)	286.6 (10.0%)	1710.6 (59.8%)	2859.5	283

Note: 1) All energy dissipations are calculated from just prior to negative going current zero crossing (120μs after 658A is flowing in the valve about to recover), up to an elapsed time of 400μs later.

2) Figures in brackets are a percentage of the total damping circuit energy dissipation resulting from recovery of valve 6.

3) C_d = 2.28μF, R_d = 32.8Ω

4) α = 90 + DOV operation.

TABLE 5

REVERSE RECOVERY

Effect of Transformer representation upon recovery overshoot and damping circuit dissipation during recovery.

	Recovery overshoot (%)	Damping circuit energy Dissipation (Joules) Valve 3	Valve 4	Valve 5	Valve 6 (recovering)	Total
Single-section transformer representation	37.6	544.2 (20.1%)	259 (9.6%)	255 (9.4%)	1642.1 (60.8%)	2701
Five-section transformer representation	35.4	523.5 (20.3%	243 (9.4%)	241 (9.3%)	1574.8 (60.9%)	2583

Note: 1) All energy dissipations are calculated from just prior to negative going current zero crossing (120μs after 658A in the valve about to recover), up to an elapsed time of 400μs later.

2) Figures in brackets are a percentage of the total damping circuit energy dissipation resulting from recovery of valve 6.

3) $C_d = 2.28\mu F$, $R_d = 32.8\Omega$

4) $\alpha = 90 +$ DOV operation

TABLE 6

REVERSE RECOVERY

Continuous operation: Dissipation at recovery (Joules)

Firing/ Extinction Angle	Recovering Valve (V6)		Series Valve (V3)		Valve (V5)		Valve (V4)		Total Dissipation	
	R_D	SA	R_D	SA	R_D	SA	R_D	SA	R_D	SA
$\alpha = 6°$	332.1	0.007	108.7	0.008	57.9	0.169	58.6	0.169	557.4	0.353
$\alpha = 12°$	361.3	0.008	118.2	0.007	63.1	0.164	63.9	0.165	606.5	0.344
$\alpha = 15°$	383.3	0.008	125.4	0.007	67	0.16	67.8	0.16	643.5	0.335
$\gamma = 14°$	63.9	0.0004	20.2	0.079	11.5	0.018	11.7	0.018	107.3	0.116
$\gamma = 15°$	72.7	0.0005	23	0.089	13.1	0.017	13.2	0.017	122	0.124
$\gamma = 16°$	82	0.0006	26	0.098	14.7	0.017	14.9	0.017	137.6	0.133

Notation:

R_D : Damping resistance (100 levels)

SA : Surge Arrester

Note:

1) $C_d = 2.28\mu F$ $R_d = 30\,\Omega$

2) Dissipations calculated up to an elapsed time of approximatley 400μs after, negative going, current zero crossing.

TABLE 7

CURRENT PRE-ESTABLISHED IN SURGE ARRESTER

Rate-of-rise of thyristor current [A μs^{-1}]

Elapsed Time	Surge Arrester Co-ordinating Current at 400kV		
	3kA	2kA	1kA
(0<t<1μs)	152	152	152
(1<t<2μs)	171	170	170
(2<t<3μs)	242	240	236
(3<t<4μs)	470	460	443
(4<t<5μs)	867	807	662
(5<t<6μs)	2037	1861	1475

TABLE 8

CURRENT PRE-ESTABLISHED IN SURGE ARRESTER

Magnitude of First Current Peak* (A)

5421	4495	3487

* These current peaks occur at an elapsed time of approximately 7μs after valve turn-on.

TABLE 9

COMMUTATION FAILURE - INRUSH PREDICTIONS

	$\frac{di}{dt}_m$ [A μs^{-1}]	$i_{1\,(pk)}$ [A]	$i_{1\,(tr)}$ [A]
Proposed reactor characteristics Delayed Valve (V3)	1890(4.5μs)	4033	478
Sellindge converter station Delayed Valve (V3)	242	1900	98

TABLE 10

VALVE-FIRING TRANSIENT INTERACTION: 12 PULSE NOTCH

Parameters of notch referred to one level*, for both a single-section and a five-section transformer representation.

$\gamma = 15°$, $U_o = 20.47°$, peak line-line voltage = 245.5kV

	Single-section Transformer Representation	Five-section Transformer Representation (With End-effects)
Magnitude of voltage notch across a level	327.9V	345V
Magnitude of voltage notch across a thyristor	286V	302.8V
Magnitude of voltage notch (per thyristor)/firing voltage x $\frac{100\%}{1}$	20%	21.26%
Time of voltage notch with respect to current zero	530μs	530μs
dV/dt across a level, immediately following positive going voltage zero crossing across the level	72V μs^{-1}	81V μs^{-1}
Maximum dV/dt across a level, following positive going voltage zero crossing across the thyristor	51V μs^{-1}	64V μs^{-1}
Maximum dV/dt across a thyristor, following positive going voltage zero crossing across the thyristor	51V μs^{-1}	46.3V μs^{-1}
Time of thyristor voltage zero with respect to V9 firing	7.38μs	6.41μs
Duration of positive excursion of voltage notch, per level	8.01μs	7.36μs
Duration of positive excursion of voltage notch, per thyristor	7.62μs	6.32μs

* Assuming 100 levels constitute a valve, neglecting voltages sharing errors and redundancy, and assuming distributed inductance.

TABLE 11

VALVE RESPONSE TO IMPULSE TEST VOLTAGES

Switching-Impulse: Initial Conditions

i) 400kV across thyristors within off-state valve, (t = 102.7μs)

Valve-voltage	399kV
Sum of Thyristor voltages	400kV
Voltage across damping capacitors	219.5kV
Voltage across damping resistors	180.5kV
Valve-current	65.6A

ii) Maximum current flowing in off-state valve, (t = 70μs)

Valve-voltage	337.5kV
Sum of Thyristor voltages	337.5kV
Voltage across damping capacitors	135kV
Voltage across damping resistors	202.5kV
Valve-current	73.6A

iii) Point in time between i) and ii), (t = 90μs)

Valve-voltage	378.8kV
Sum of Thyristor voltages	380.1kV
Voltage across damping capacitors	187.9kV
Voltage across damping resistors	192.2kV
Valve-current	69.9A

TABLE 12

VALVE RESPONSE TO IMPULSE TEST VOLTAGES

Switching impulse: inrush predictions

	$\frac{di}{dt}_m$ ($A\,\mu s^{-1}$)	$i_{1(pk)}$ (A)	$i_{1(tr)}$ (A)	$\frac{di_2}{dt}$ ($A\,\mu s^{-1}$)	$i_{2(pk)}$ (A)	$\frac{dV}{dt}_T$ ($V\,\mu s^{-1}$)	$\frac{dV}{dt}_L$ ($V\,\mu s^{-1}$)	$E_{(45)}$ (Joules)
Static Initial Conditions								
Worst Case Repetitive (400kV) (Chapter 6.4.9)	166(3.5μs)	826(4.3μs)	163	28.1	465	684	791	362.2
Dynamic Initial Conditions								
Sum of thyristor Voltages = 400kV (102.7μs)	638(4.6μs)	1346(5.6μs)	117.5	40.2	510	1160	1350	368.3
Maximum Valve Current (70μs)	165(6μs)	805(6.5μs)	129	30.2	428	640	700	255
t = 90μs	621(4.9μs)	1200(5.8μs)	121	37.2	483	1000	1170	329

TABLE 13

VALVE RESPONSE TO IMPULSE TEST VOLTAGES

Lighting-Impulse: Initial Conditions

i. 400kV across thyristors within the off-state valve, (t = 2.41us).

Valve-voltage	471kV
Sum of thyristor voltages	400kV
Voltage across damping capacitors	8.2kV
Voltage across damping resistors	391.8kV
Valve-current	142.5A

ii. 1μs after dV/dt across a thyristor level in the off-state valve exceeds 1kV μs^{-1} (t =1.1μs).

Valve-voltage	475.2kV
Sum of thyristor voltages	278.5kV
Voltage across damping capacitors	2.0kV
Voltage across damping resistors	276.5kV
Valve-current	100.5A

TABLE 14

VALVE RESPONSE TO IMPULSE TEST VOLTAGES

Front-of-Wave: Initial Conditions

1μs after dV/dt across a thyristor level in the off-state valve exceeds 1kV μs^{-1} (t = 1μs).

Valve-voltage	489.2kV
Sum of thyristor voltages	321.5kV
Voltage across damping capacitors	2.5kV
Voltage across damping resistors	319kV
Valve-current	116A

TABLE 15

VALVE RESPONSE TO IMPULSE TEST VOLTAGES

Lightning-impulse and front-of-wave impulse: inrush predictions

	$\frac{di}{dt}_m$ ($A\ \mu s^{-1}$)	$i_{1(pk)}/t$ (A)	$i_{1(tr)}$ (A)	$\frac{di_2}{dt}$ ($A\ \mu s^{-1}$)	$i_{2(pk)}$ (A)	$\frac{dV_T}{dt}$ ($V\ \mu s^{-1}$)	$\frac{dV_L}{dt}$ ($V\ \mu s^{-1}$)	$E_{(45)}$ (Joules)
Static Initial Conditions								
Worst Case Repetitive (400kV) (Chapter 6.4.9)	166(3.5μs)	826(4.3μs)	163	28.1	465	684	791	362.2
Dynamic Initial Conditions - Lightning Impulse								
Sum of thyristor Voltages = 400kV (2.41μs)	900(3.9μs)	1465(5μs)	-3.46	45.7	457	1420	1610	524
1μs after dV/dt_{-1} exceeds 1kV μs^{-1} (t = 1.1μs)	810(4.3μs)	1377(5.5μs)	6.5	45	456	1340	1530	541
Dynamic Initial Conditions - Front-of-wave Impulse								
1μs after dV/dt_{-1} exceeds 1kV μs^{-1} (t = 1μs)	947(3.96μs)	1520(5μs)	-4.17	48	476	1470	1690	577

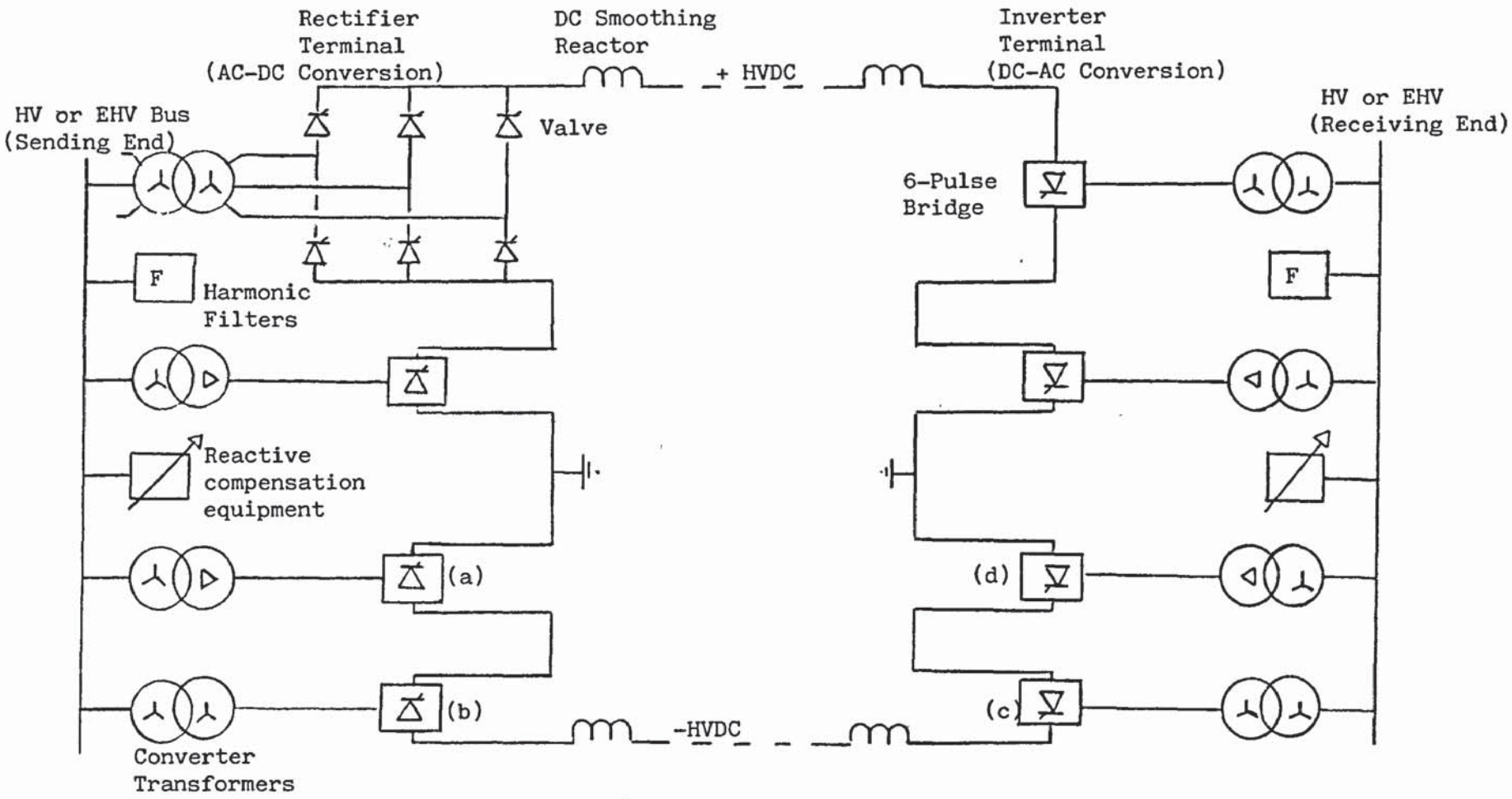

Fig.2.1 - Schematic of a bipolar, HVDC transmission scheme
(a) + (b) forms a 12-pulse bridge
(a) + (b) + (c) + (d) forms a pole

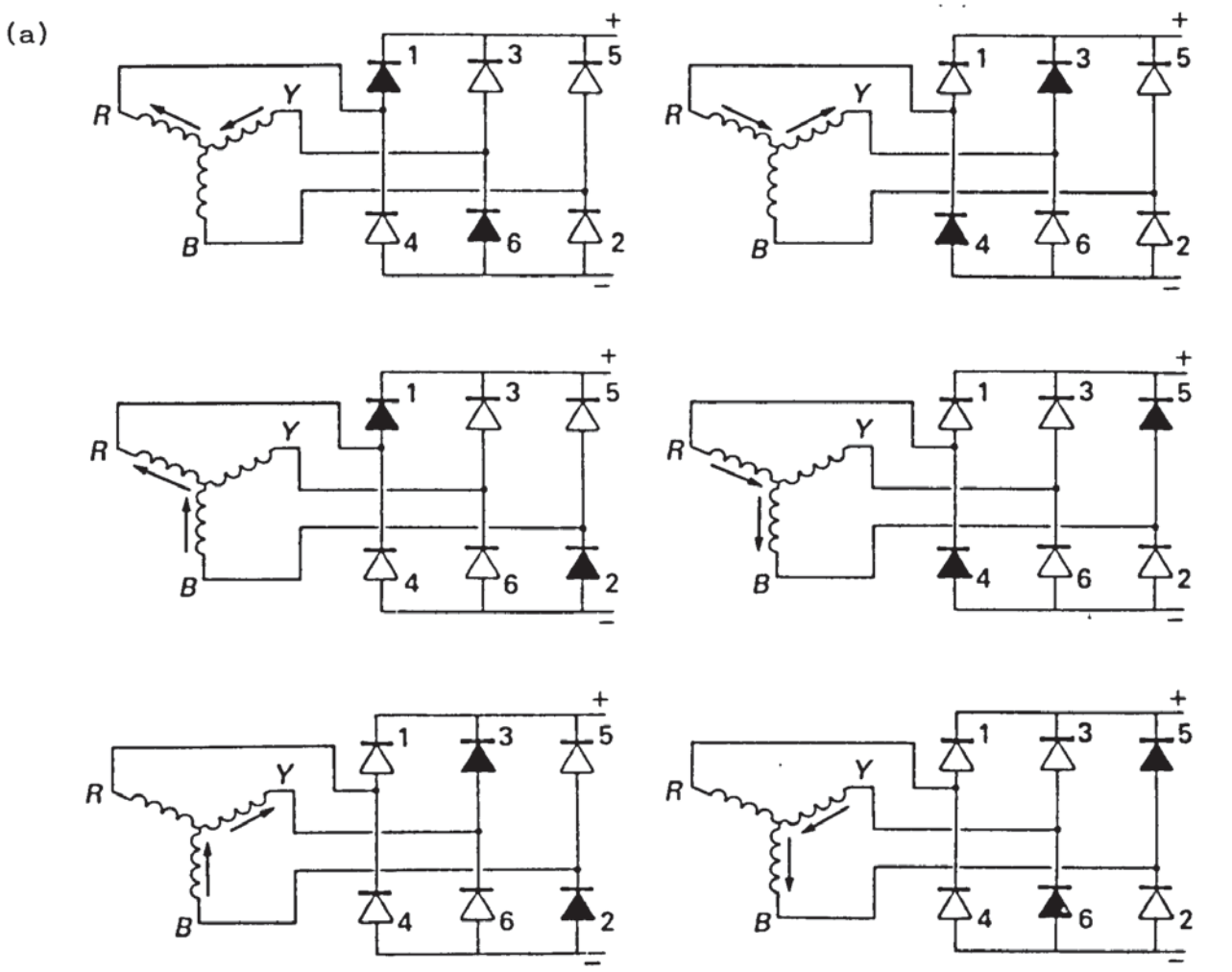

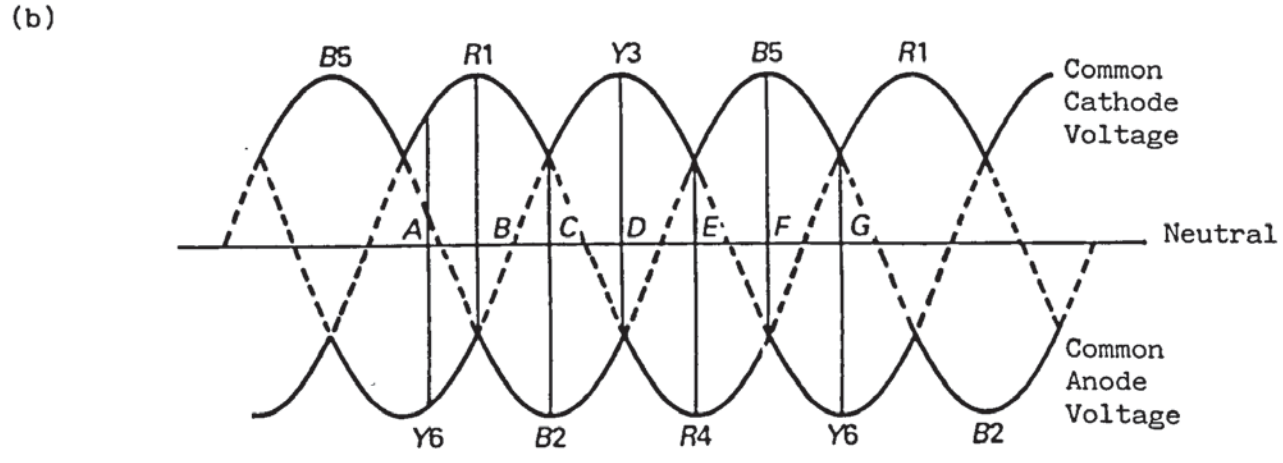

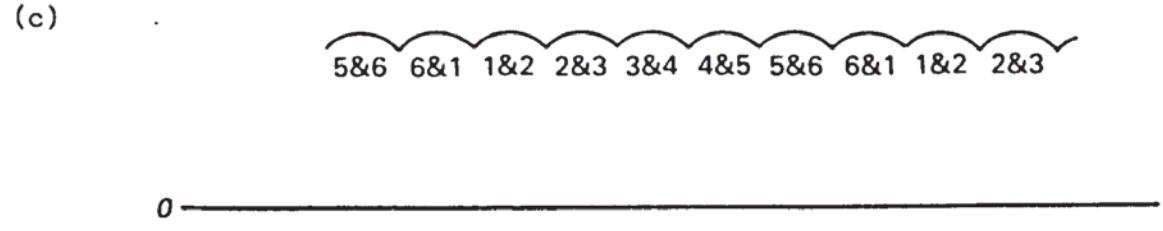

Fig.2.2 - Bridge conducting sequence and DC voltage waveforms
(a) Sequence of conduction
(b) Common anode and common cathode voltages
(c) Common cathode voltage with respect to the common anode.

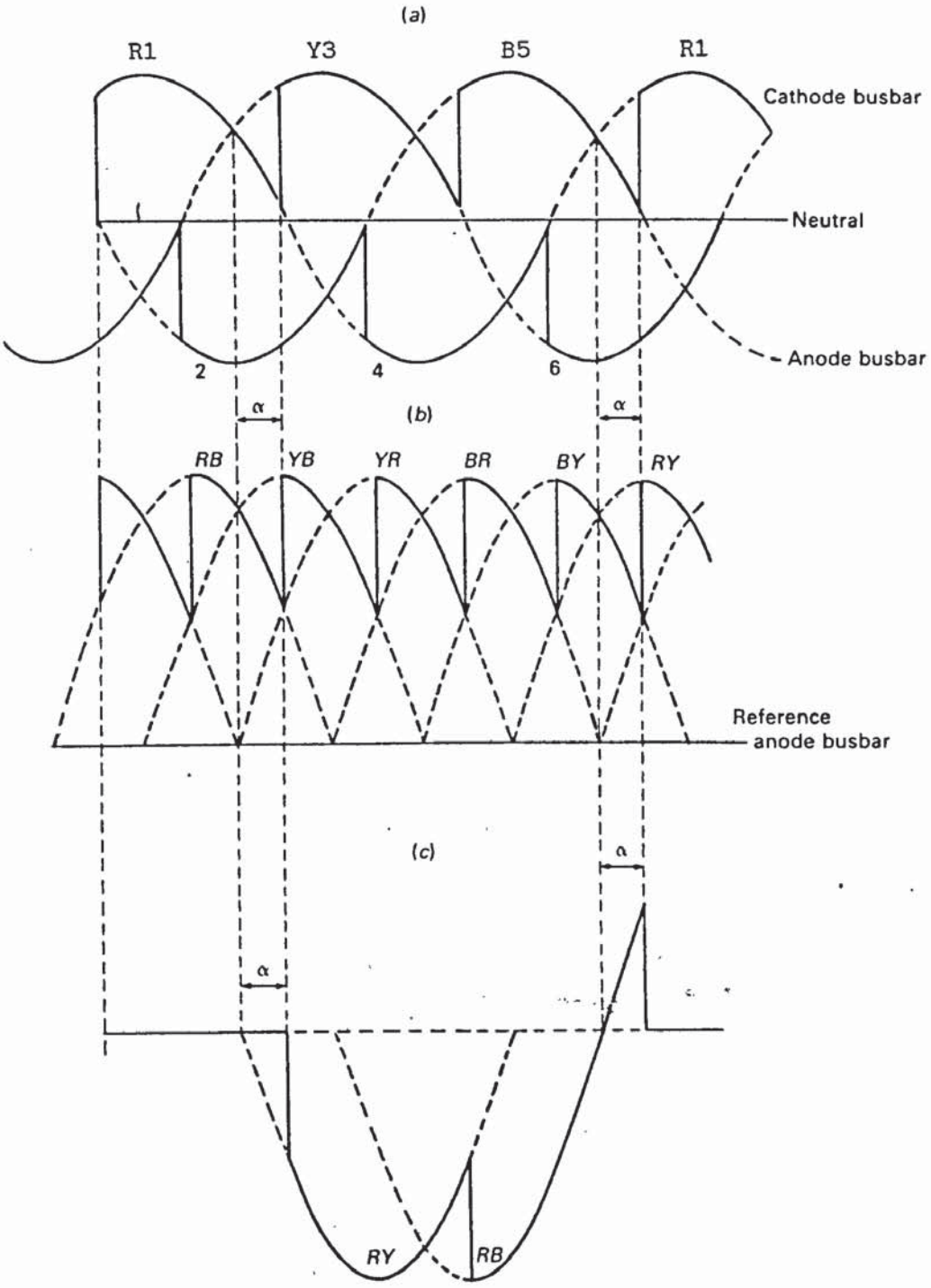

Fig.2.3 - Effect of firing delay on voltage waveforms
(a) Common anode and common cathode voltages
(b) Direct voltage
(c) Voltage across valve 1.

(a)

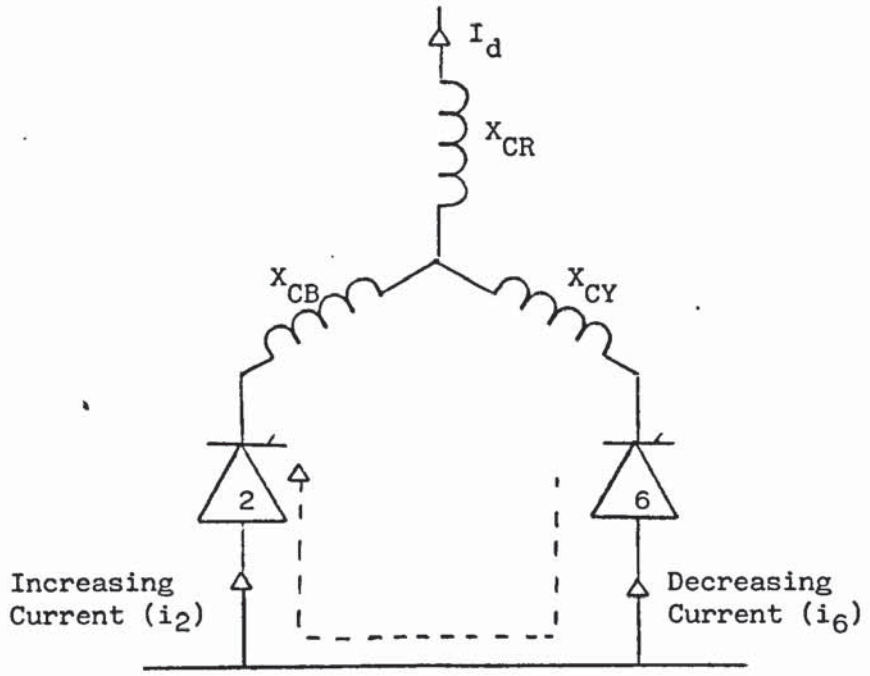

X_{CR}, X_{CY}, X_{CB} Leakage reactance of the red, yellow and blue phase, respectively, of a converter transformer.

i_2, i_6 Currents flowing in valves 2 and 6, respectively.

(b)

(c)

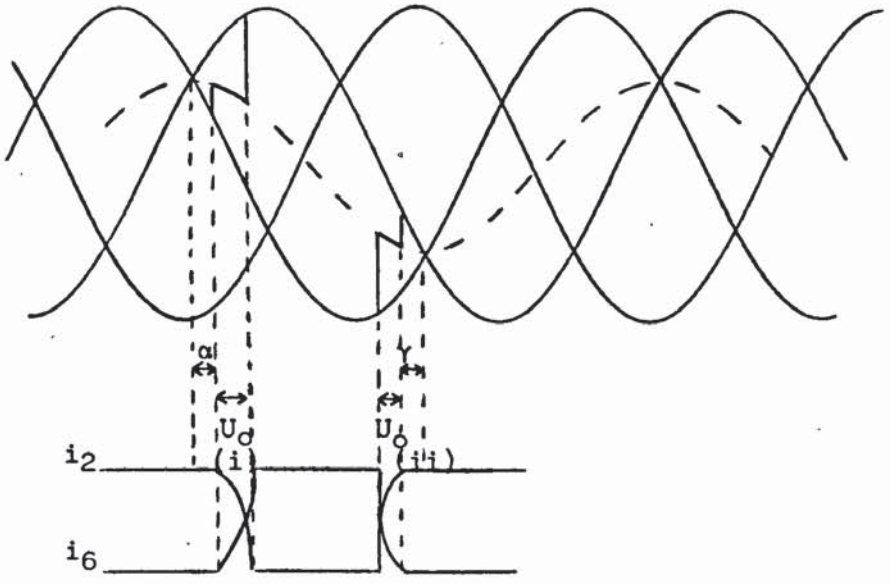

Fig.2.4 - The commutation process.
(a) Simplified equivalent circuit showing the commutation of current from valve 6 to valve 2.
(b) Voltage waveforms showing (i) Rectification
(ii) Inversion
(c) Current waveforms showing (i) Rectification
(ii) Inversion

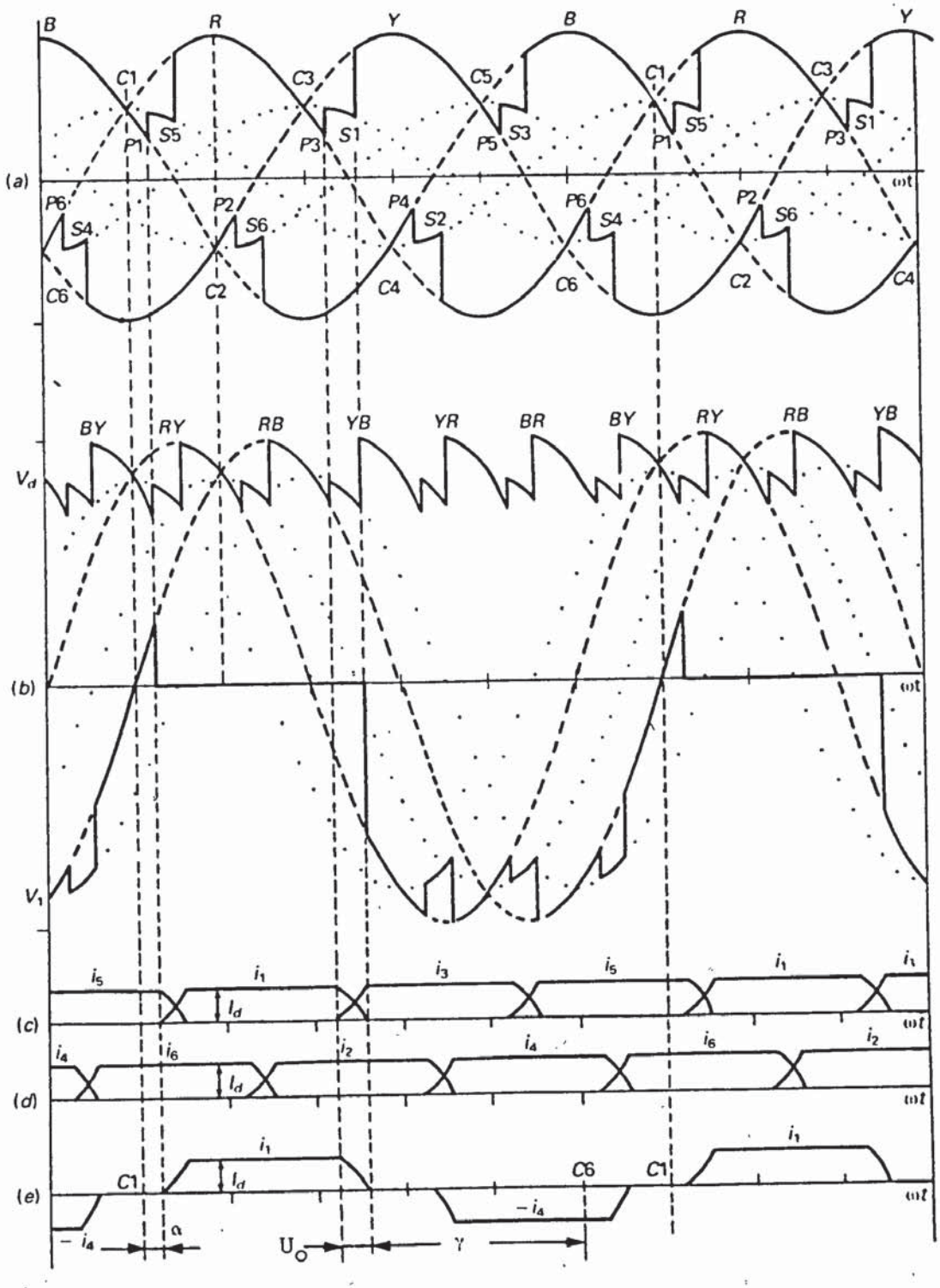

Fig.2.5 - Typical, 6-pulse bridge, voltage and current waveforms during rectification.

(a) Common cathode and common anode voltages with respect to the transformer neutral.

(b) Direct bridge voltage, V_d, and voltage across valve 1, V_1.

(c),(d) Valve currents i_1 to i_6.

(e) AC line current of the red phase.

C Instant of valve-voltage reversal

P Firing instant.

S Instant at which current commutation is completed.

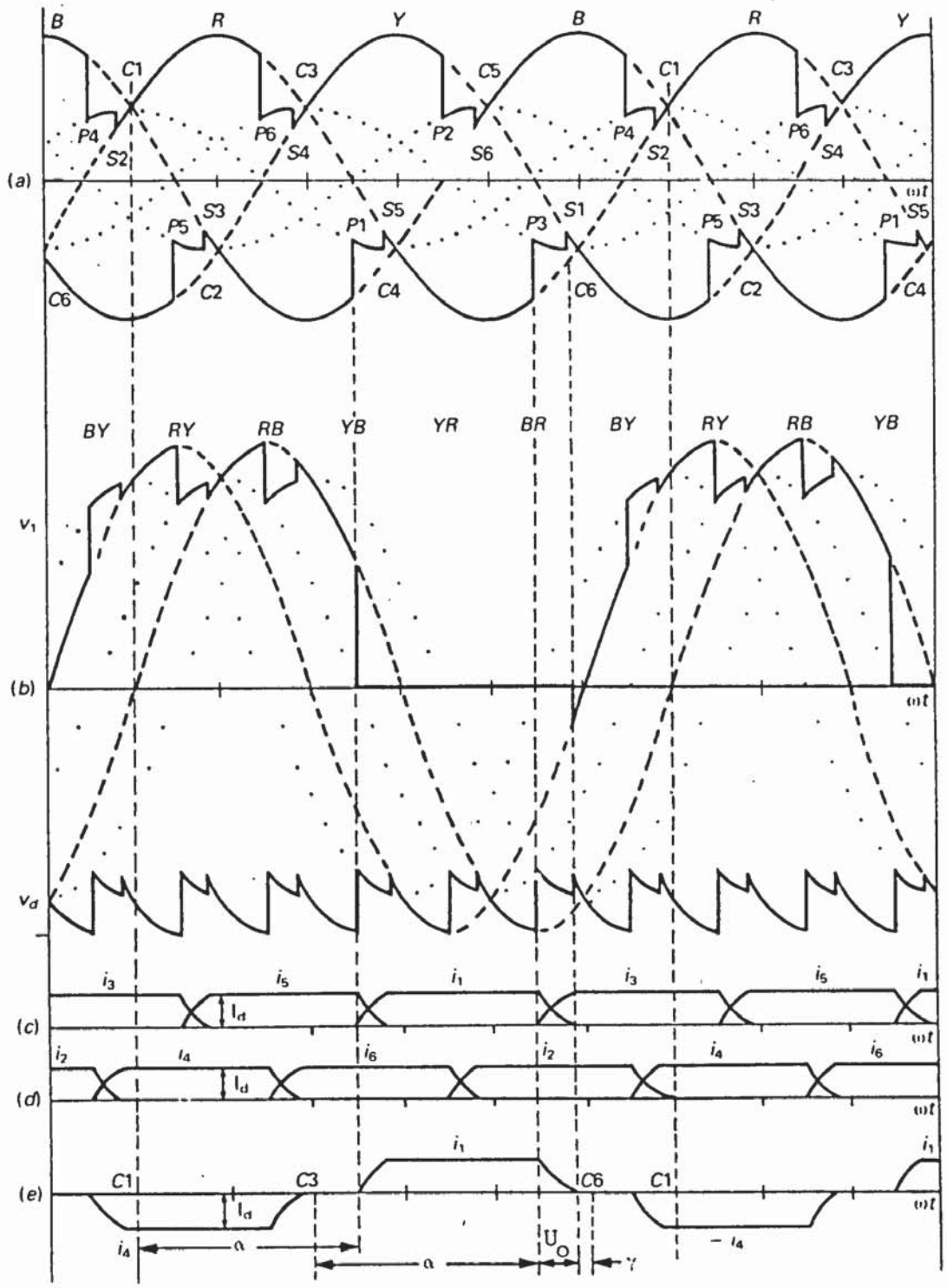

Fig.2.6 - Typical, 6-pulse bridge, voltage and current waveforms during inversion.

(a) Common anode and common cathode voltage with respect to the transformer neutral.

(b) Voltage across valve 1, V_1, and direct bridge voltage, V_d.

(c),(d) Valve currents i_1 to i_6

(e) AC line current of the red phase.

P Firing Instant

S Instant at which current commutation is completed.

C Instant of valve-voltage reversal.

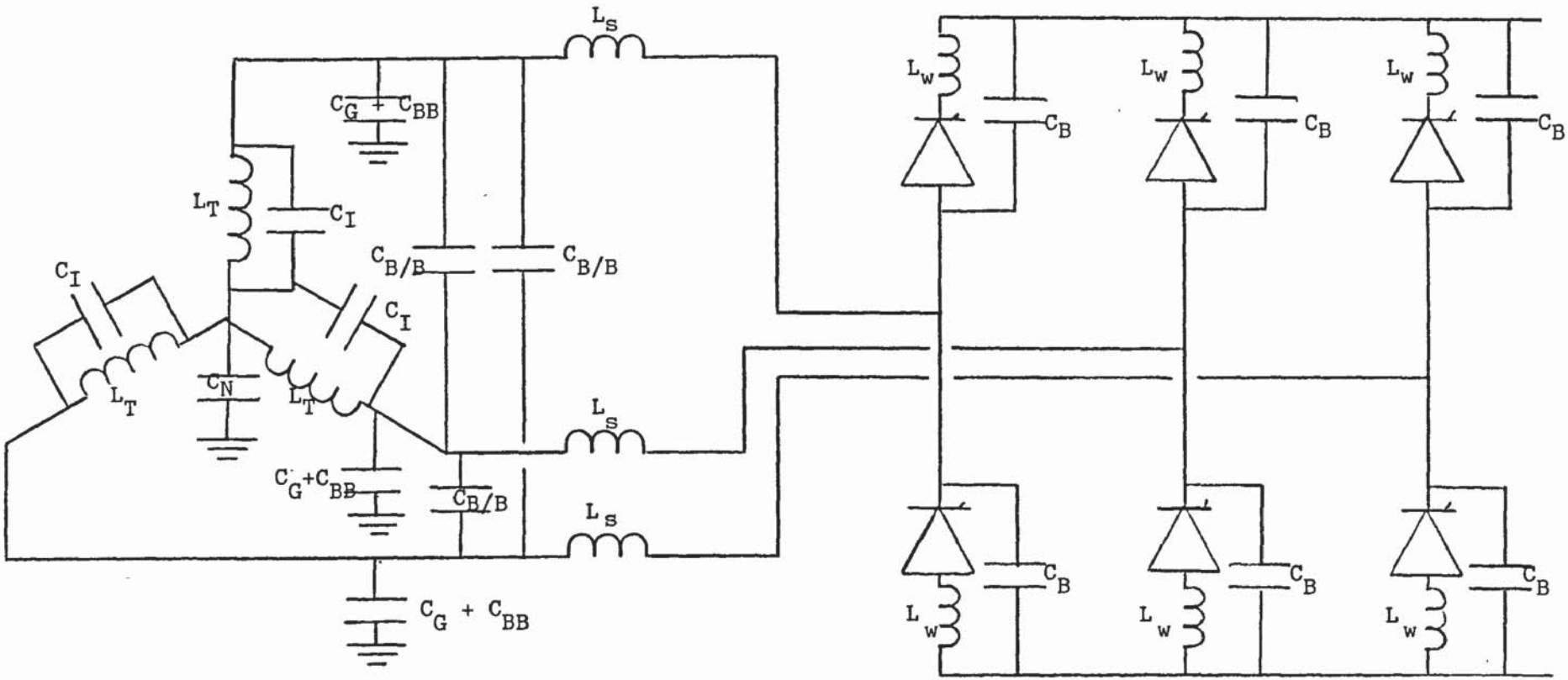

Fig.2.7 - Schematic of a six-pulse bridge showing stray capacitances and inductances as lumped parameters.

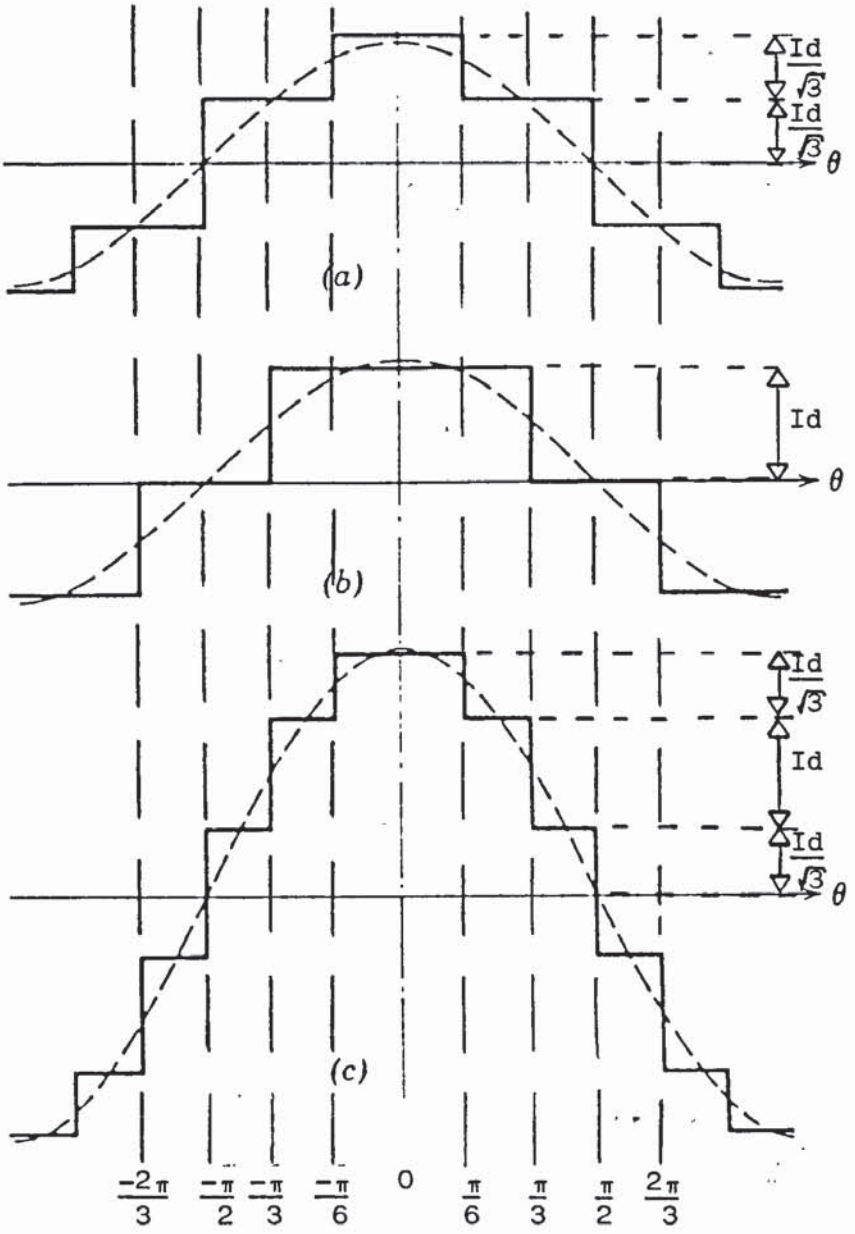

Fig.2.8 - Alternating line current for a bridge converter; commutating reactance neglected.

(a) 6-pulse bridge with a YΔ - connected transformer.
(b) 6-pulse bridge with a YY - connected transformer.
(c) 12-pulse bridge constructed from two 6-pulse bridges ((a) + (b)); connected in parallel on the primary and in series on the secondary.

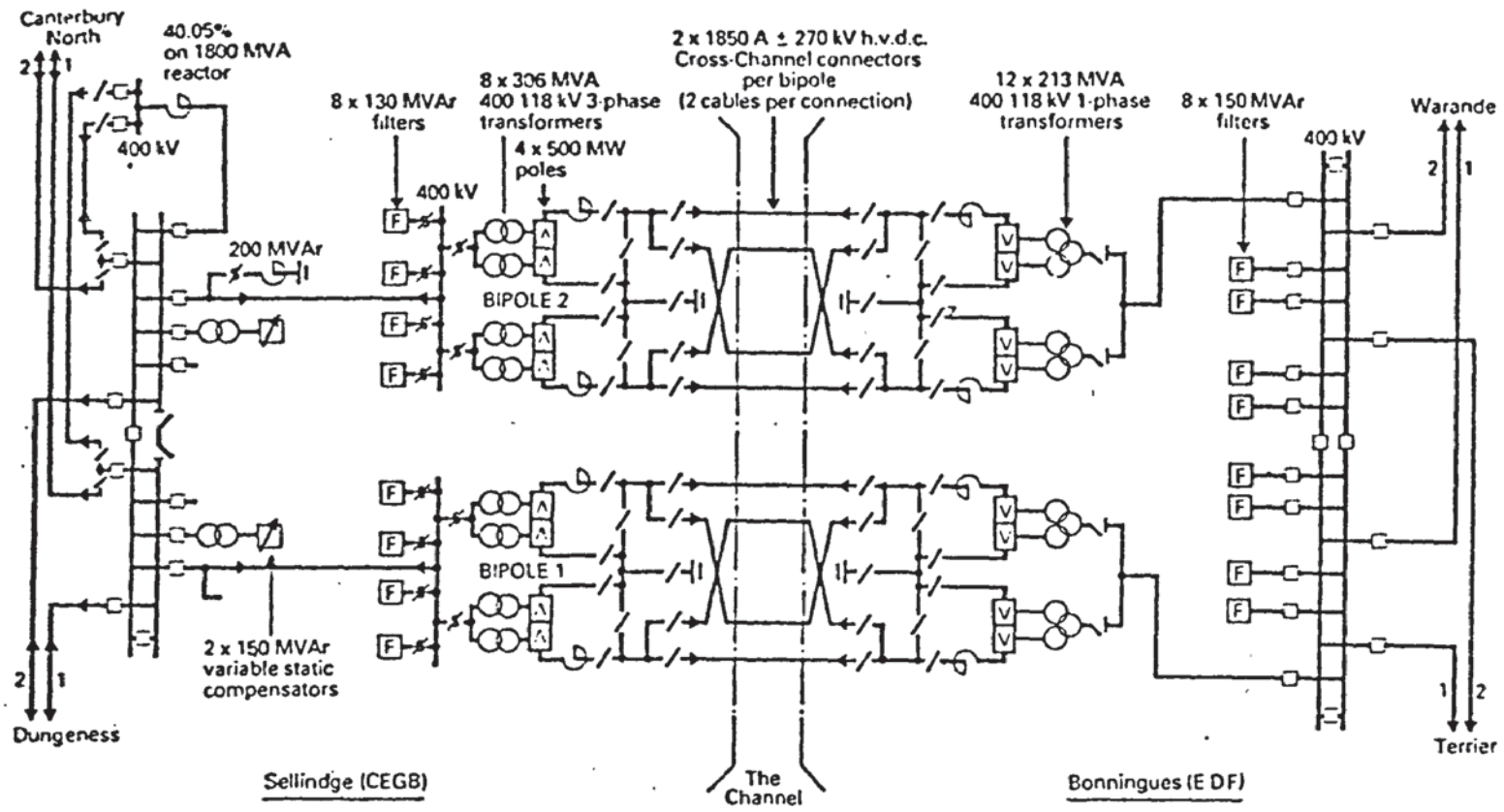

Fig.2.9 - Schematic showing the general arrangement of the proposed 2000 MW Cross-Channel Link.

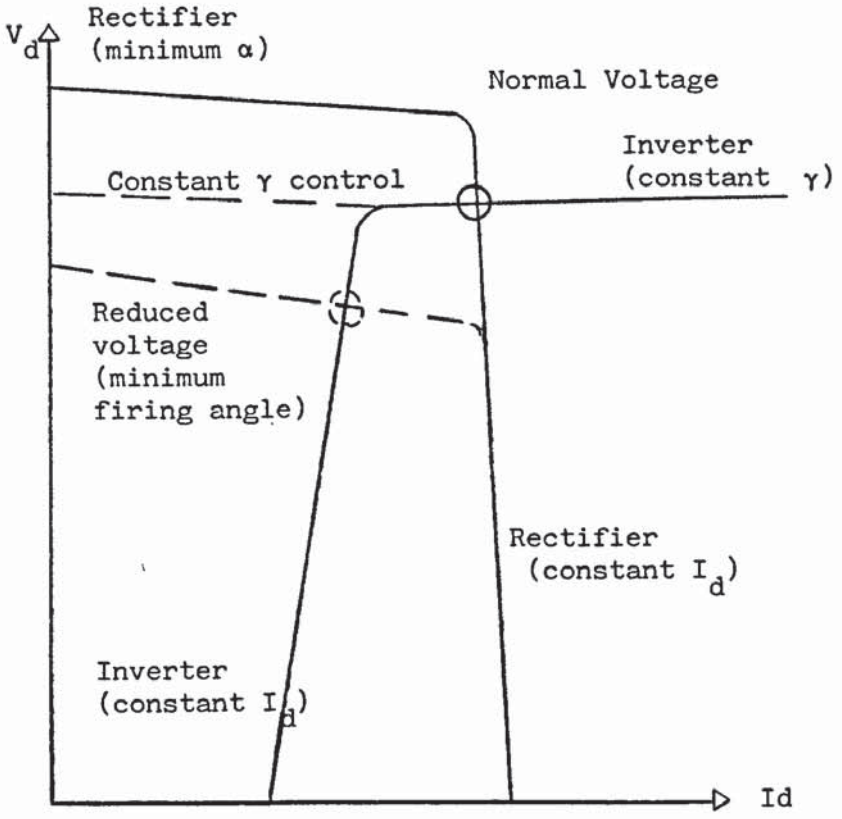

Fig.2.10 - General characteristics of an HVDC control system.

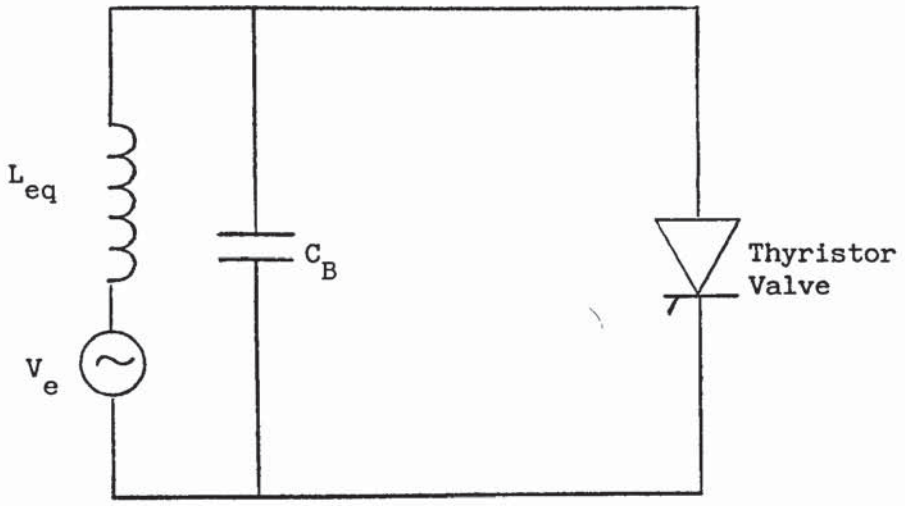

Fig.3.1 - Simplified, single-phase, equivalent circuit of a converter station used in discussion of voltage oscillations at thyristor turn-off.

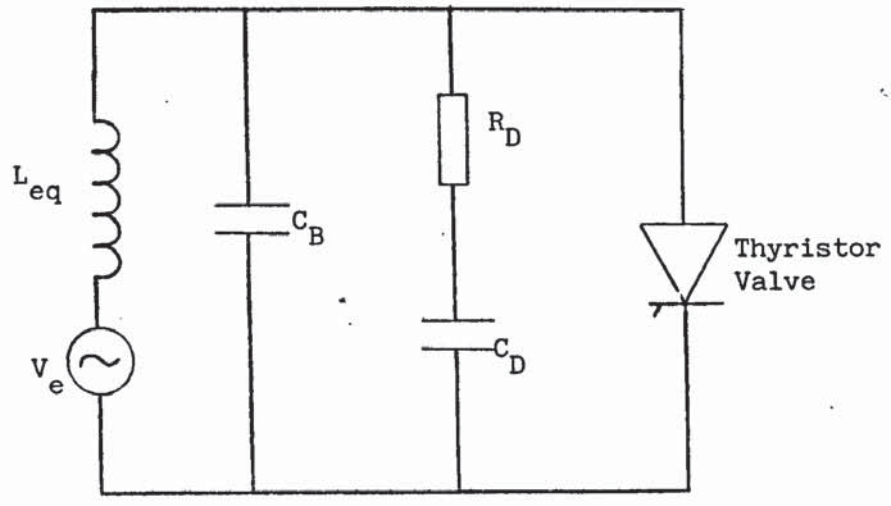

Fig.3.2 - Simplified, single-phase, equivalent circuit of a converter station with damping components (R_D and C_D) to limit the magnitude of recovery overvoltage at thyristor turn-off.

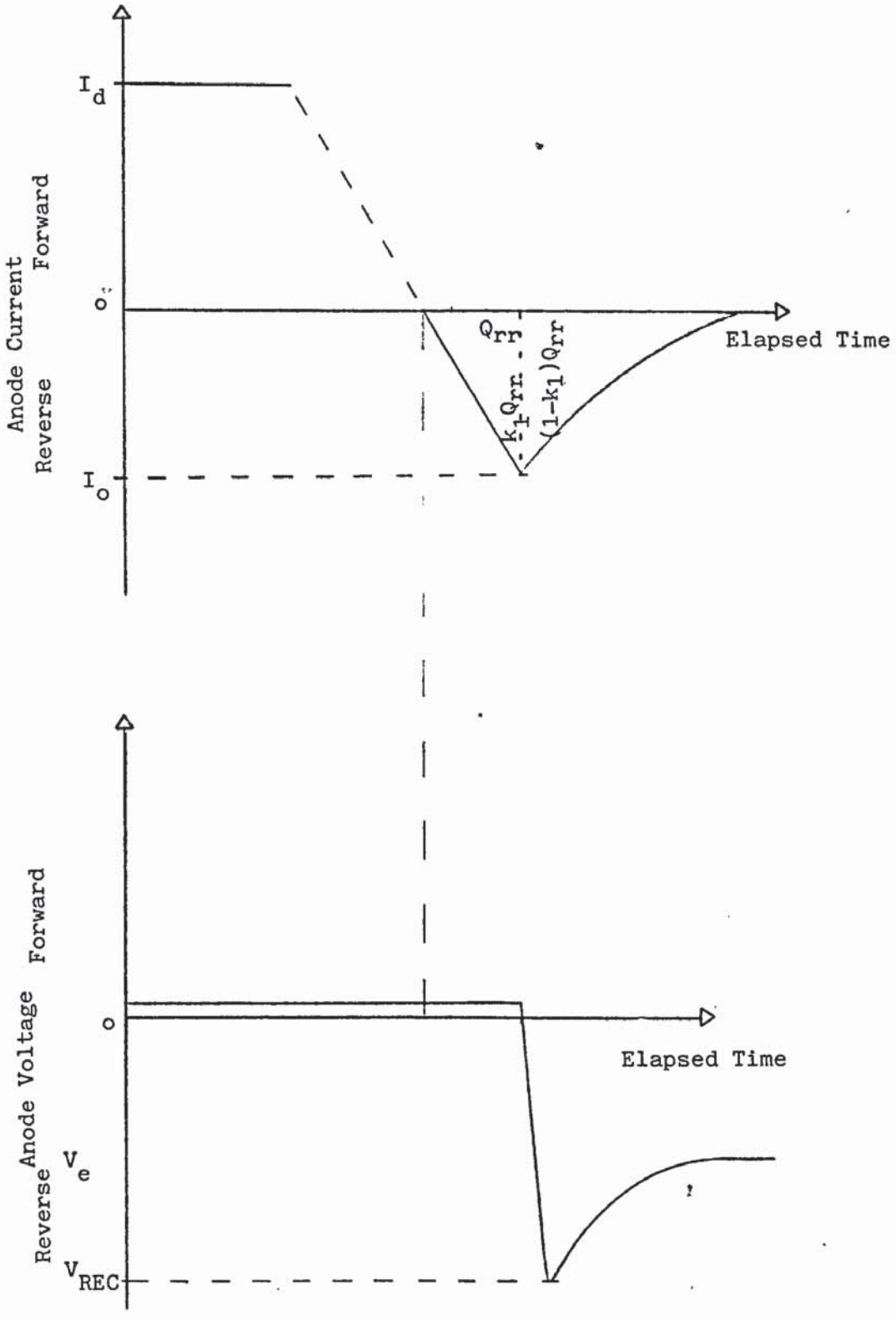

Fig.3.3 - Thyristor anode current and anode voltage during recovery.

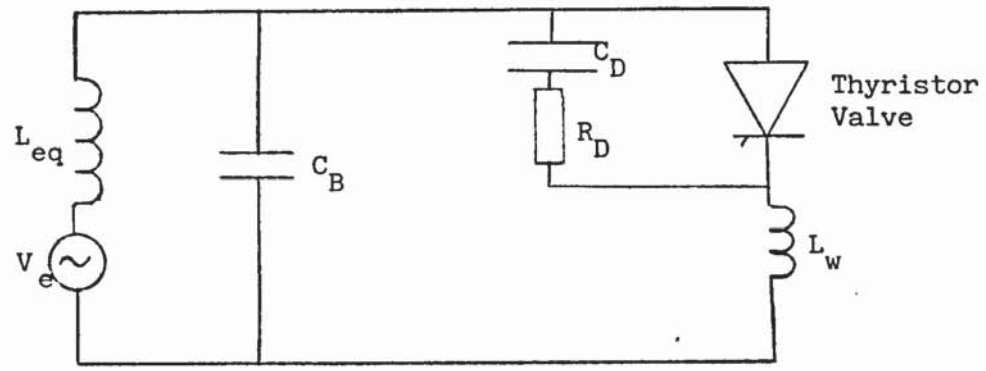

Fig.3.4 - Simplified, single-phase, equivalent circuit of a thyristor valve during turn-on.

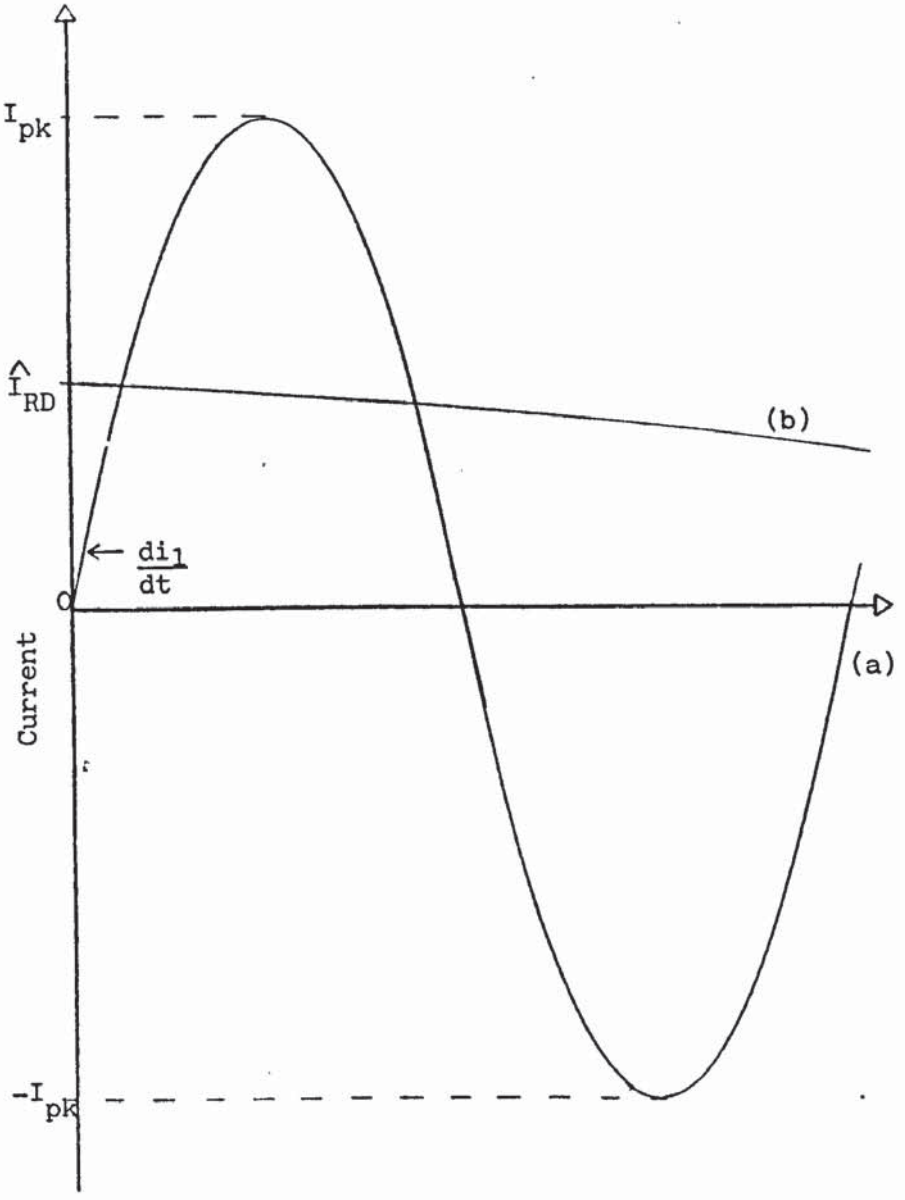

Fig.3.5 - Constituents of thyristor inrush current, (simplified circuit, fig.3.4)
(a) Displacement current from shunt-stray capacitance.
(b) Discharge-current from damping-circuit.

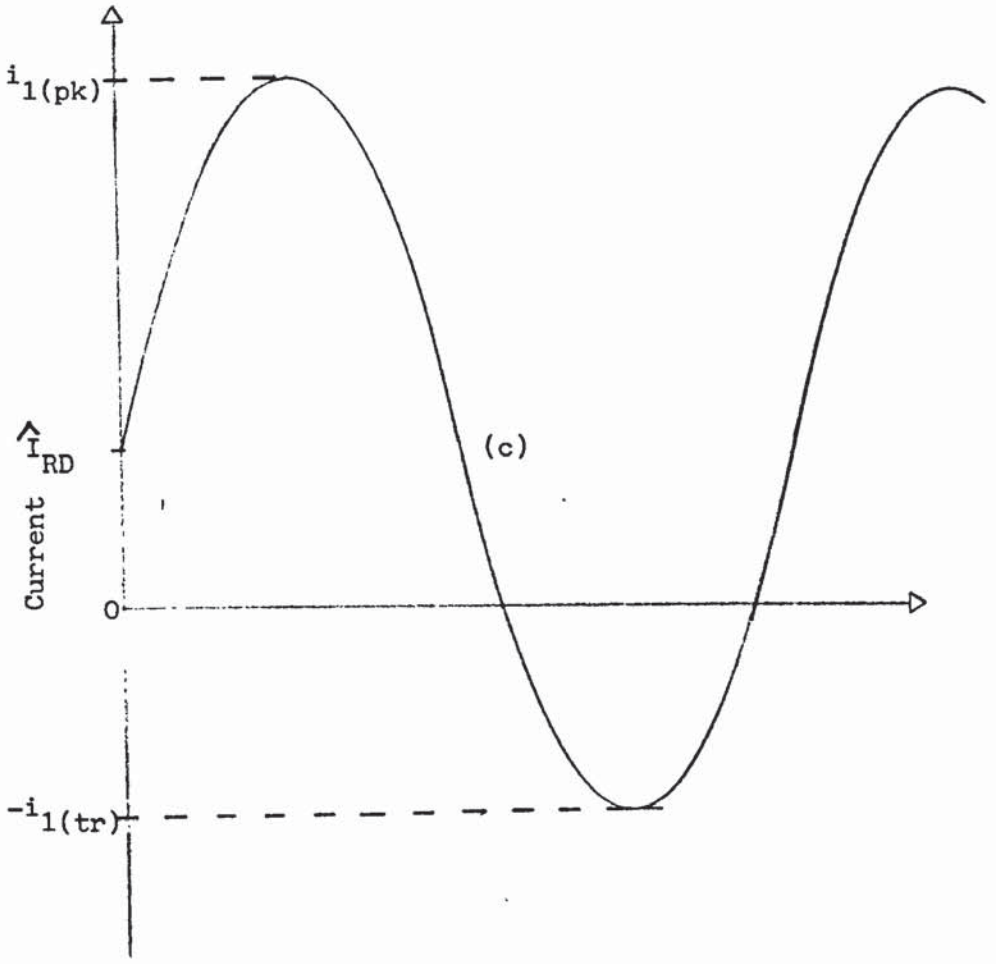

Fig.3.5 (c) Thyristor inrush current, (simplified circuit, fig.3.4), sum of 3.5(a) and (b)

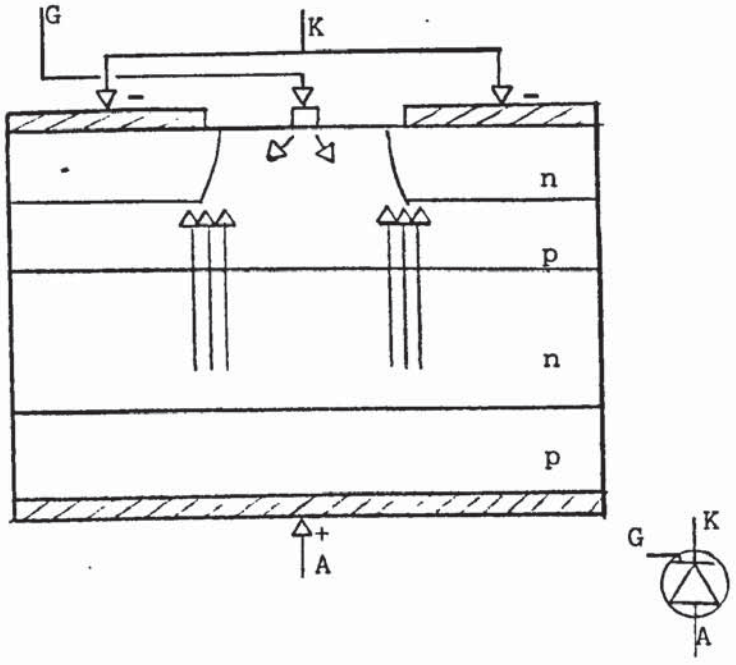

Fig.3.6 - Conventional, centre gate, thyristor
G Gate
A Anode
K Cathode

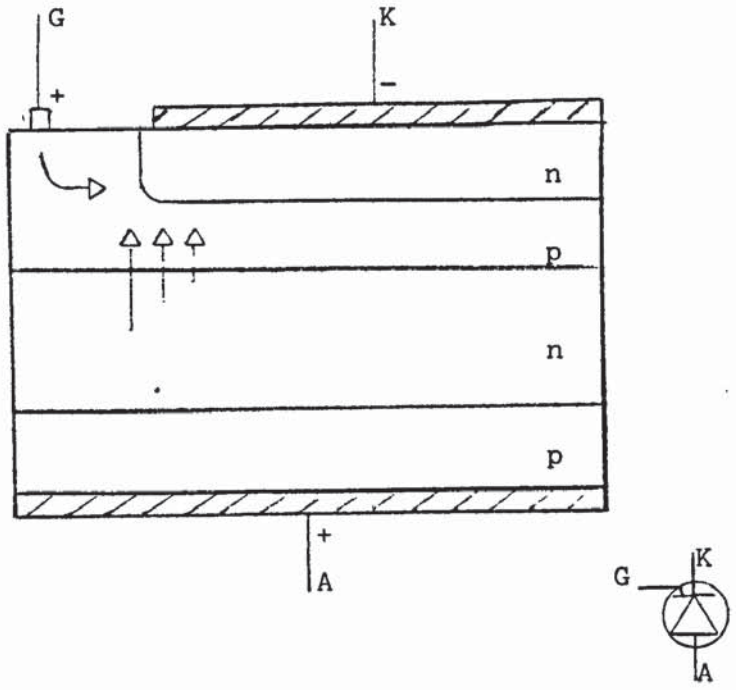

Fig.3.7 - Conventional side gate thyristor.

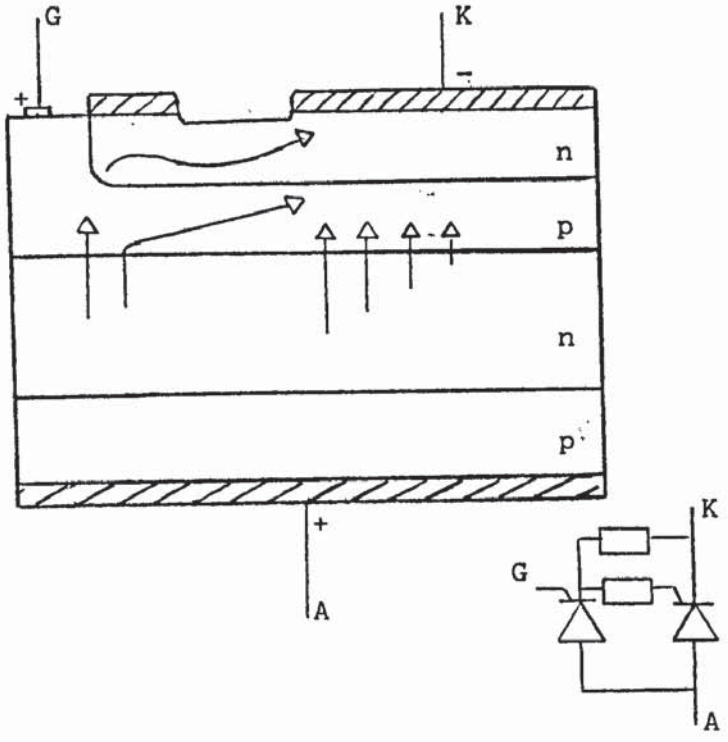

Fig.3.8 - Field initiated gate thyristor.

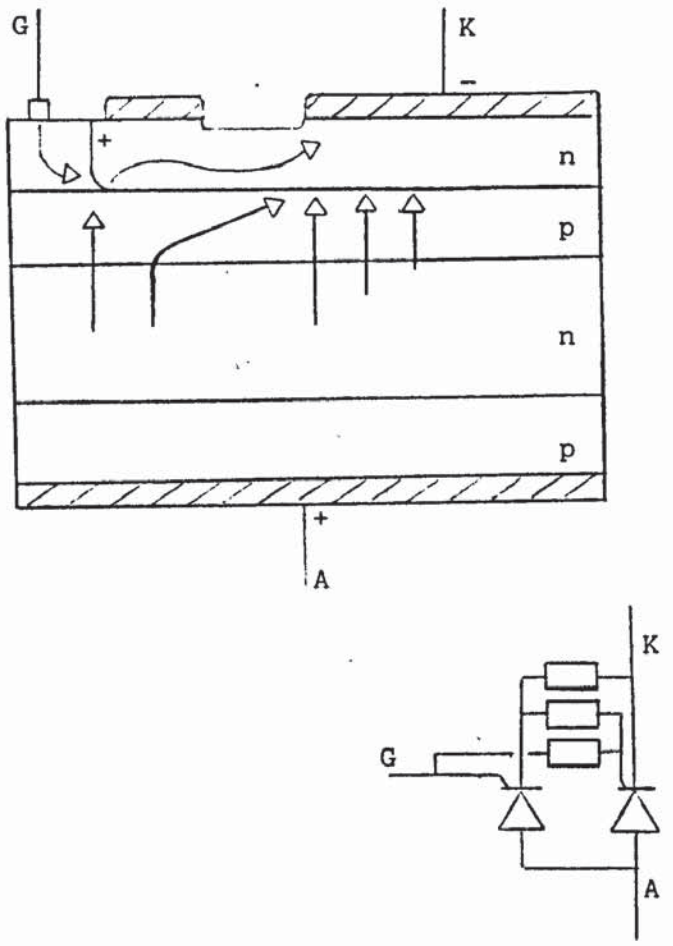

Fig.3.9 - N+ Gate Thyristor.

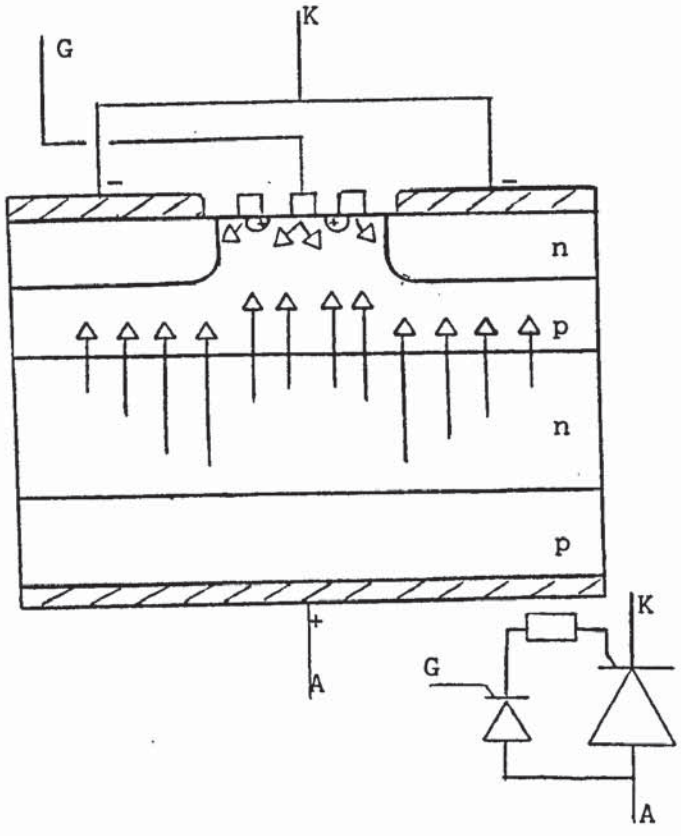

Fig.3.10 - Amplifying-gate thyristor.

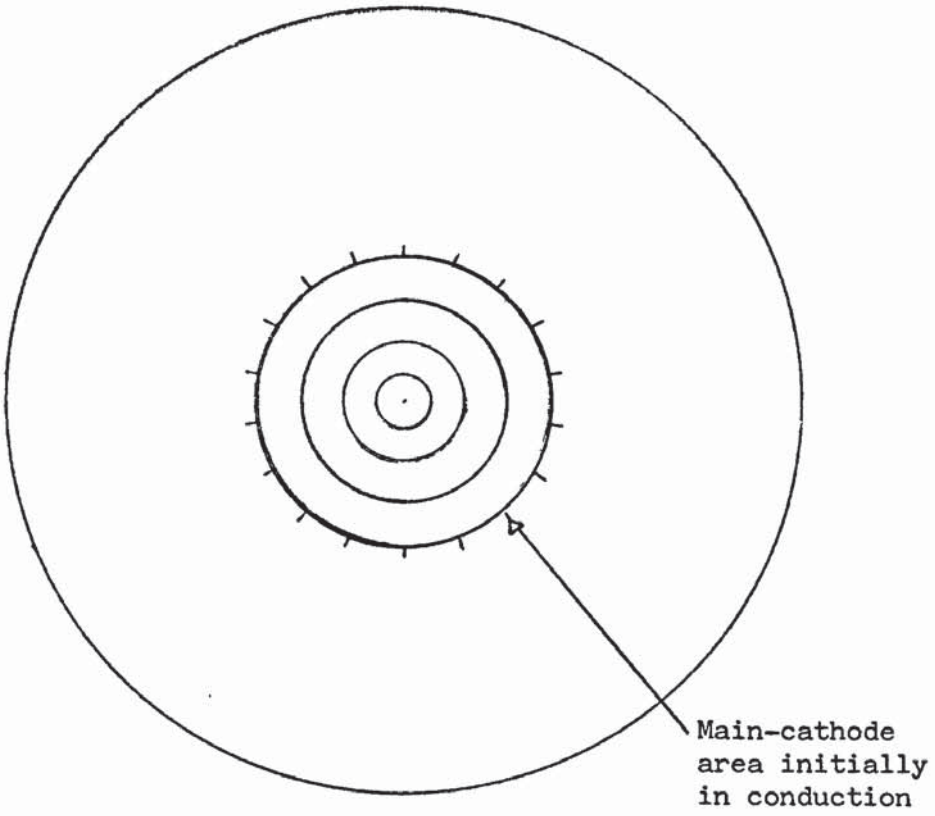

Fig.3.11 - Plan view of amplifying-gate thyristor.

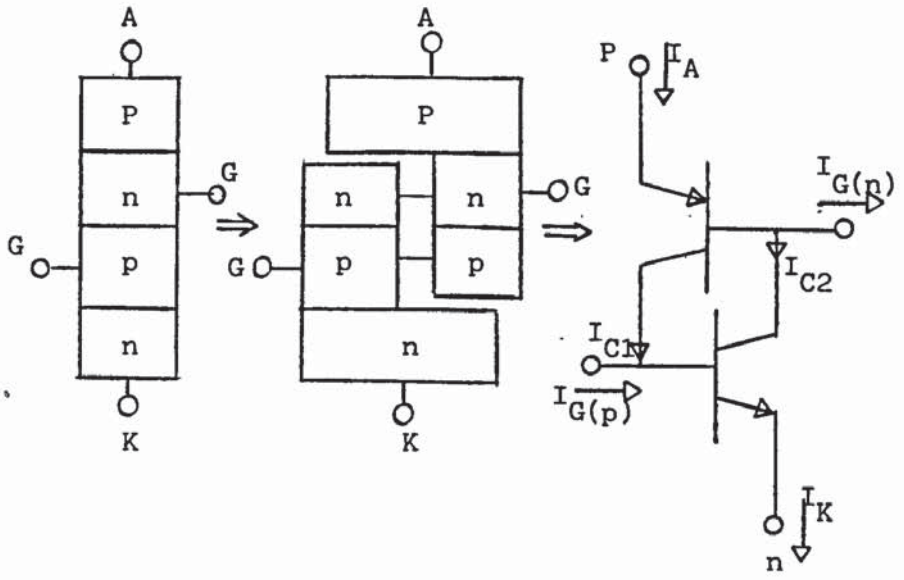

Fig.3.12 - Two transistor analogue of a p-n-p-n structure.

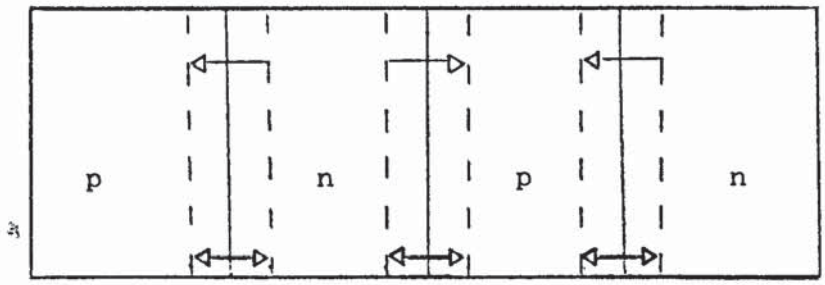

⟶ Direction of electric field, from region of of excess positive charge to region of excess negative charge.

⟷ Depletion layer

Fig.3.13(a) p-n-p-n structure with zero bias

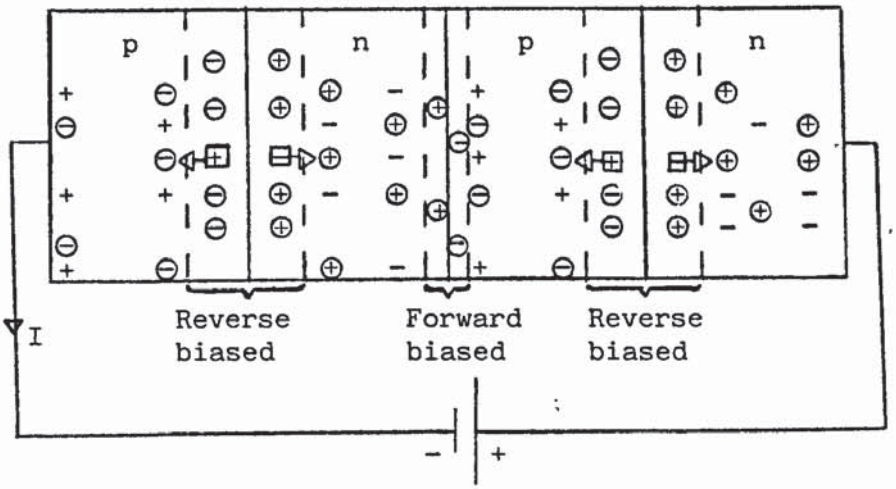

\- Free electron

\+ Free hole

⊖ Fixed acceptor impurity ion

⊕ Fixed donor impurity ion

Fig.3.13(b) - Reverse biased p-n-p-n structure

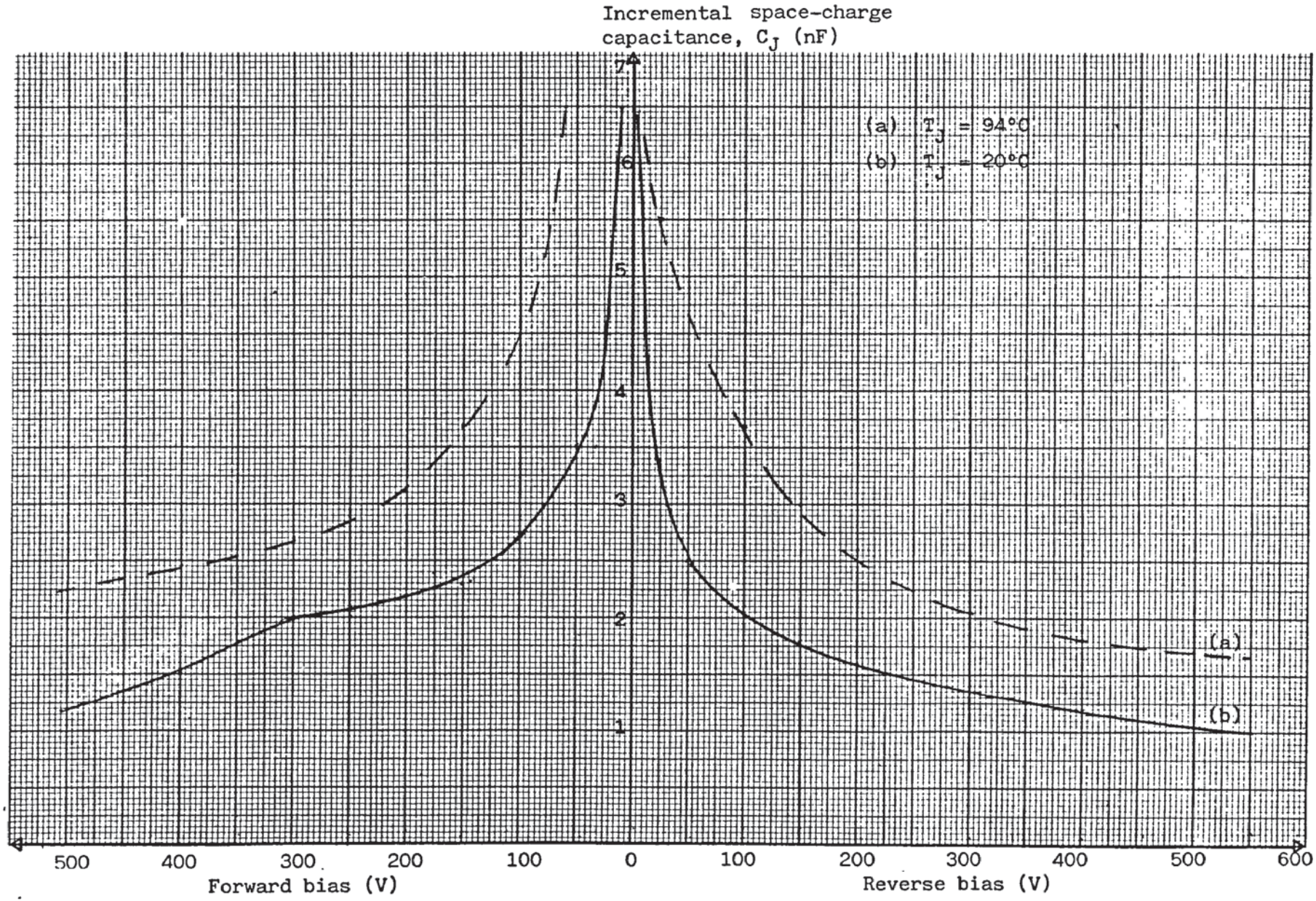

Fig.3.14 - Small signal capacitance, C_J, versus DC voltage (56mm thyristor)

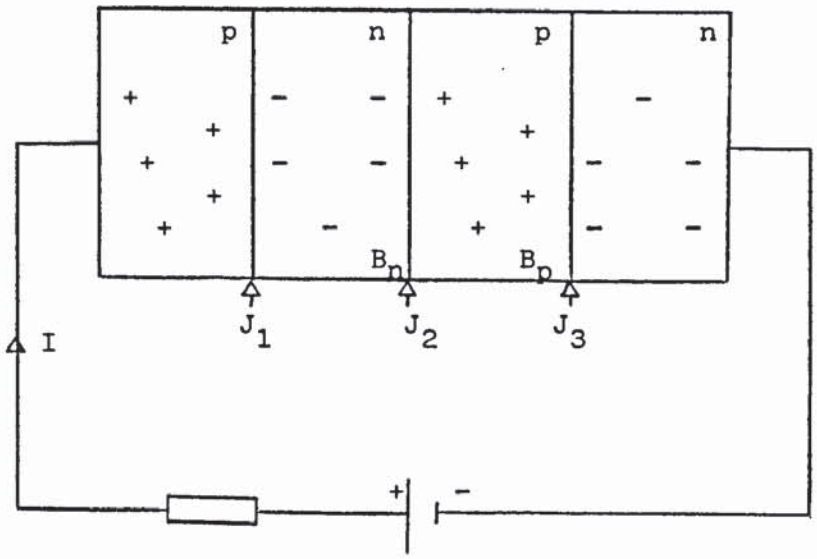

Fig.3.15 - Forward biased p-n-p-n structure in its conducting state

J_1, J_2, J_3 p-n junctions

B_n, B_p Base regions

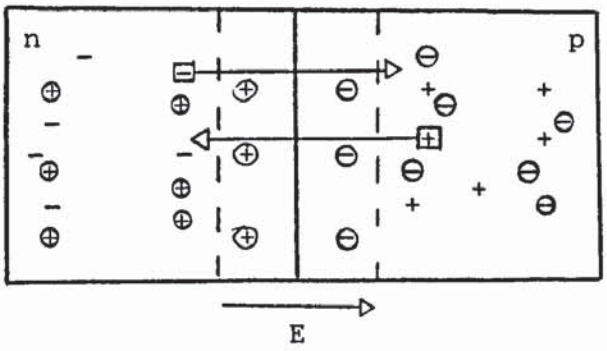

- Free electron
+ Free hole
⊖ Fixed acceptor impurity ion
⊕ Fixed donor impurity ion

Fig.3.16 - Abrupt junction model of a p-n structure with zero bias.

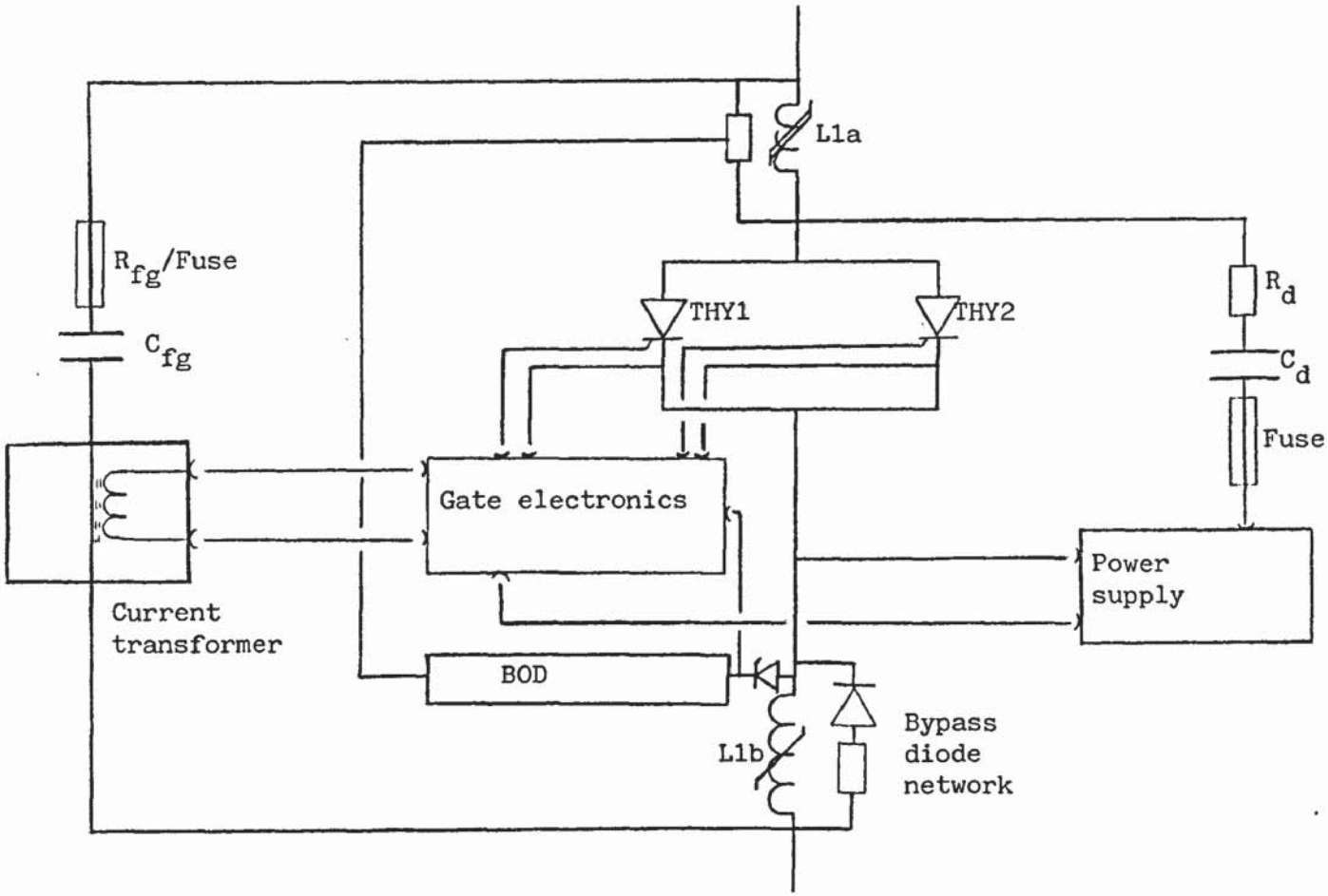

Fig.3.17 - Simplified circuit diagram of a thyristor module (Sellindge converter station design)

L1a Ferrite saturating reactor.
L1b Quasi-linear reactor.
THY1, THY2 56mm thyristors.

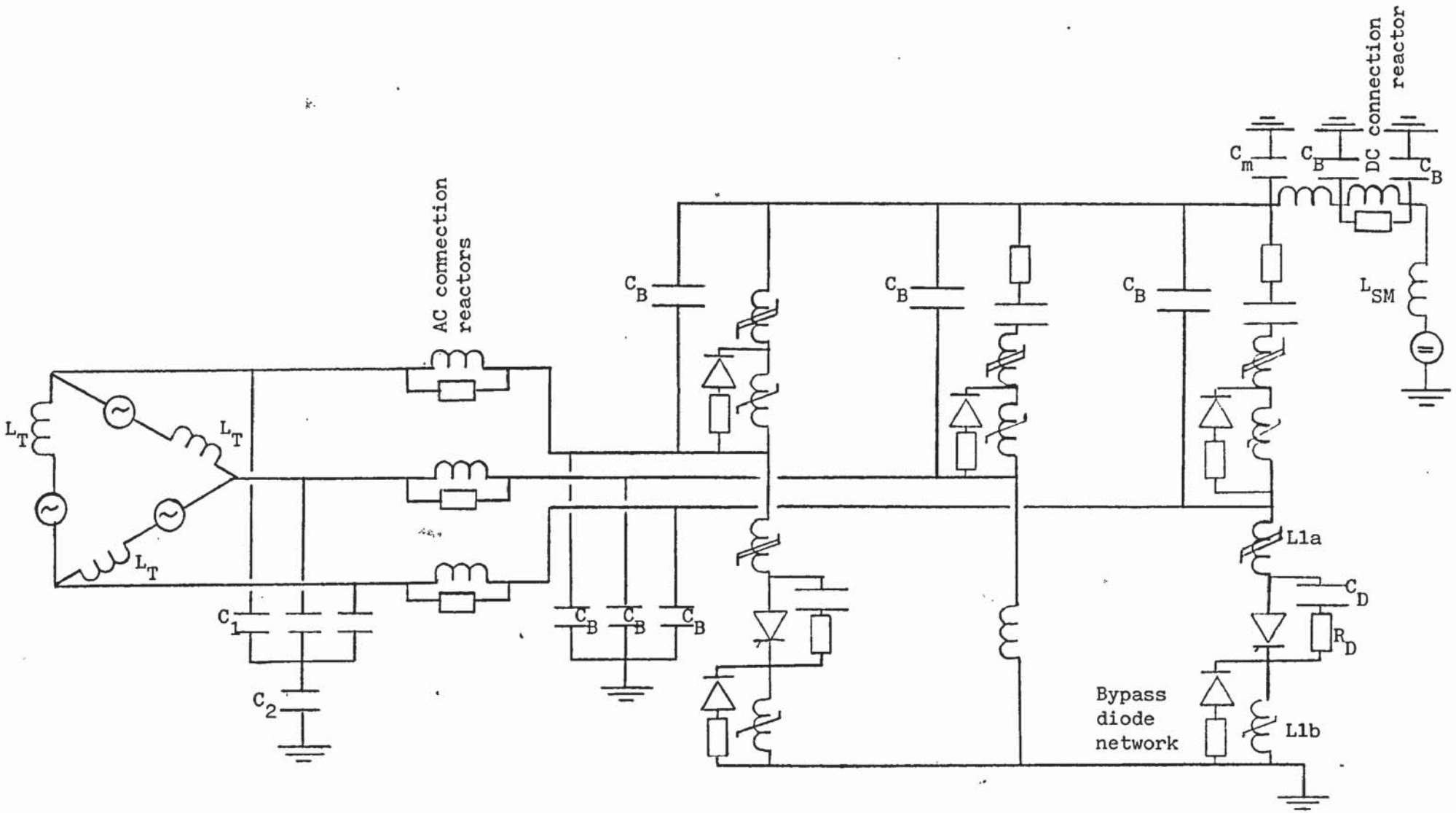

Fig.3.18 - Equivalent circuit for calculating 'repetitive' inrush current for the Sellindge Converter station.

C1, C2 Transformer electrostatic model (see Chapter 4.5.1)
L1a Ferrite saturating reactor
L1b Quasi-linear reactor

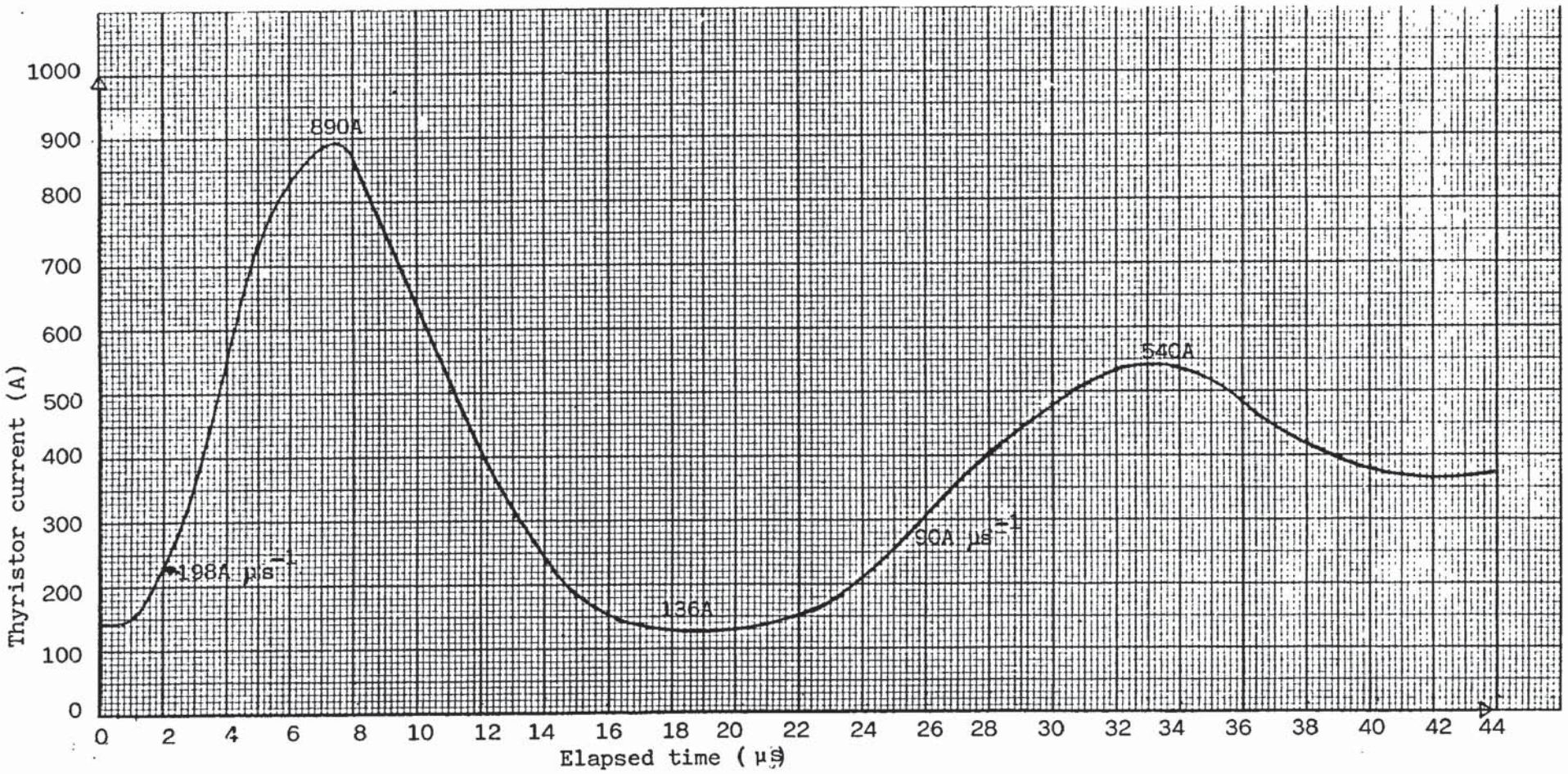

Fig.3.19 - Worst-case, repetitive, thyristor inrush current for the Sellindge converter station.

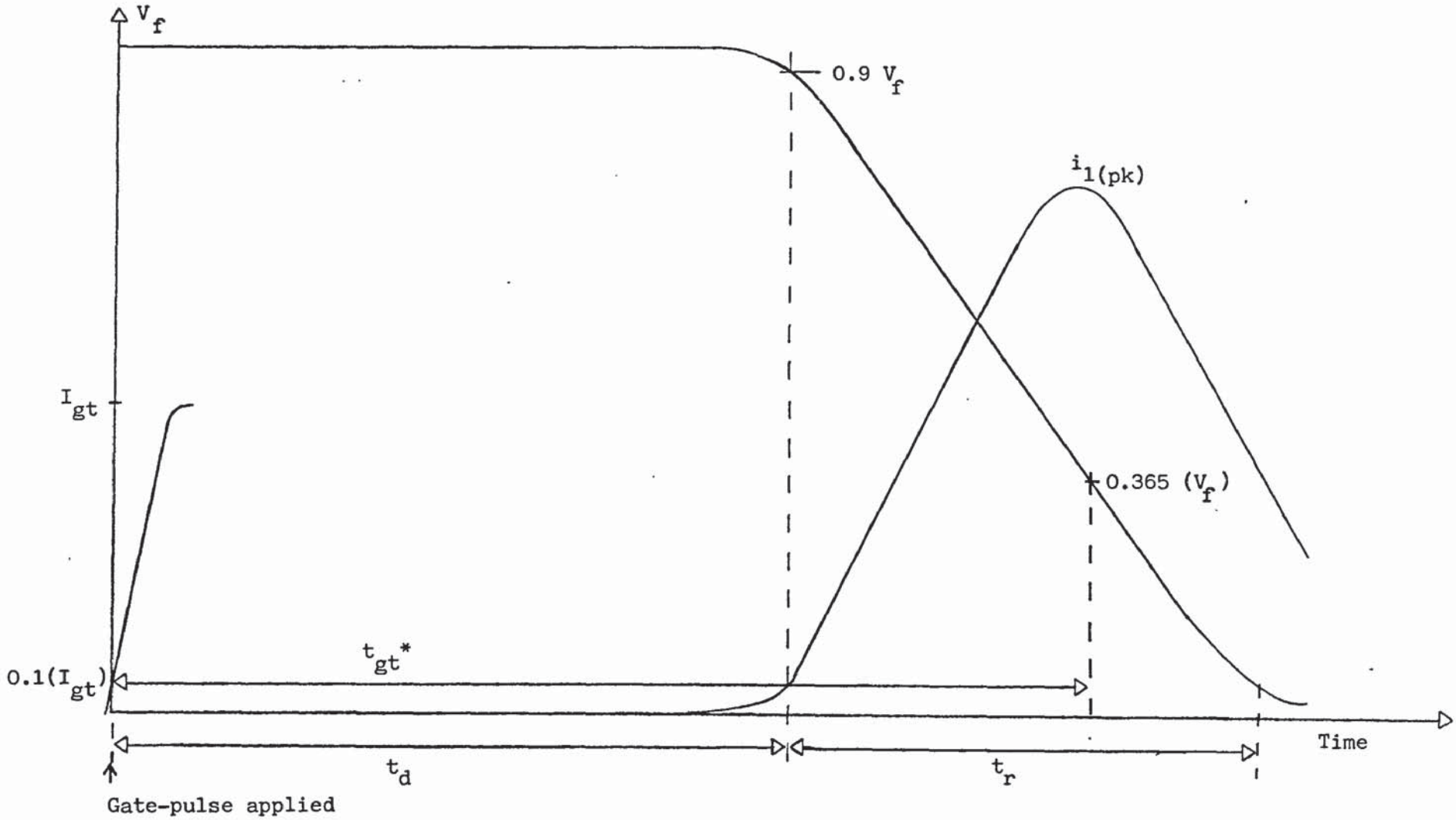

Fig.4.1 - Thyristor anode voltage and current during turn-on.

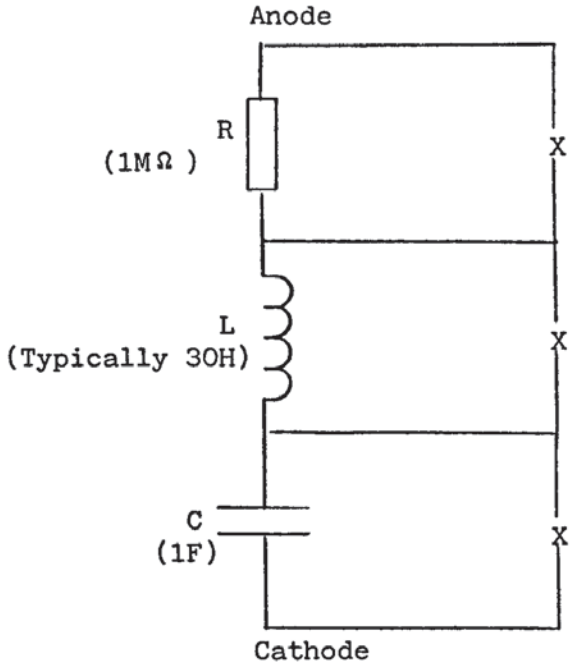

Fig.4.2 - 'Conventional' thyristor representation during reverse recovery.

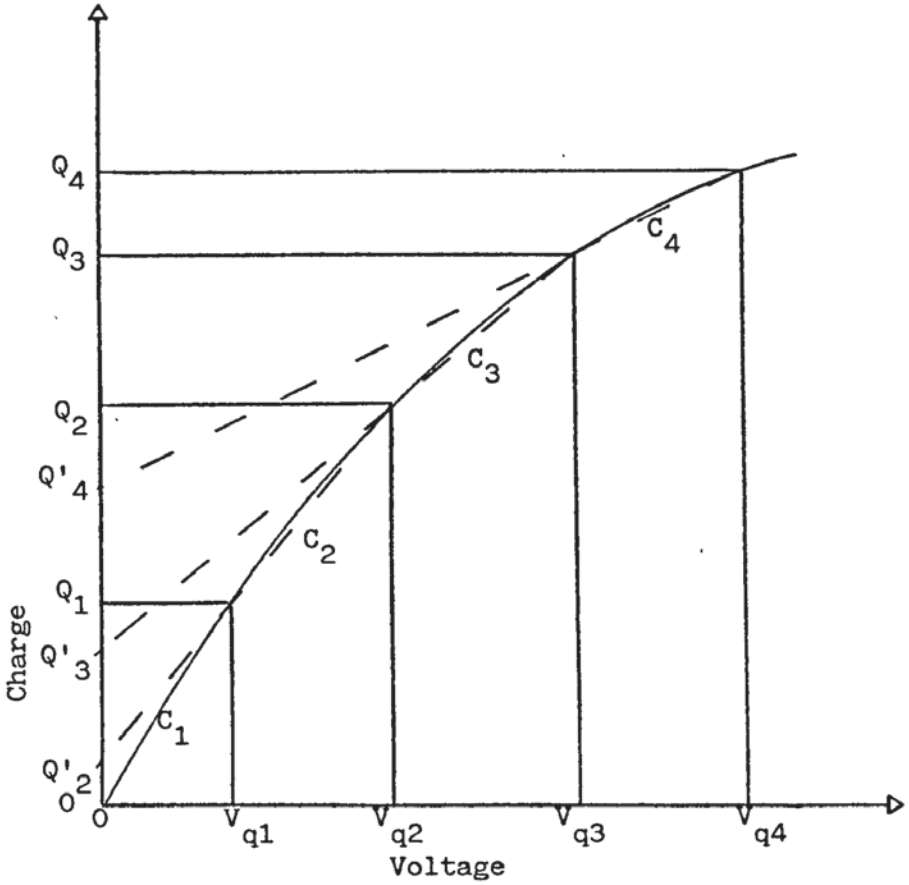

Fig.4.3 - Piece-wise linear representation of a voltage dependent capacitance

C_1, C_2, C_3, C_4 Value of incremental capacitance.

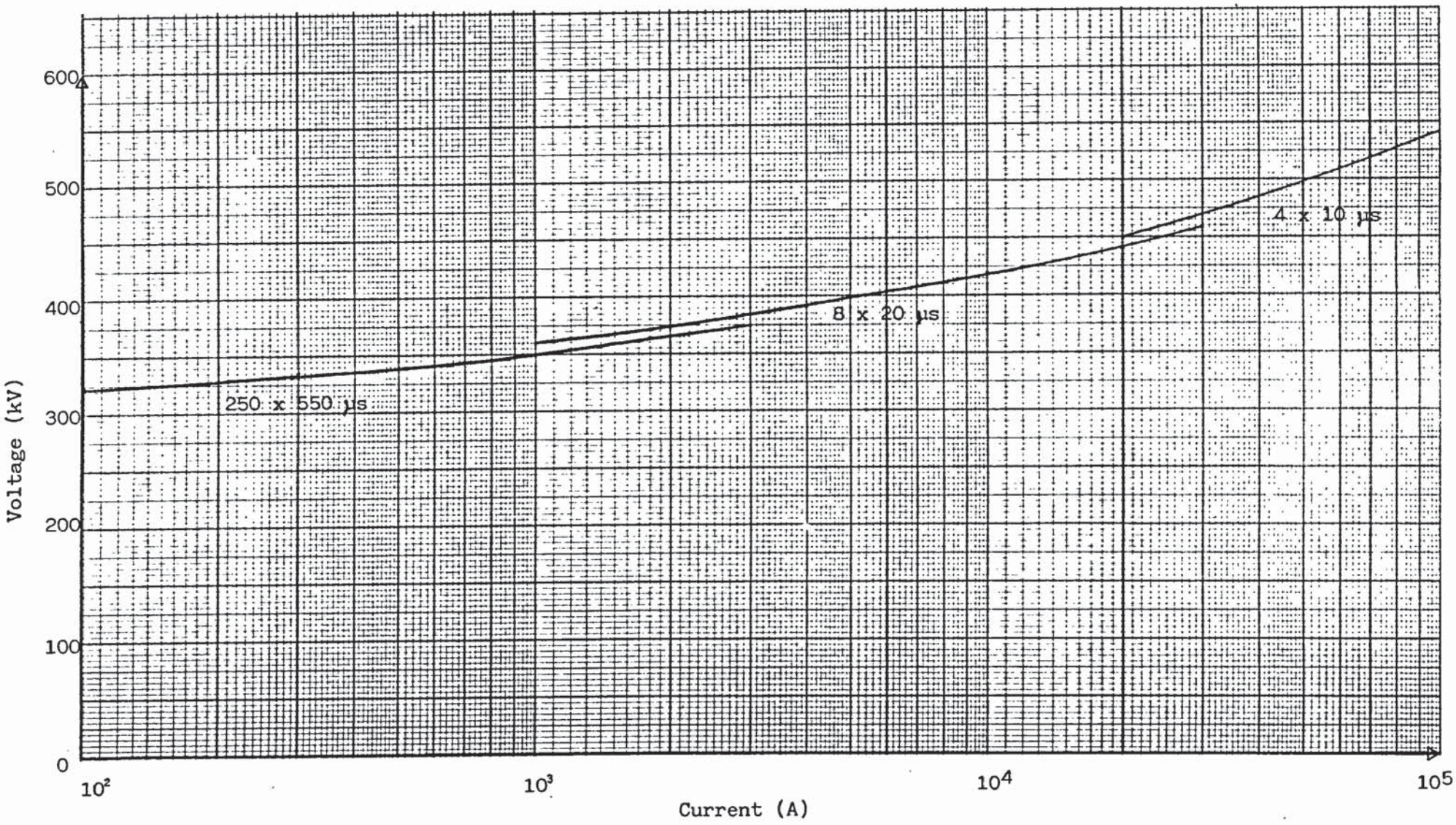

Fig.4.4 - Dependence of the voltage versus current characteristic of a surge arrester upon impulse waveshape.

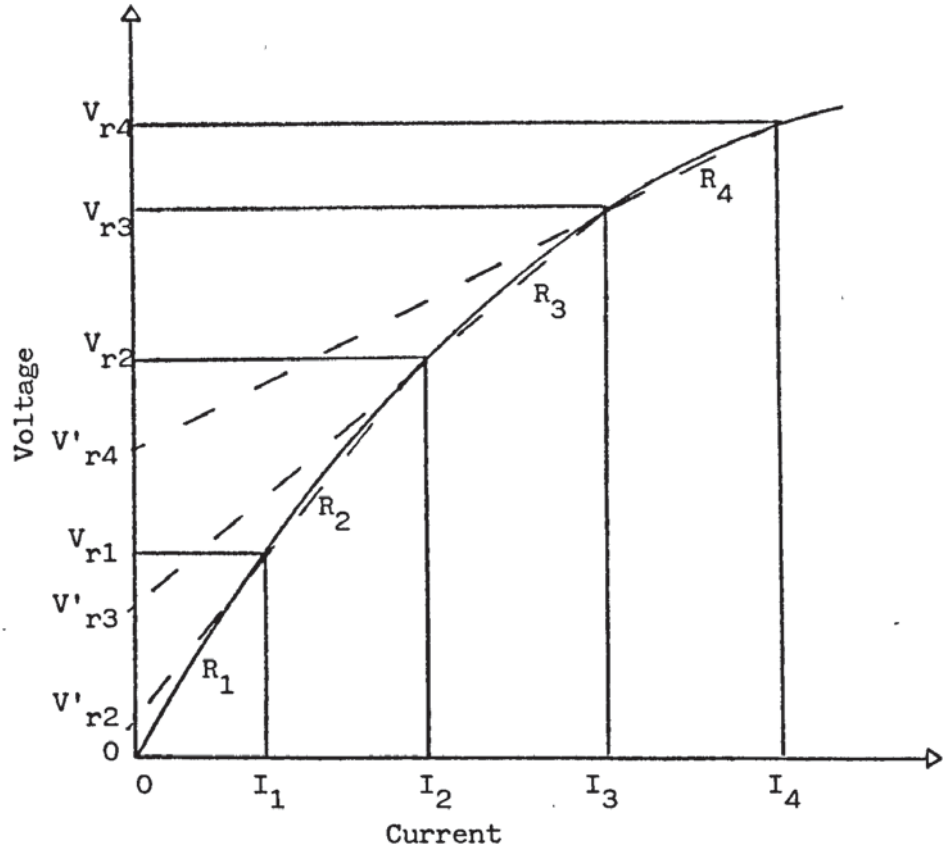

Fig.4.5 - Piece-wise linear representation of a current dependent resistance.
R_1, R_2, R_3, R_4 Value of incremental resistance.

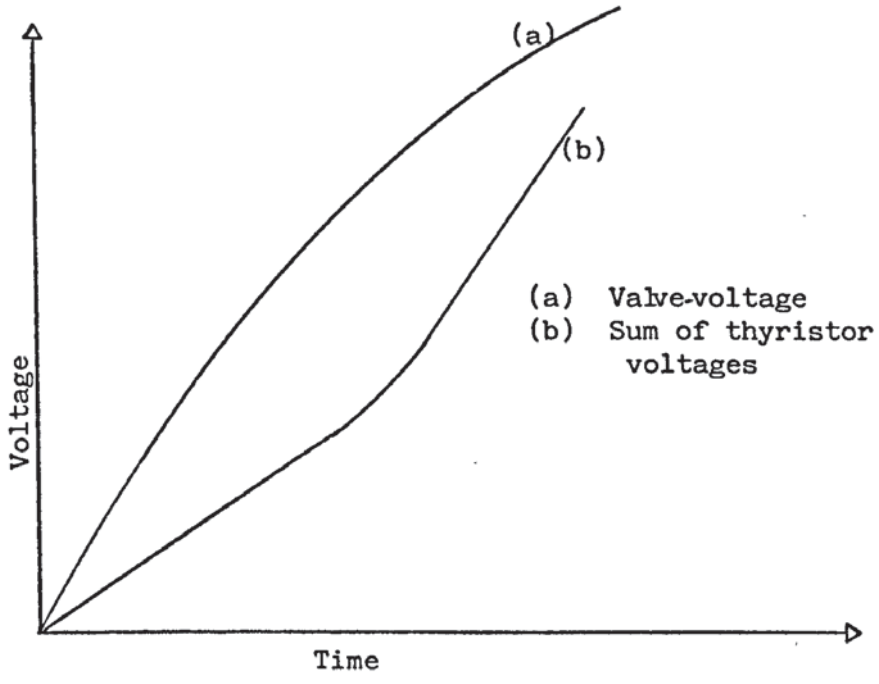

Fig.4.6 - For a fast wavefront (e.g. 0.25/5μs), with saturating reactors in a valve, the sum of thyristor voltages lags behind the applied valve-voltage.

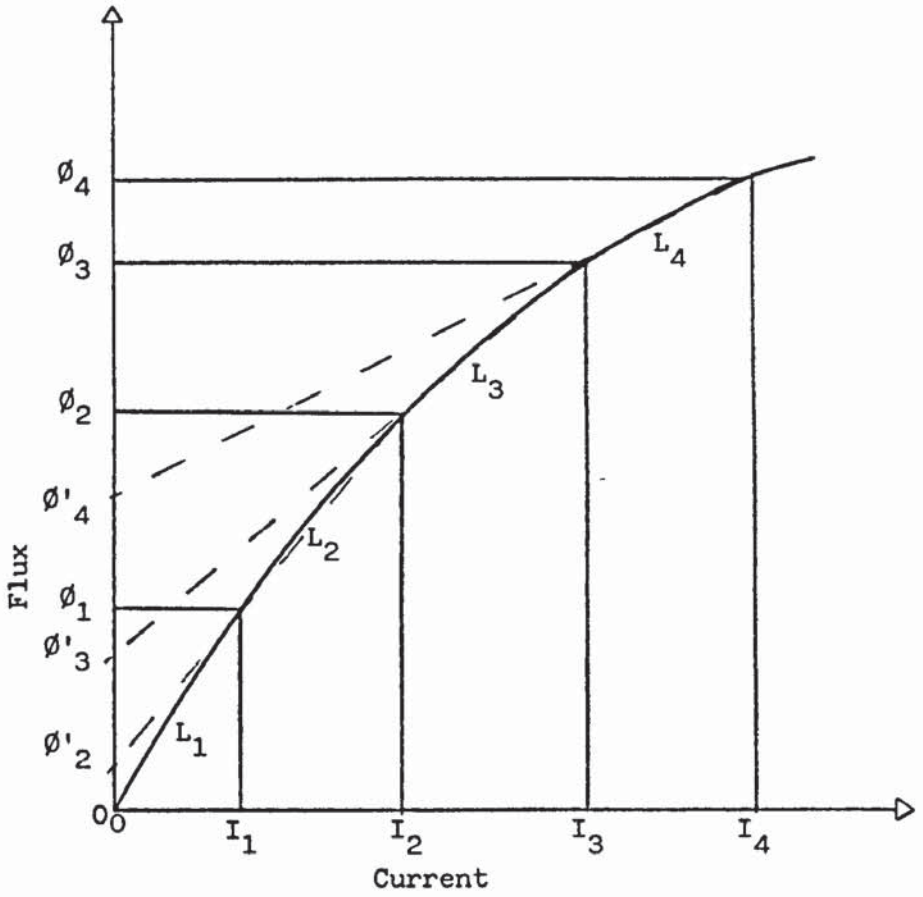

Fig.4.7 - Piece-wise linear representation of a current dependent inductance.
L_1, L_2, L_3, L_4 Value of incremental inductance

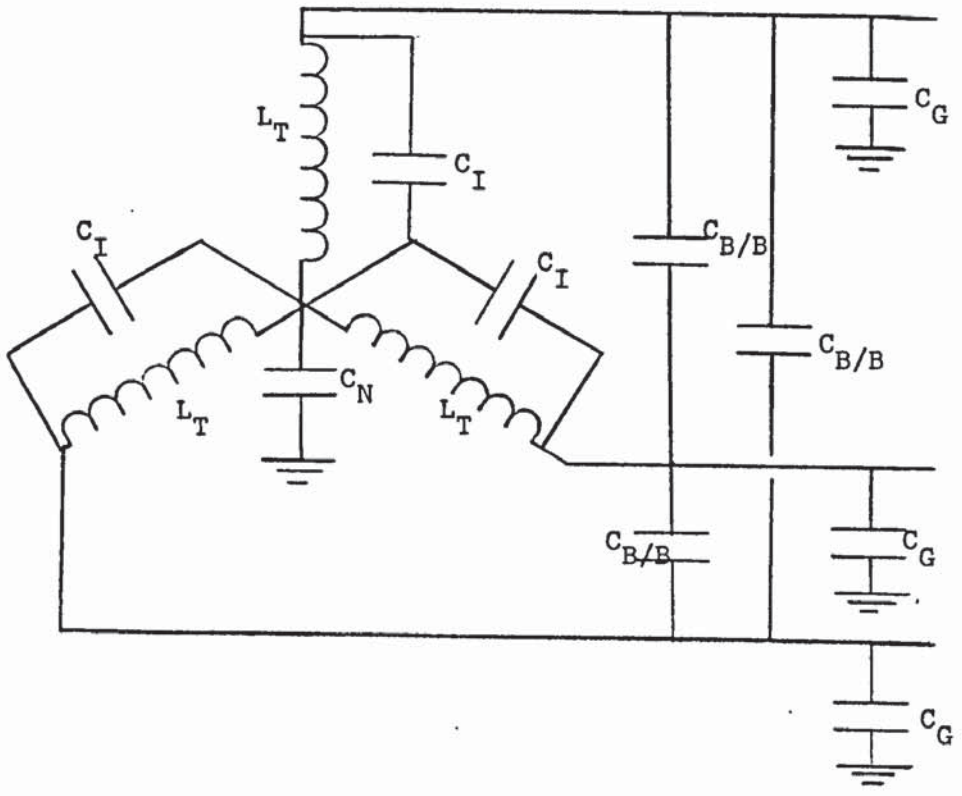

Fig.4.8 - Single-section, lumped representation of the converter transformer secondary with stray capacitances.

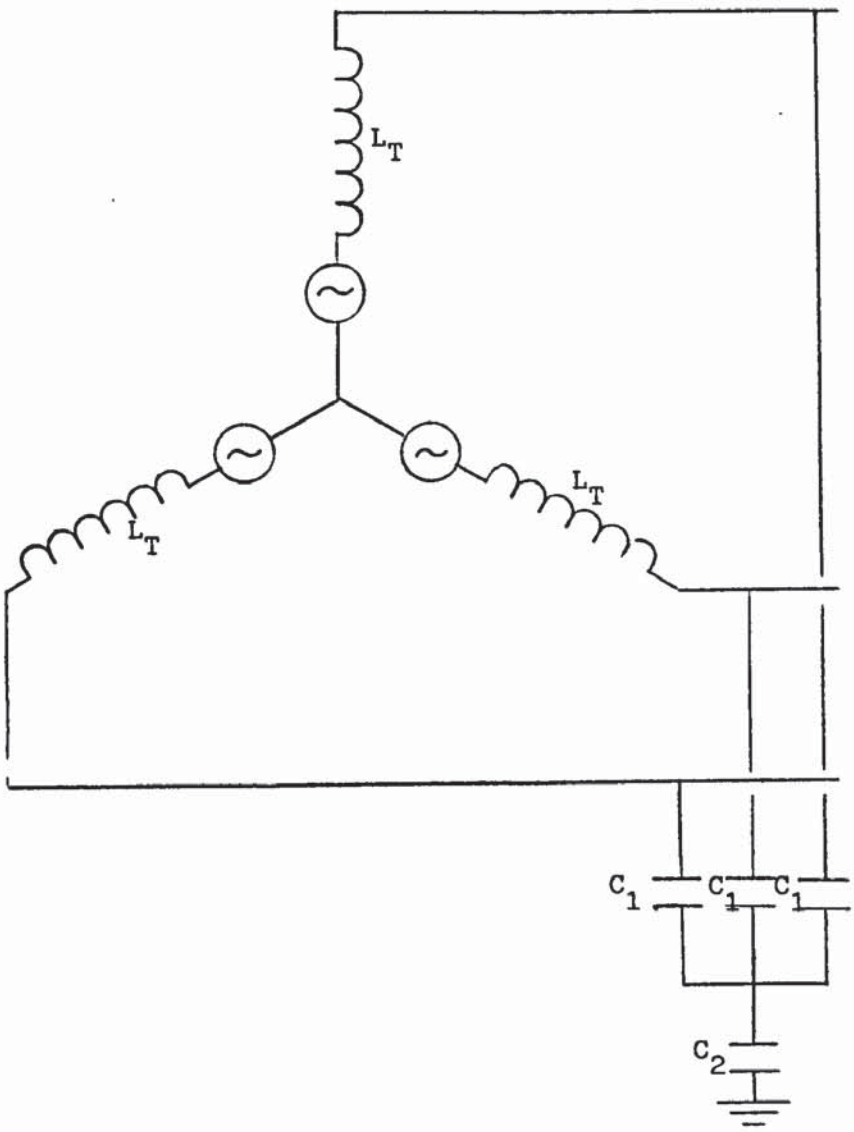

Fig.4.9 - Lumped, equivalent capacitance representation of the converter transformer, secondary, stray capacitances.

C_1, C_2 Transformer electrostatic model.

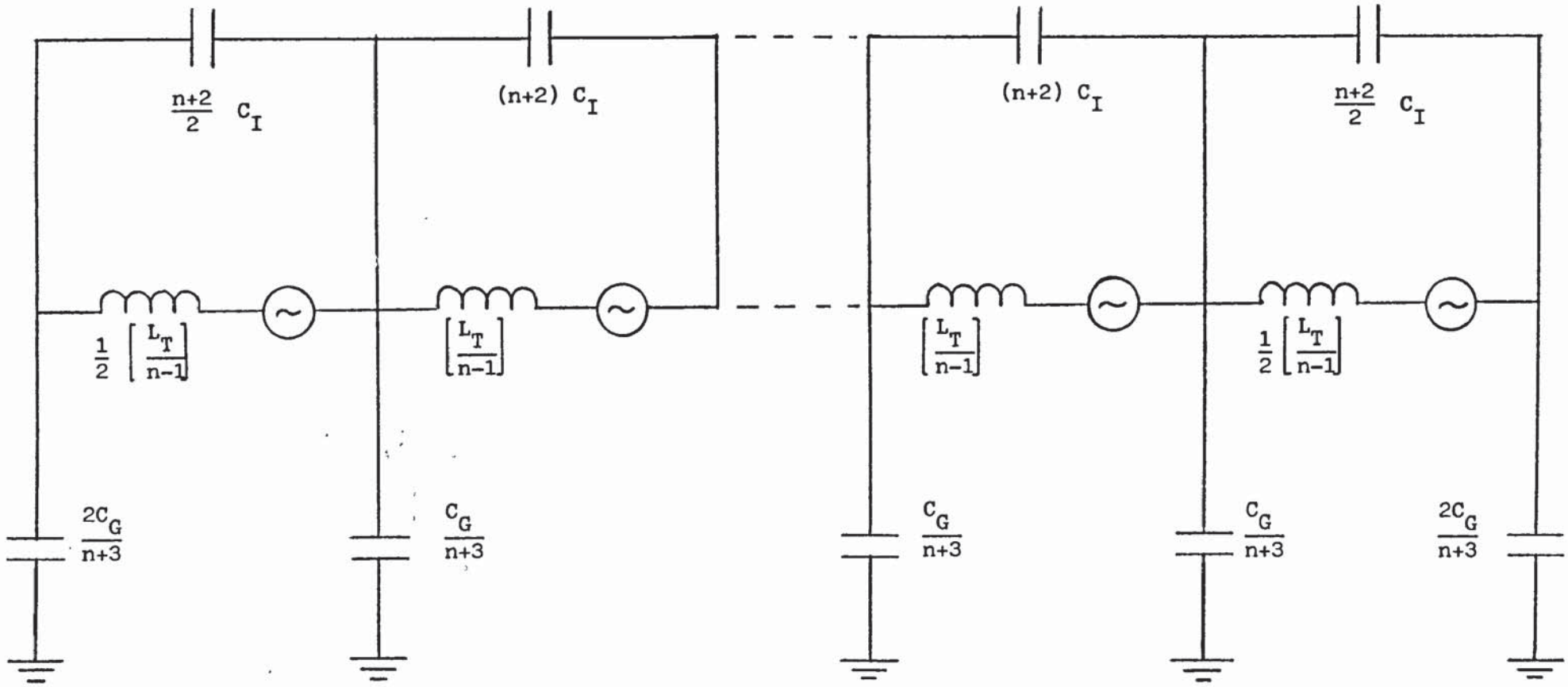

Fig.4.10 - One-phase of an n-section, 3-phase, representation of a transformer secondary including end-effects but not high-frequency resistance.

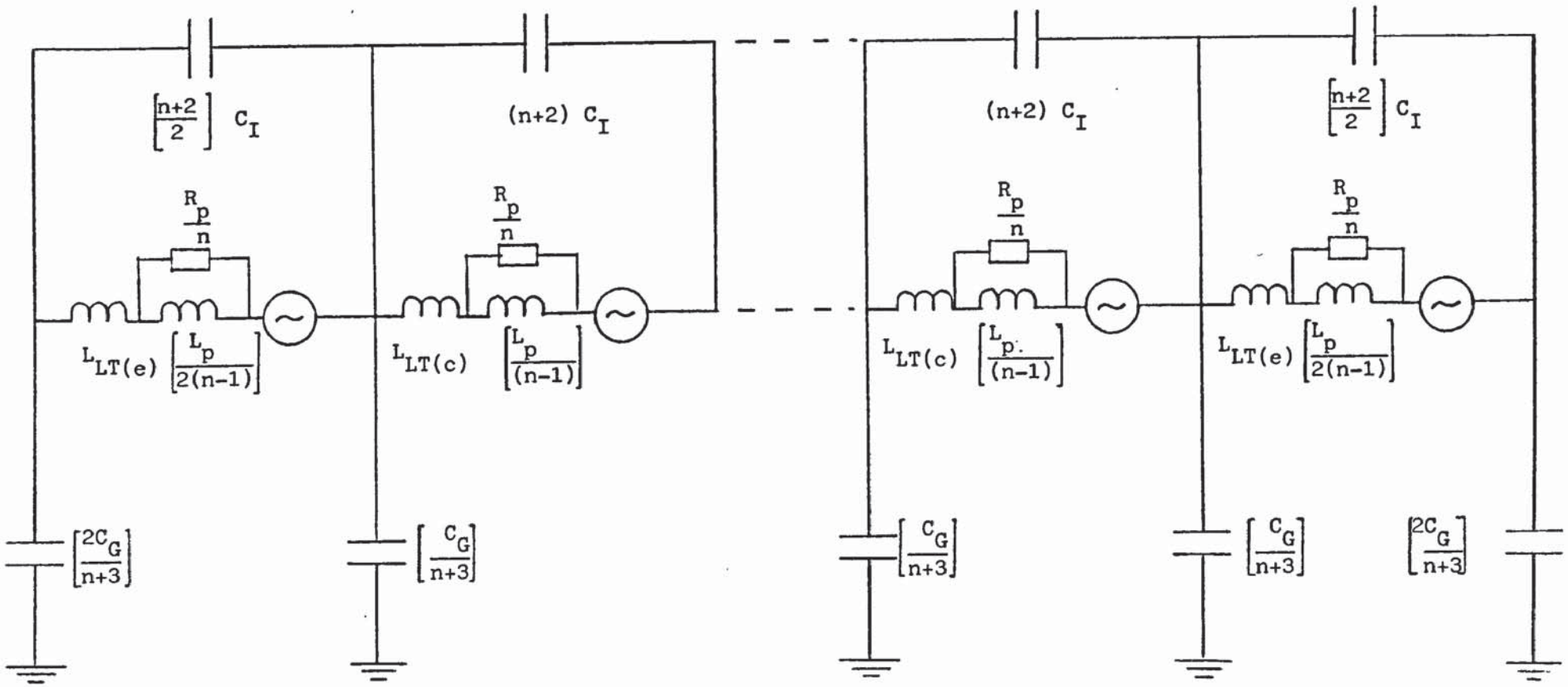

Fig.4.11 - One-phase of an n-section, 3-phase, representation of a transformer secondary including end-effects and high-frequency resistance.

$L_{LT(e)}$ Series-inductance of an end-section

$L_{LT(c)}$ Series-inductance of a central-section

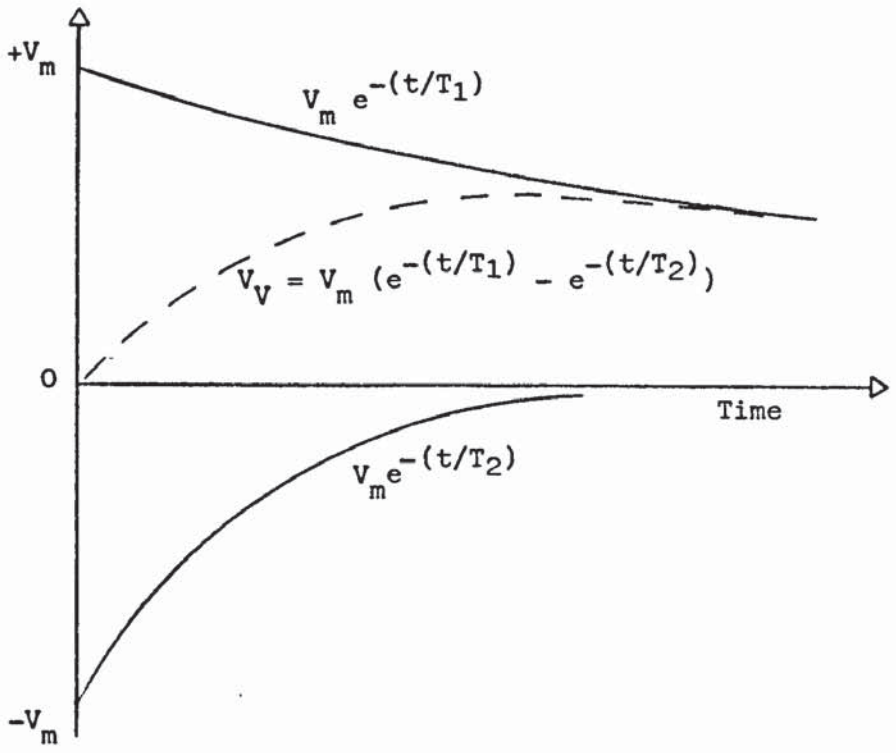

Fig.4.12 - Mathematical derivation of an impulse.

T_1, T_2 Time constants

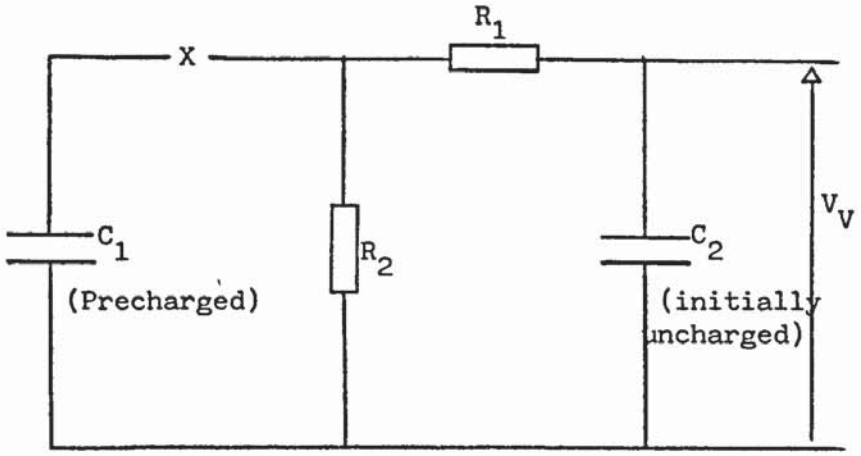

Fig.4.13 - Equivalent circuit of an impulse generator.

C_1, C_2, R_1, R_2 Circuit components of an impulse generator.

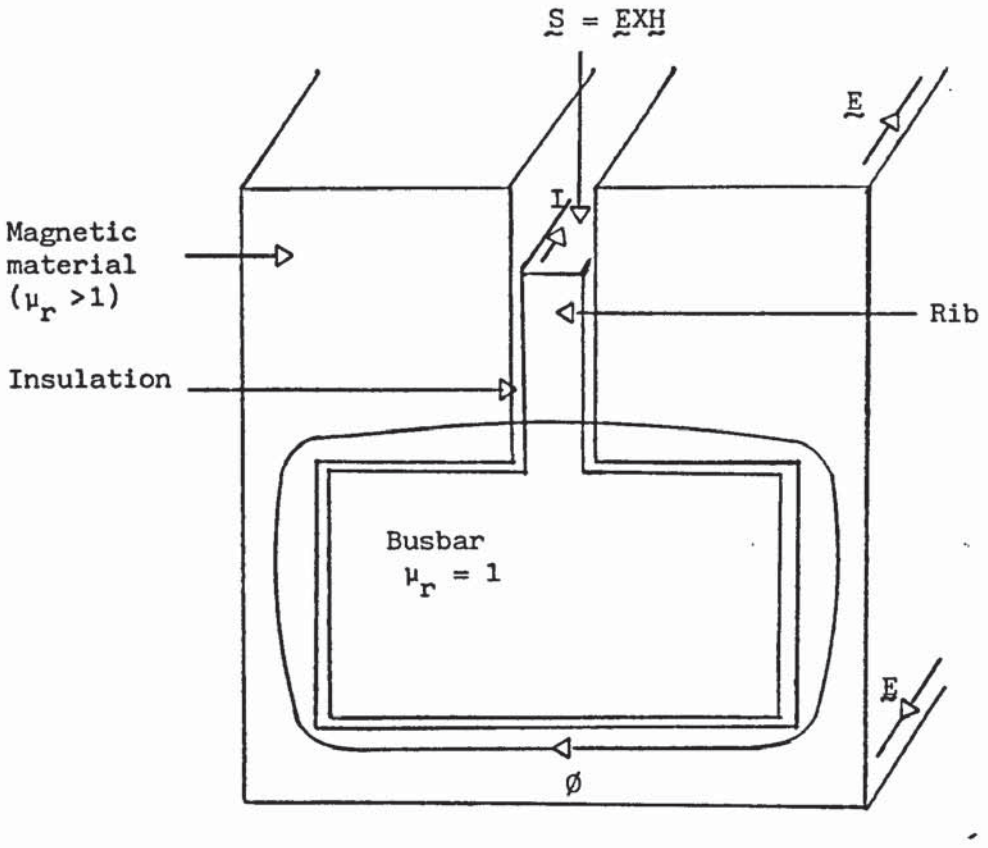

Fig.5.1 - Cross-section of a ribbed busbar housed in a semi-closed slot.

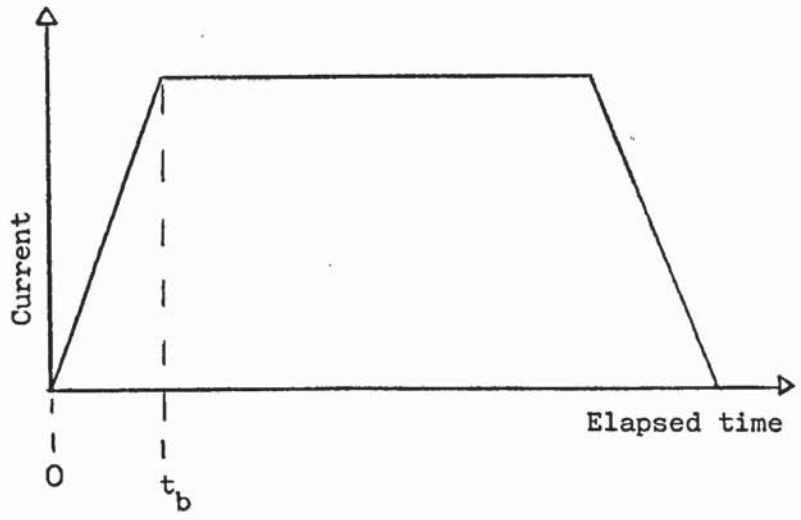

Fig.5.2 - Representation of valve inrush-current by a trapezoidal current.

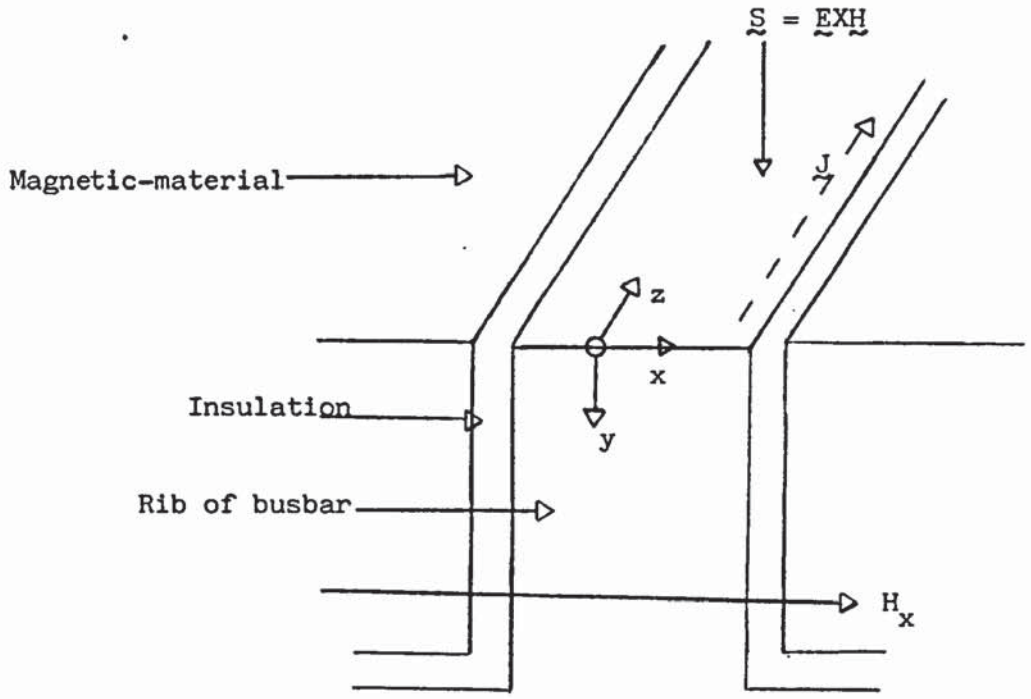

Fig.5.3 - Cross-section of an infinite busbar housed in a semi-closed slot.

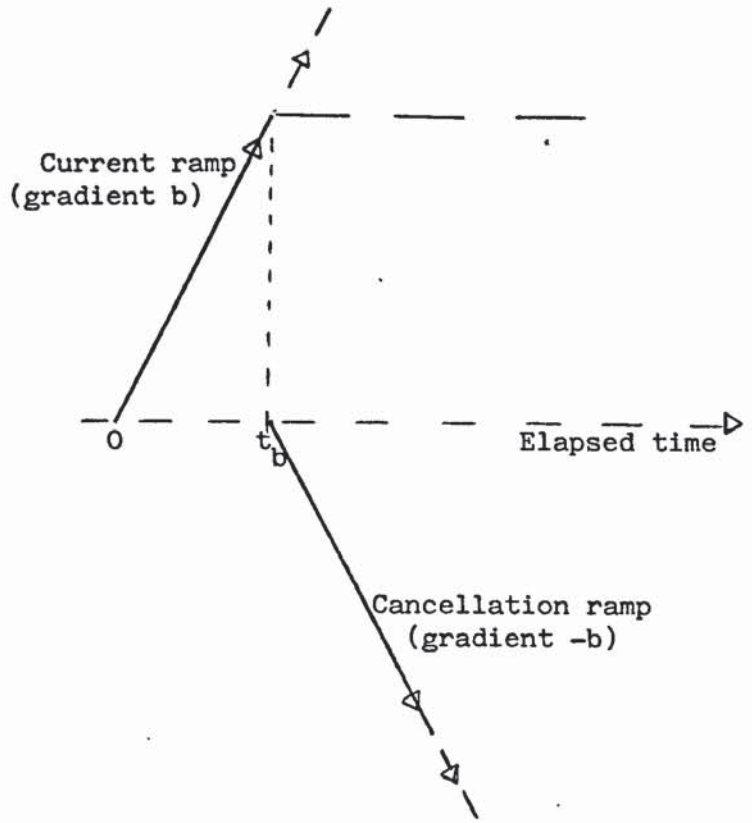

Fig.5.4 - 'Trapezoidal' surface-excitation of current represented by the sum of current ramps.

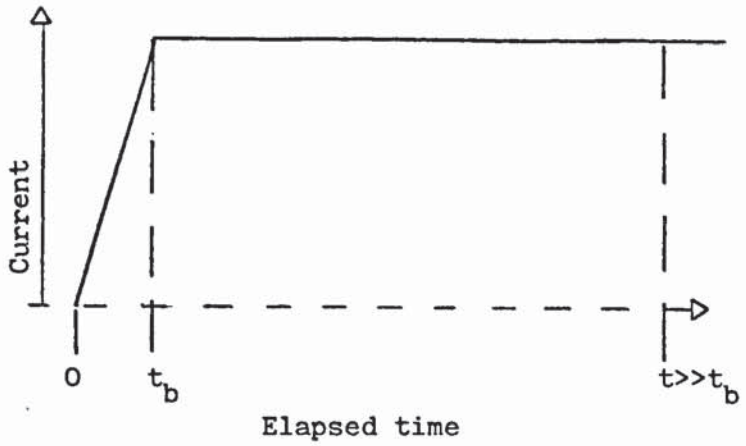

Fig.5.5 - 'Trapezoidal' current pulse.
If elapsed time $t>>t_b$ then the current pulse is assumed to be a simple step.

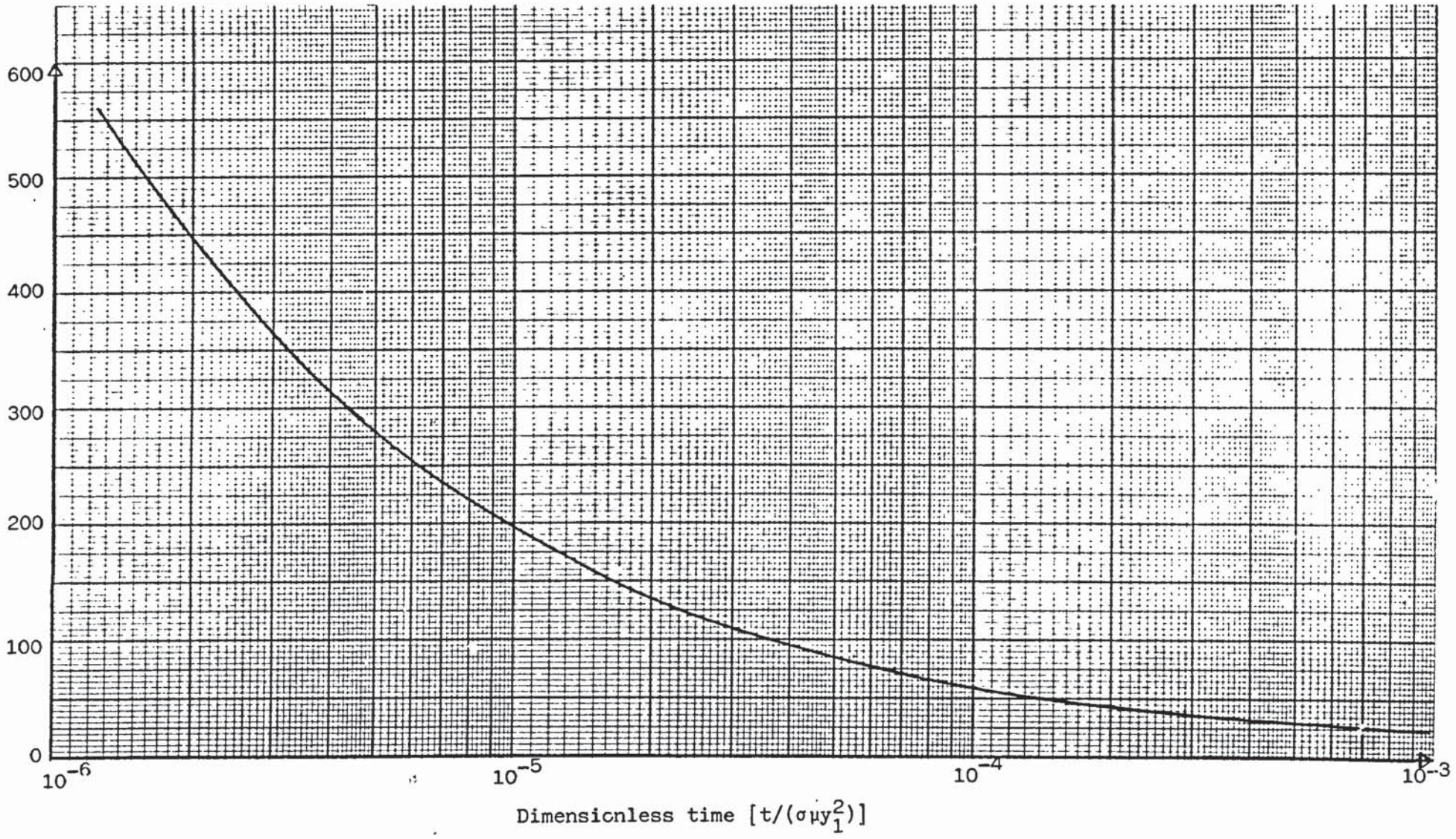

Fig.5.6 - Dependence of the transient resistance ratio upon the dimensionless time, for a current ramp surface excitation.

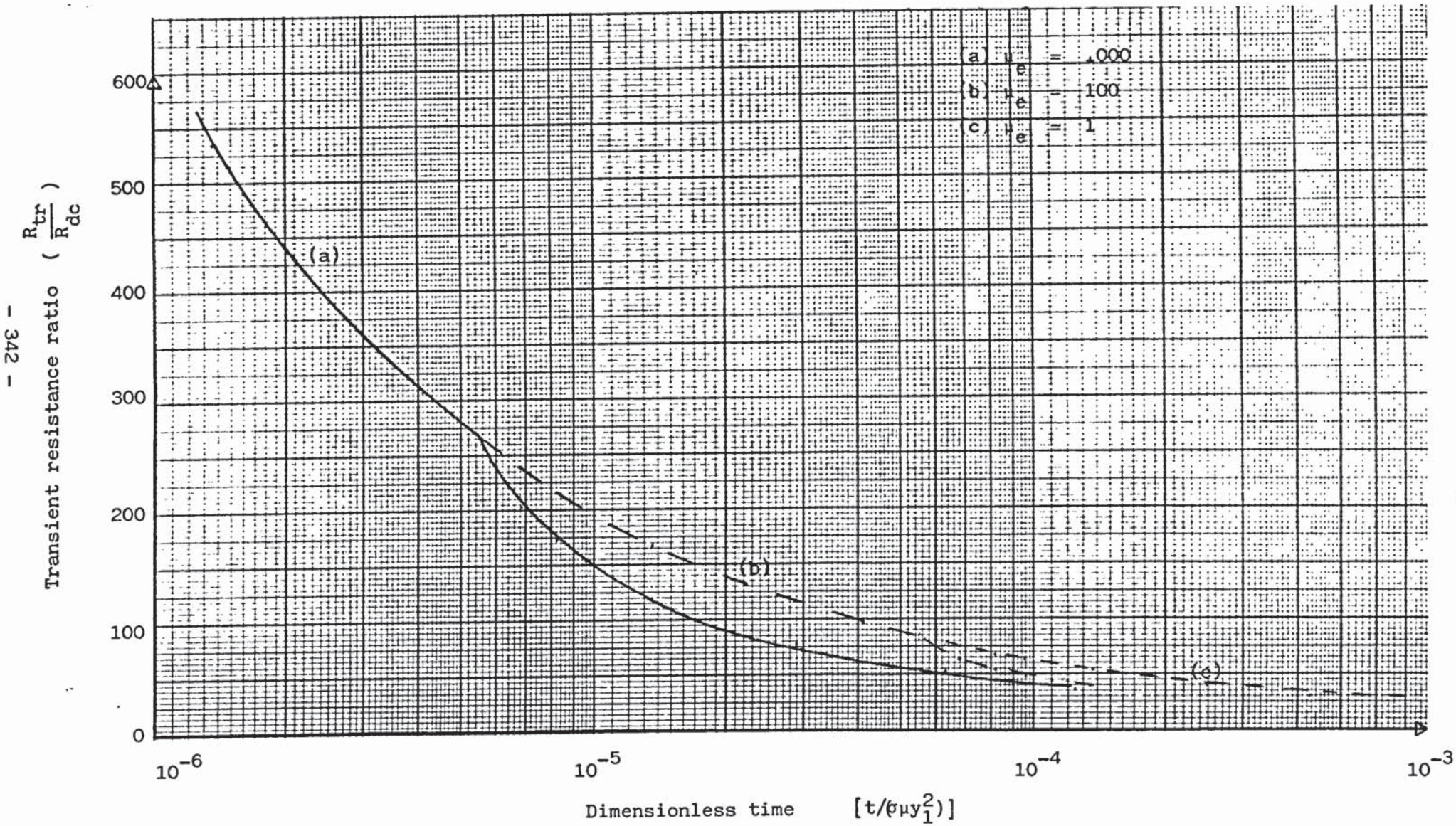

Fig.5.7 - Dependence of the transient resistance ratio upon the dimensionless time, for a trapezoidal current (see fig.5.4) surface excitation (t_b = 0.4 μs).

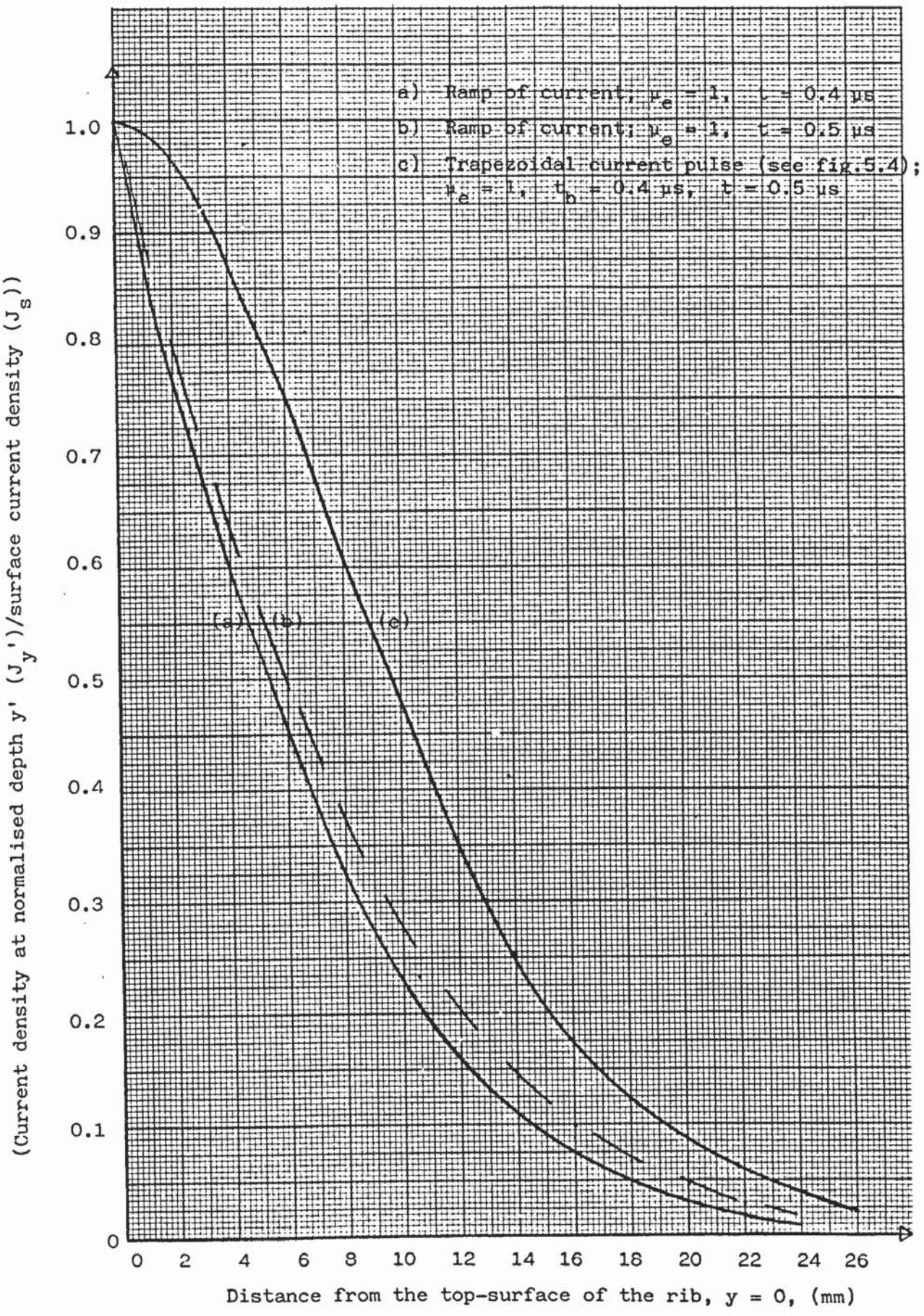

Fig.5.8 - Dependence of the current density within the rib upon the distance from the top-surface (y = 0) of the rib, the surface-excitation and the elapsed time.

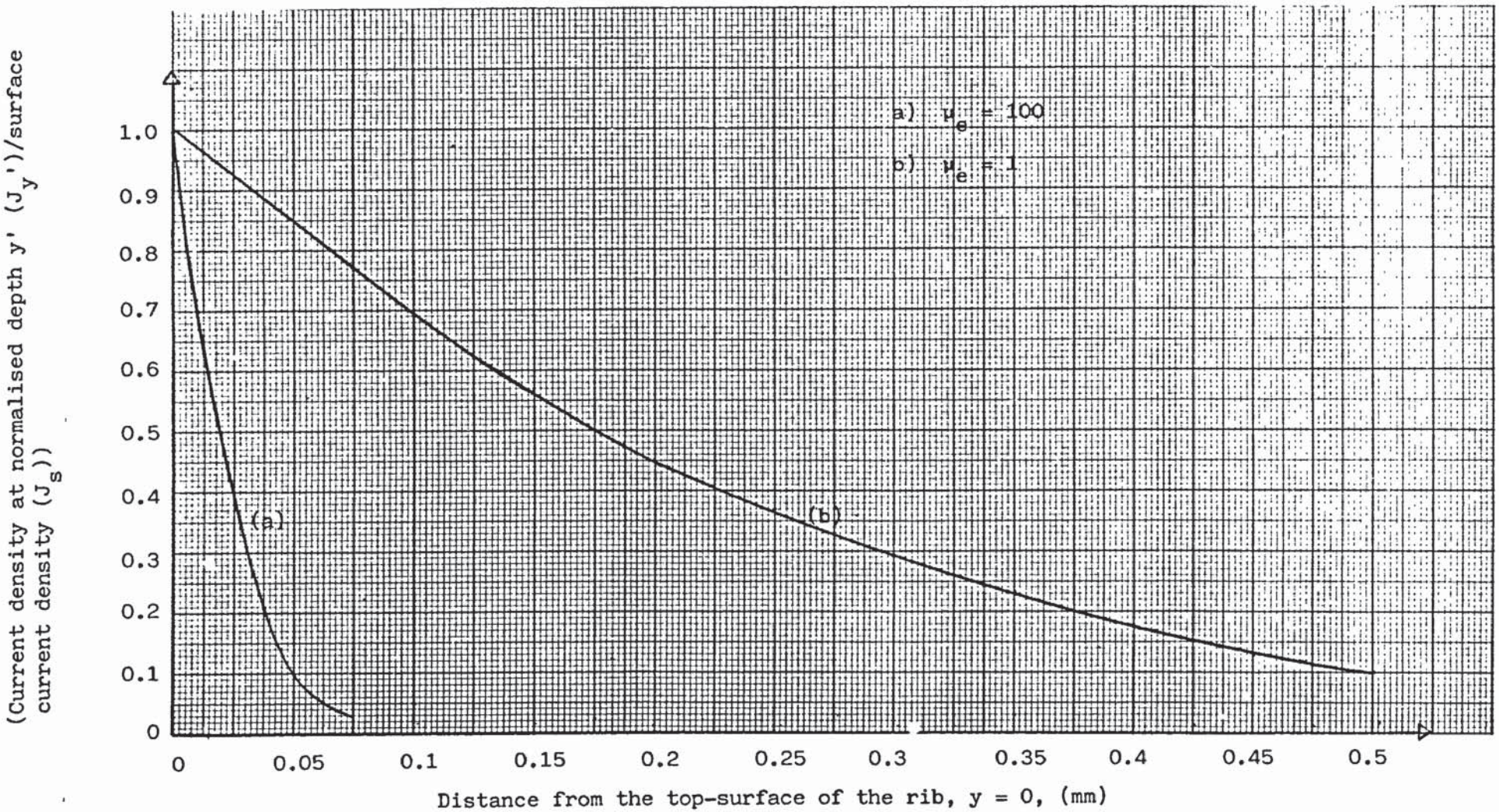

Fig.5.9 - Dependence of the current density within the rib upon the distance from the top surface (y = 0) of the rib and the effective relative permeability of the magnetic circuit t = 4.85 μs, (current ramp surface excitation, $\rho = 1.724 \times 10^{-8}$ Ω.m)

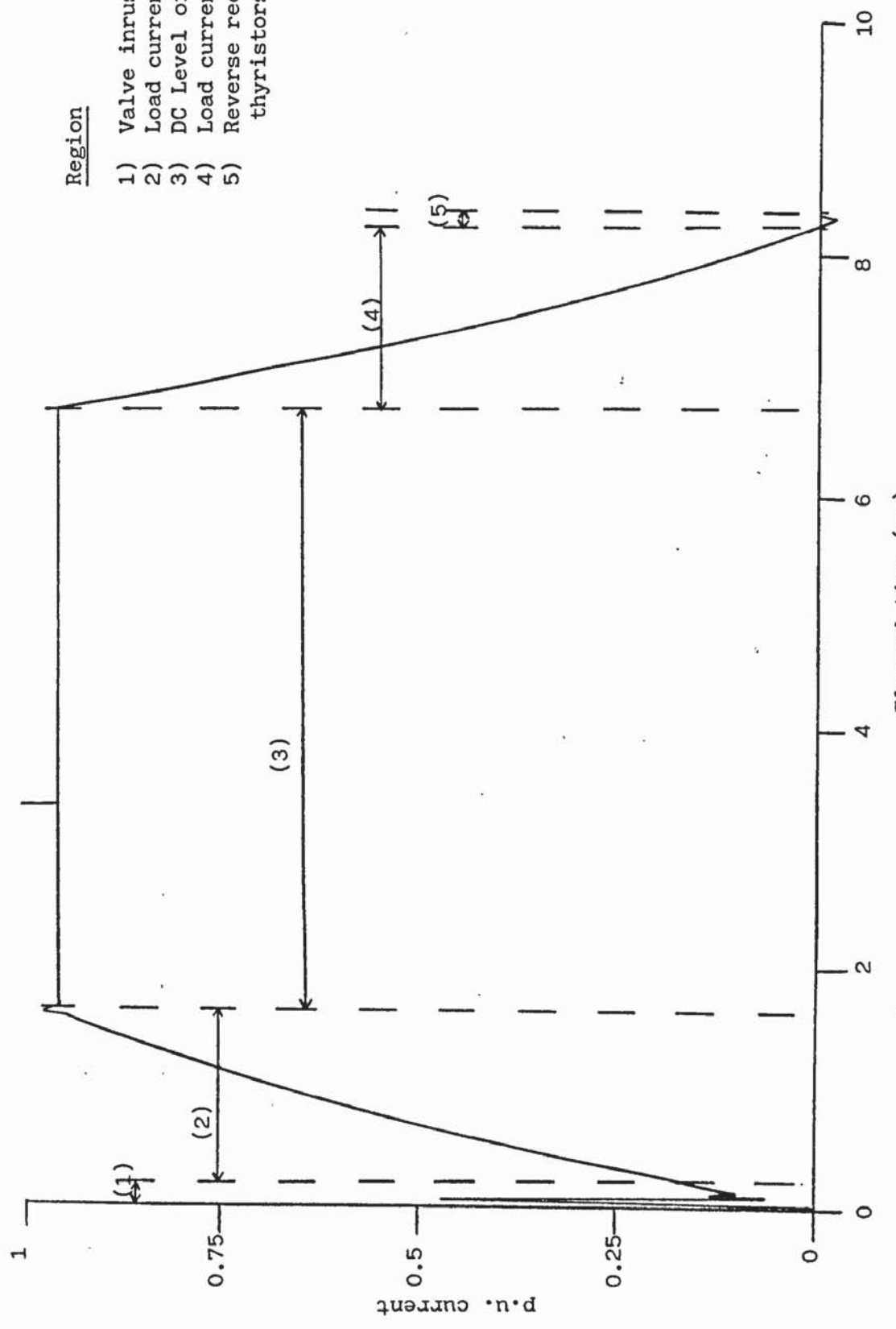

Fig. 6.1 - Typical Valve Current for 50 Hz Operation.

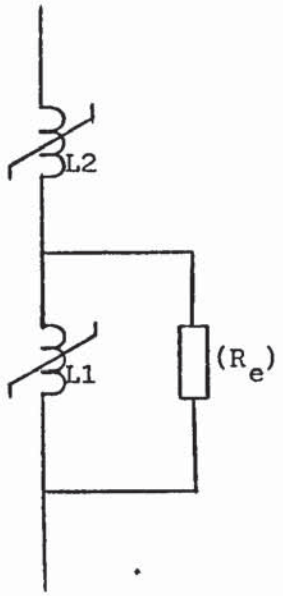

Fig.6.2 - Representation of a lossless magnetic material (L2) in series with a lossy magnetic material (L1); eddy-current losses are represented by resistance R_e.

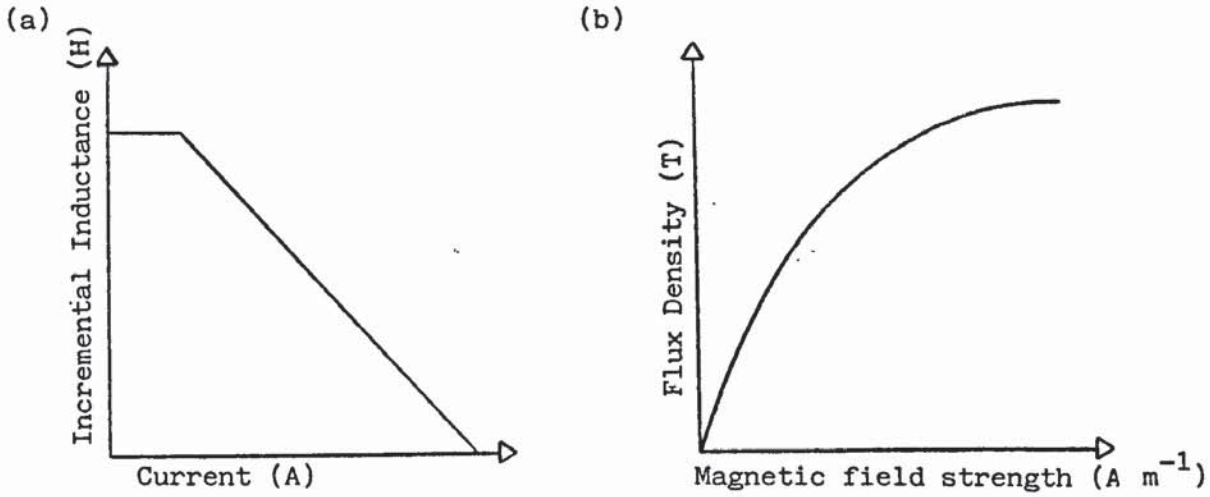

Fig.6.3 - General form of characteristics assumed for the 'inductive characteristic' of reactor parts L1 and L2.
a) Incremental inductance with current
b) B-H curve

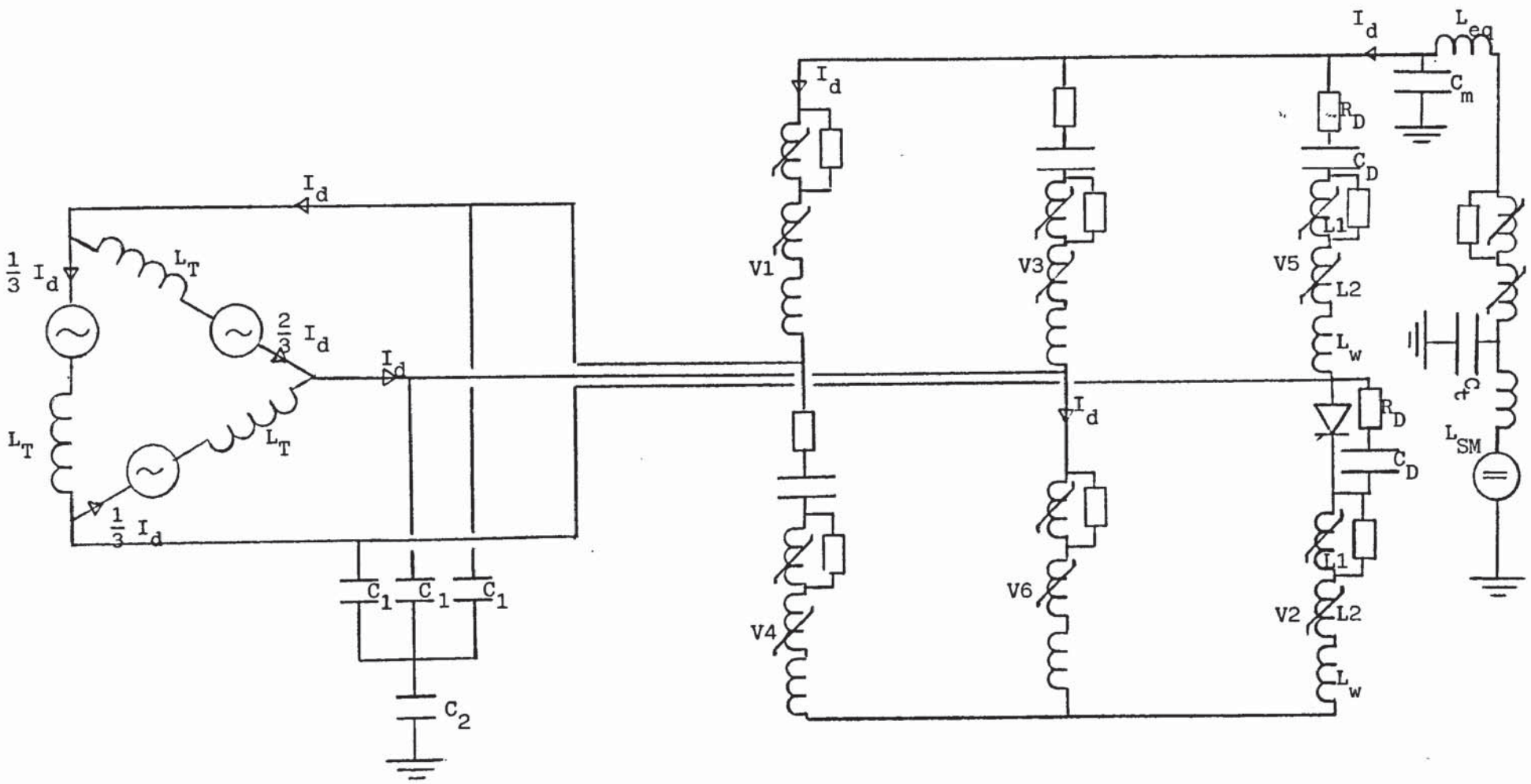

Fig.6.4 - Equivalent circuit of a six-pulse bridge, for coherent turn-on studies.
C_1, C_2 Transformer electrostatic model.
VN Valve firing sequence

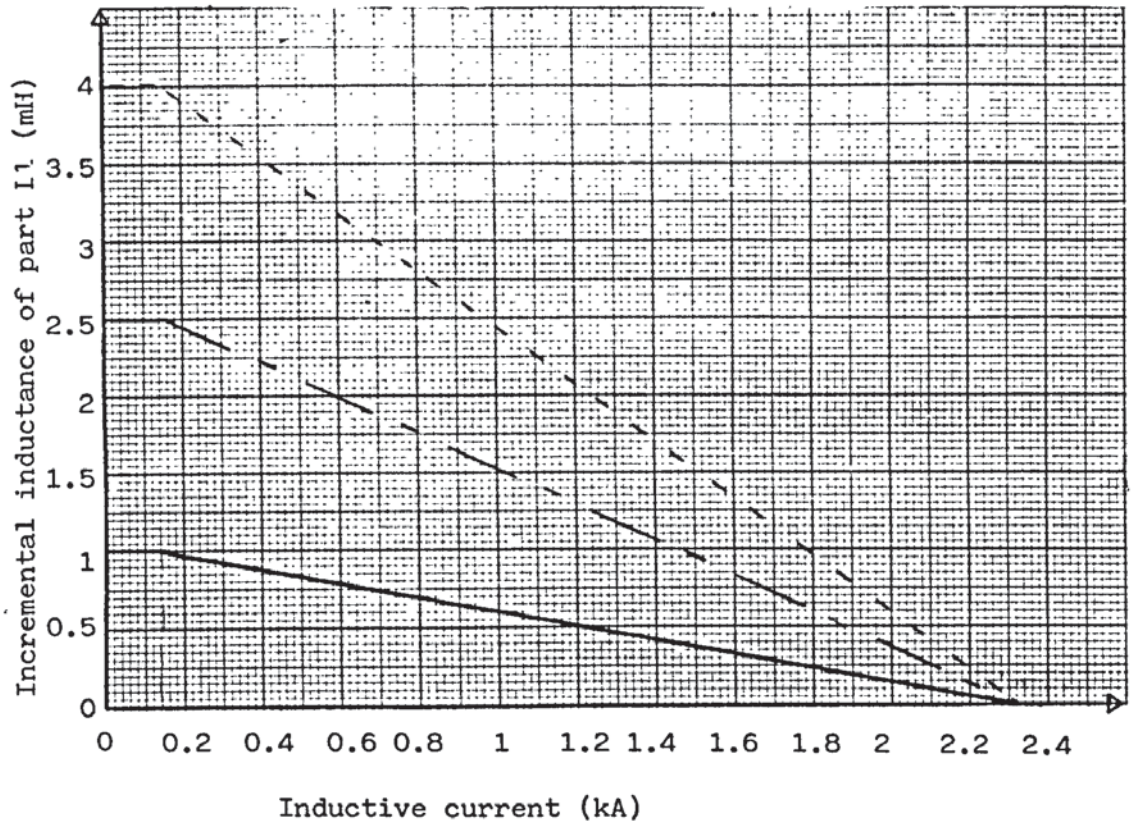

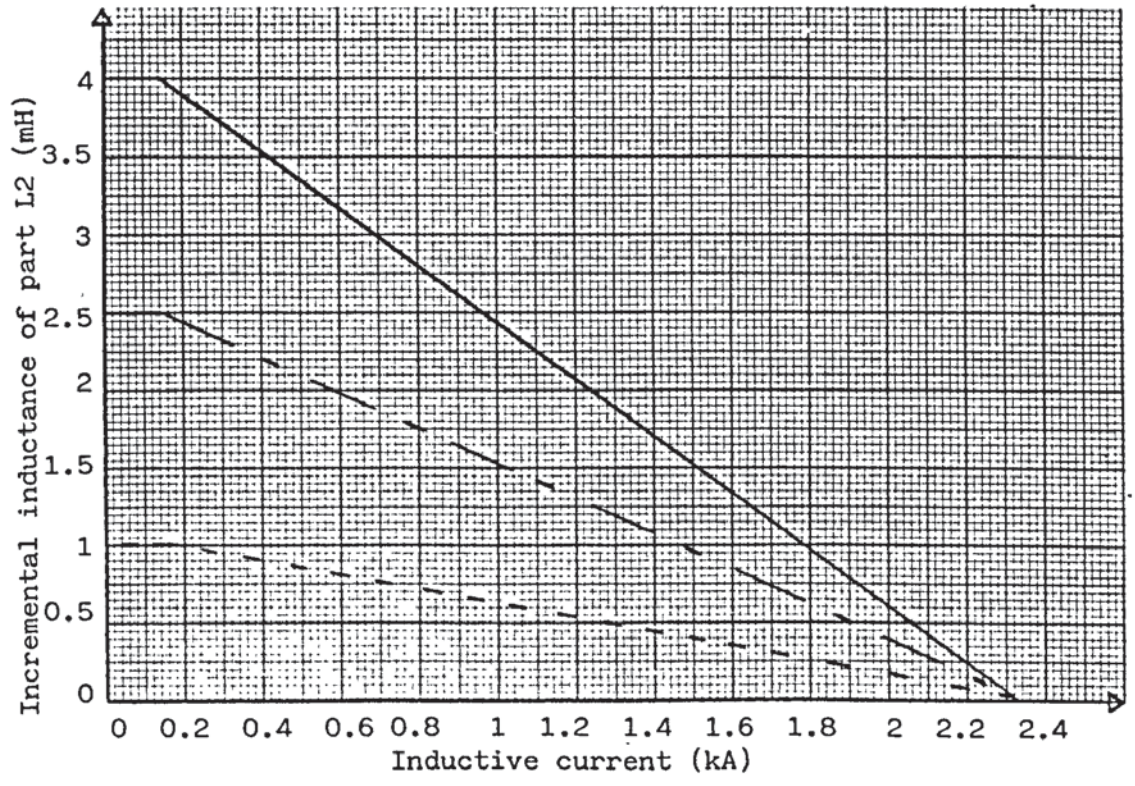

Fig.6.5 - General form of incremental inductance with current characteristics, utilised to assess the optimum relative magnitude of the inductance values.

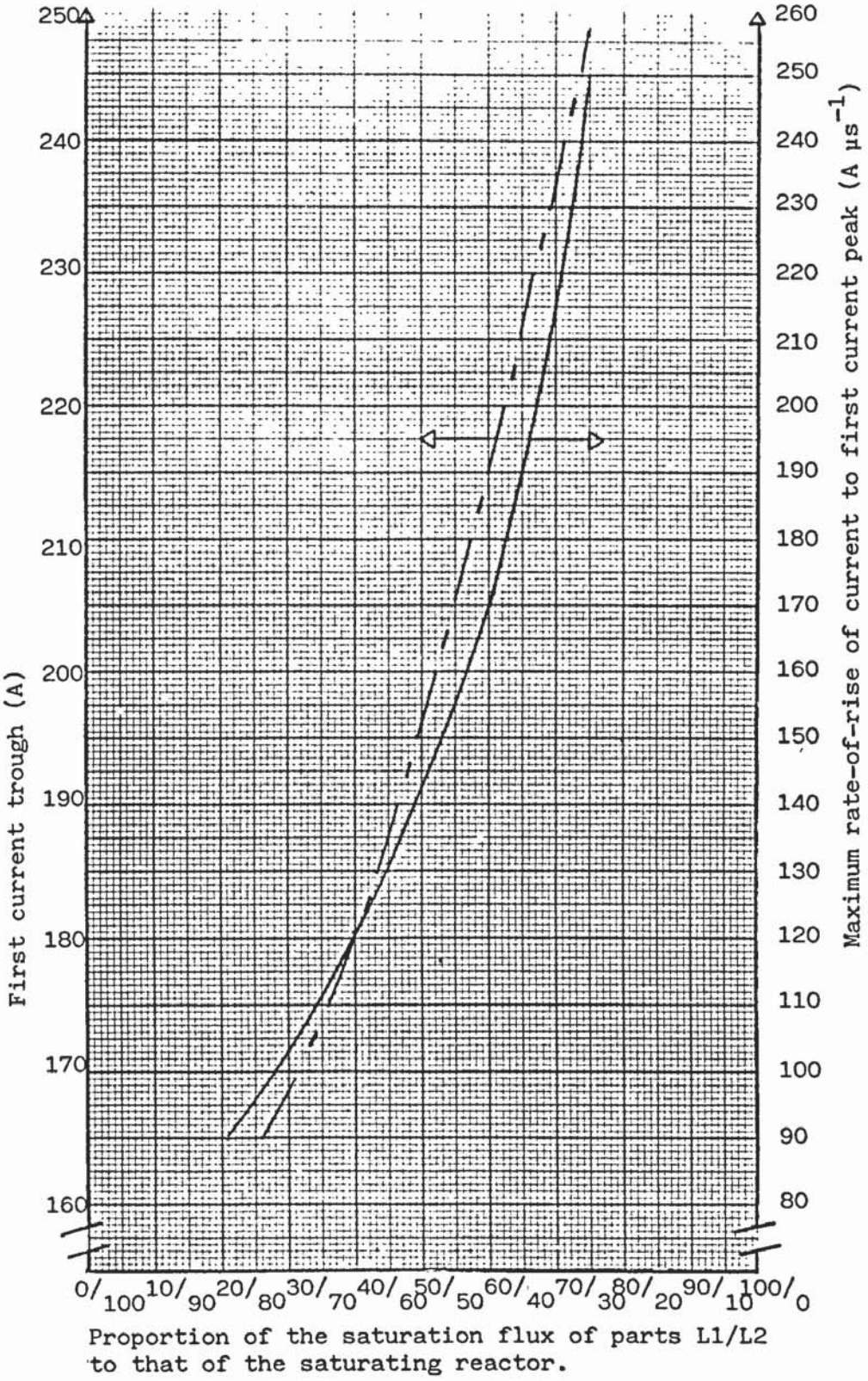

Fig.6.6 - Dependence of the magnitude of first current trough and the maximum di/dt to first current peak upon the proportion of the saturation flux of parts L1/L2 to that of the saturating-reactor.

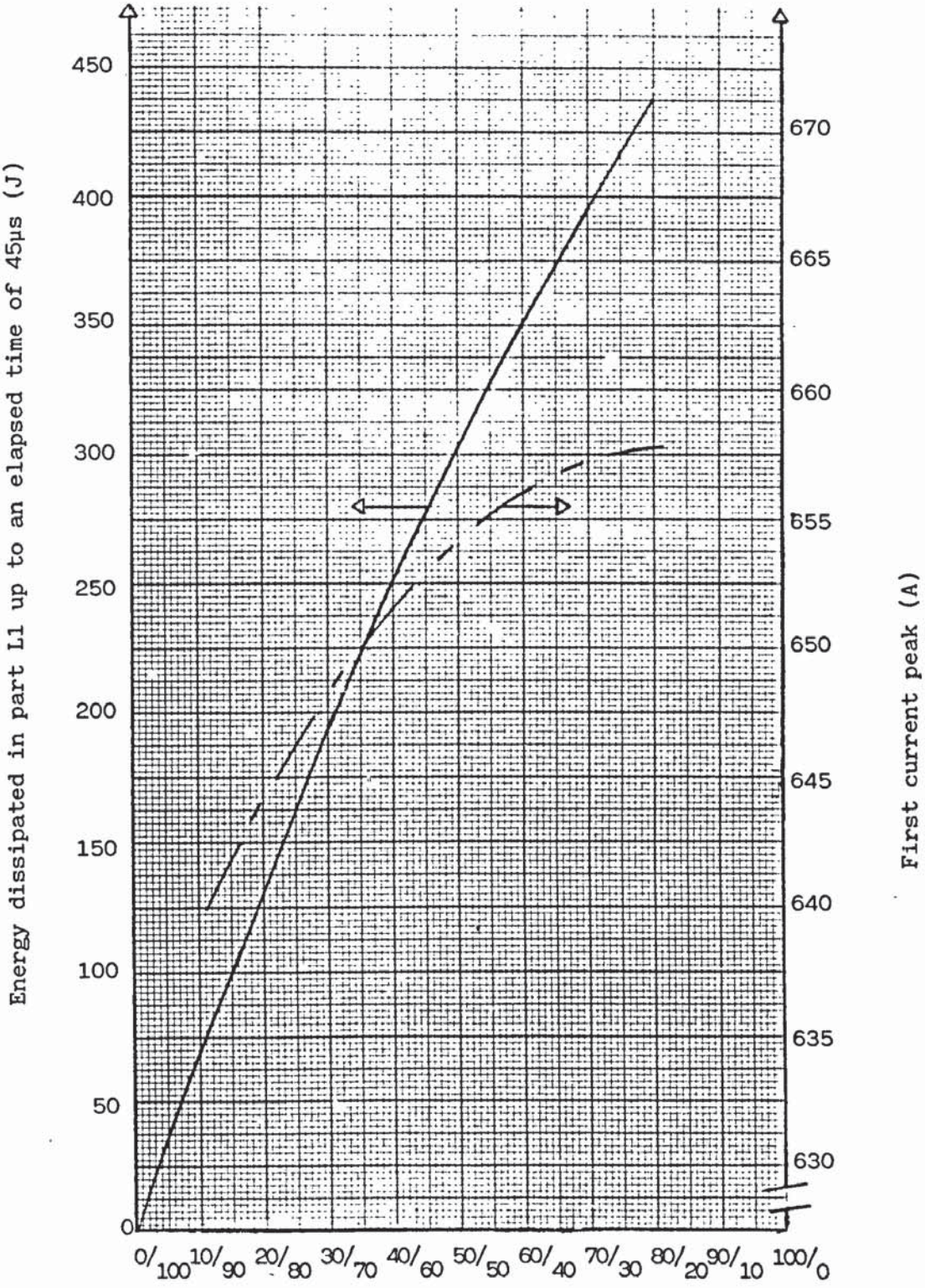

Fig.6.7 - Dependence of the energy dissipation in part L1 up to an elapsed time of 45µs and the magnitude of the first current peak upon the proportion of the saturation flux of parts L1/L2 to that of the saturating reactor.

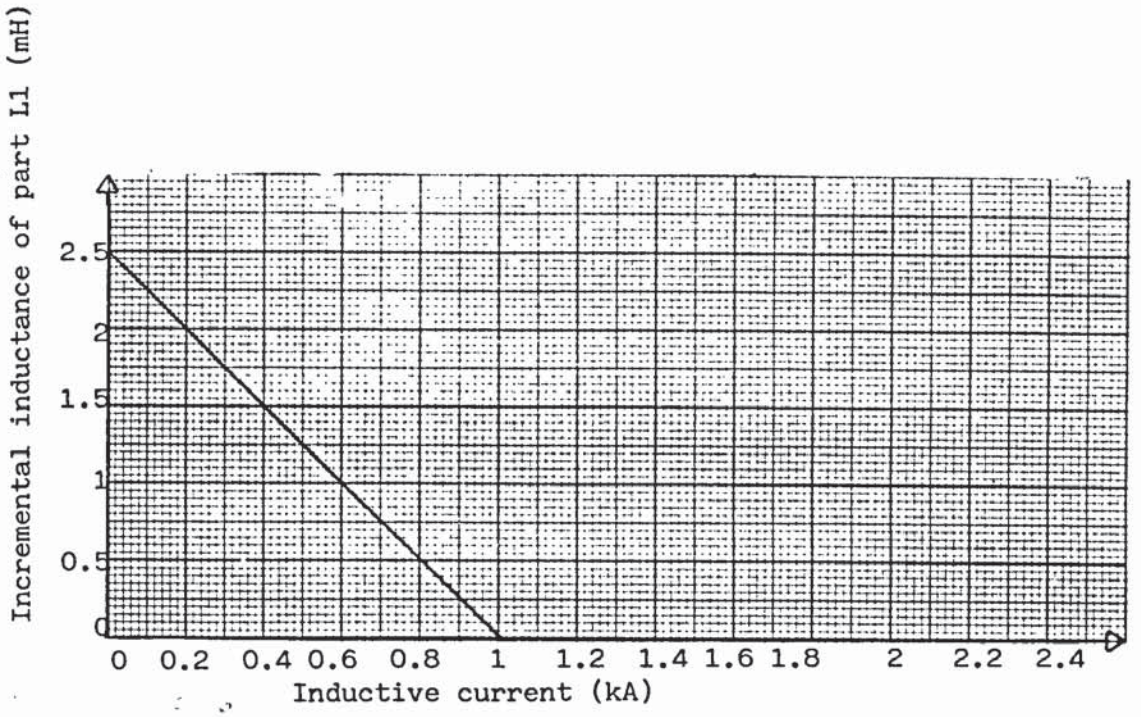

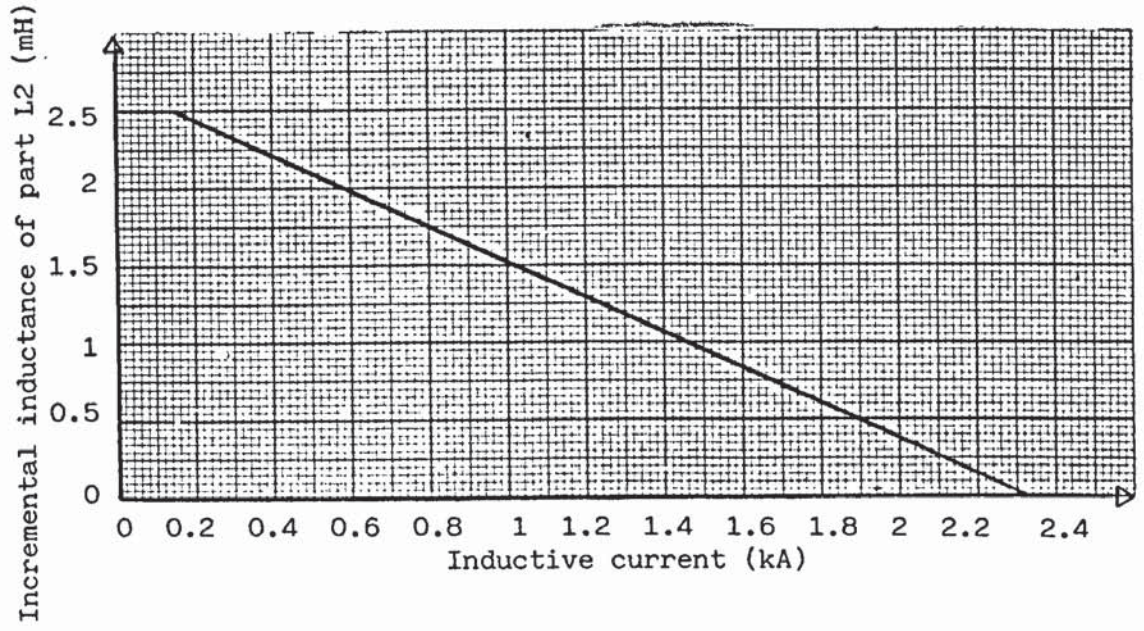

Fig.6.8 - General form of incremental inductance with current characteristics, utilised to assess the optimum value for the reflected resistance of part L1.

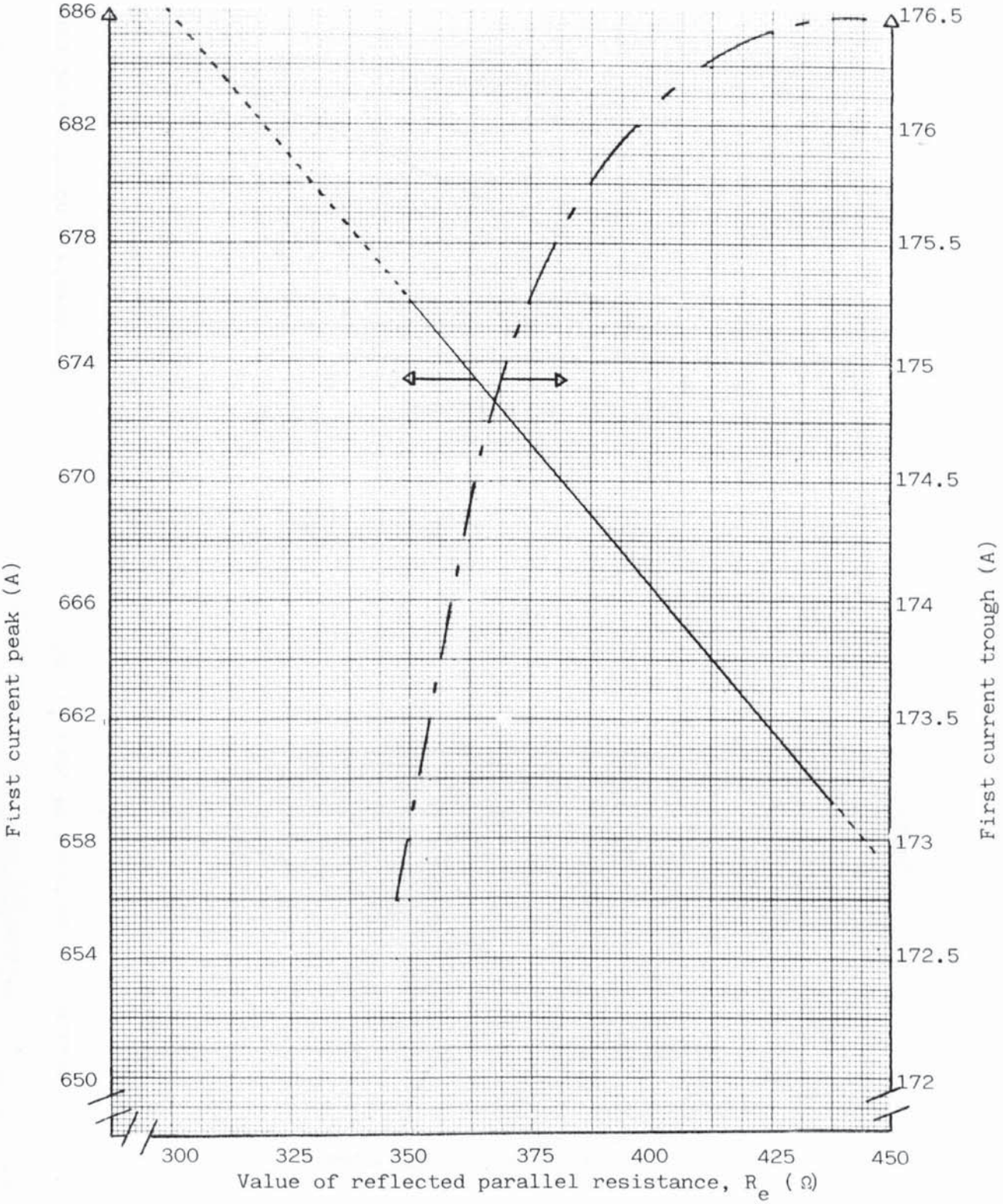

Fig.6.9 - Dependence of the magnitude of the first current peak and the first current trough upon the value of reflected parallel resistance.

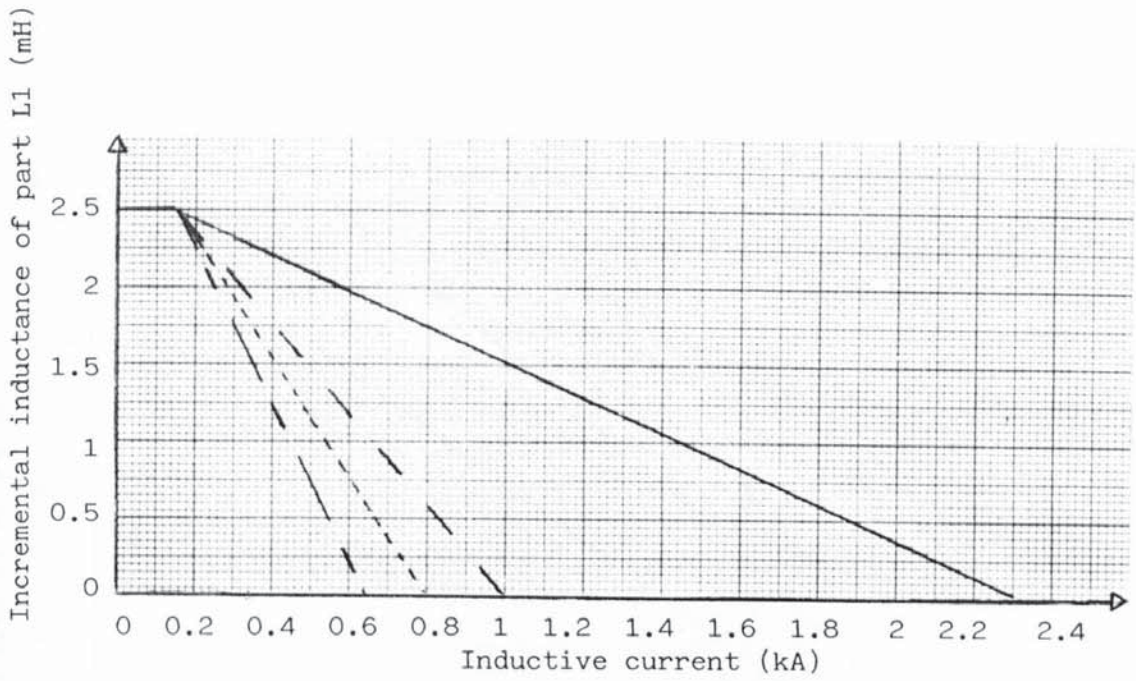

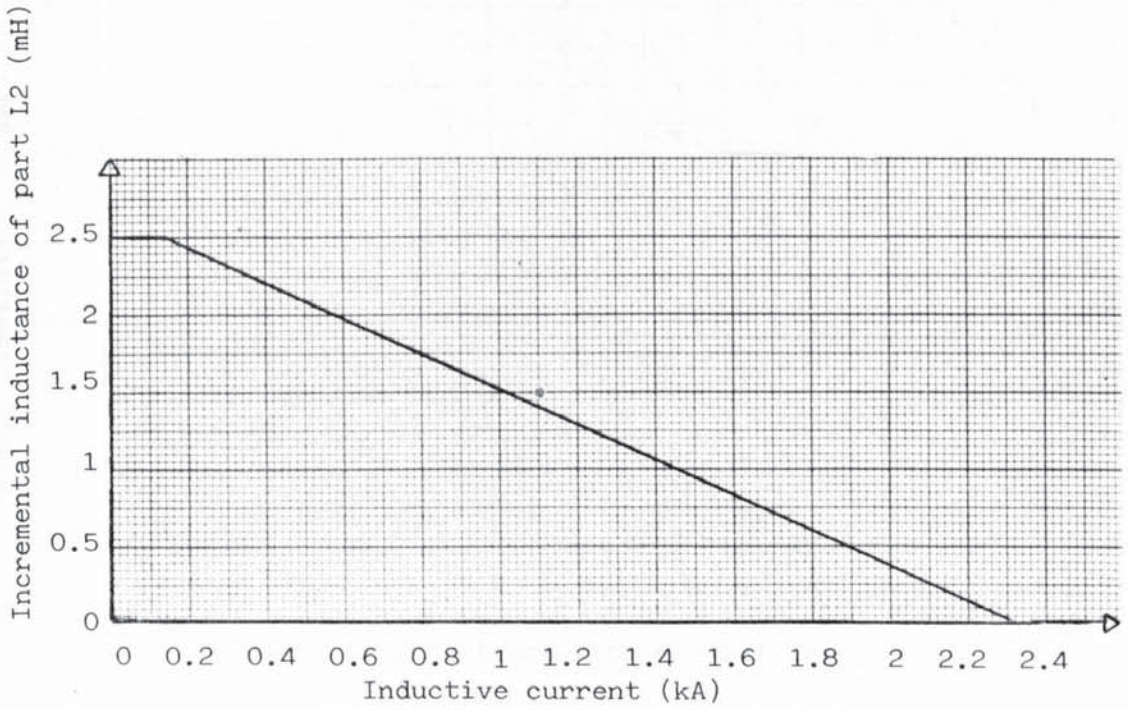

Fig.6.10 - General form of incremental inductance with current characteristics, utilised to optimise the inductance characteristic of part L1.

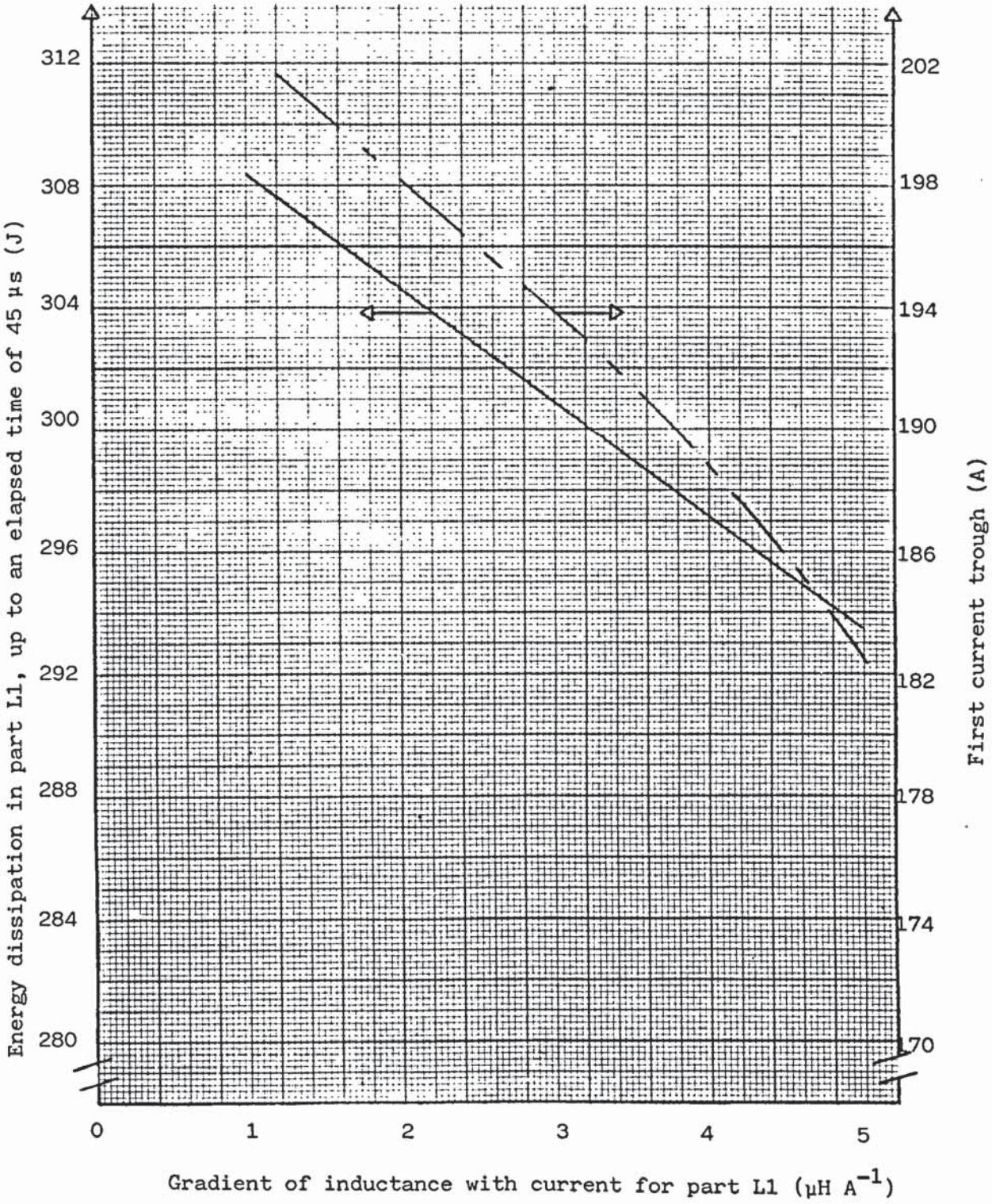

Fig.6.11 - Dependence of the energy dissipation in part L1 and the magnitude of first current trough upon the gradient of the inductance with current characteristic of part L1.

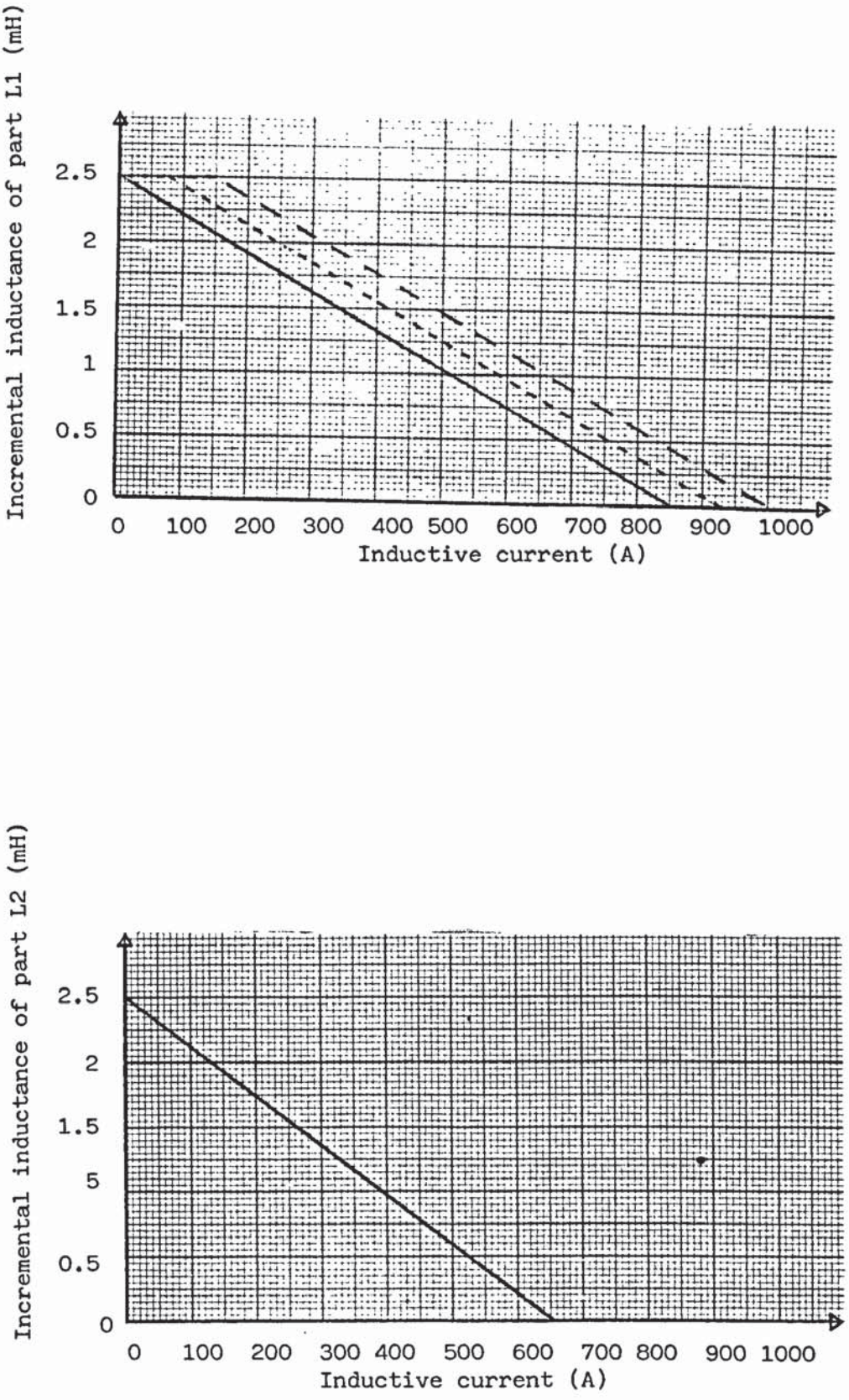

Fig.6.12 - General form of incremental inductance with current characteristic, utilised to assess the optimum interval of constant inductance for part L1.

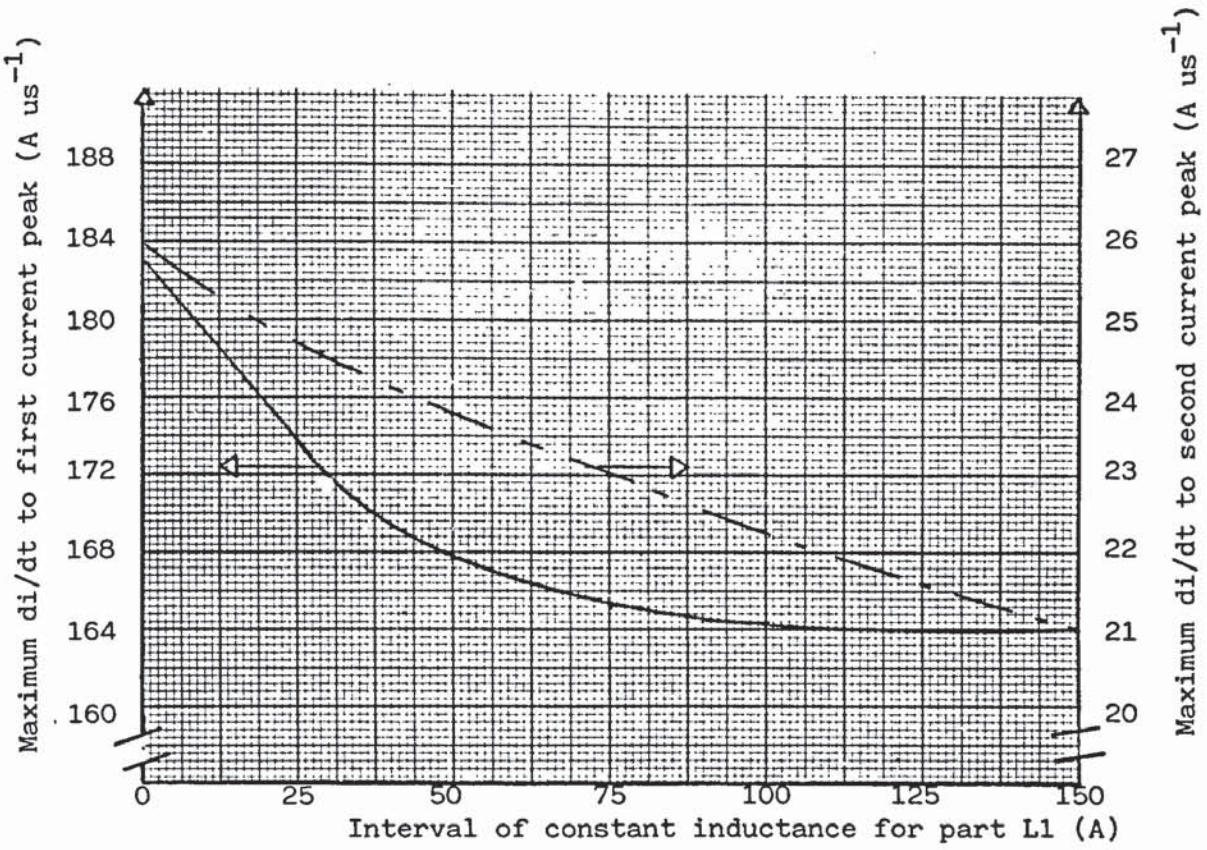

Fig.6.13 - Dependence of the maximum di/dt to both first current peak and second current peak upon the interval of constant inductance for part L1.

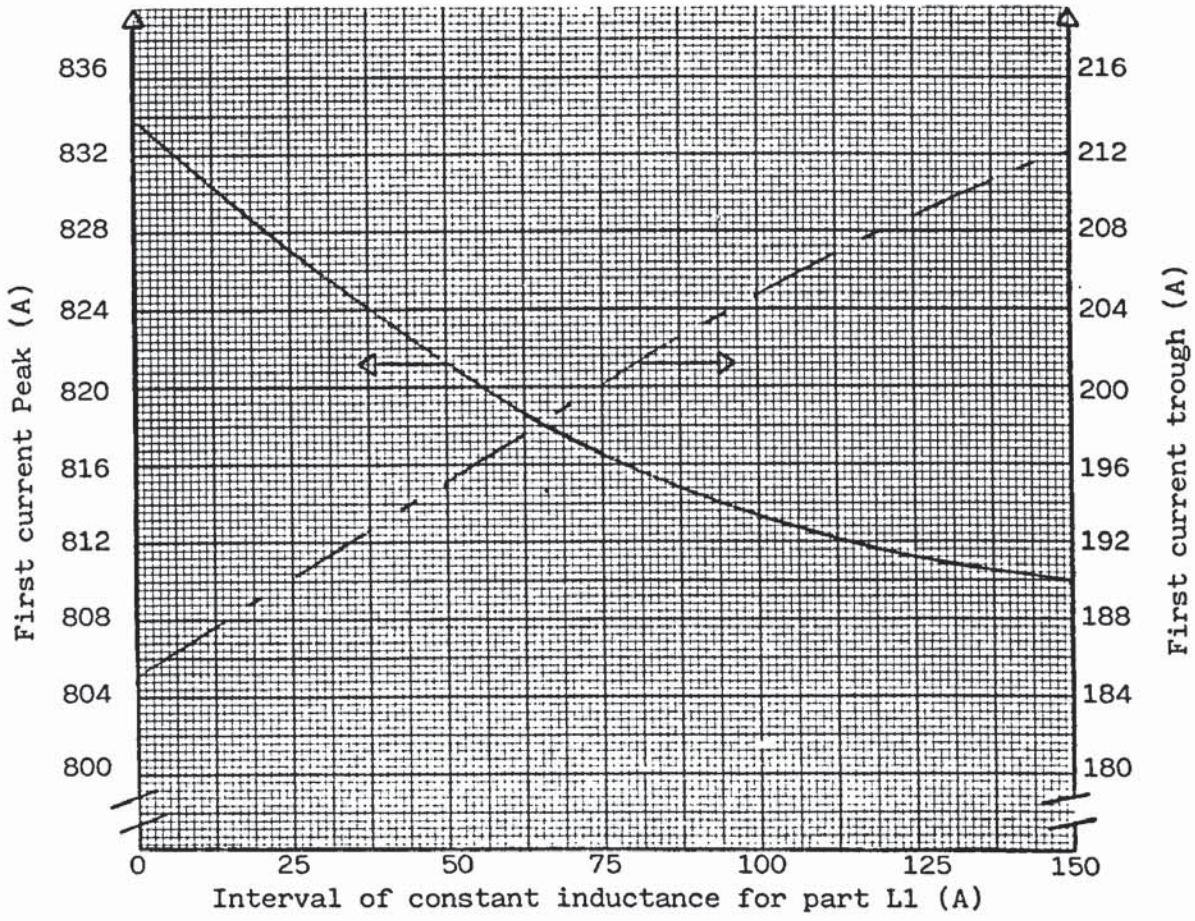

Fig.6.14 - Dependence of the magnitude of both the first current peak and the first current trough upon the interval of constant inductance for part L1.

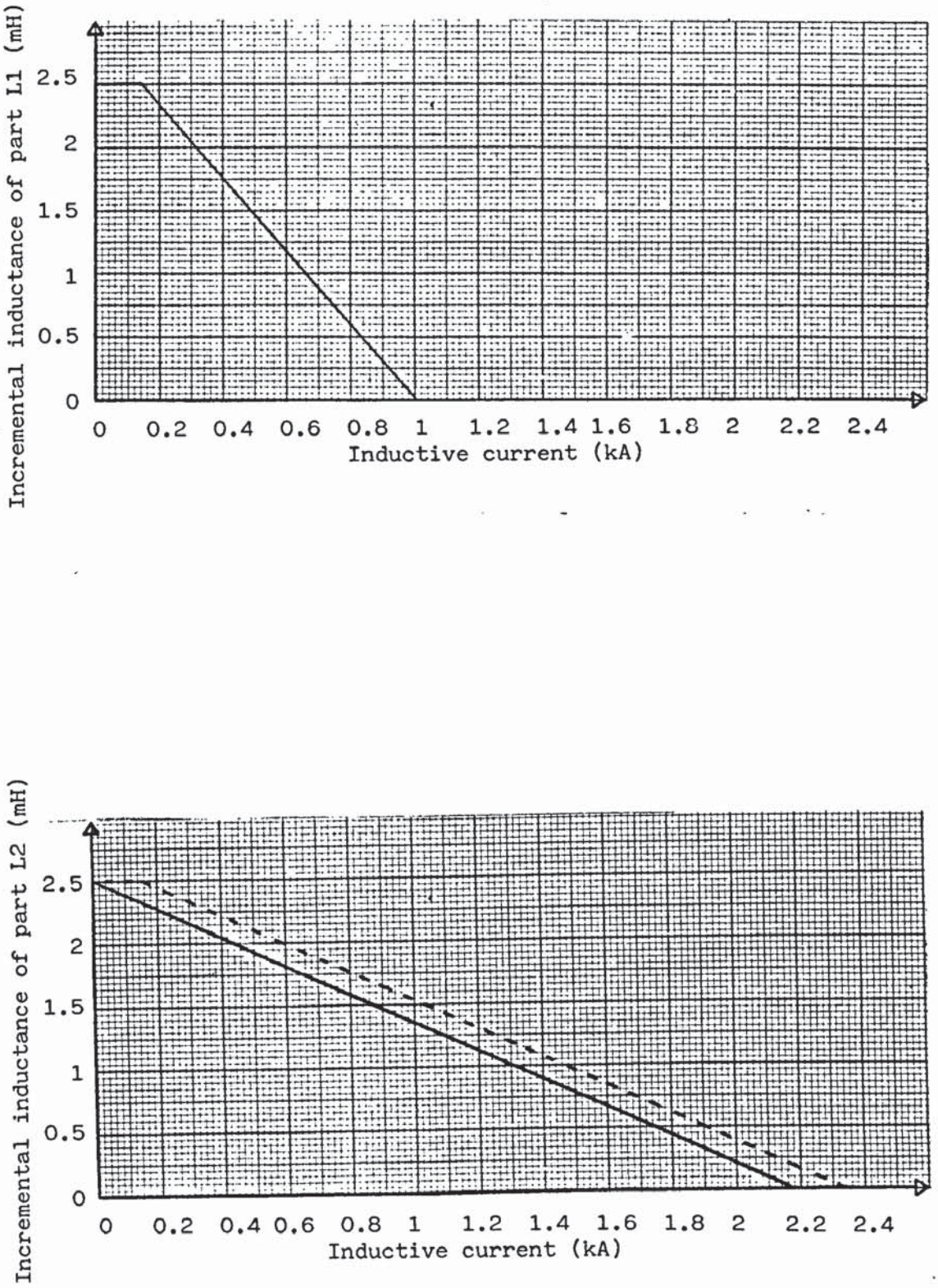

Fig.6.15 - General form of incremental inductance with current characteristics, utilised to assess the optimum interval of constant inductance for part L2.

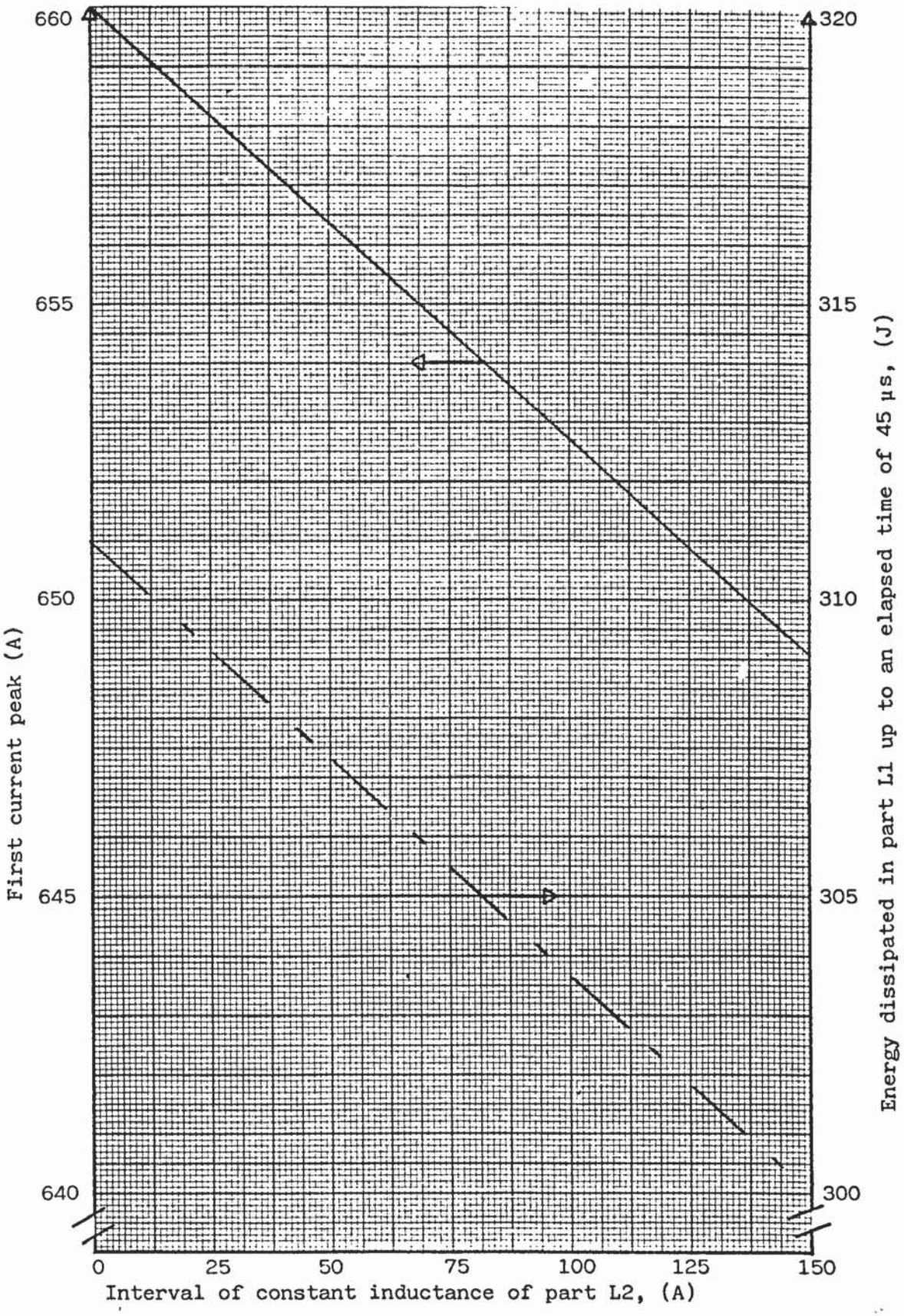

Fig.6.16 - Dependence of the magnitude of the first current peak, and the energy dissipation in part L1 up to an elapsed time of 45 μs, upon the interval of constant inductance of part L2.

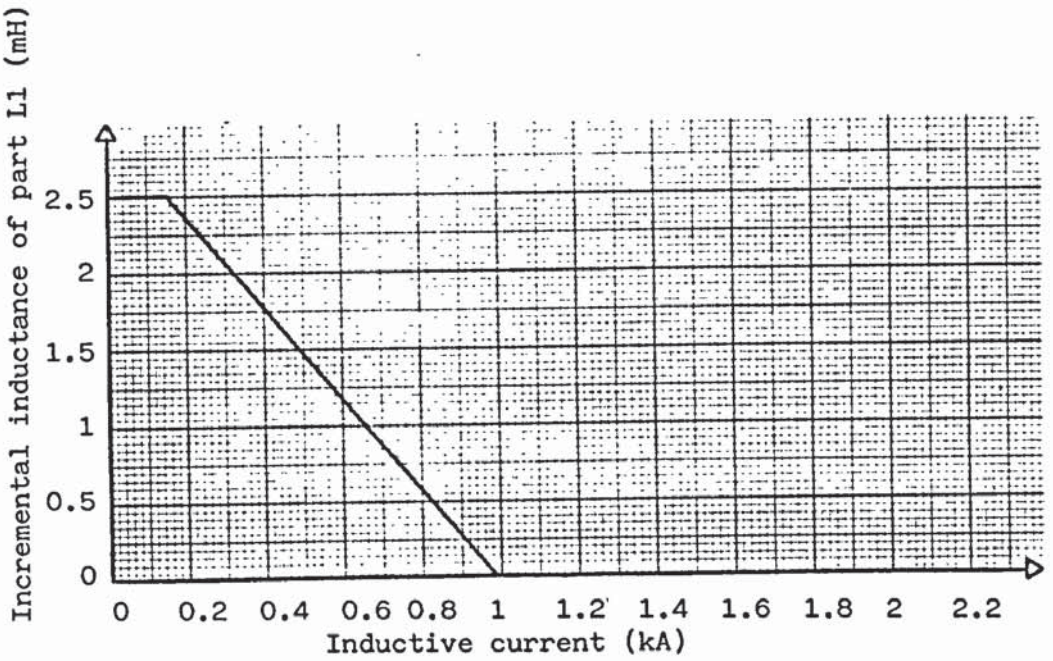

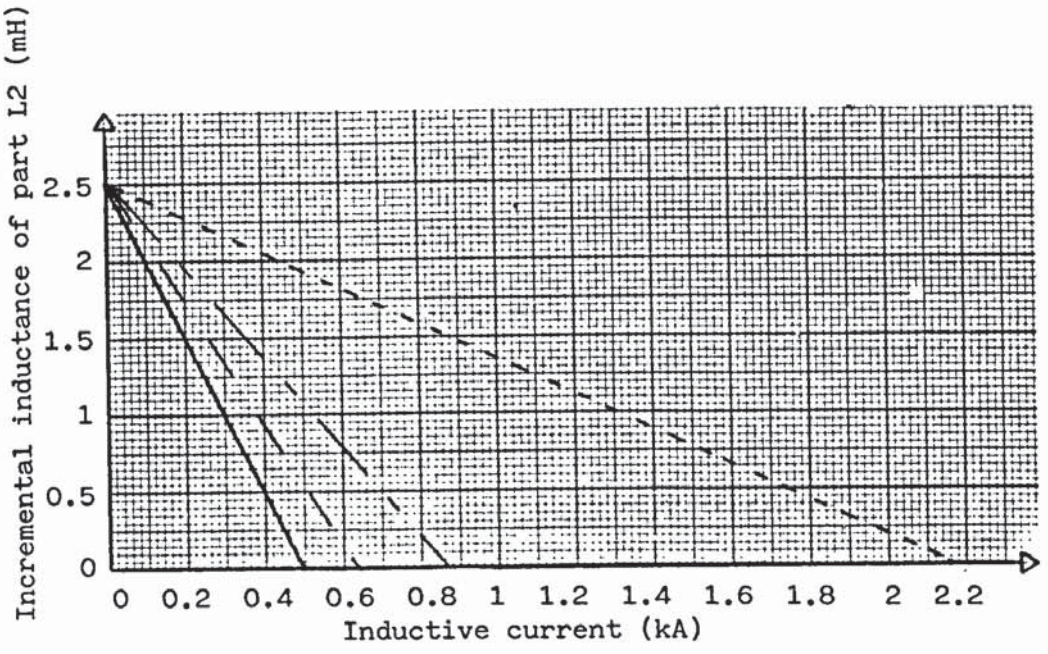

Fig.6.17 - General form of the incremental inductance with current characteristics, utilised to optimise the inductance characteristic of part L2.

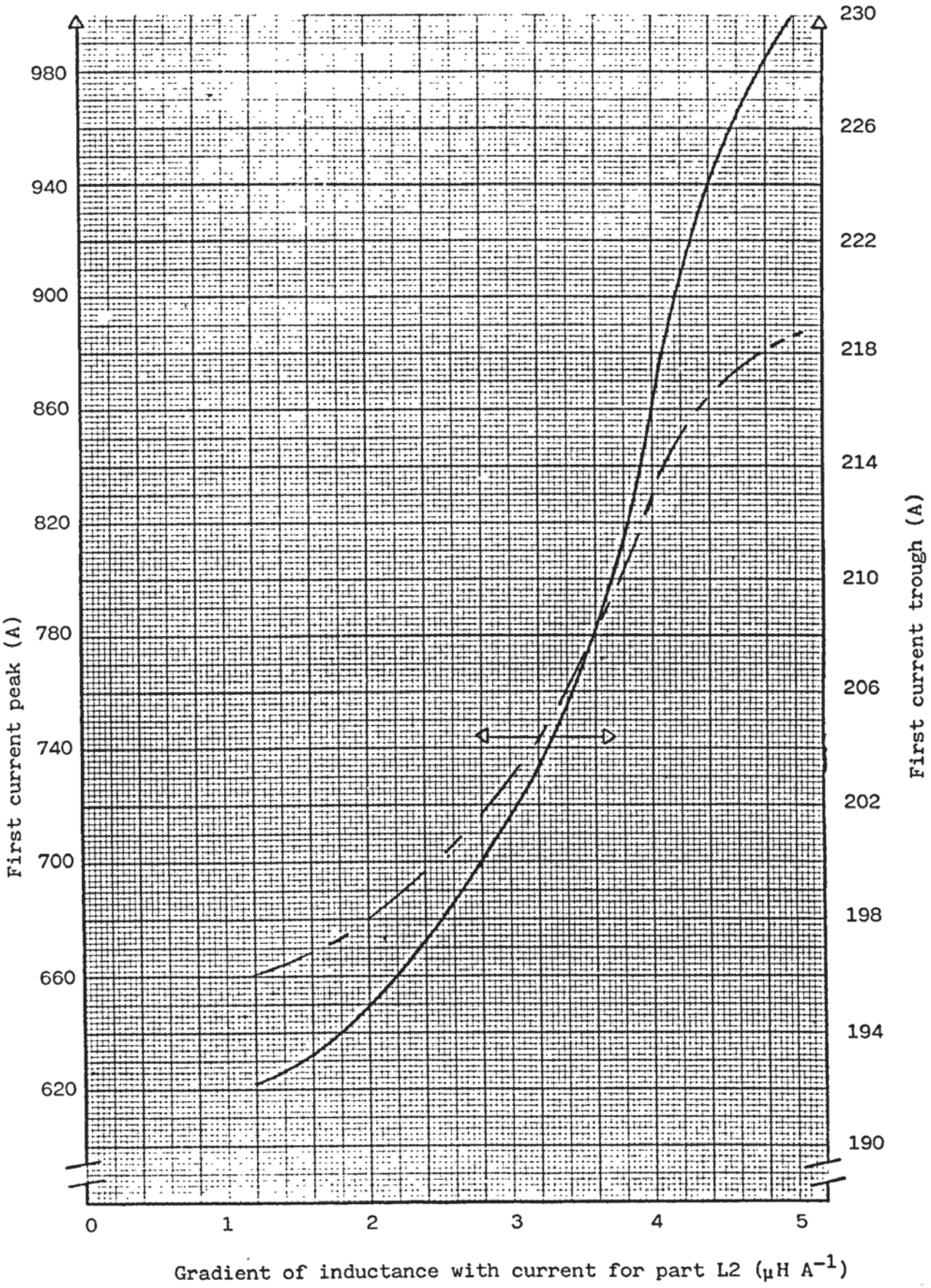

Fig.6.18 - Dependence of both the magnitude of first current peak and first current trough upon the gradient of the inductance with current characteristic of part L2.

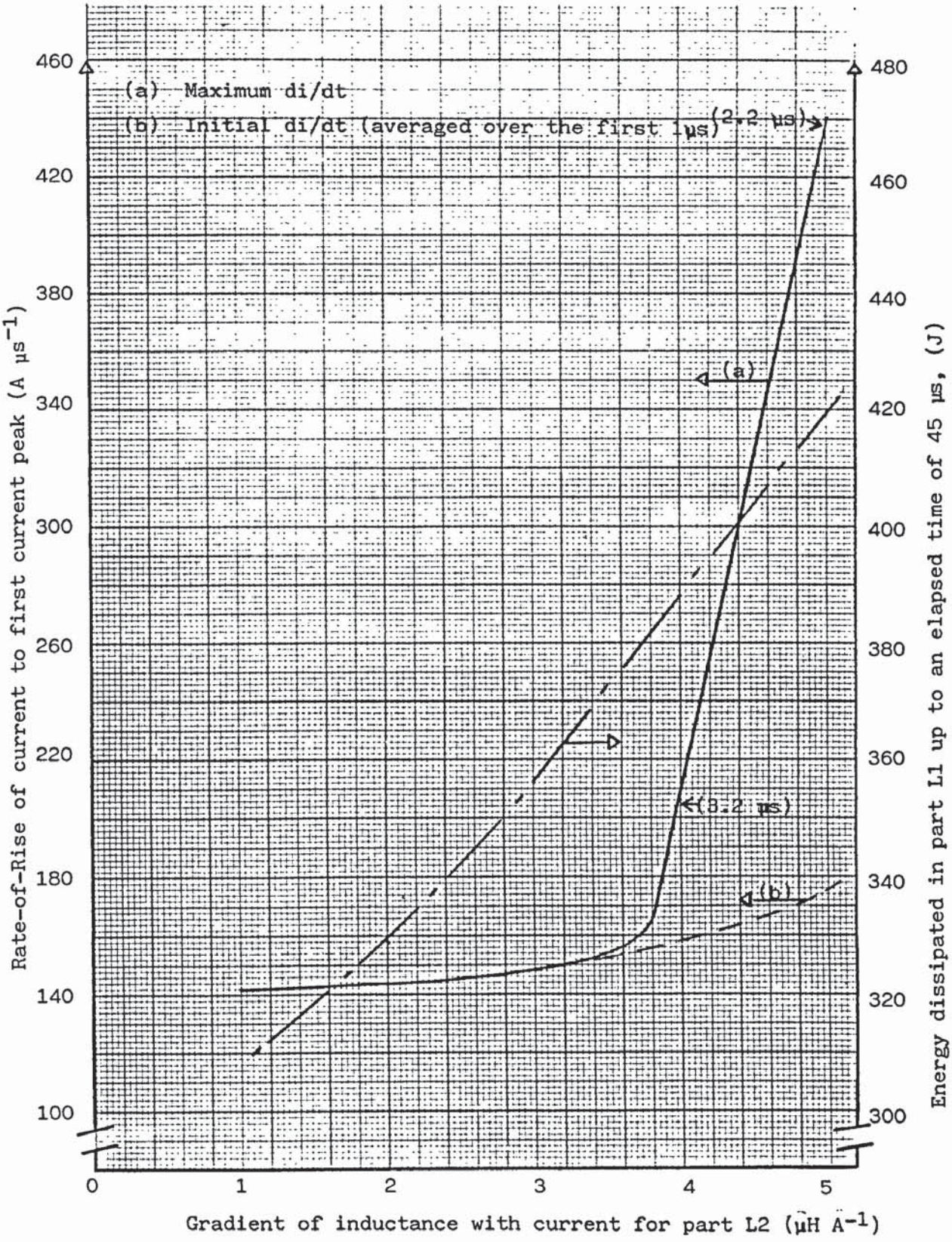

Fig.6.19 - Dependence of the initial and maximum di/dt to first-current peak, and the energy dissipation in part L1 (up to an elapsed time of 45 μs), upon the gradient of inductance with current for part L2.

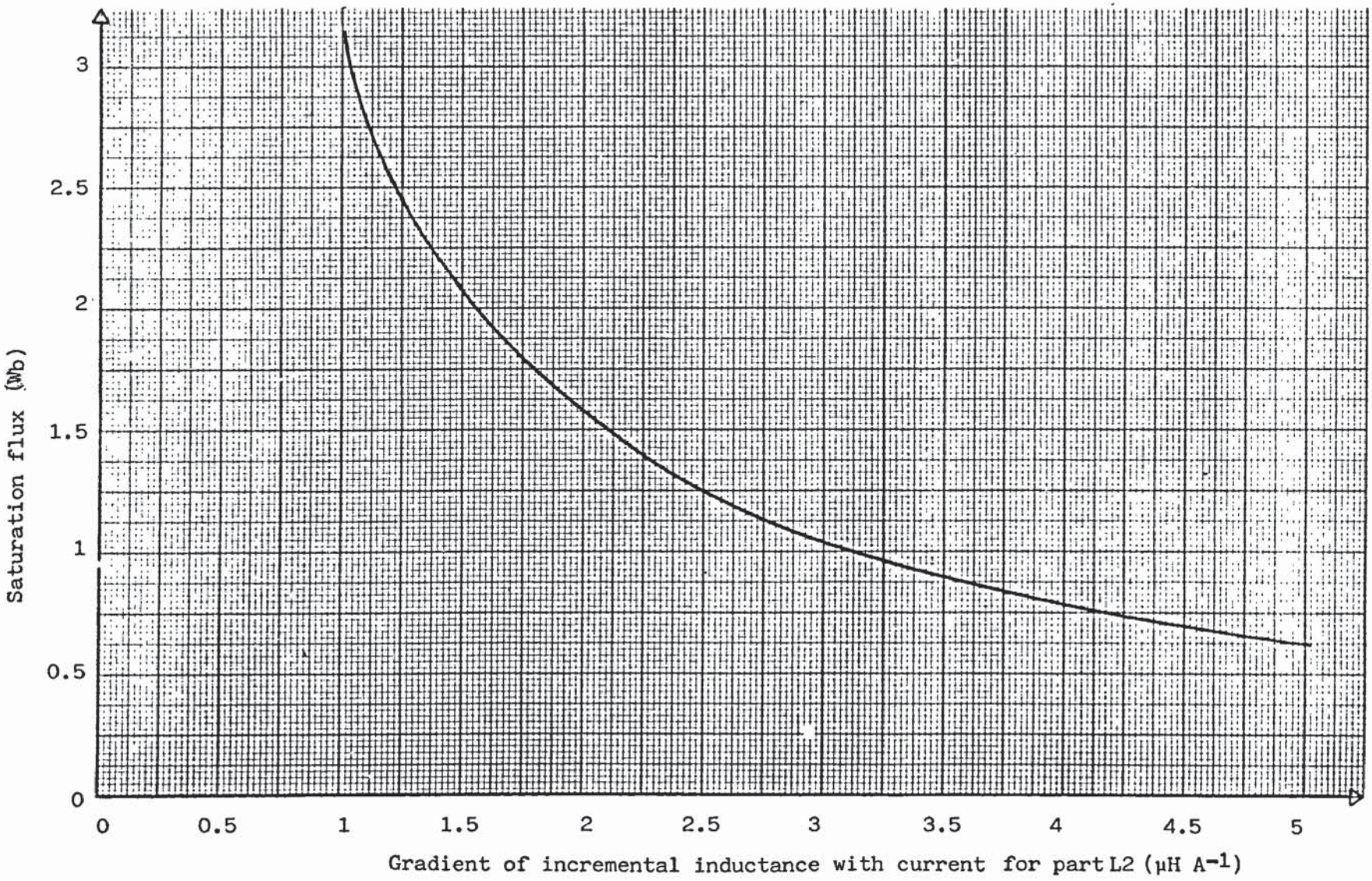

Fig.6.20 - Dependence of the saturation flux requirement of part L2 upon the gradient of the inductance with current for part L2.

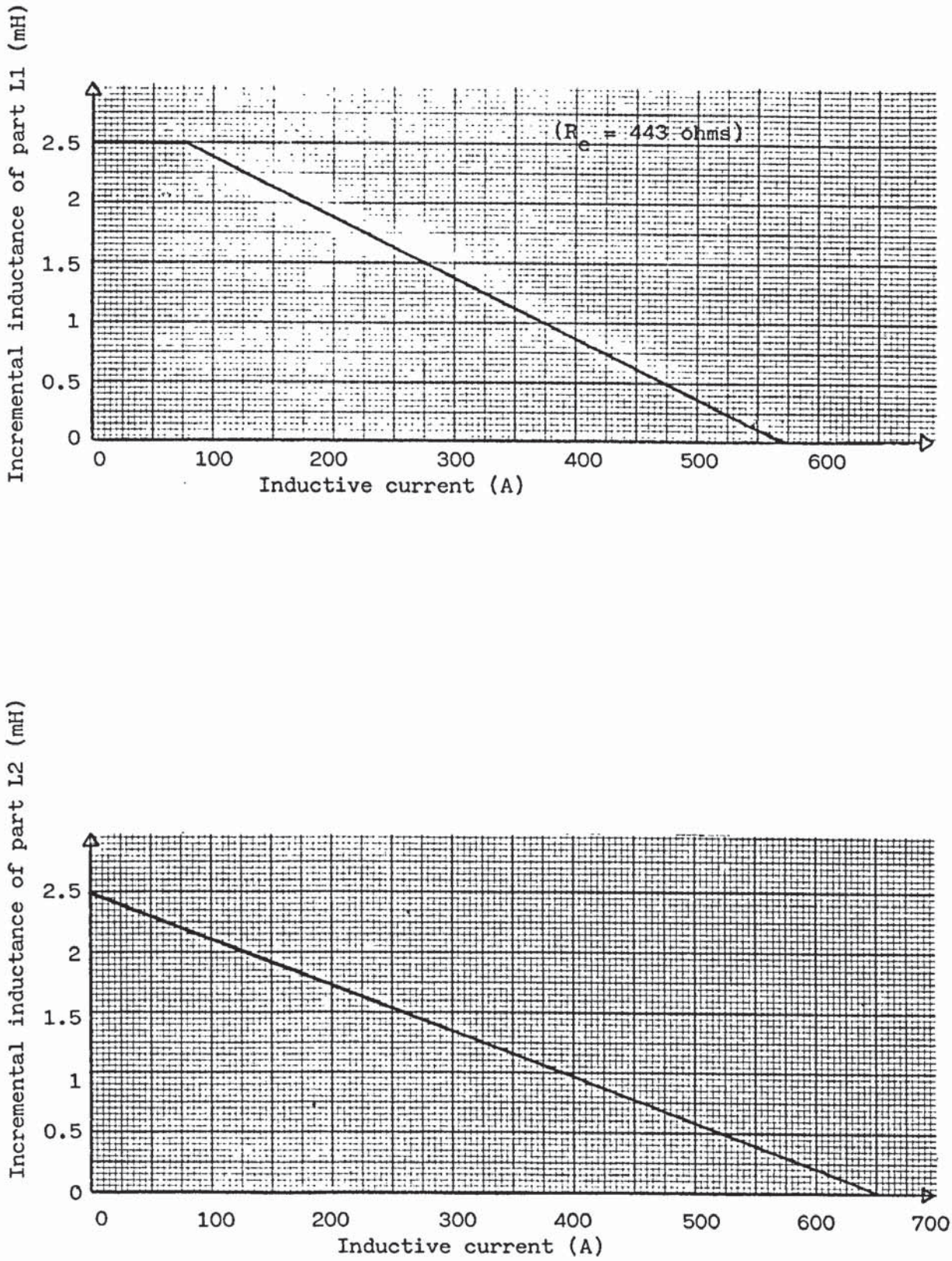

Fig.6.21 - Proposed inductance with current characteristics for parts L1 and L2 respectively.

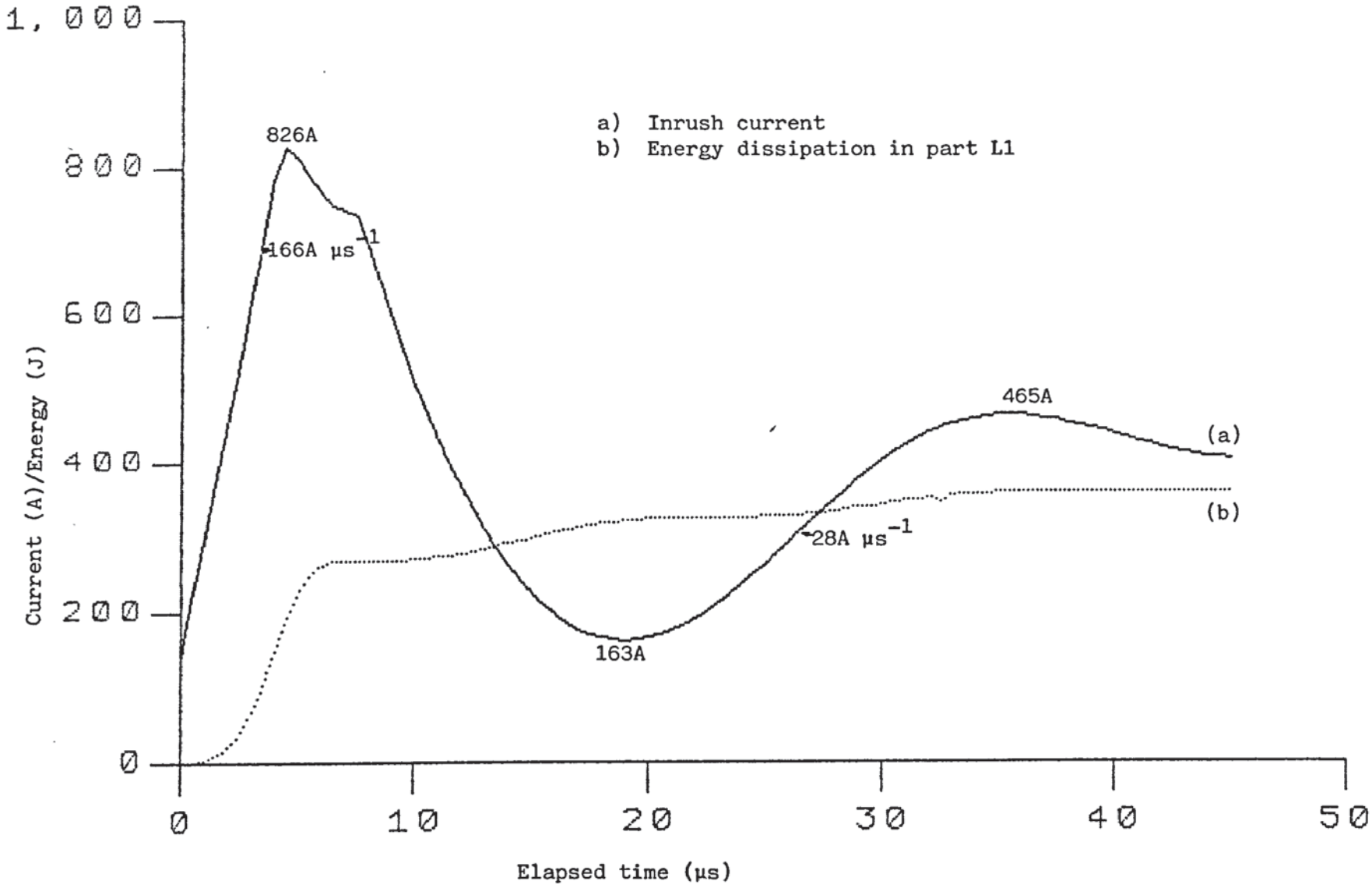

Fig.6.22 - Thyristor inrush current and energy dissipation in part L1 during worst-case repetitive inrush. (Proposed characteristics represented (see figure 6.21)).

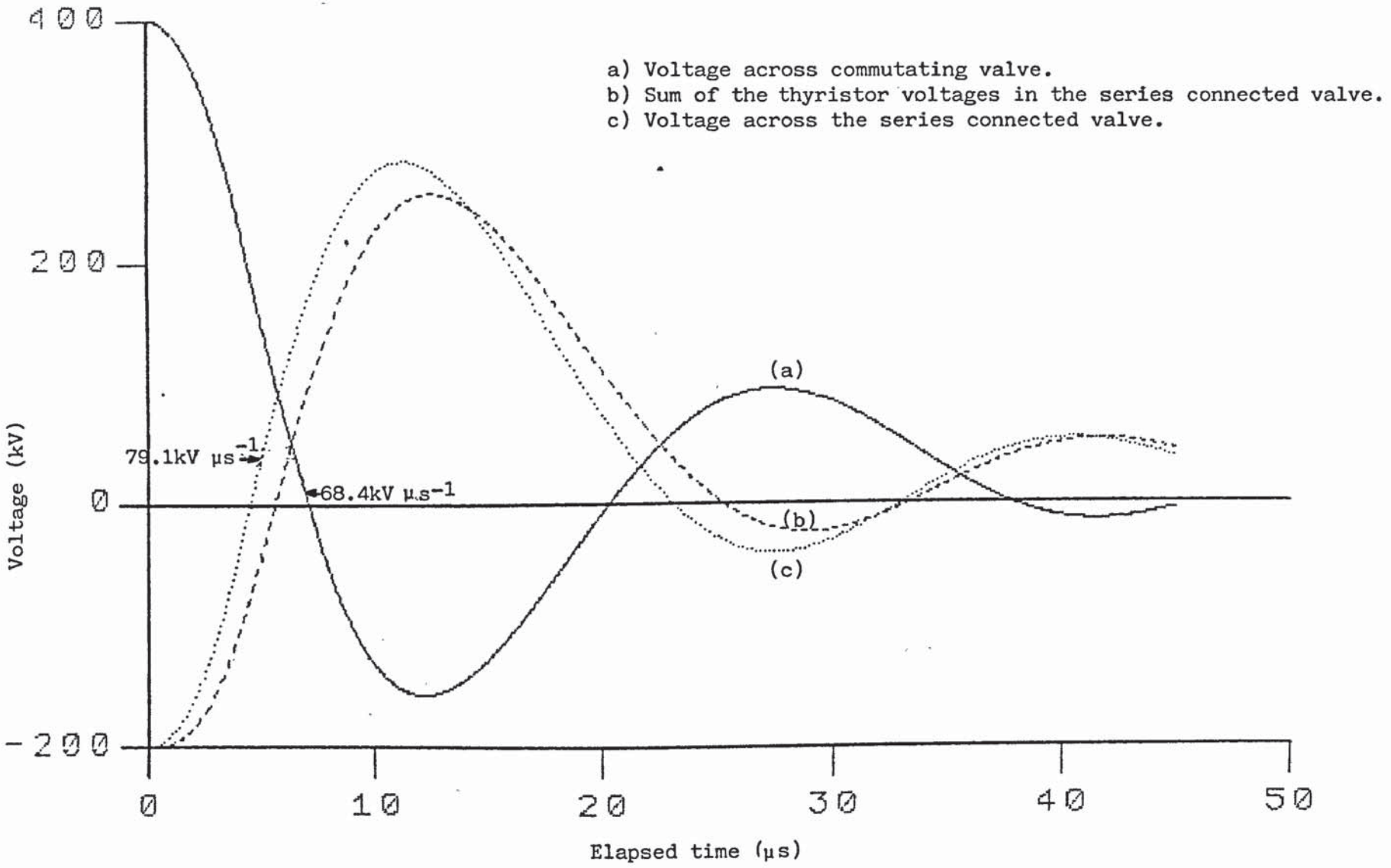

Fig.6.23 - Voltage across commutating valve and voltage associated with series connected valve for worst-case repetitive turn-on, (proposed characteristics represented (see figure 6.21)).

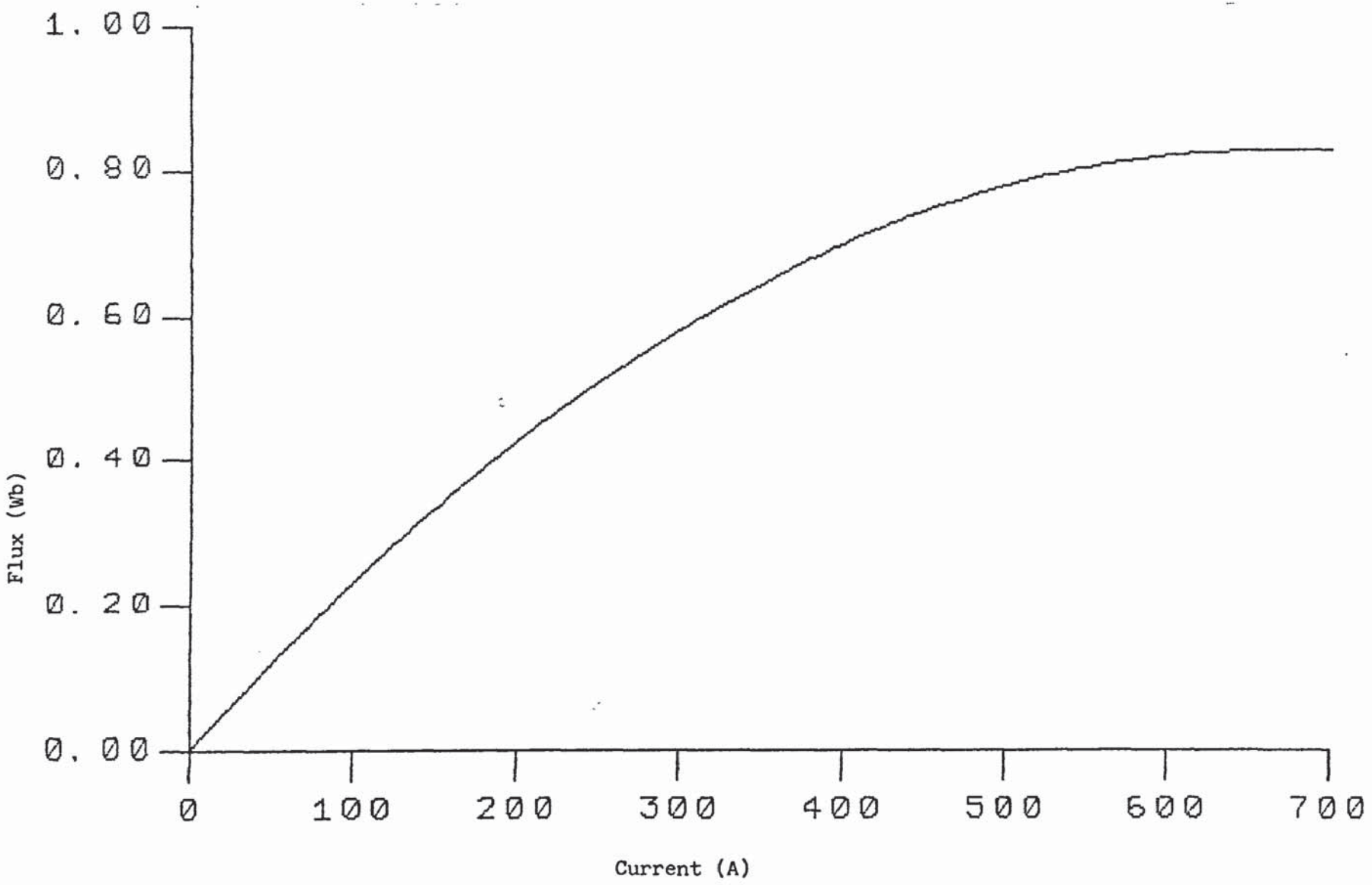

Fig.6.24 - Flux-current curve for the proposed inductance with current characteristic, for part L2.

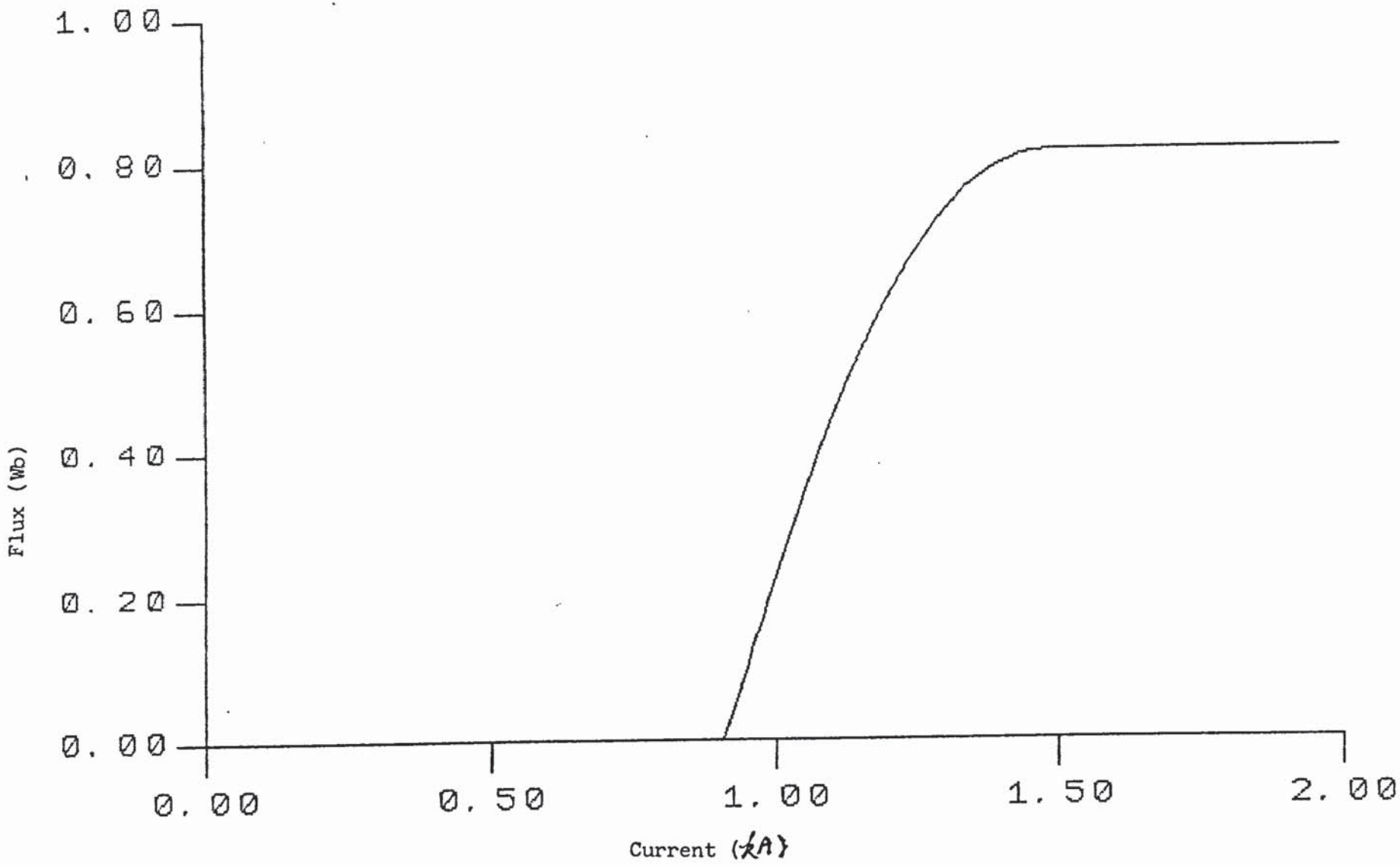

Fig.6.25 - Flux-current curve for the proposed characteristic for part L1, (fixed B-field, equivalent to 4kV per level for a 100 level valve, applied to part L1).

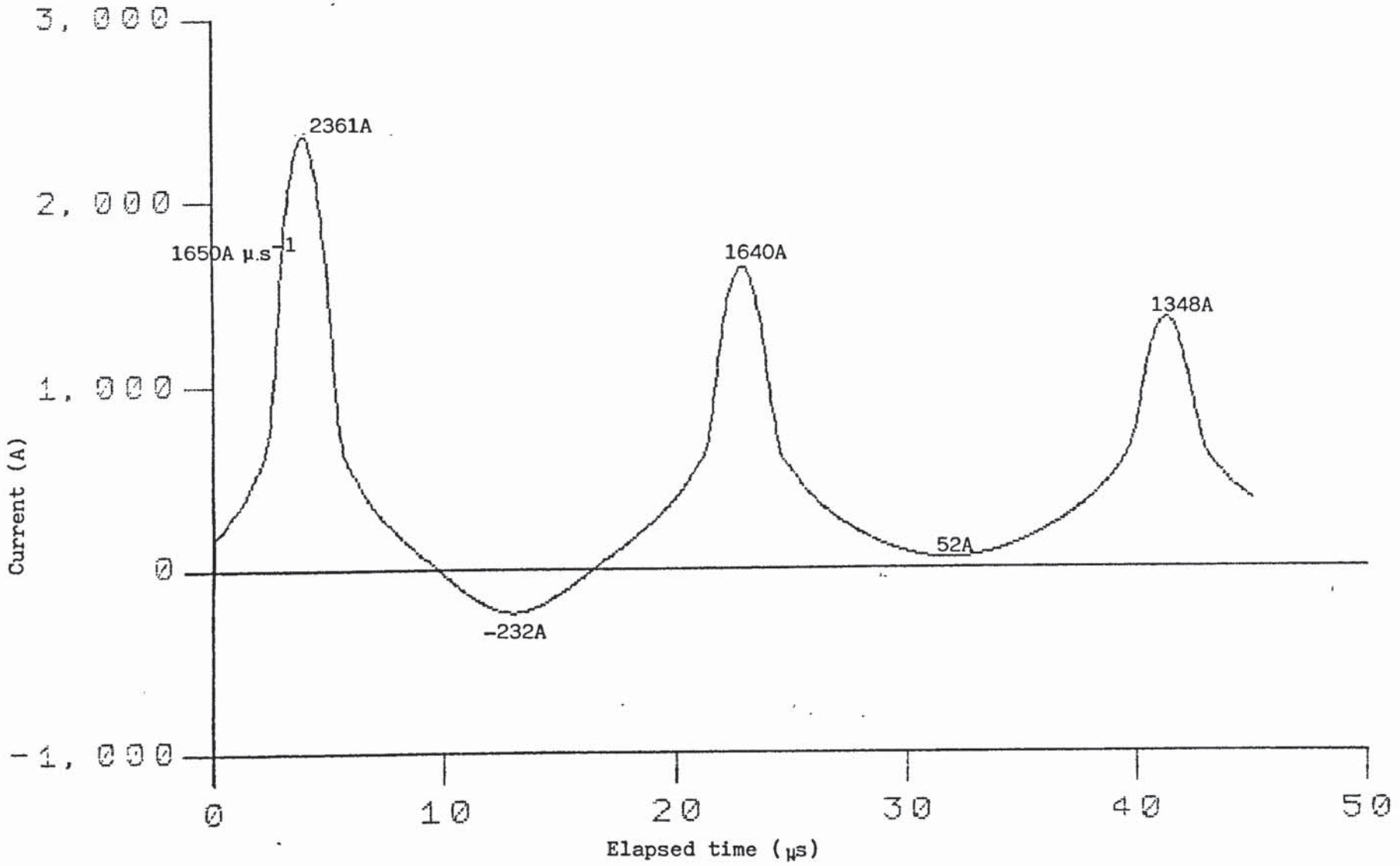

Fig.6.26 - Thyristor inrush prediction during worst-case repetitive inrush. Proposed characteristic for part L2 (figure 6.21) is modelled; part L1 is not modelled.

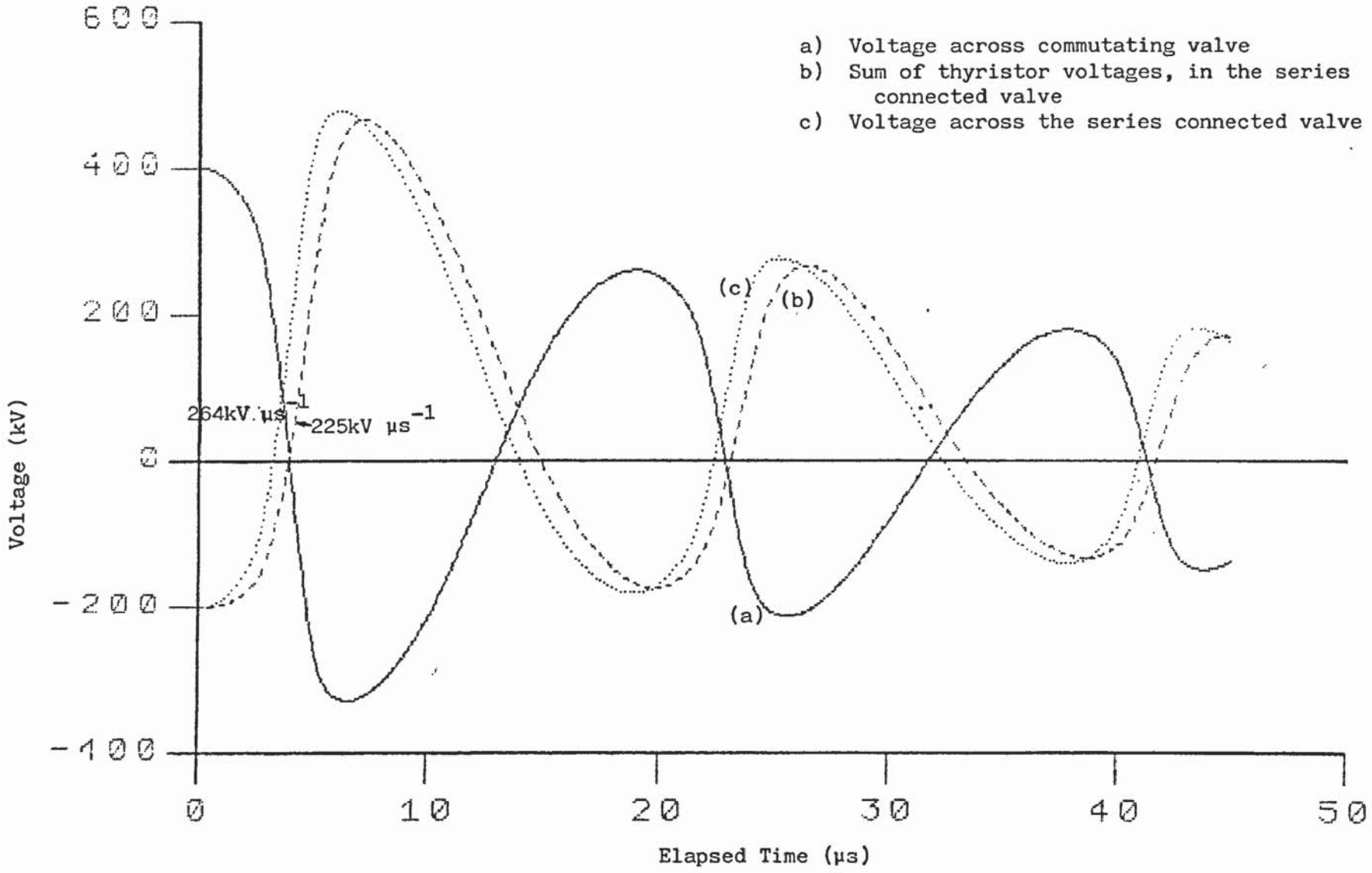

Fig. 6.27 Voltage across commutating valve and voltage associated with series connected valve for worst-case repetitive turn-on. Proposed characteristic for part L2 (Figure 6.21) is modelled; part L1 is not modelled.

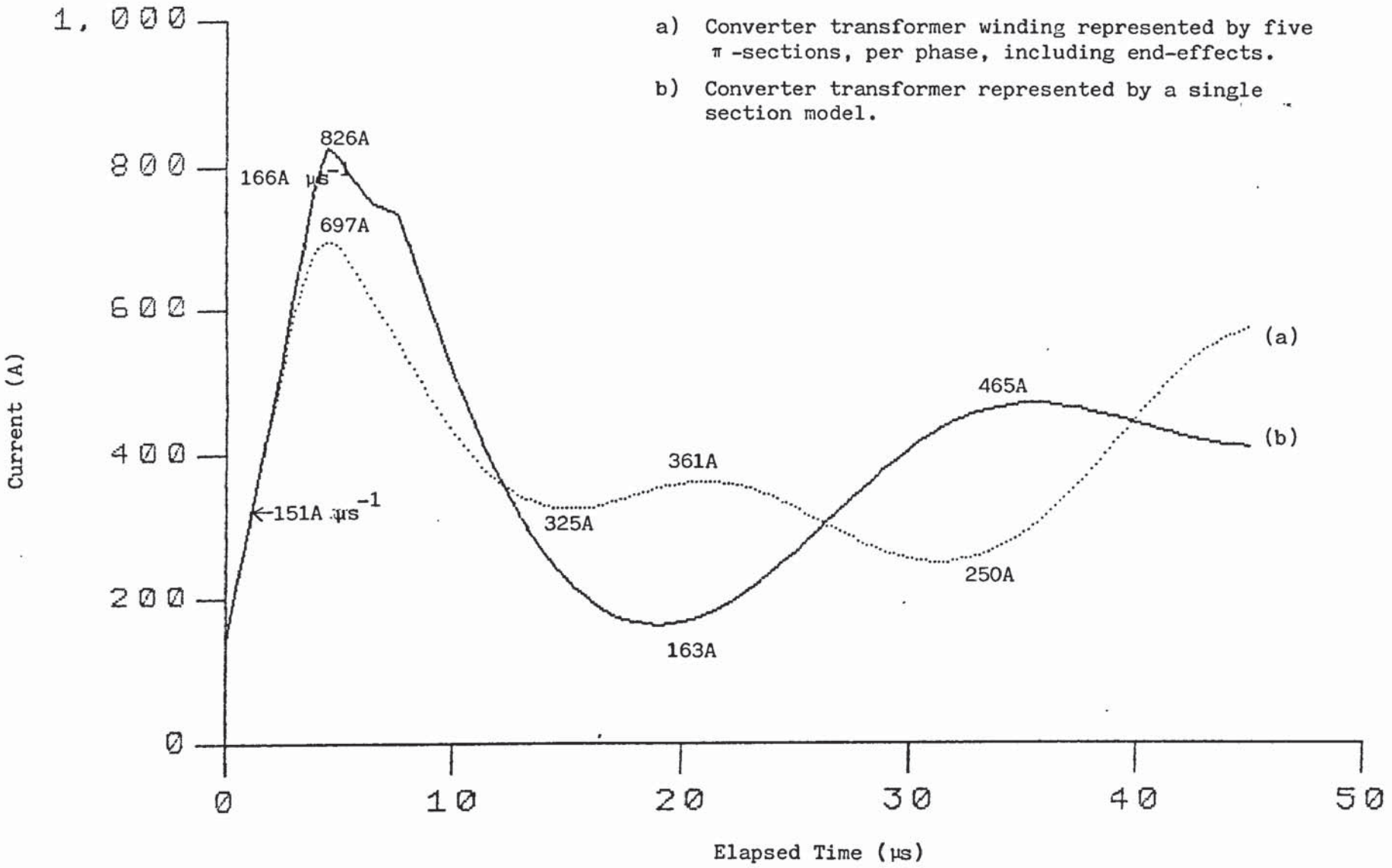

Fig. 6.28 - Comparison of predictions of thyristor inrush current during worst-case repetitive turn-on (Proposed reactor characteristics.(Figure 6.21)).

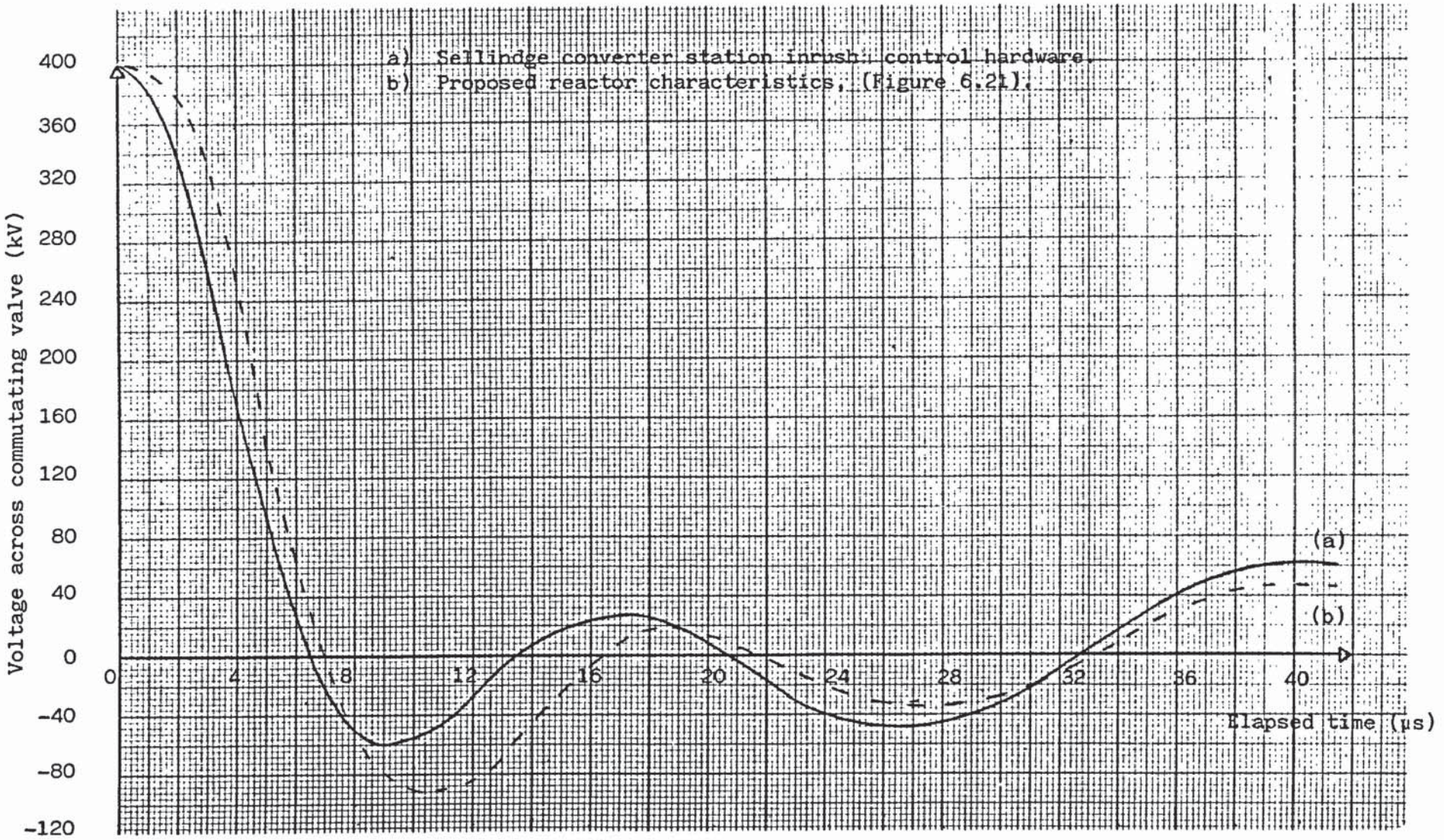

Fig. 6.29 - Comparison of predicted valve-voltage collapse during worst-case repetitive turn-on. Converter transformer is represented by five π-sections including end-effects.

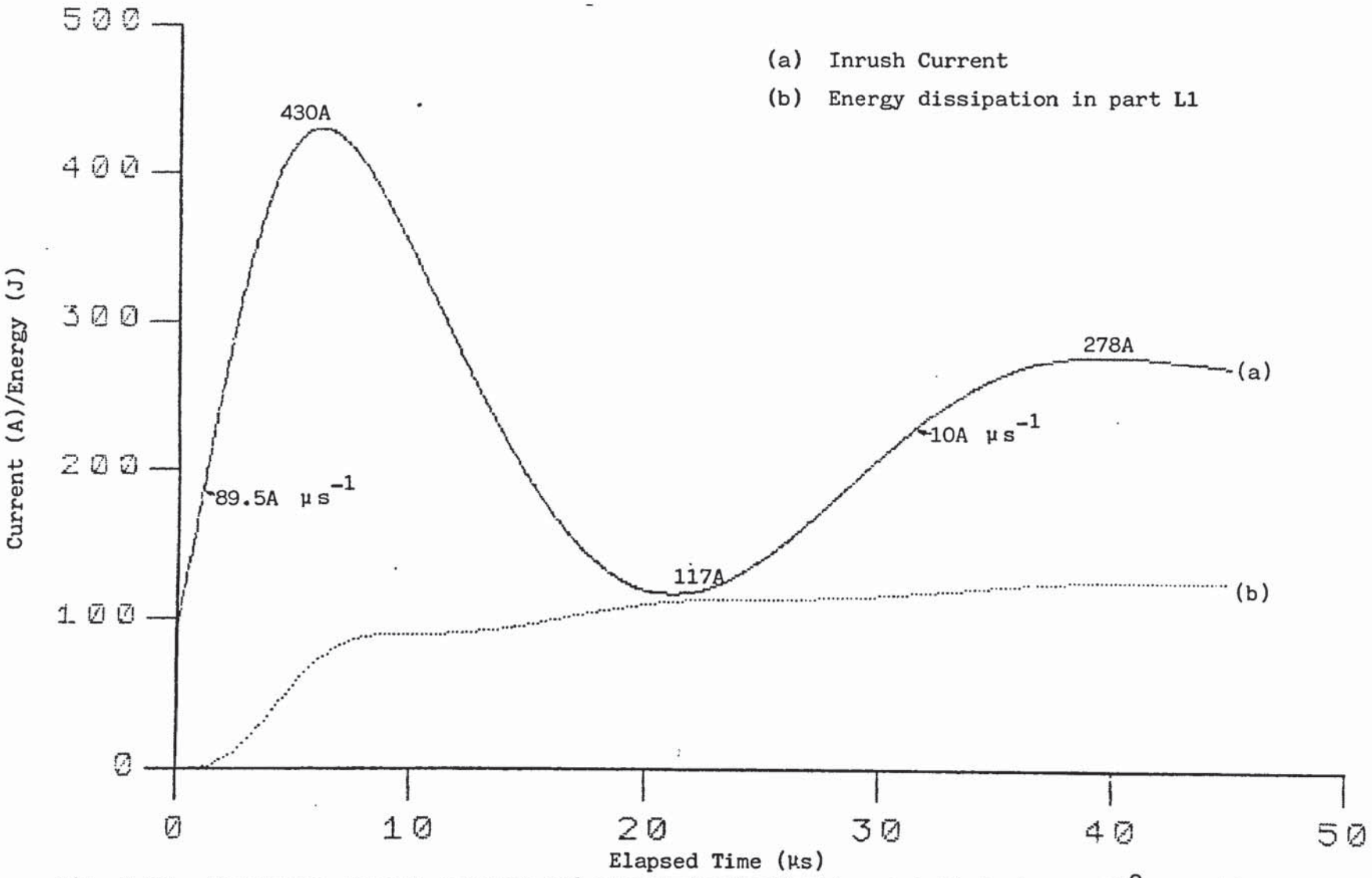

Fig. 6.30 - Thyristor inrush current and energy dissipation in part L1 during $\alpha = 90^{o}$ operation. (Proposed characteristics represented (see Figure 6.21)).

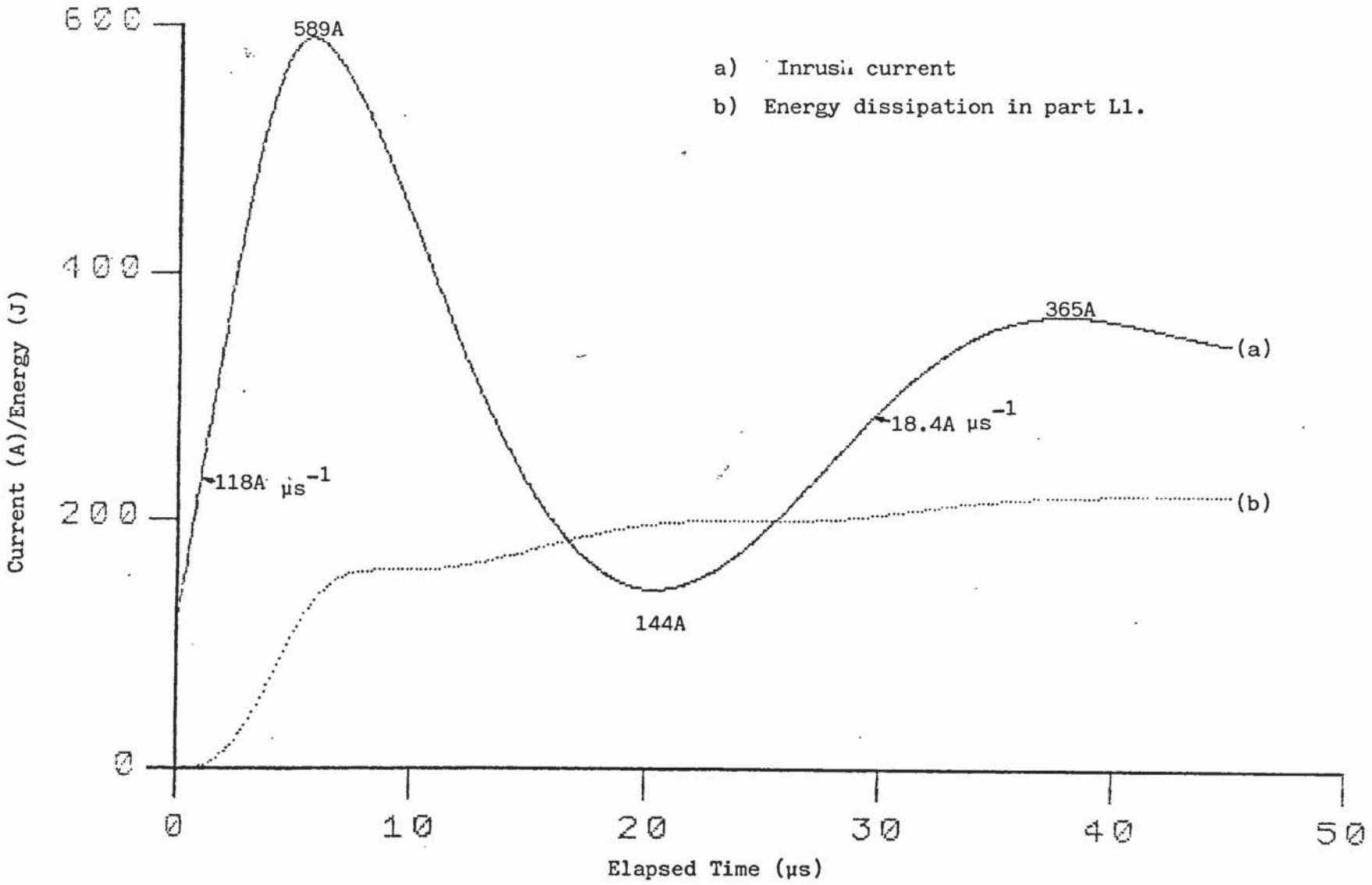

Fig. 6.31 - Thyristor inrush current and energy dissipation in part L1 during $\alpha = 90^{\circ}$ + DOV operation. (Proposed characteristics represented (see Figure 6.21)).

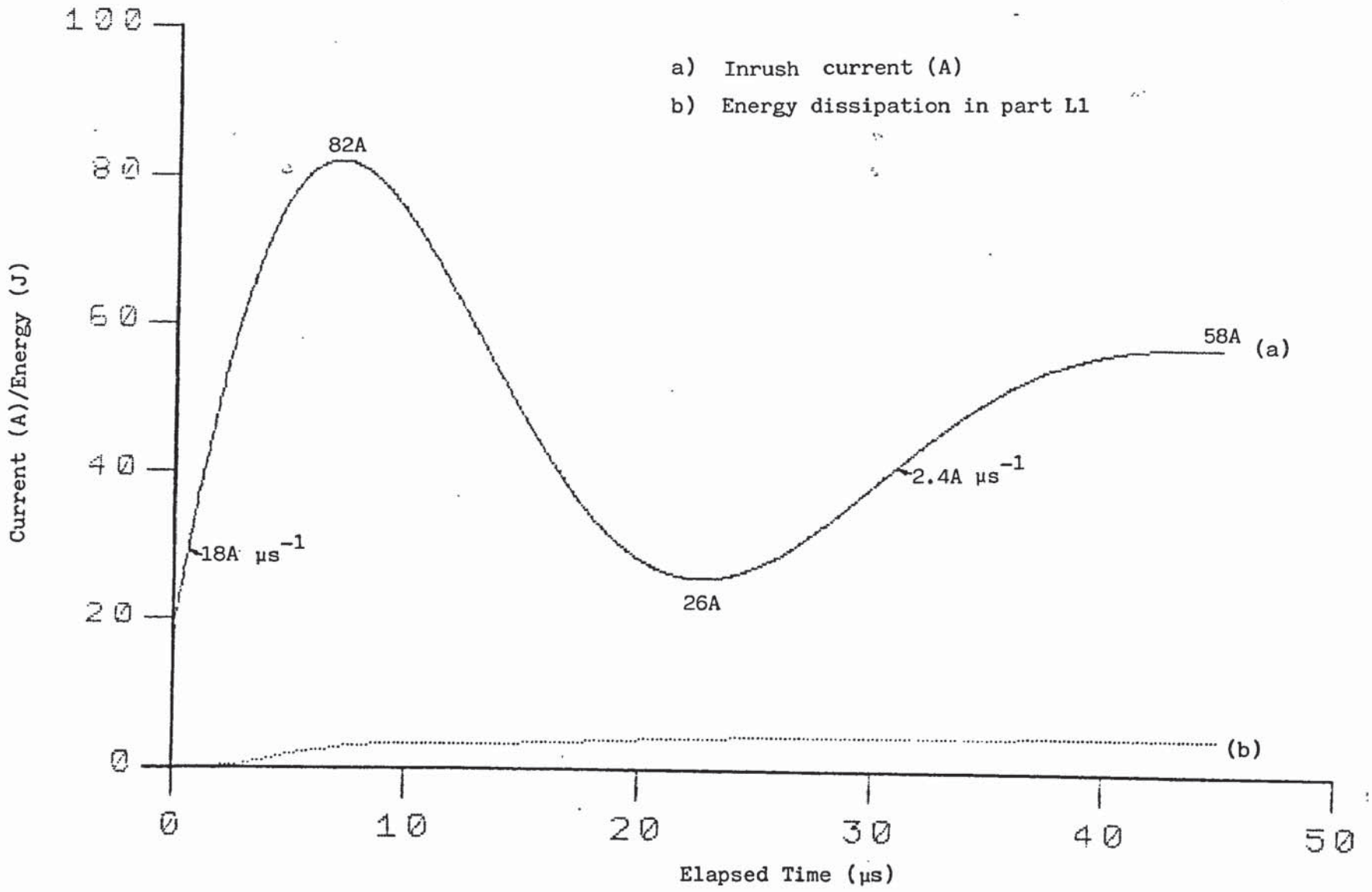

Fig. 6.32 - Thyristor inrush current and energy dissipation in part L1 during $\alpha = 12^{o}$ operation (Proposed characteristics represented (see Figure 6.21))

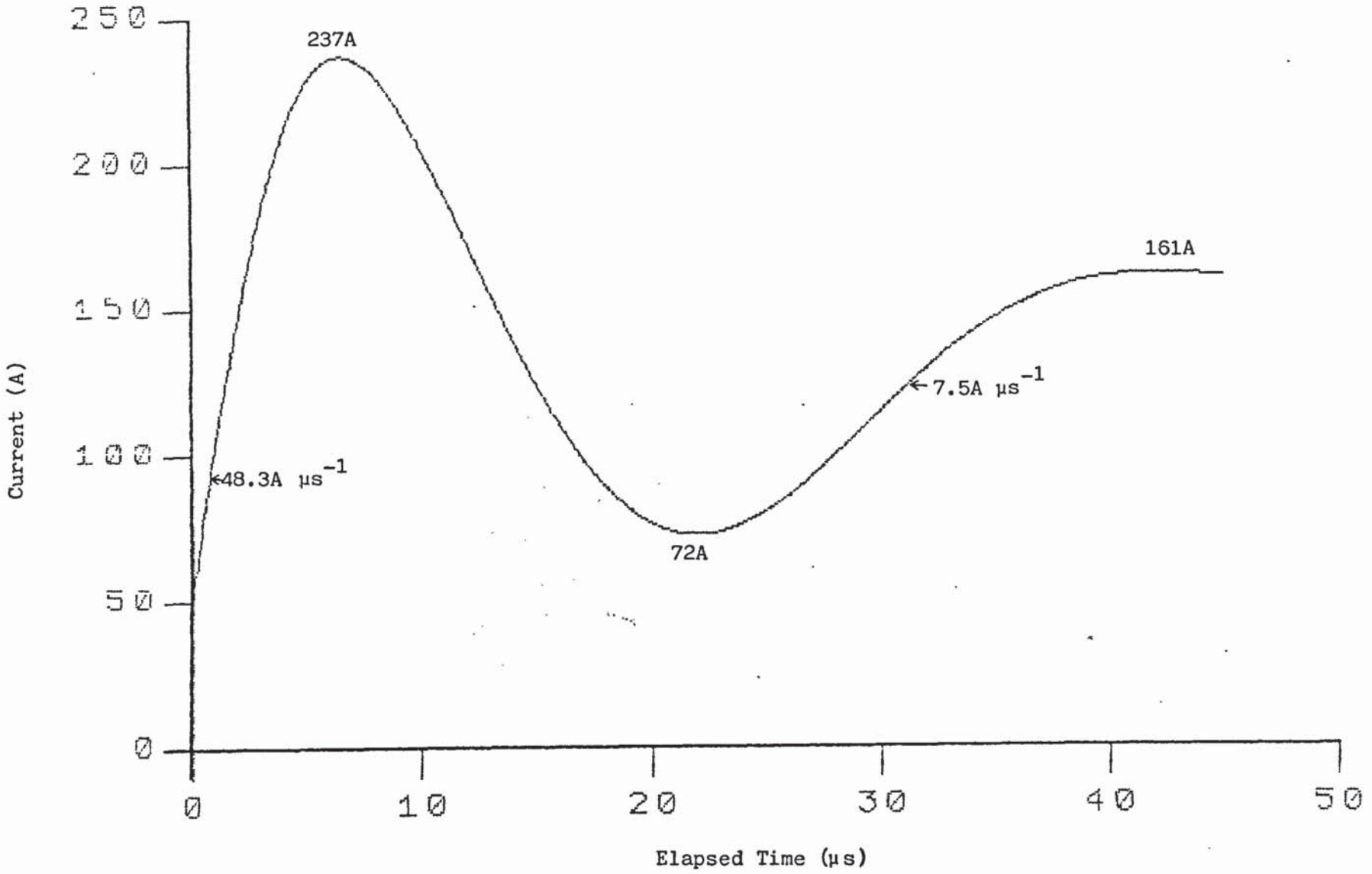

Fig. 6.33 - Thyristor inrush current during $\gamma = 15^{o}$ operation. (Proposed characteristics represented (see figure 6.21))

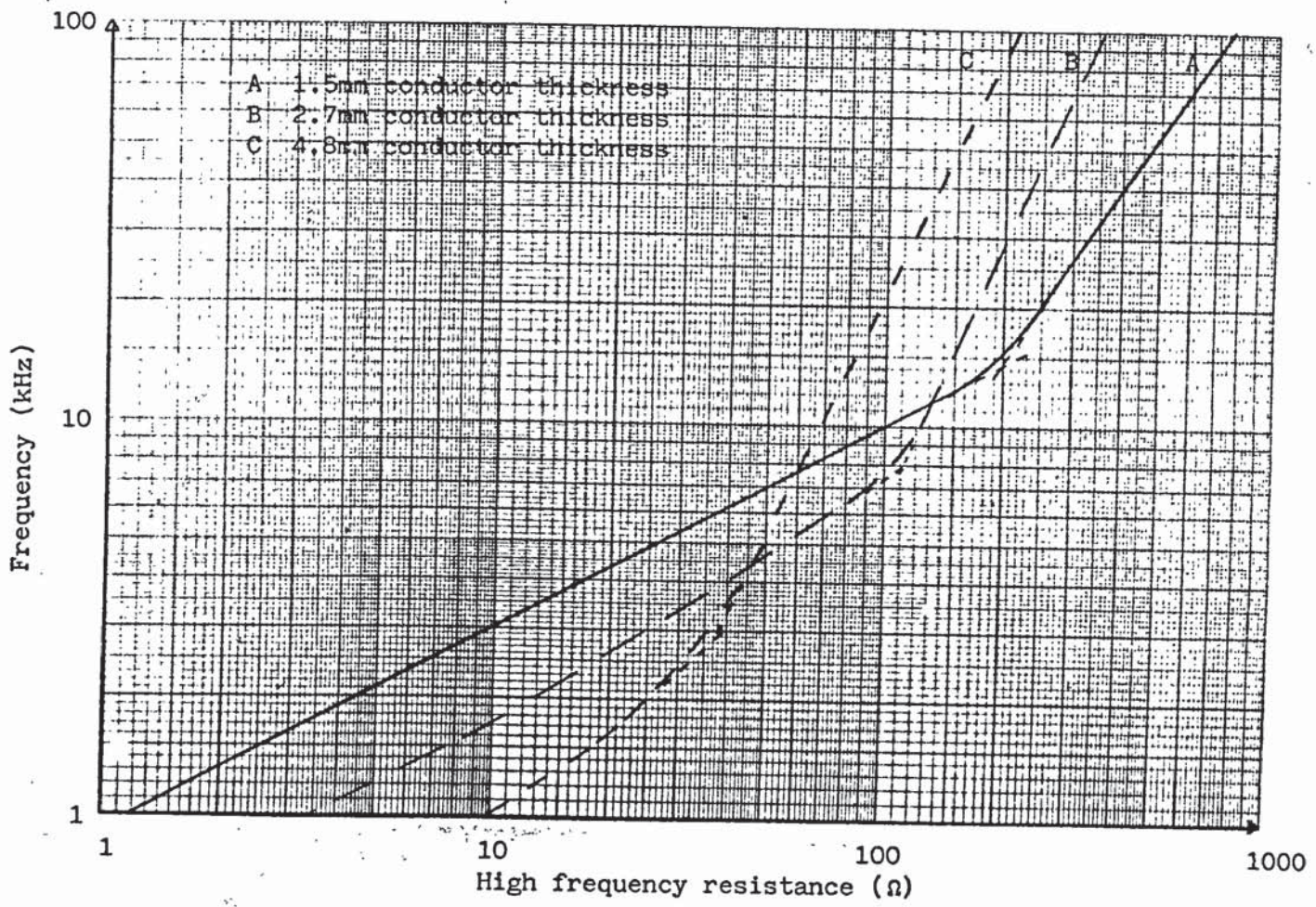

Fig.7.1 - Typical high frequency resistance characteristics of a transformer winding.

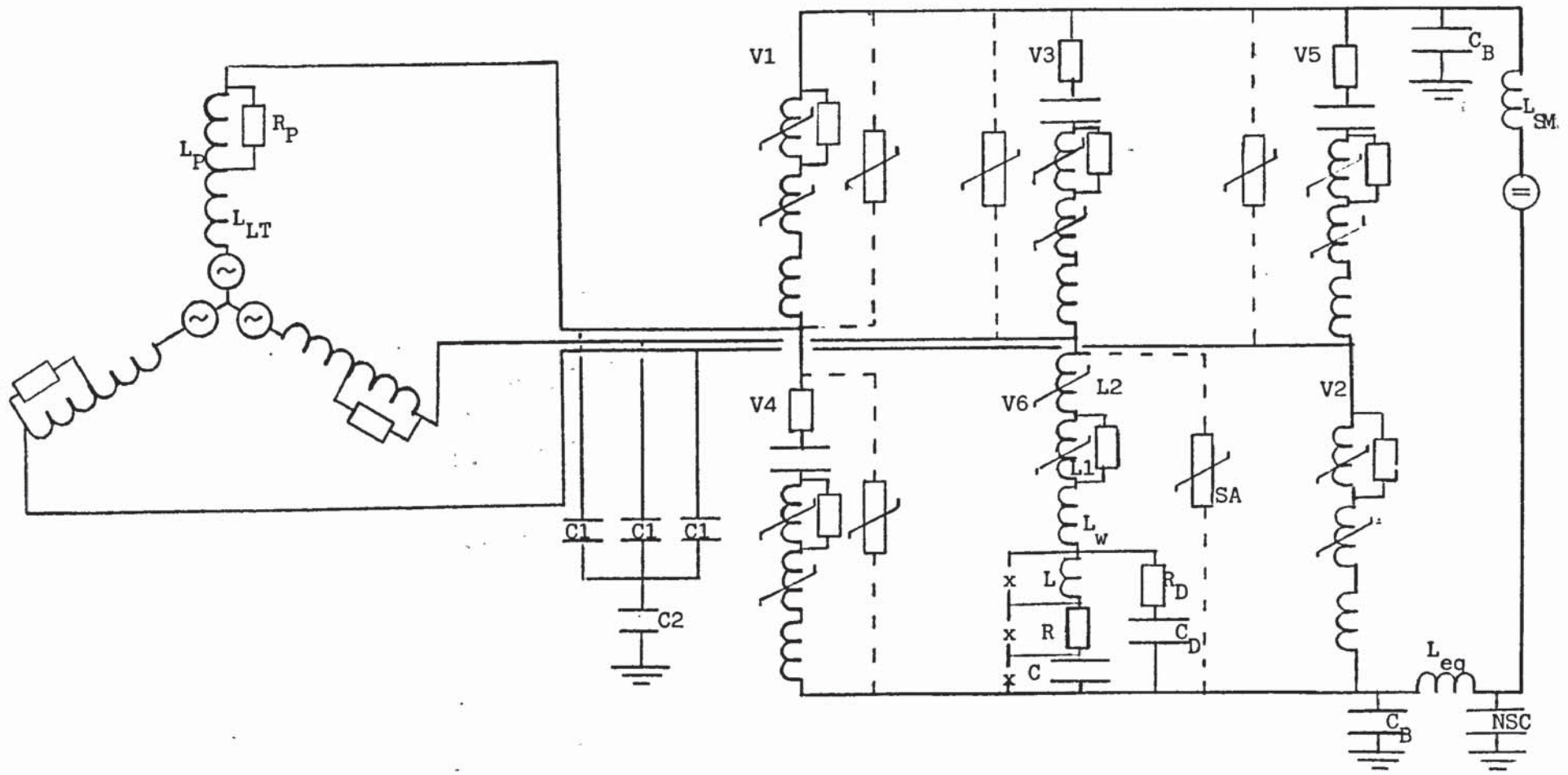

Fig.7.2 - Simplified equivalent circuit of a converter station at turn-off of a thyristor valve.
R, L, C Conventional thyristor representation during reverse recovery.
C1, C2 Transformer electrostatic model.
NSC Neutral surge capacitors. SA Surge arrester.
VN ...Valve firing sequence

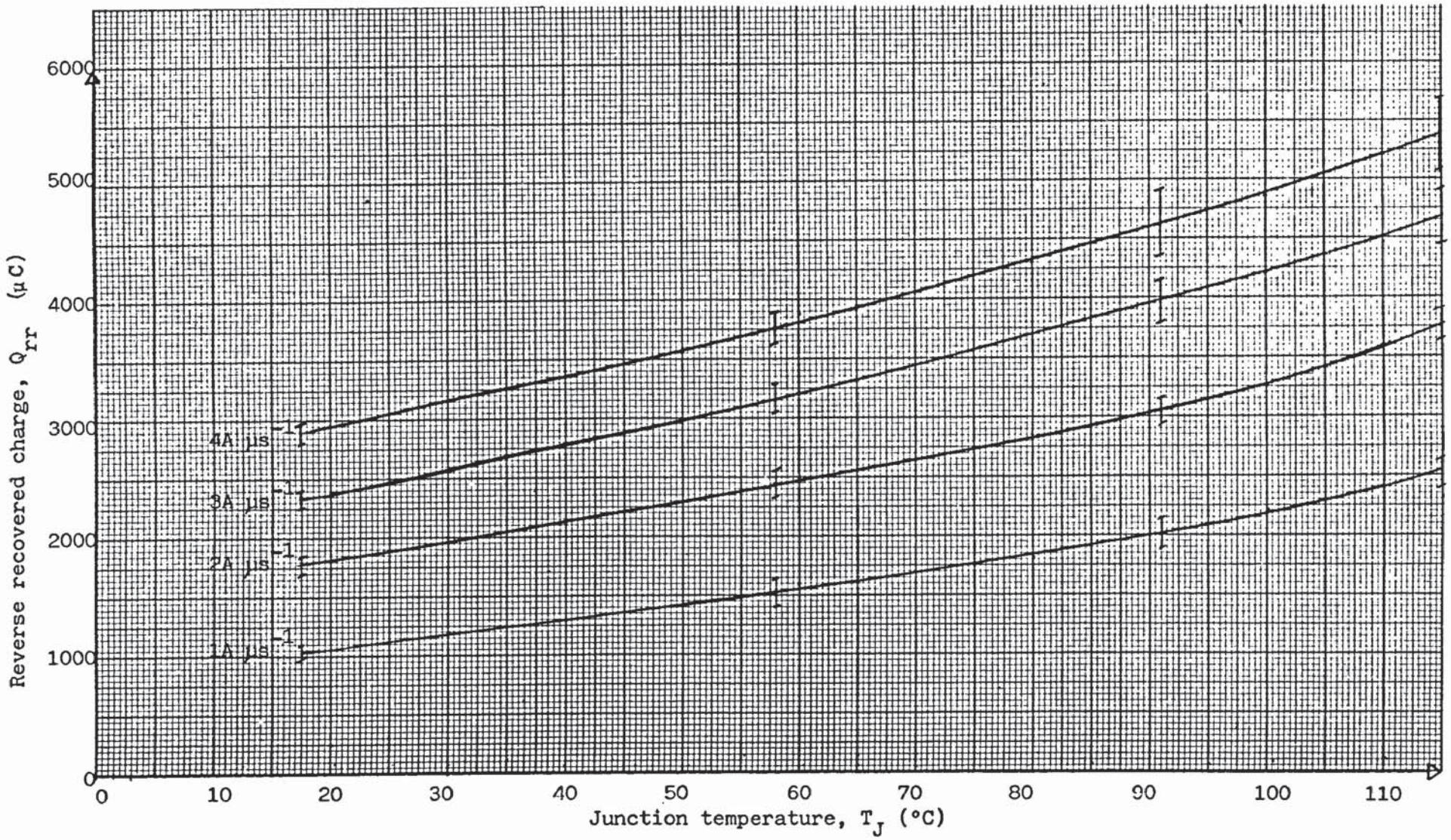

Fig.7.3 - Dependence of the reverse recovered charge upon junction temperature and thyristor di/dt at turn-off.

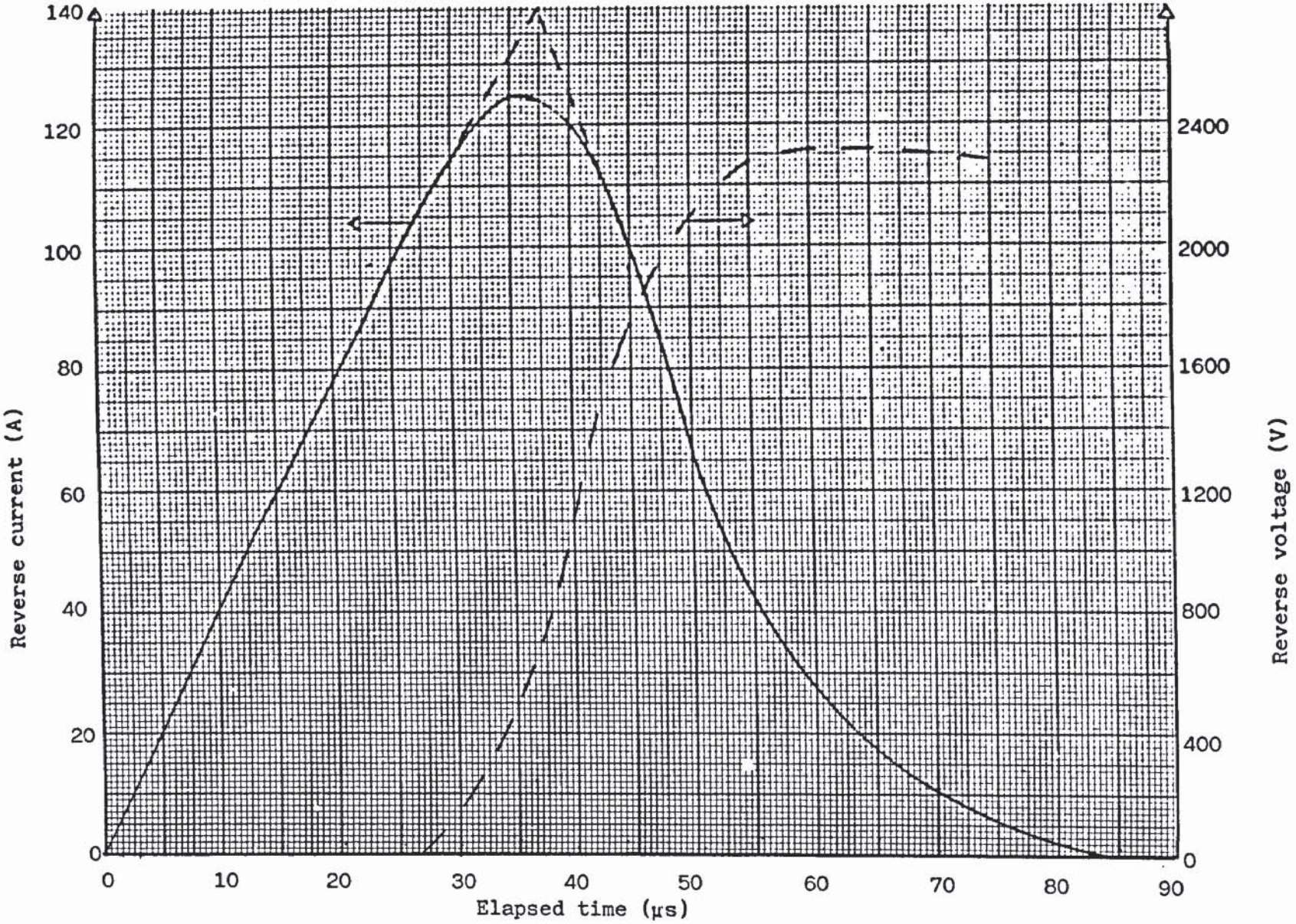

Fig.7.4 - Typical reverse current and reverse voltage waveforms, during recovery of a thyristor.
(Q_{rr} = 4810 μC, T_J = 125°C, di/dt = 4A μs^{-1})

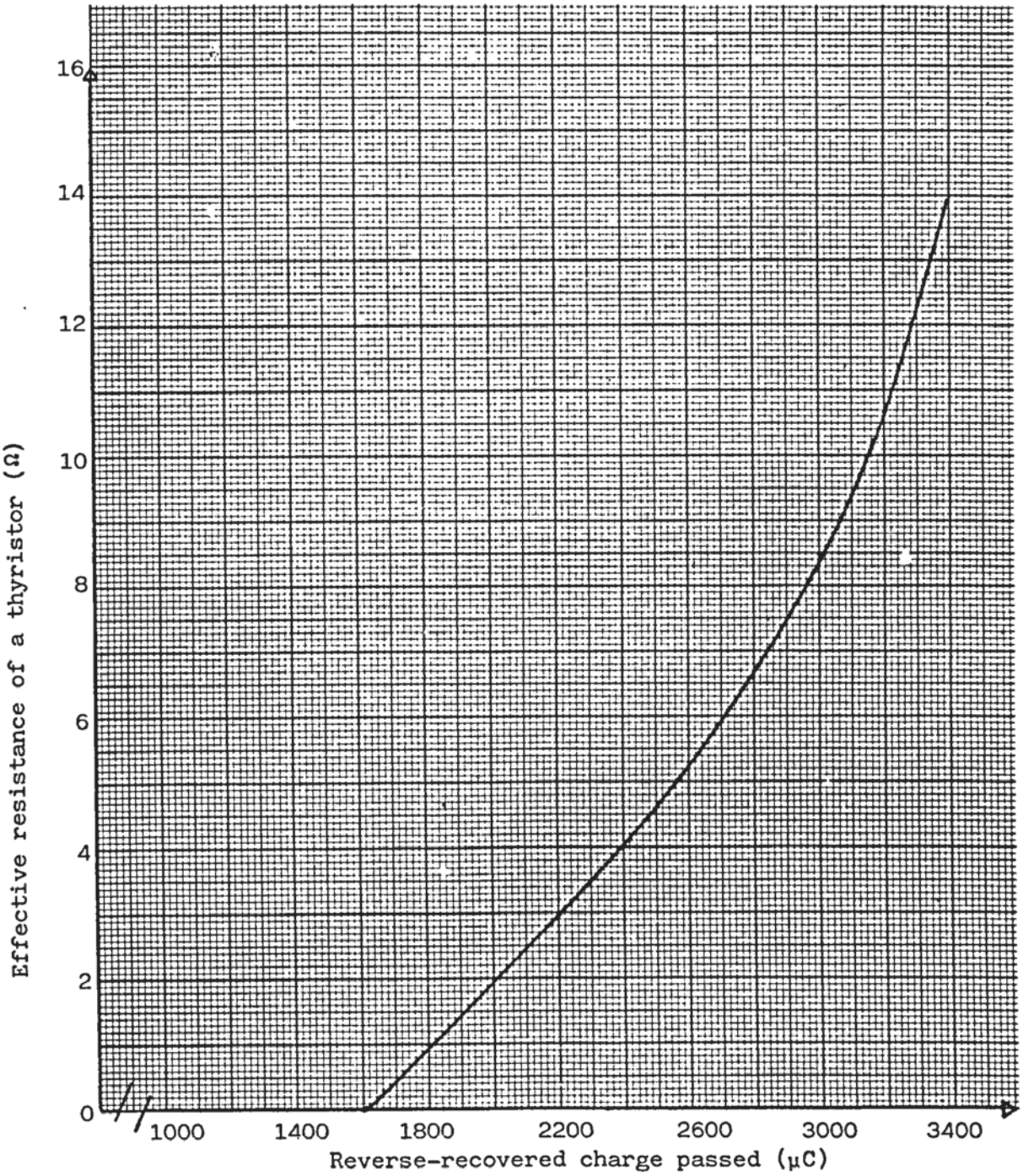

Fig.7.5 - Effective resistance of a thyristor, versus reverse recovered charge passed, during recovery.
(Q_{rr} = 4810 μC, T_J = 125°C, di/dt = 4A μs^{-1}).

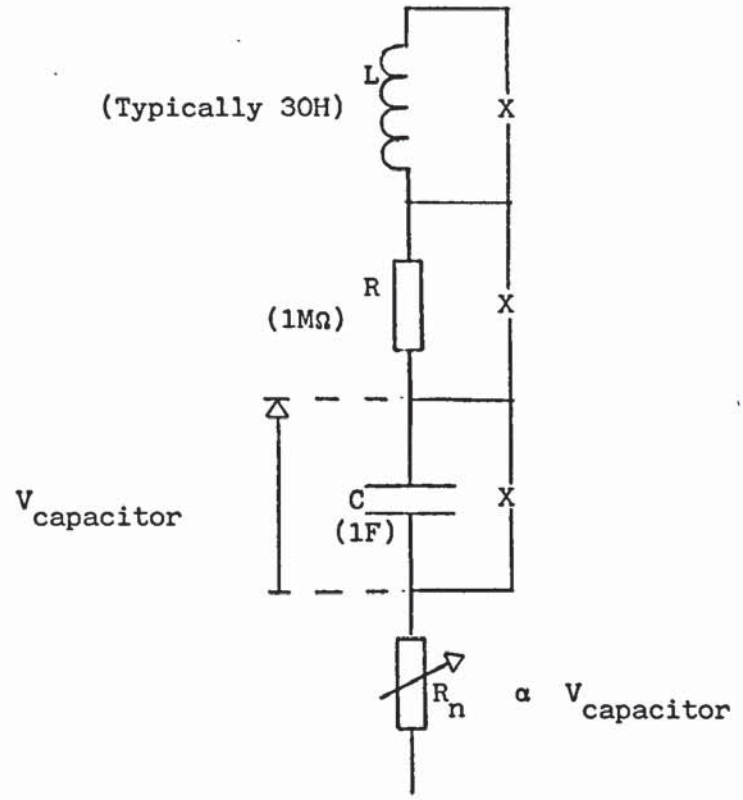

Fig.7.6 - Refined ('non-snappy') representation of thyristor during recovery.

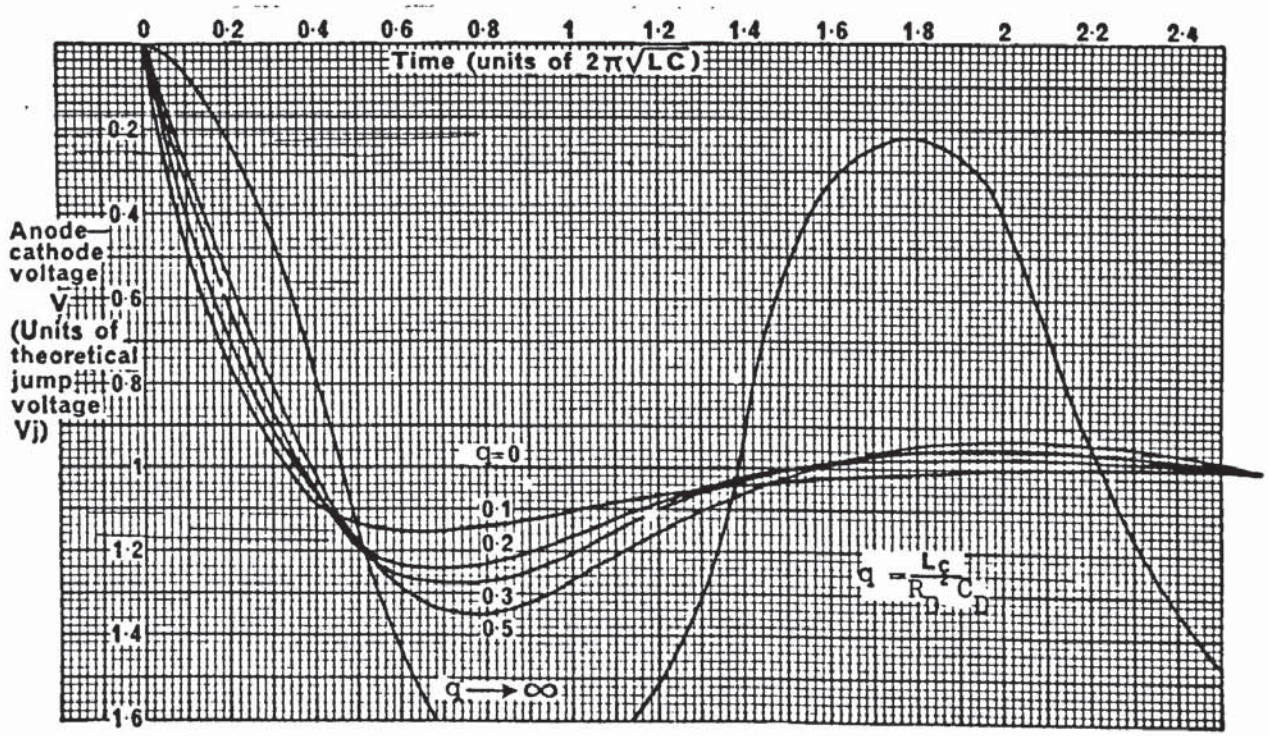

Fig.7.7 - Dependence of the theoretical overshoot factor upon both time and 'q'.

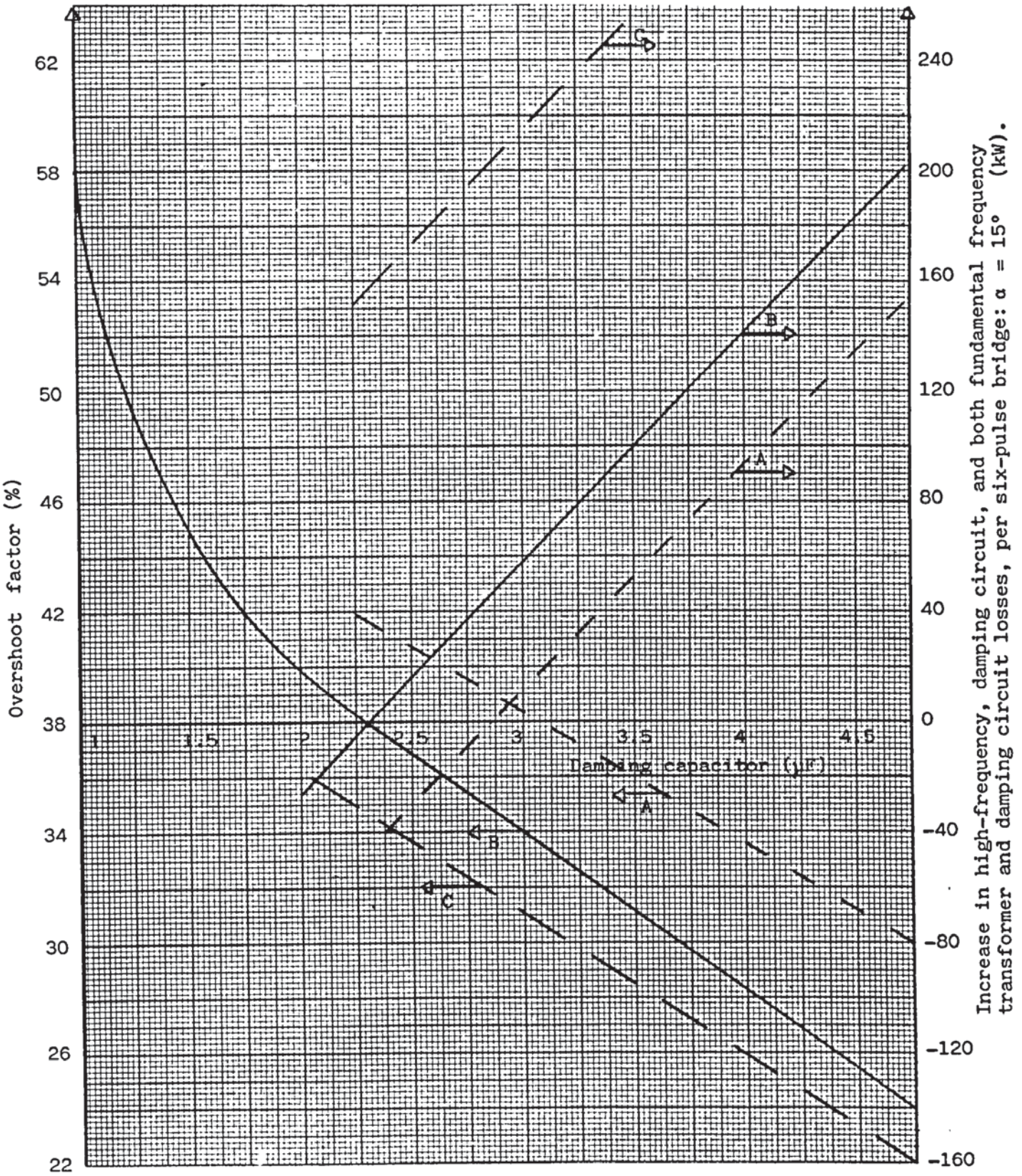

Fig.7.8 - Effect of the value of the damping capacitor upon:
a) Overshcot factor
b) Increase in high-frequency, damping circuit, and both fundamental frequency transformer and damping circuit losses, per six-pulse bridge ($\alpha = 15°$)

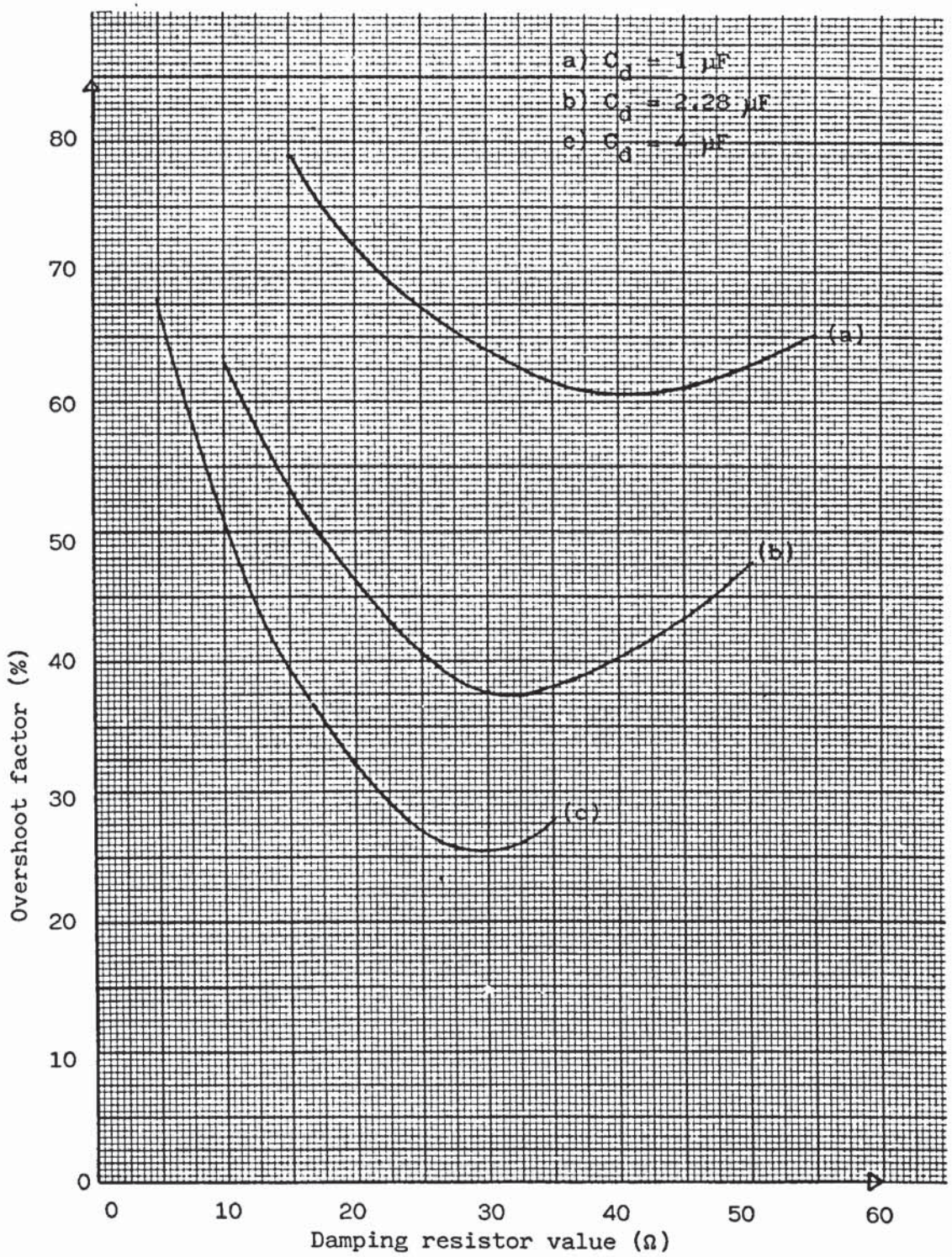

Fig.7.9 - Dependence of the overshoot factor upon the value of the damping capacitor and damping resistor.

(α = 90 + DOV operation; transformer winding design B).

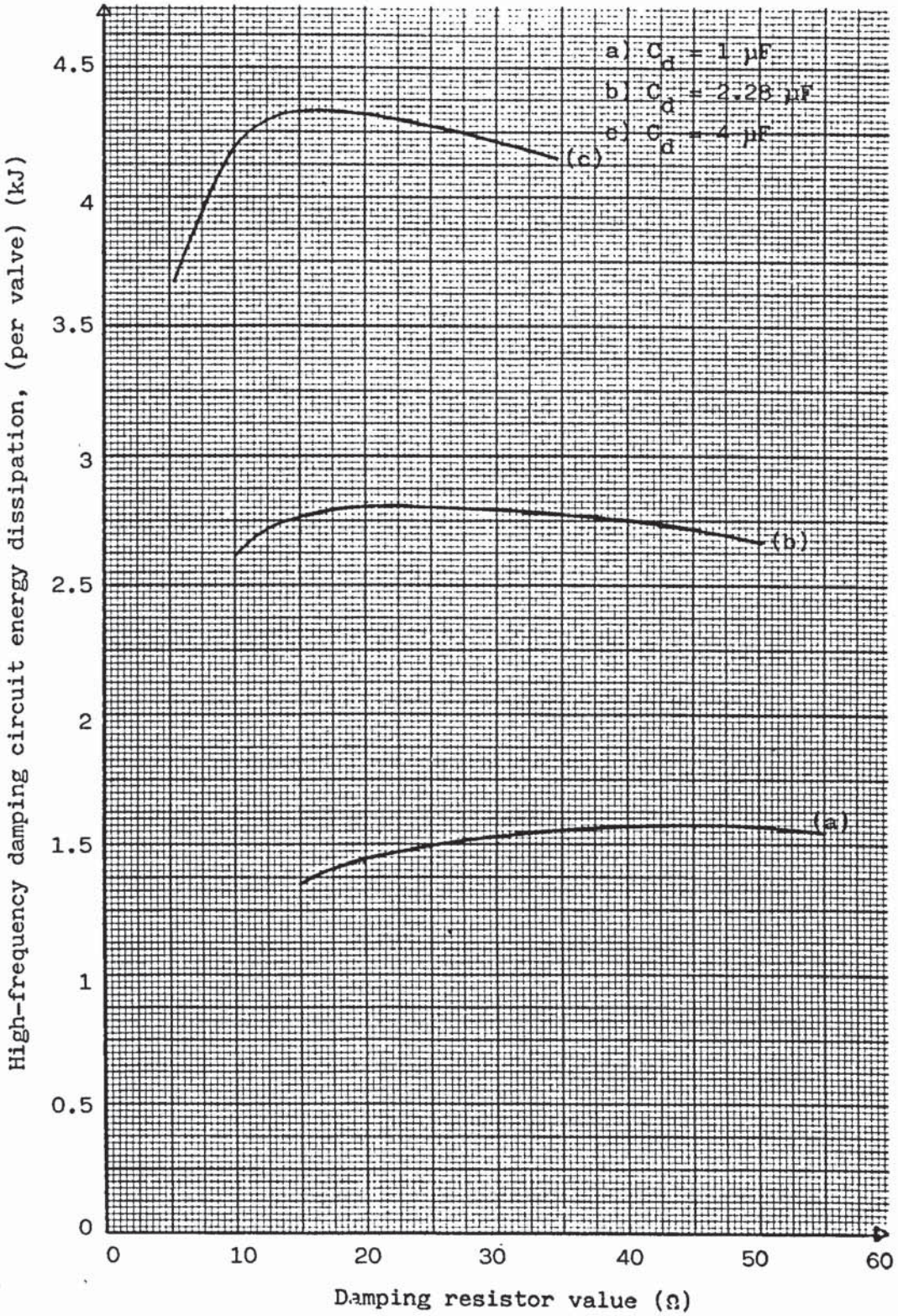

Fig.7.10 - Dependence of the high-frequency, damping circuit, energy dissipation, resulting from recovery transients throughout the six-pulse bridge, upon both the value of damping capacitor and resistor.

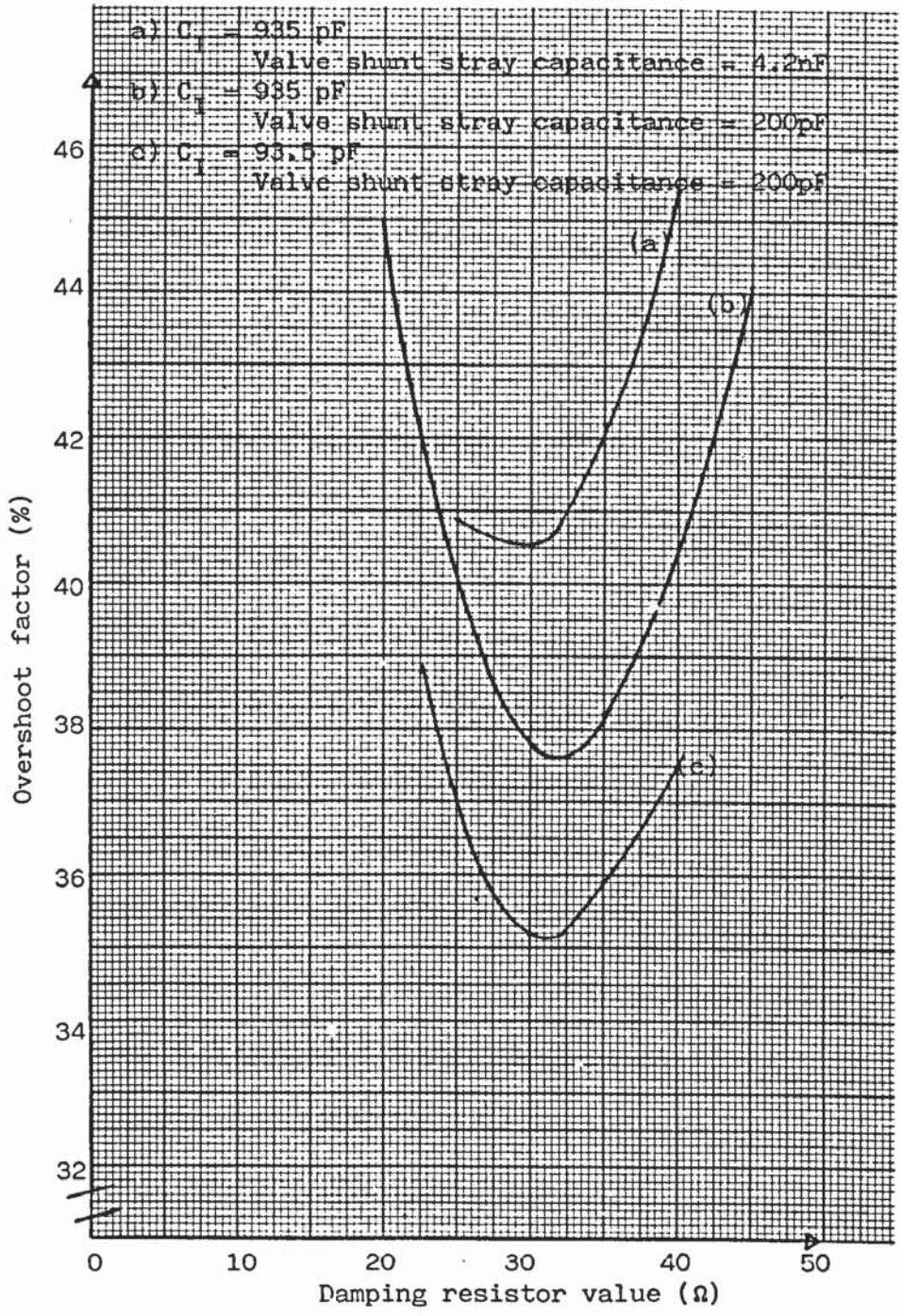

Fig.7.11 - Dependence of the overshoot factor upon ;
i) Damping resistor value
ii) Transformer series (inter-turn) capacitance
iii) Valve shunt stray capacitance.

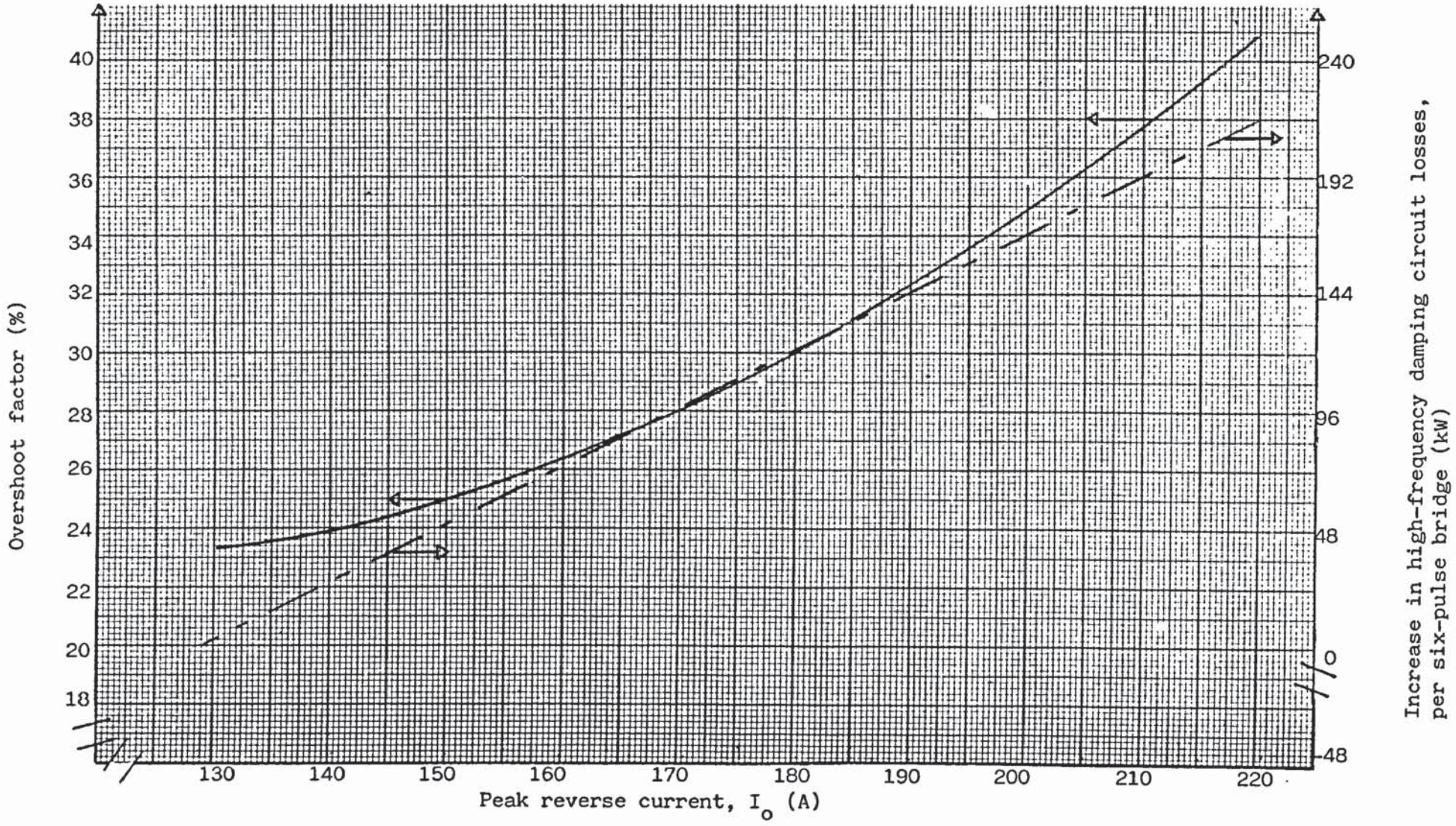

Fig.7.12 - Dependence of both the overshoot factor and the high-frequency damping circuit losses upon the value of the peak reverse current.
(Q_{rr} = 6400 µC; C_d = 4 µF; α = 90 + DOV).

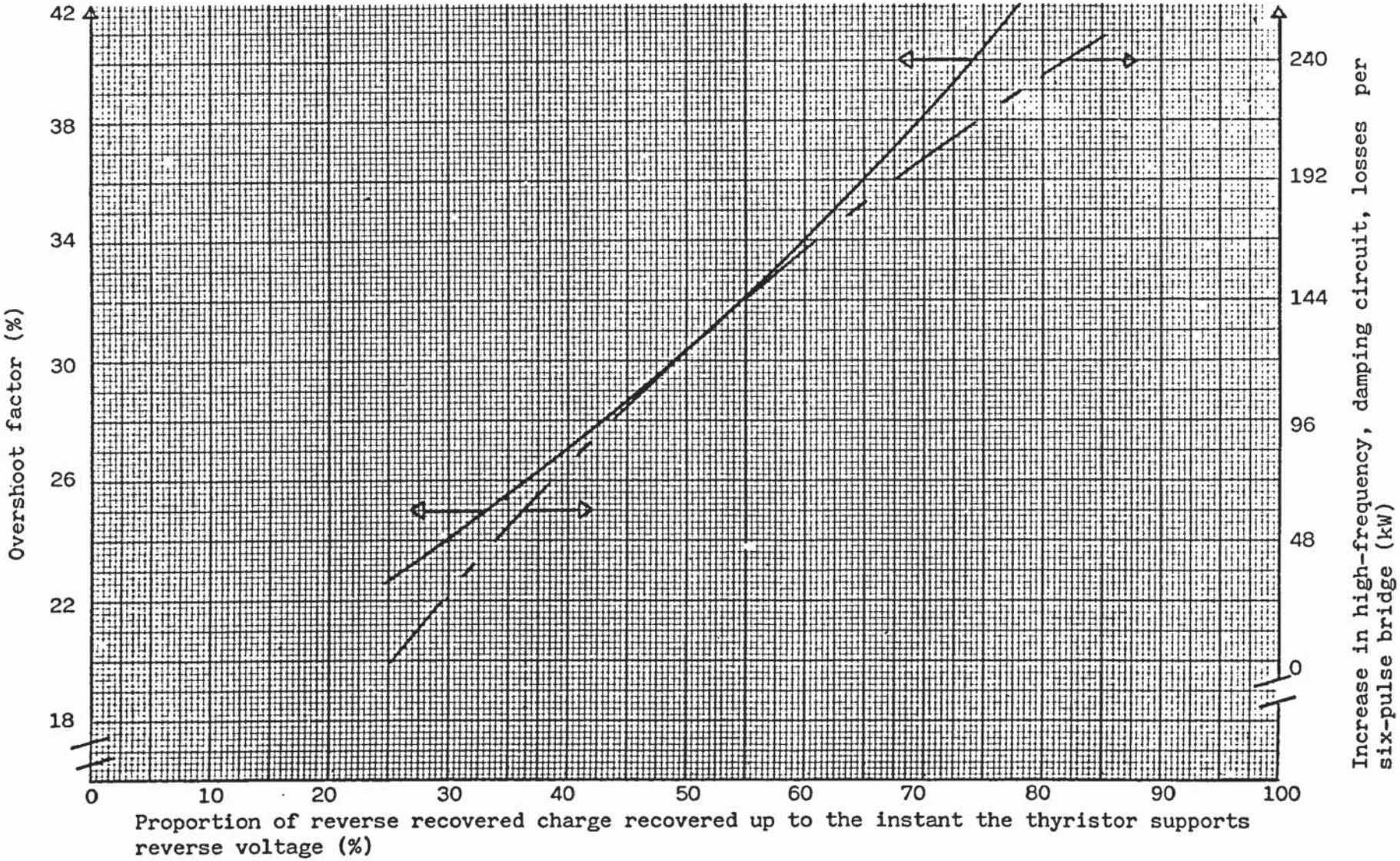

Fig.7.13 - Dependence of both the overshoot factor and the increase in high-frequency, damping circuit, losses upon the proportion of reverse recovered charge recovered up to the instant the thyristors support reverse voltage. (Q_{rr} = 6400 µC; C_d = 4 µF; α = 90 + DOV)

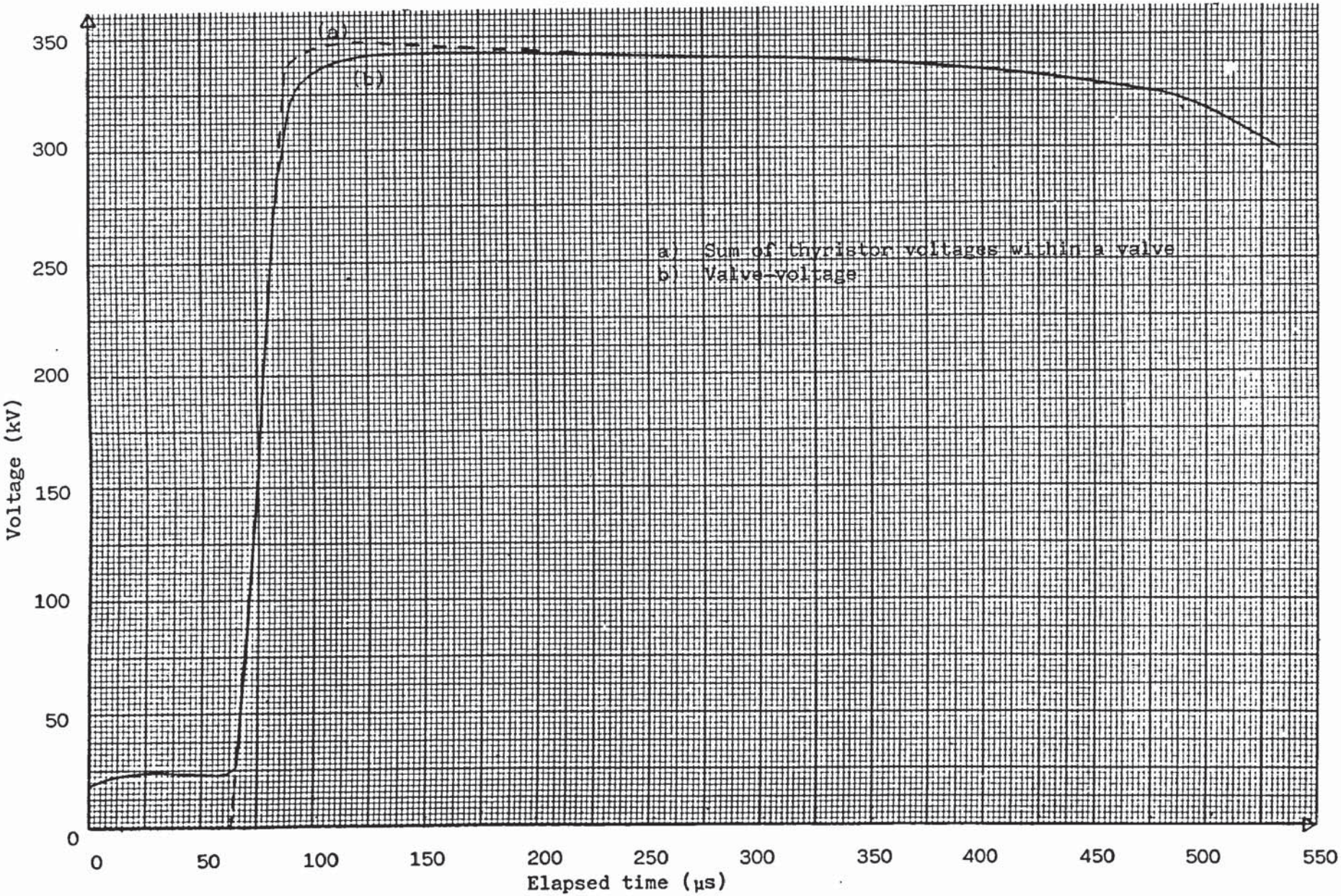

Fig.7.14 - Voltages associated with recovering valve. Minimum tolerance surge arrester, α = 90 + DOV, C_d = 2.85 µF, R_d = 30 Ω, Q_{rr} = 6400 µC split 37/63%.

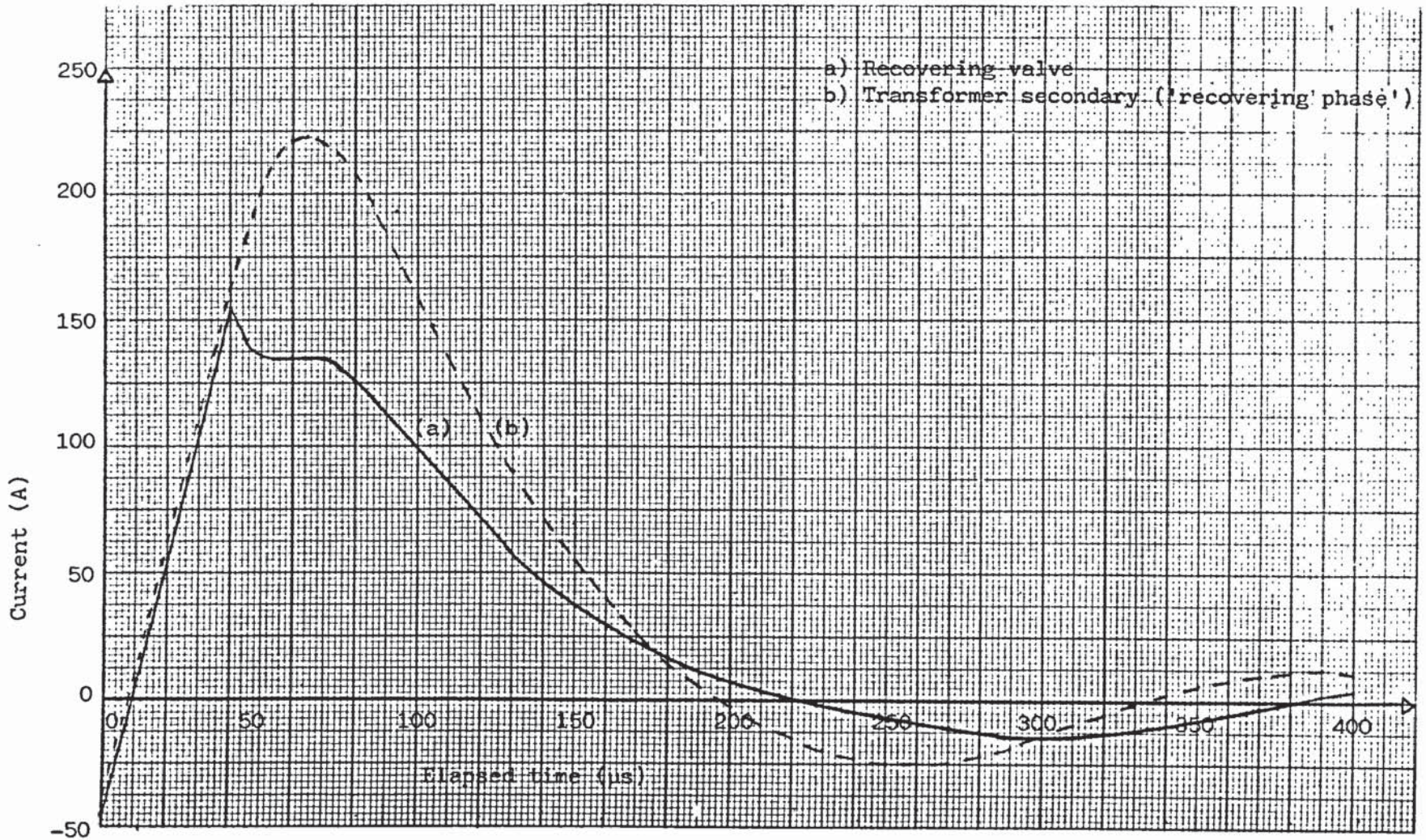

Fig.7.15 - Currents associated with a recovering valve and 'recovering phase' of a star secondary transformer winding. No surge arresters represented;
α = 90 + DOV, C_d = 2.28 μF, R_d = 30Ω, Q_{rr} = 6400 μC split 37/63.

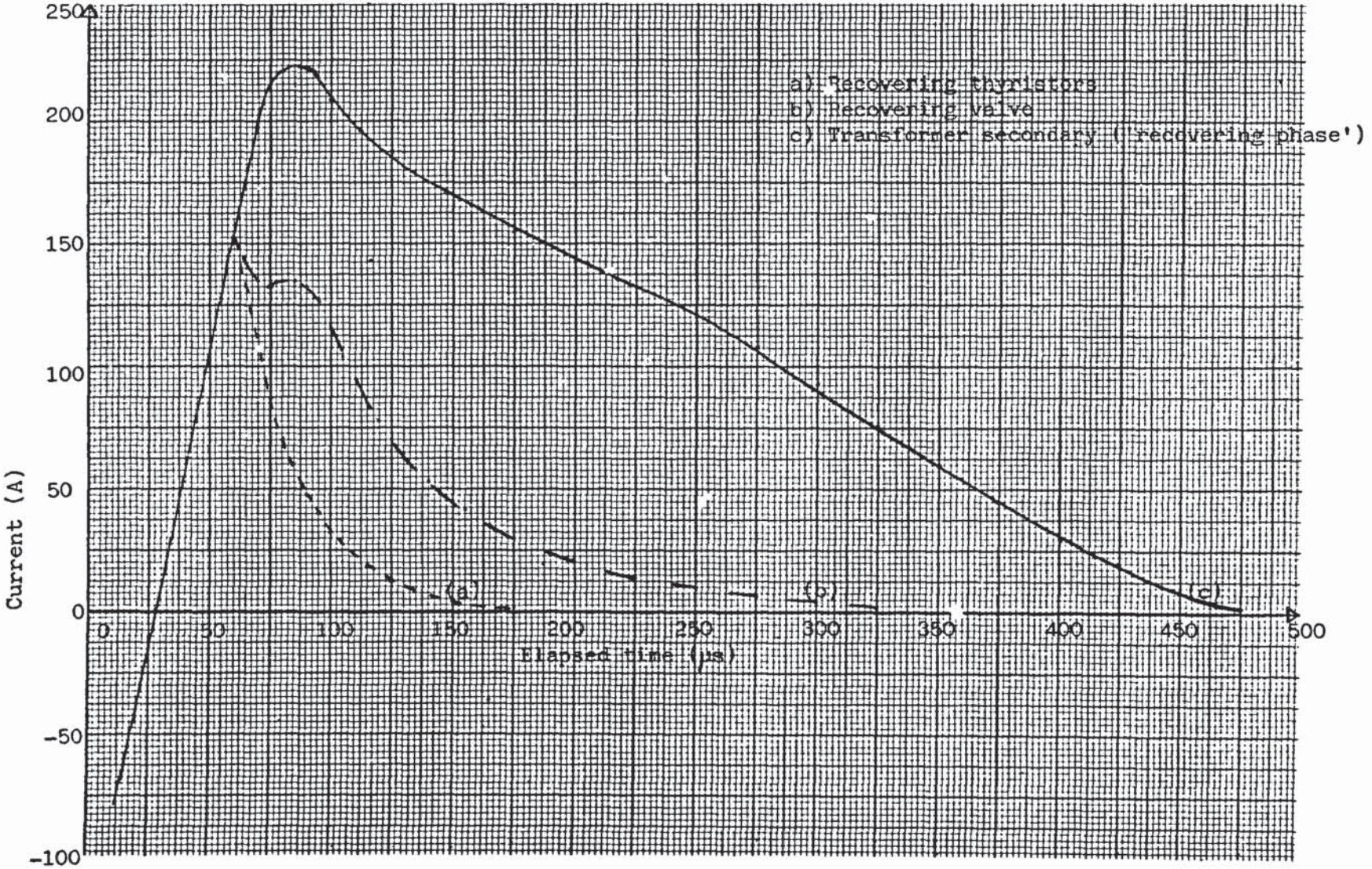

Fig.7.16 - Currents associated with a recovering valve and 'recovering phase' of a star secondary transformer winding. Minimum tolerance surge arrester, α = 90 + DOV, $C_d = 2.28\,\mu F$, $R_d = 30\Omega$, $Q_{rr} = 6400\mu C$ split 37/63%.

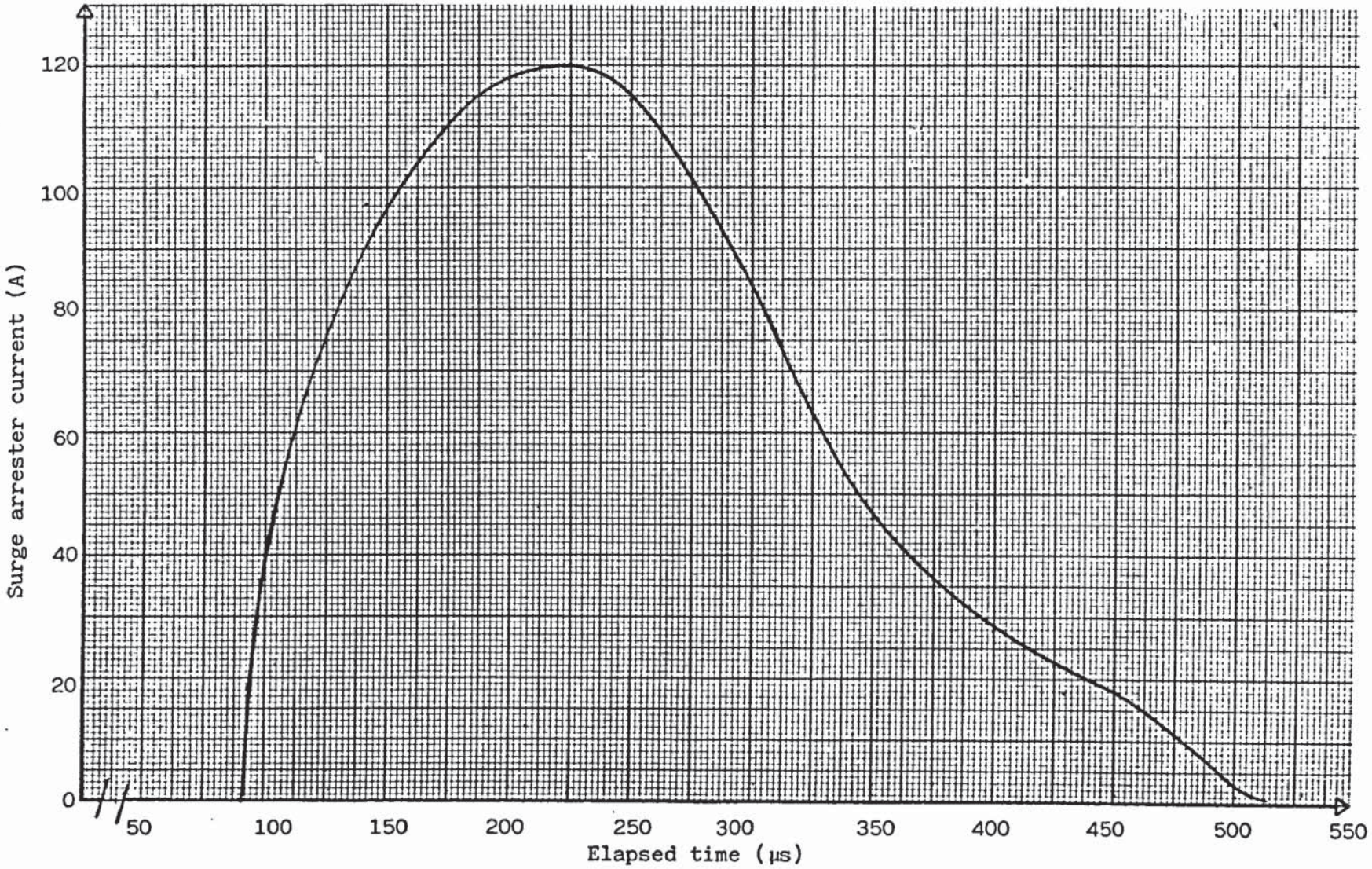

Fig.7.17 - Current through a minimum tolerance surge arrester, connected in parallel with a recovering valve. (α = 90 + DOV, C_d = 2.28 μF, R_d = 30Ω, Q_{rr} = 6400 μC split 37/63%).

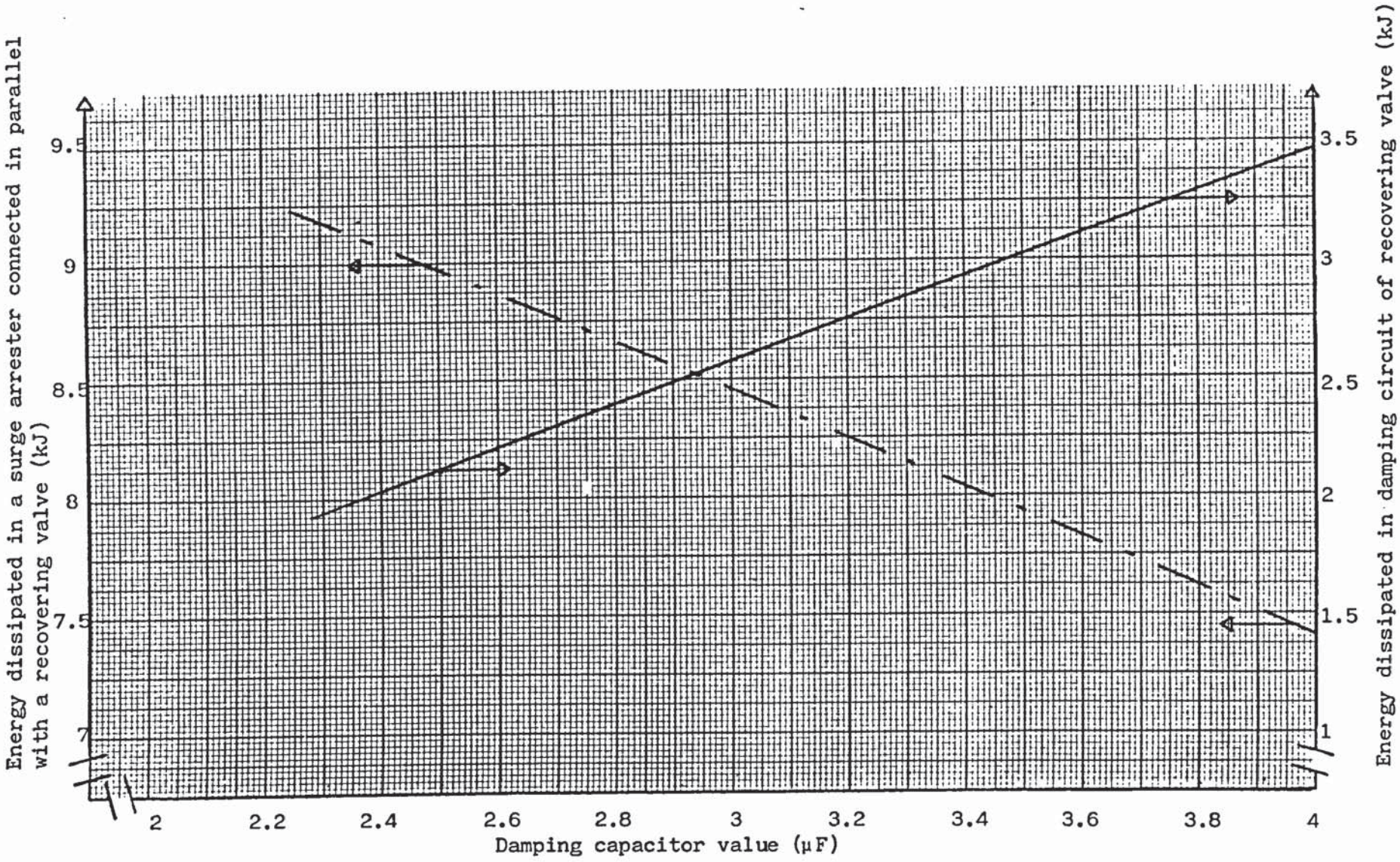

Fig.7.18 - Dependence of the energy dissipation in the valve surge arrester and in the damping resistors of the recovering valve upon the value of the damping capacitor.
(Minimum tolerance arrester, α= 90 + DOV, R_d = 30 Ω, Q_{rr} = 6400 μC split 37/63%).

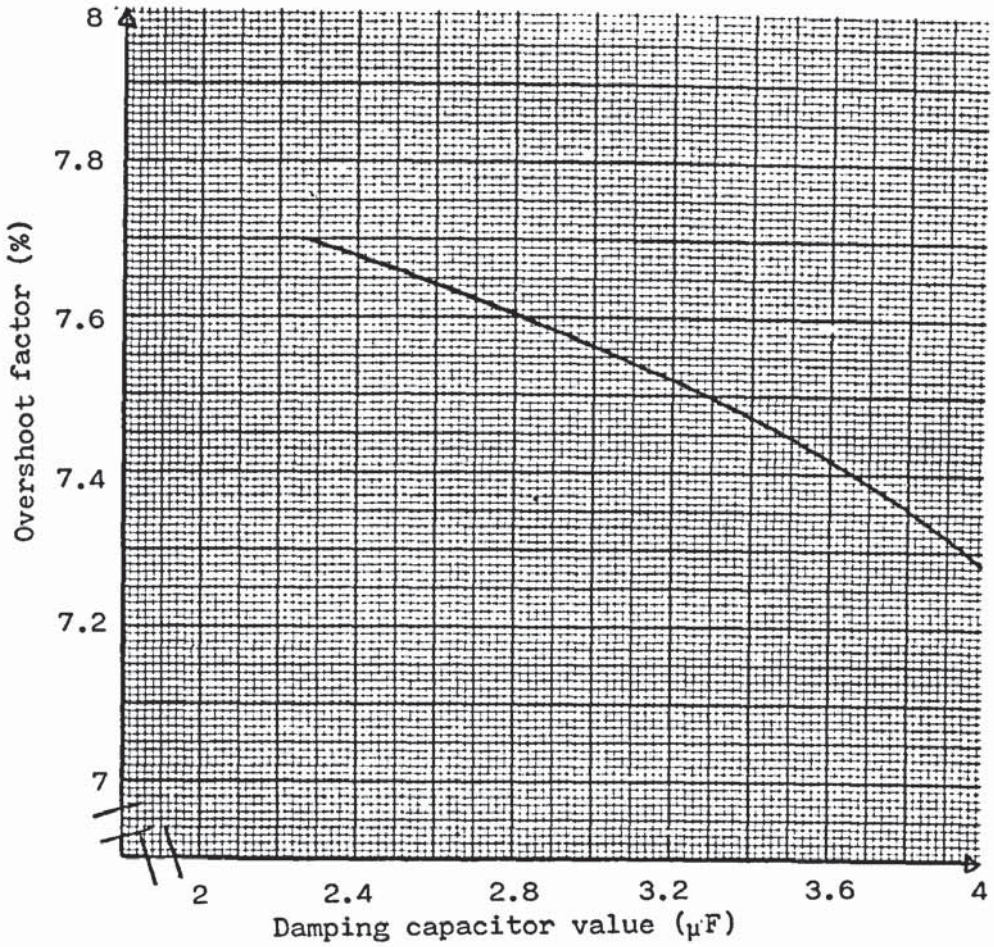

Fig.7.19 - Dependence of overshoot factor upon the value of the damping capacitor. (Minimum tolerance arrester, α= 90+DOV operation).

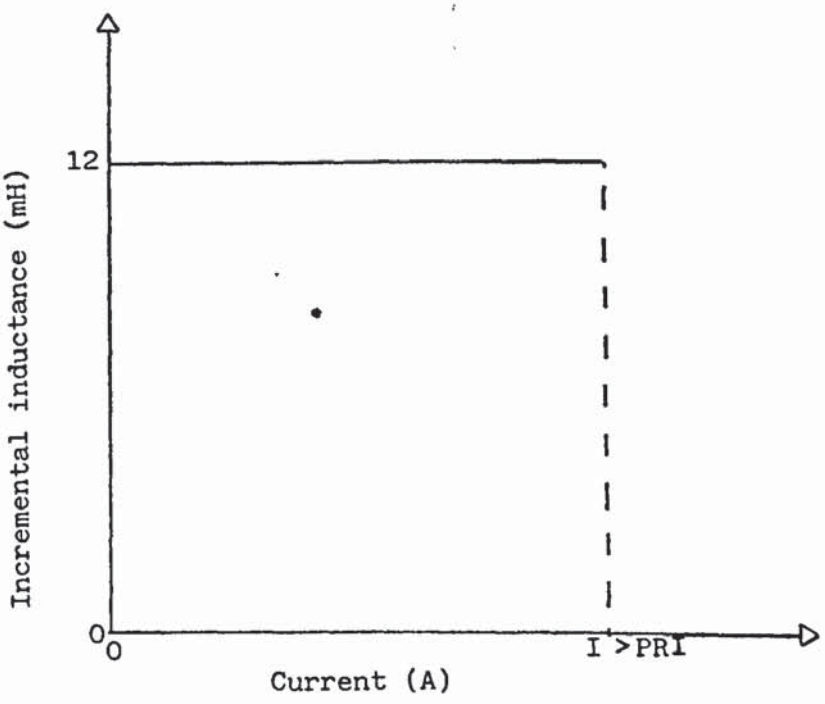

Fig.7.20 - Saturating reactor characteristic represented, in place of proposed 'two-part' reactor, to assess the dependence of the overshoot factor and damping circuit losses upon the reactor characteristic.

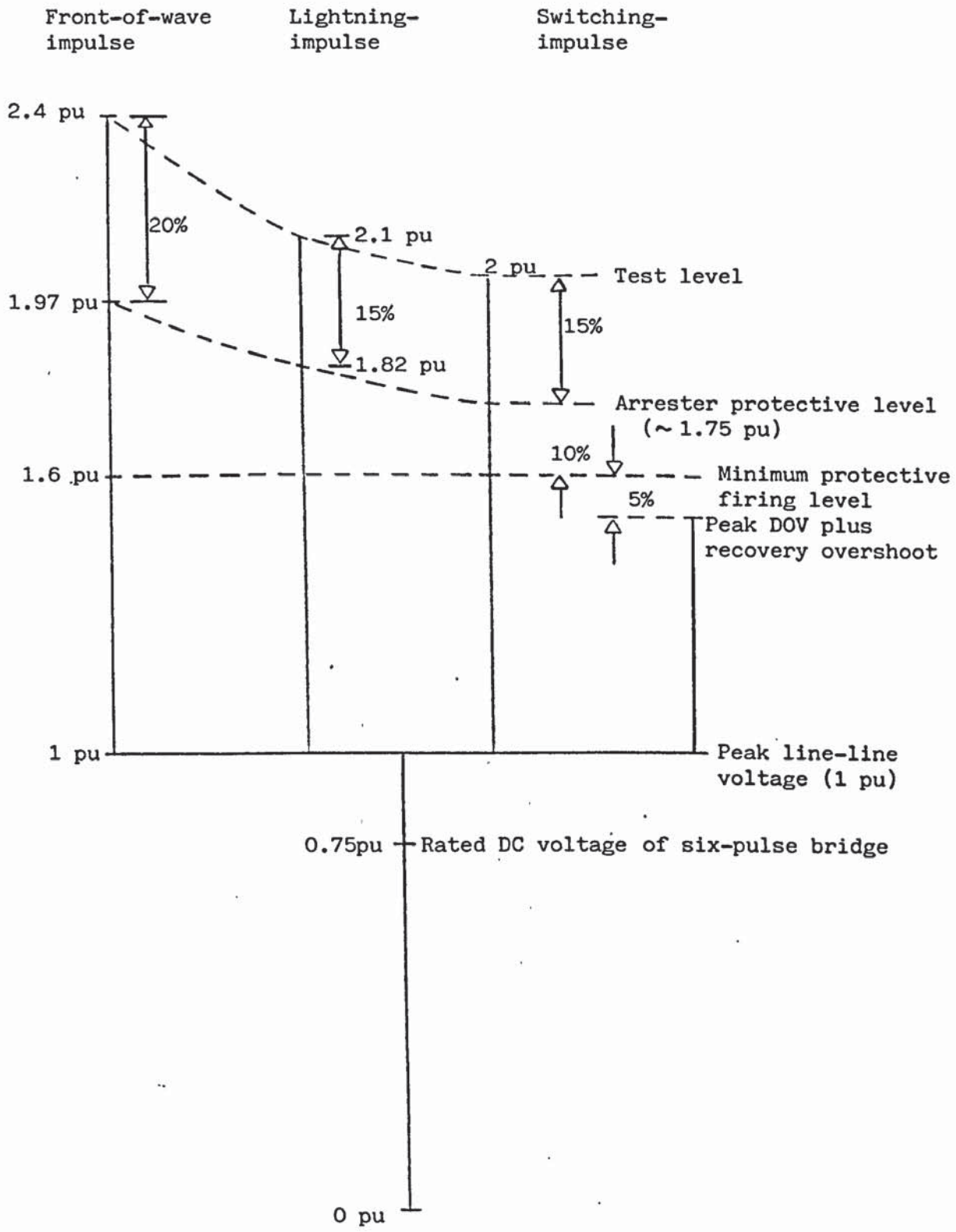

Fig.8.1 - Typical insulation co-ordination for a thyristor valve.

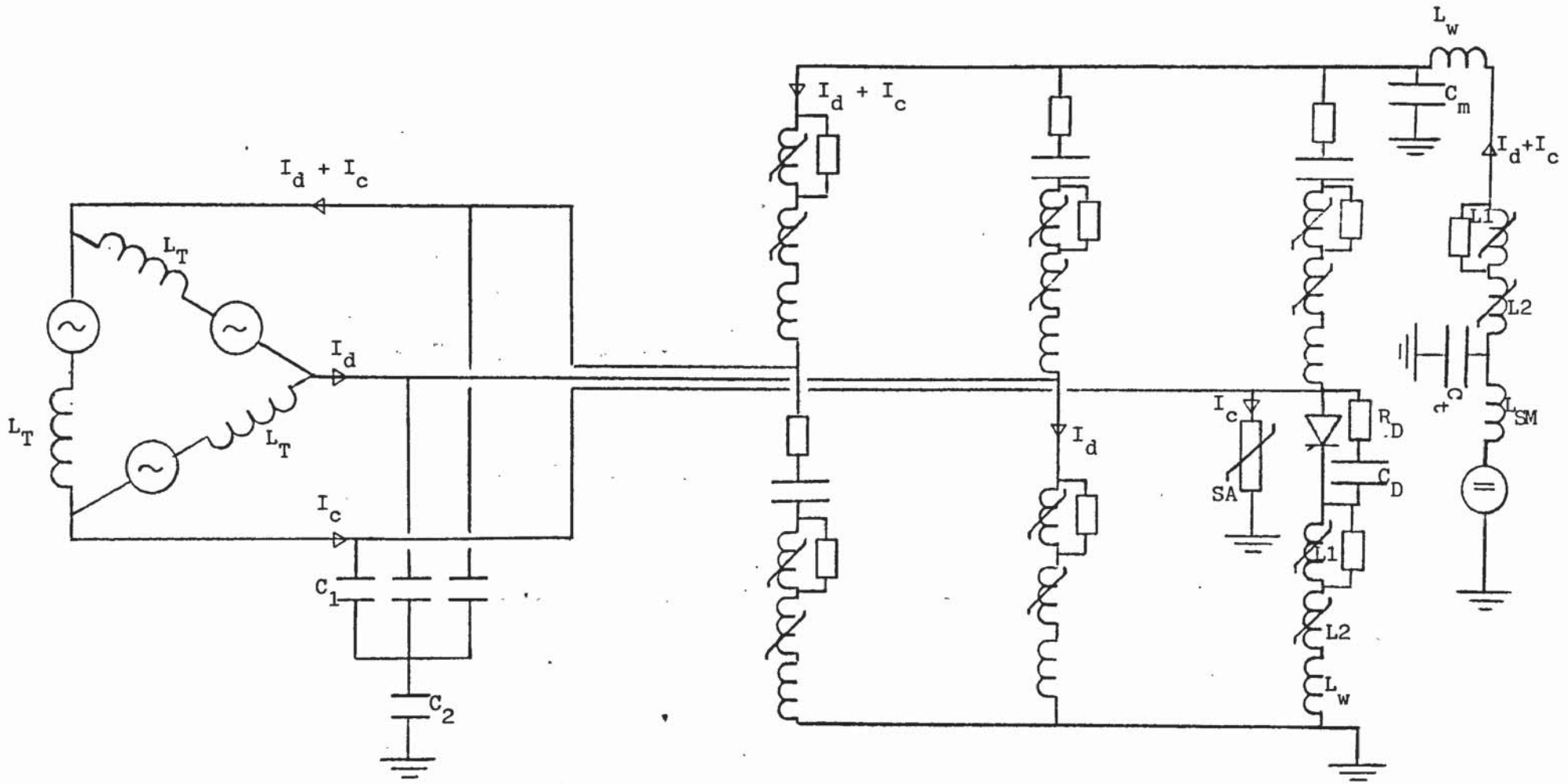

Fig.8.2 - Simplified equivalent circuit of a six-pulse bridge used for coherent turn-on studies. (Co-ordinating current (I_c) pre-established in a surge arrester (SA)). C_1, C_2 Transformer electrostatic model.

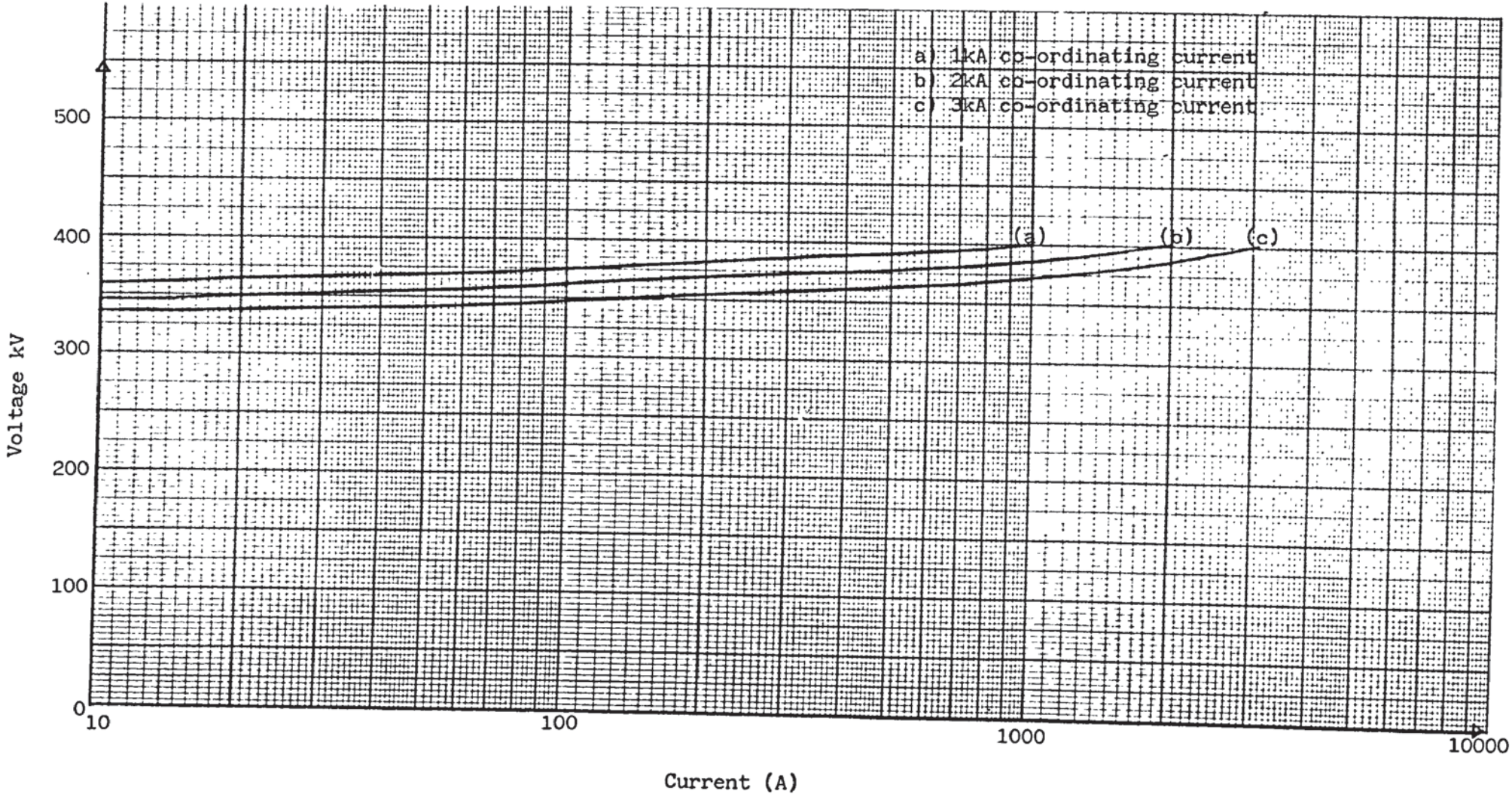

Fig.8.3 - Typical voltage-current characteristics for a surge arrester, (250/2500 μs impulse)

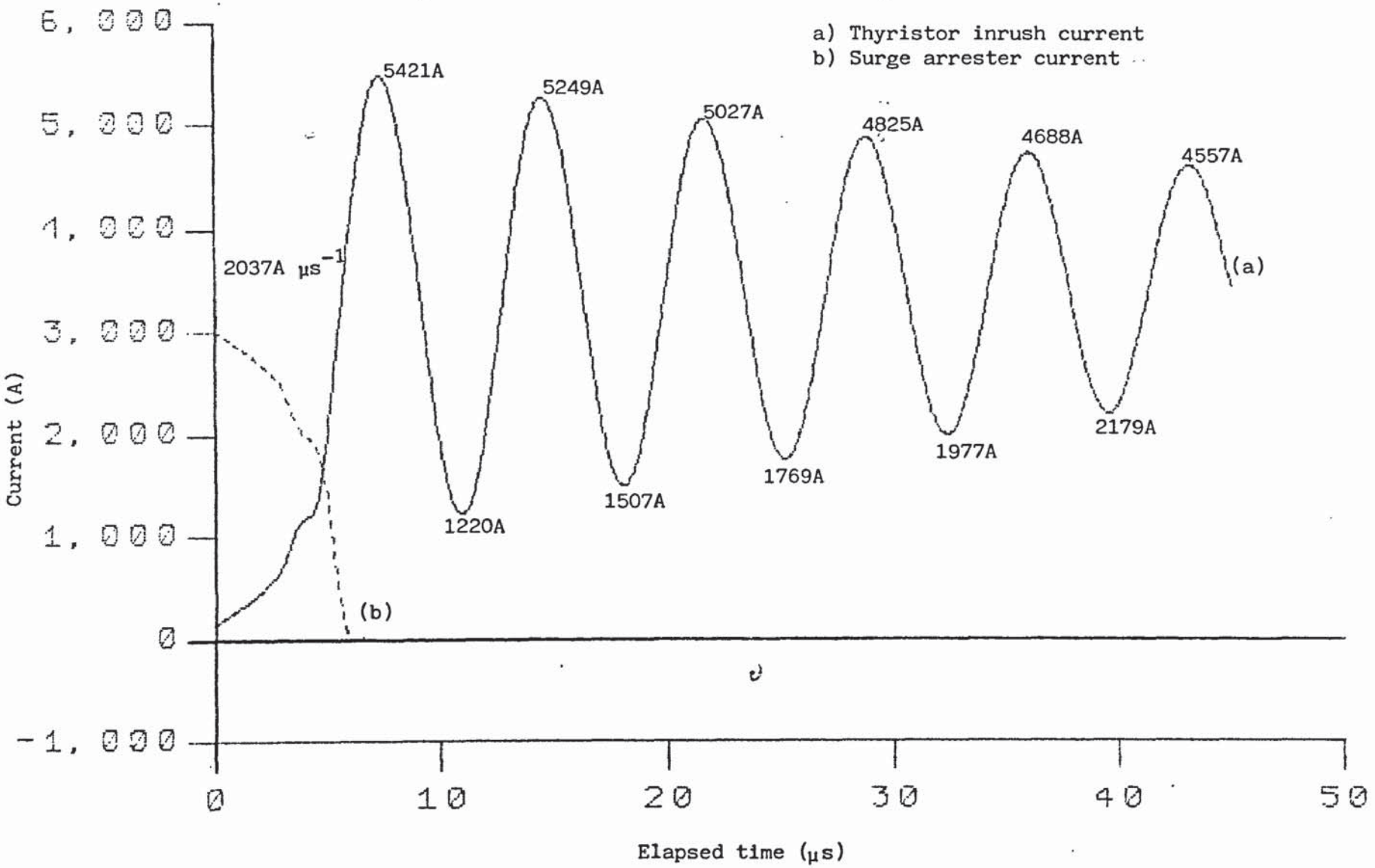

Fig.8.4 - Thyristor inrush current prediction for turn-on from a valve-voltage equal to the sum of the maximum BOD levels. 3kA co-ordinating current pre-established in the arrester.

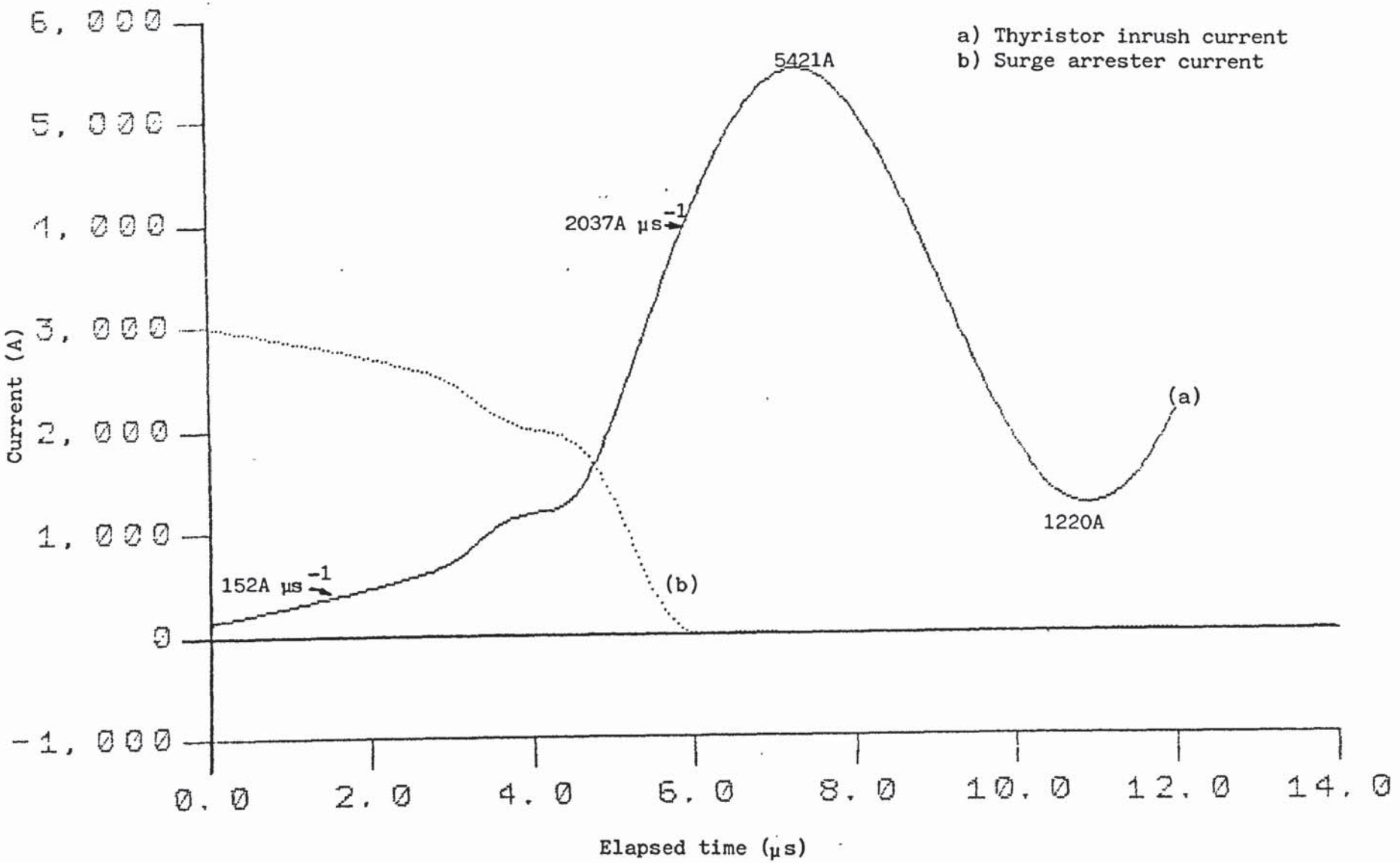

Fig.8.5 - Thyristor inrush current prediction for turn-on from a valve-voltage equal to the sum of the maximum BOD levels. 3kA co-ordinating current pre-established in the arrester.

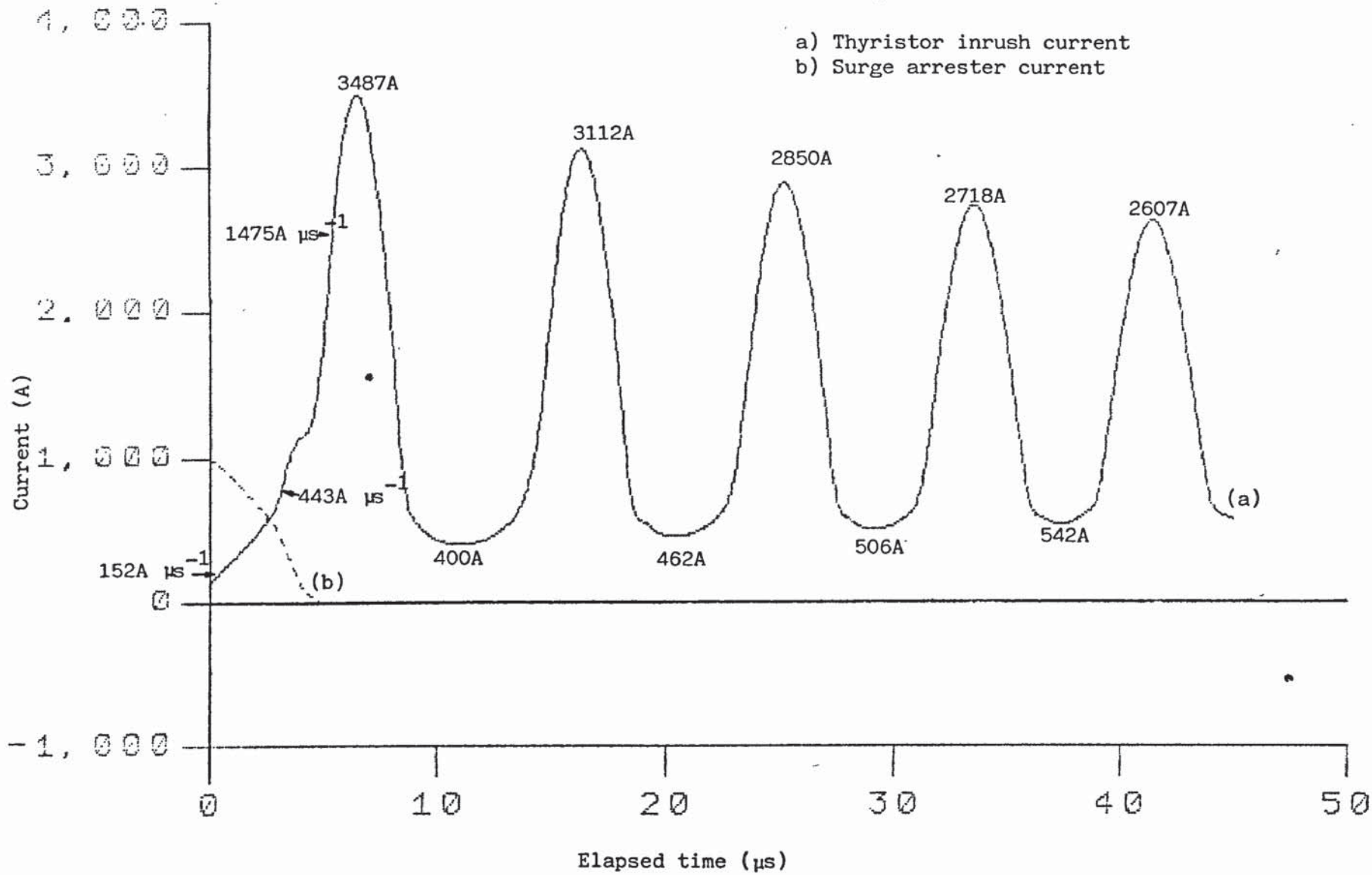

Fig.8.6 - Thyristor inrush current prediction for turn-on from a valve-voltage equal to the sum of the maximum BOD levels. 1kA co-ordinating current pre-established in the arrester.

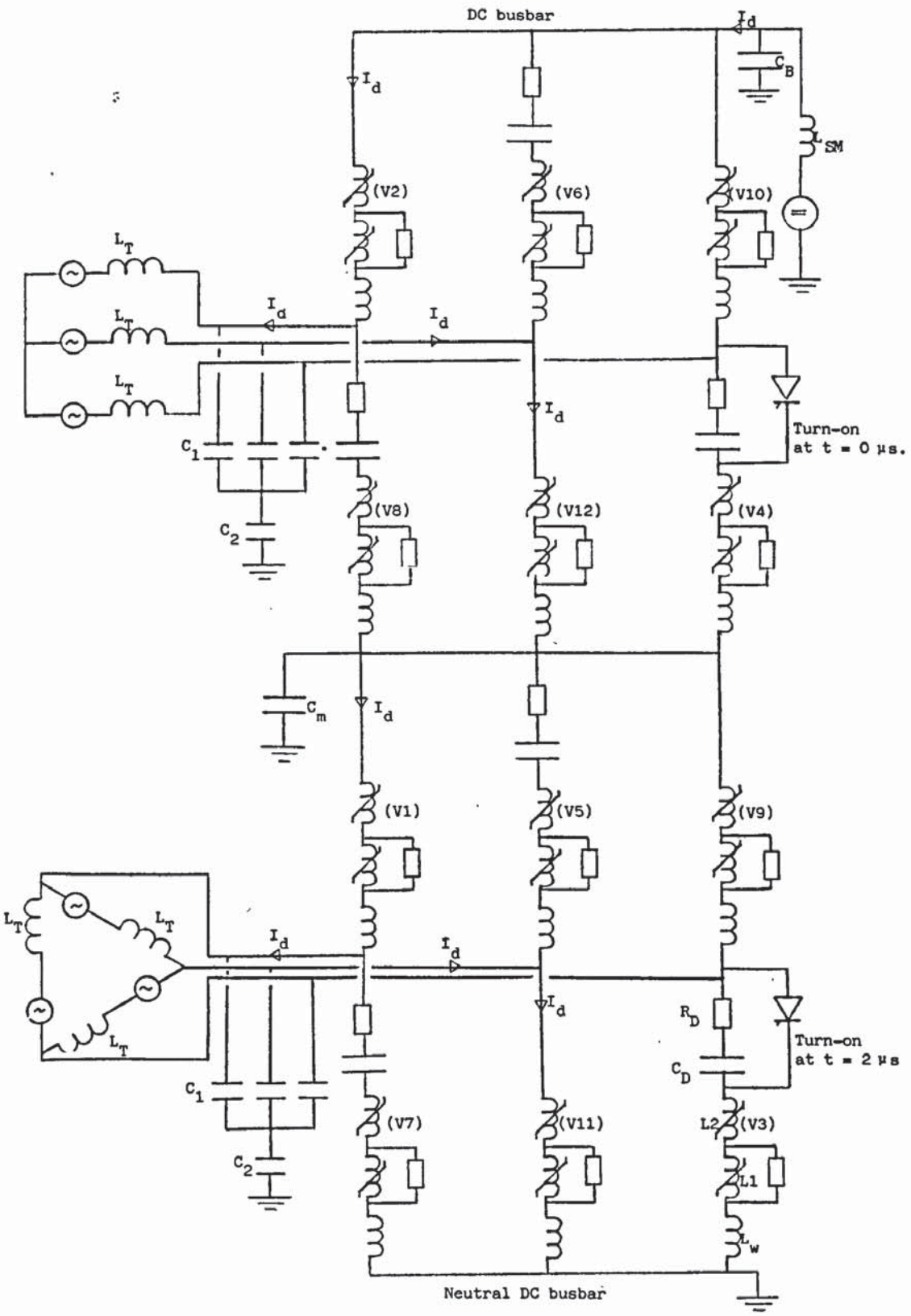

Fig.8.7 - Equivalent circuit of a 12-pulse bridge used for commutation failure studies.
C_1, C_2 Electrostatic model of stray capacitances.
(VN) 'Normal' valve firing sequence.

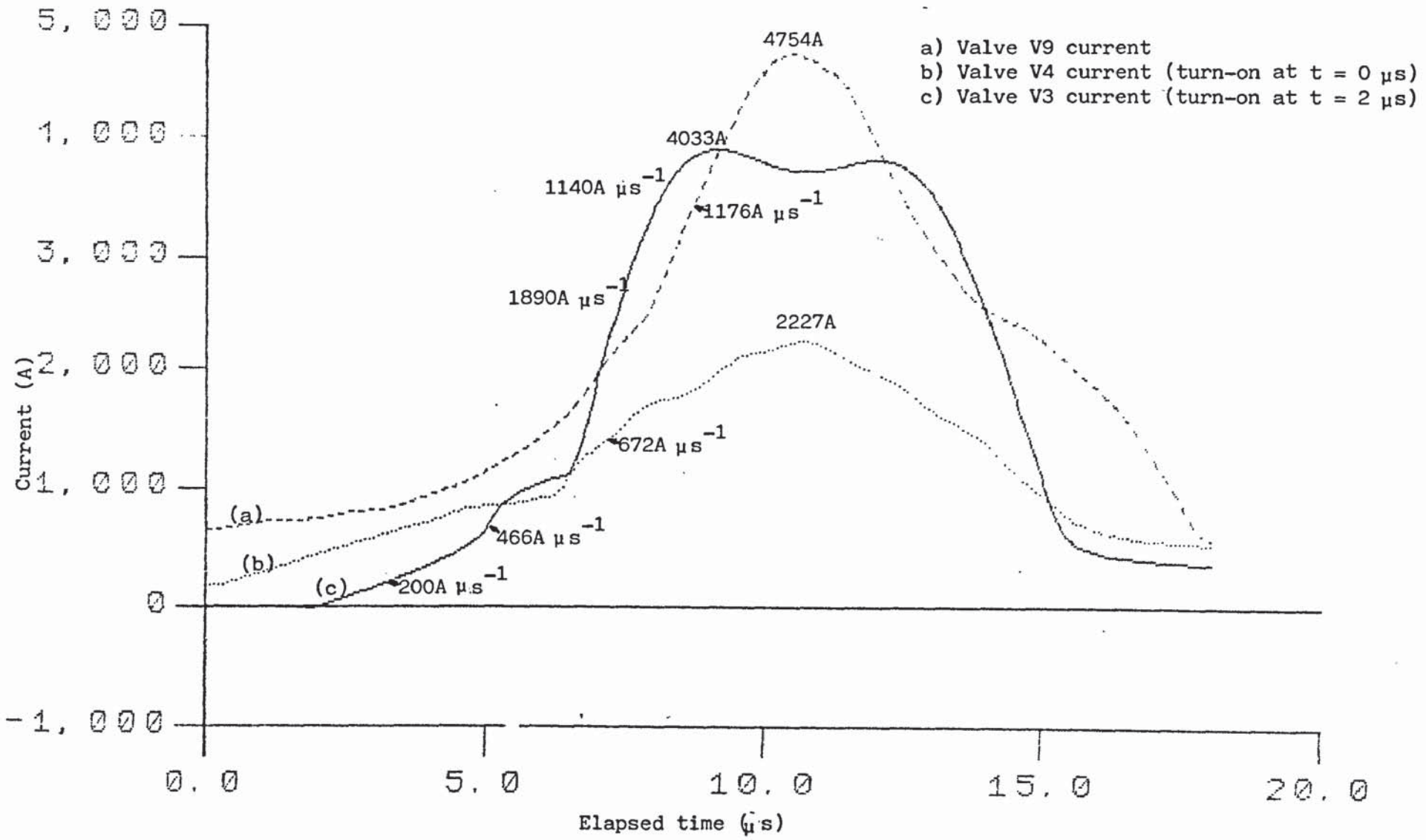

Fig.8.8 - Thyristor inrush current predictions; commutation failure from maximum system precharge. Proposed reactor represented.

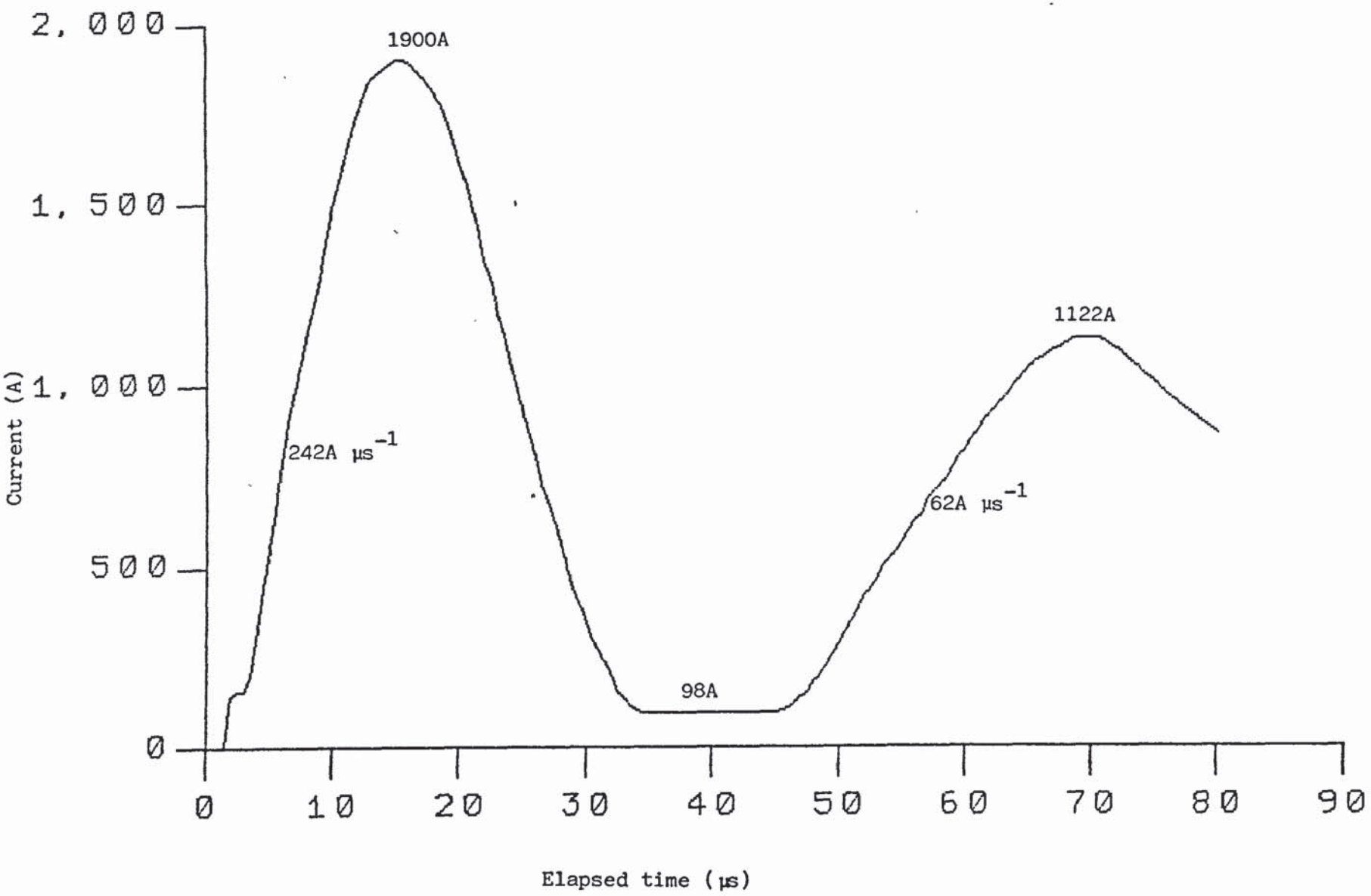

Fig.8.9 - Thyristor inrush current prediction for the Sellindge converter station; commutation failure from maximum system precharge.

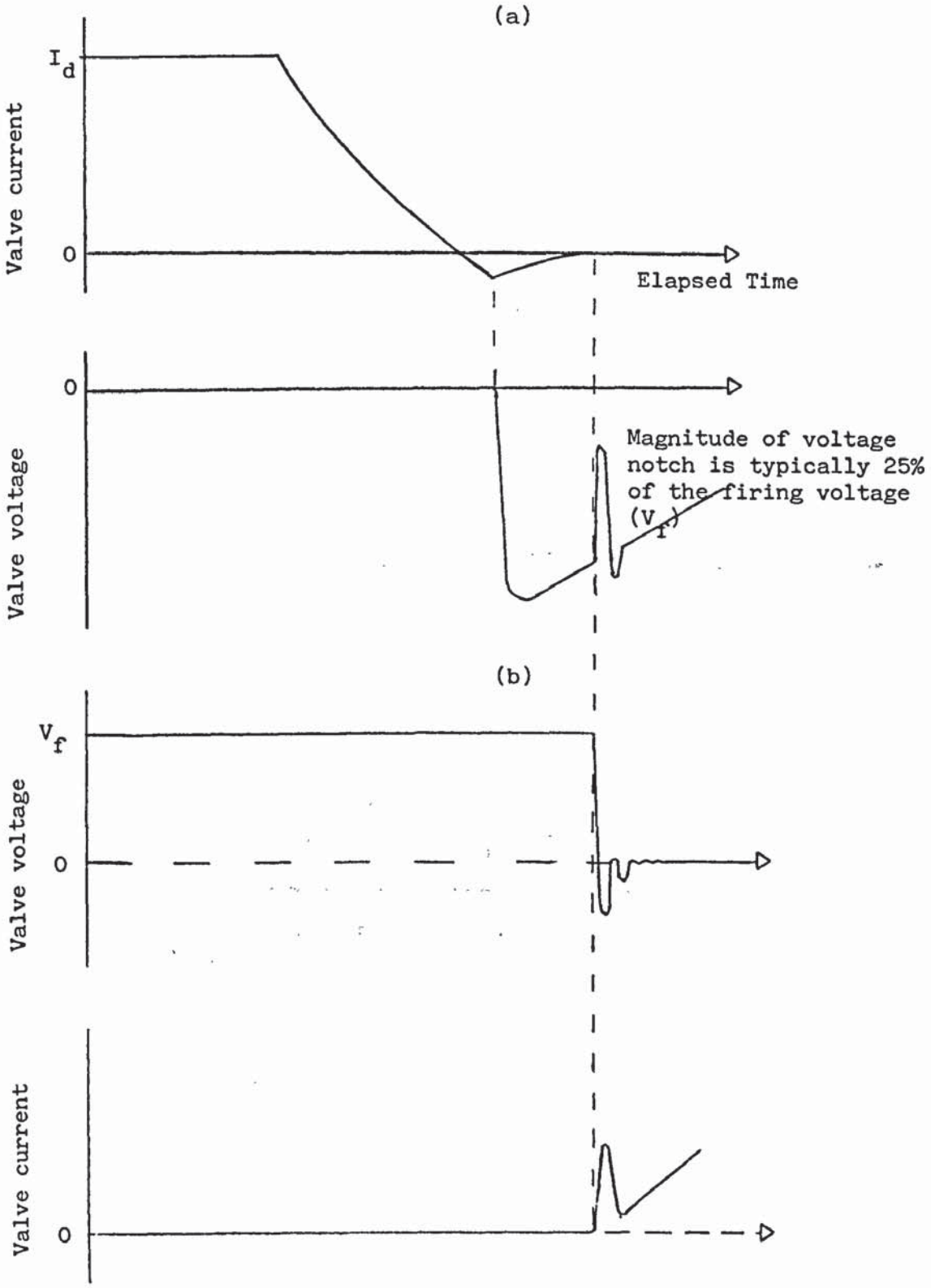

Fig.8.10 - Typical valve-current and valve-voltage waveforms;

a) Recovery
b) Turn-on

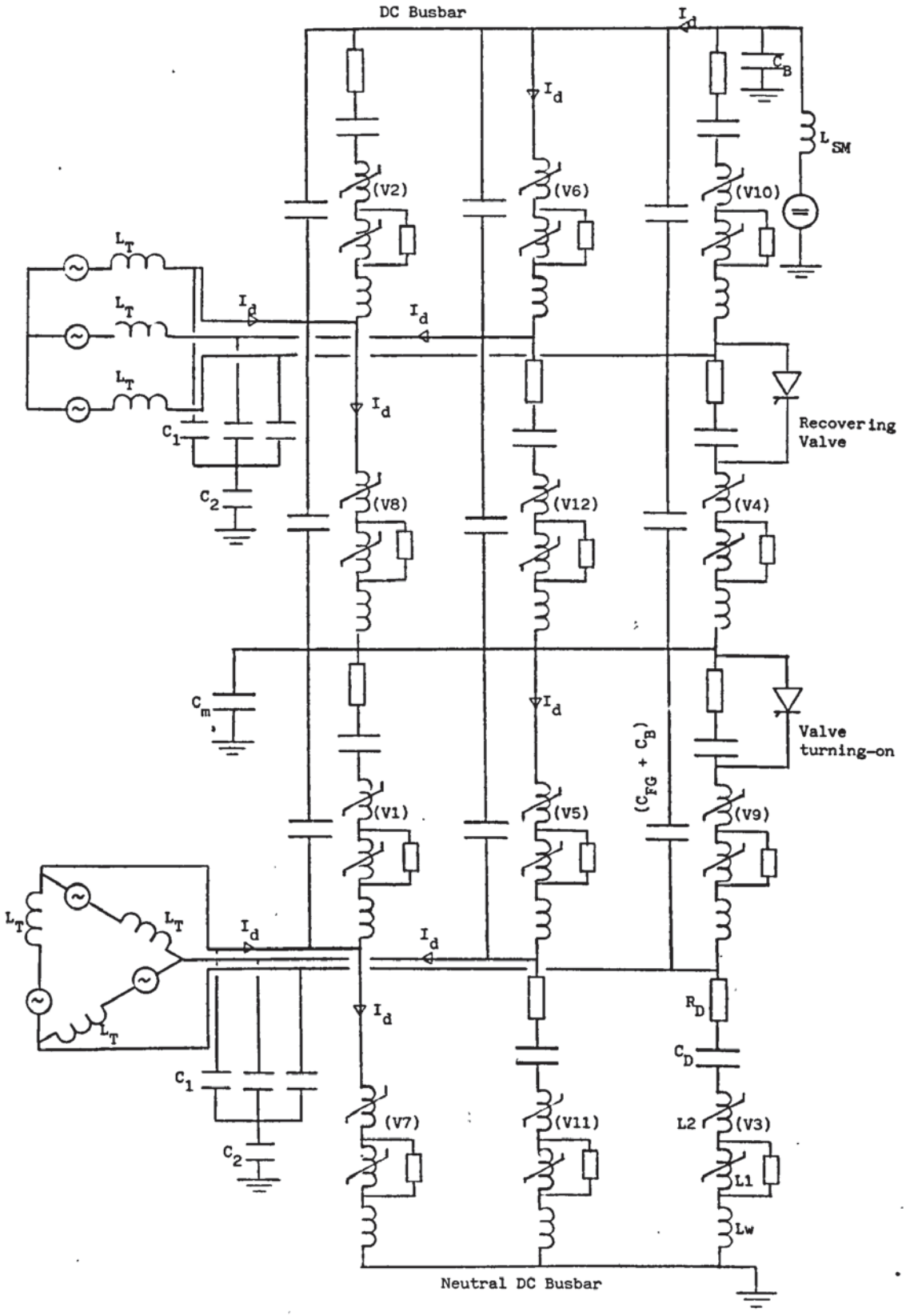

Fig.8.11 - Equivalent circuit of a 12-pulse bridge used for 12-pulse notch studies.
C_1, C_2 Electrostatic model of stray capacitances.
(VN) Valve firing sequence.

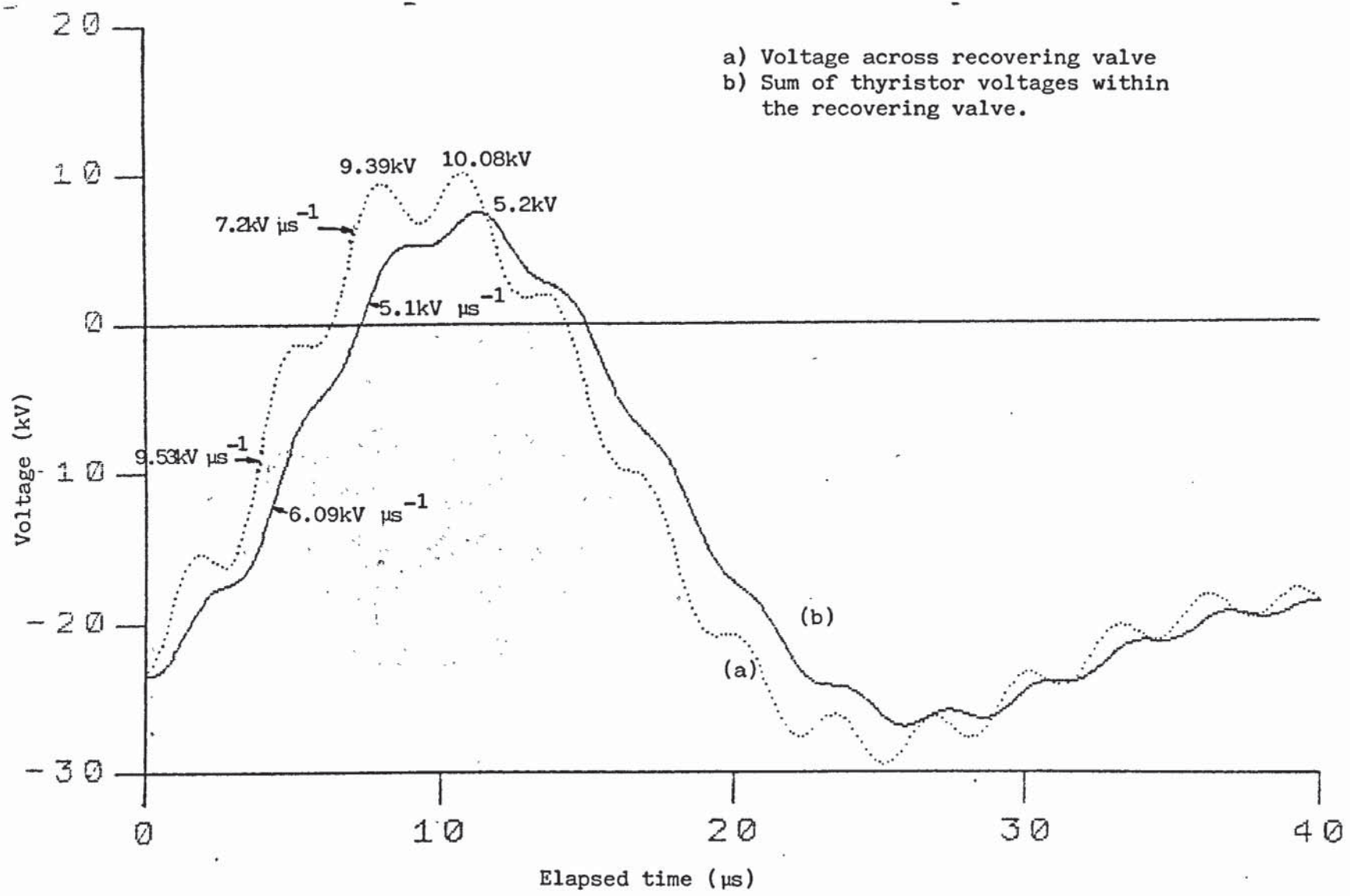

Fig.8.12 - Voltages associated with a recovering valve, sited in the bottom row of the upper six-pulse bridge, during inverter operation ($\gamma = 15°$): single-section representation of transformer secondary.

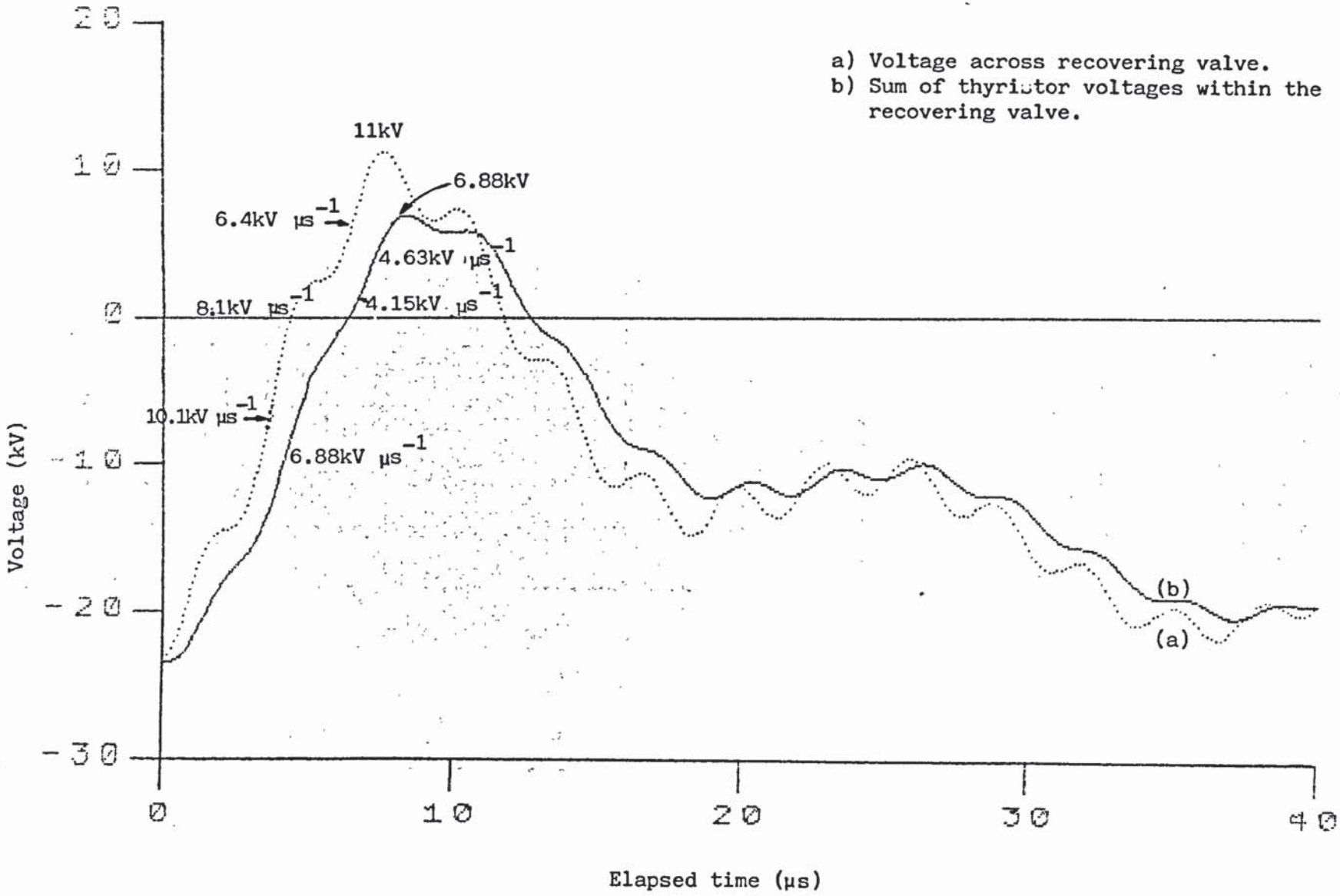

Fig.8.13 - Voltages associated with a recovering valve, sited in the bottom row of the upper six-pulse bridge, during inverter operation: refined representation of transformer secondary.

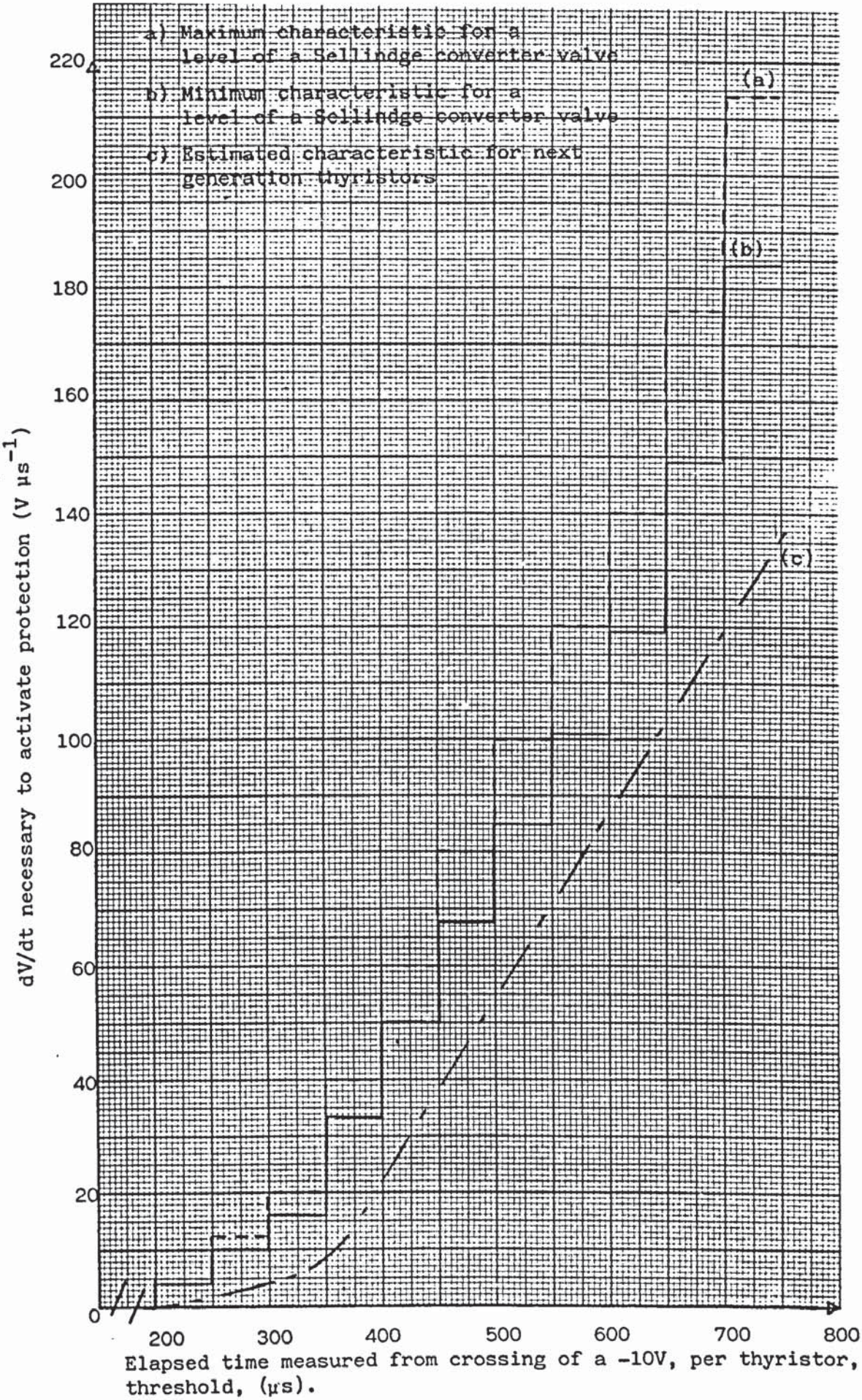

Fig.8.14 - Forward recovery protection characteristic for one level of a Sellindge converter valve together with an estimated characteristic for a next generation thyristor.

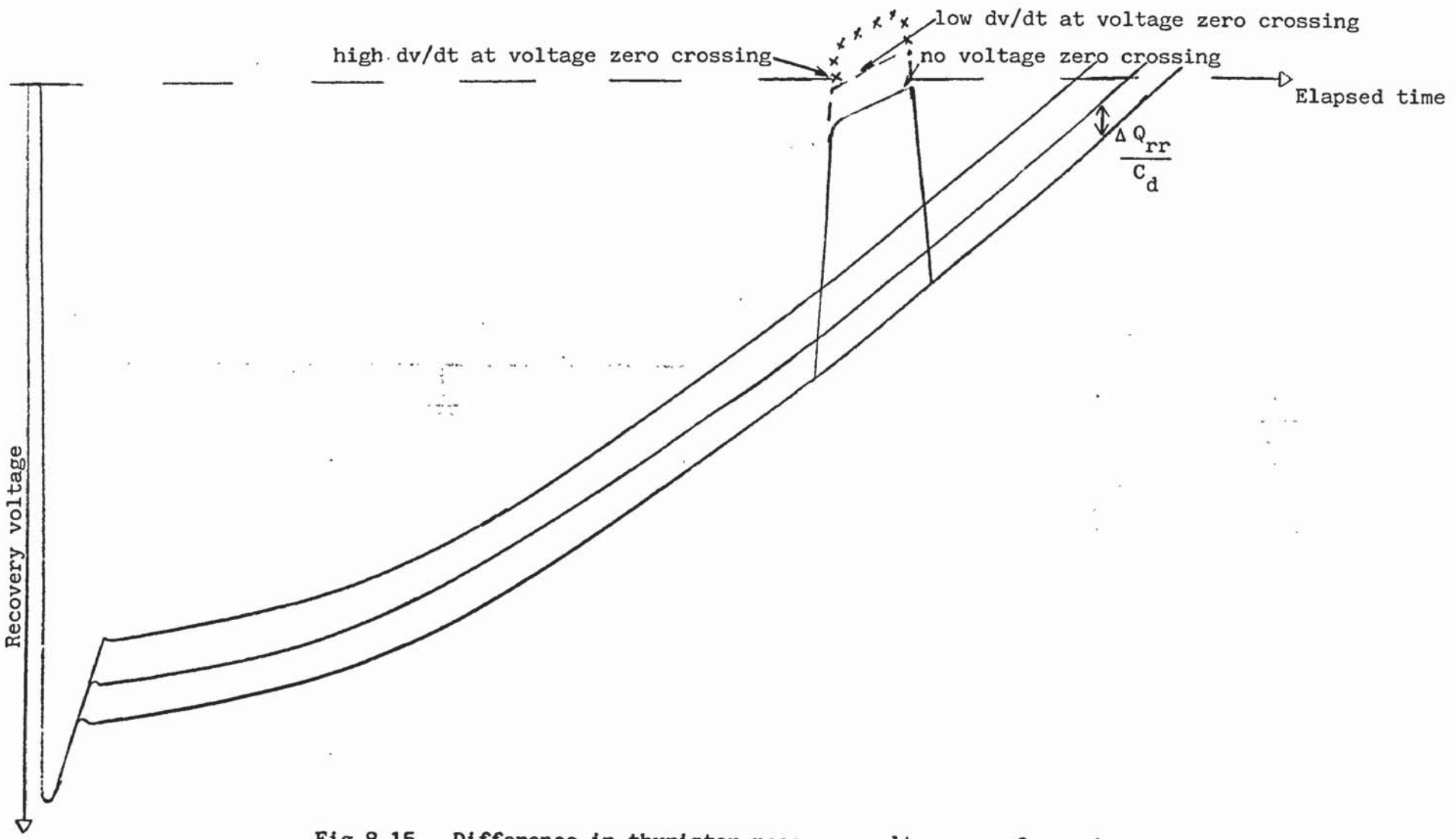

Fig.8.15 - Difference in thyristor recovery voltage waveforms due to differences in reverse recovered charge (ΔQ_{rr}) between thyristors.

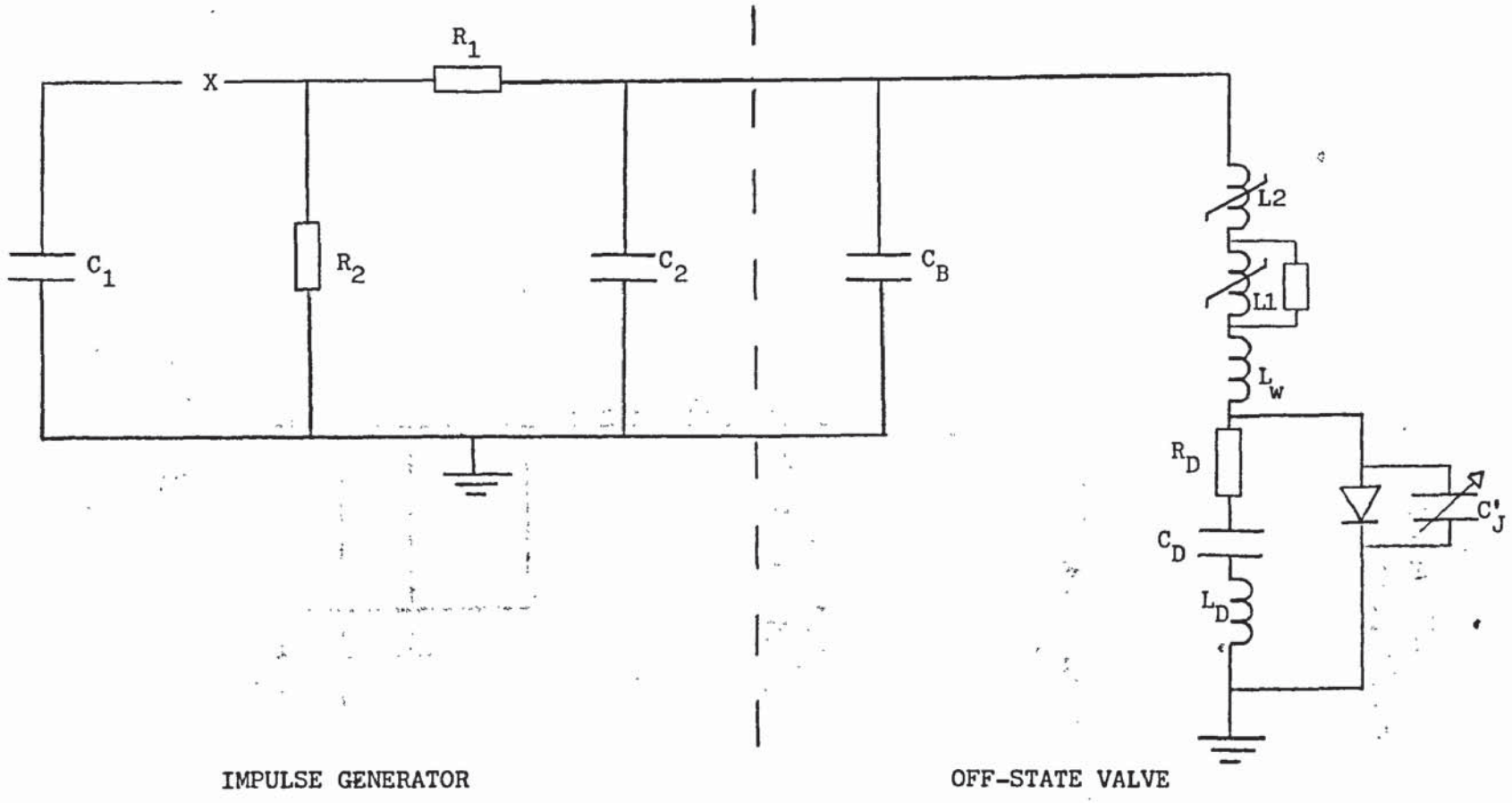

Fig.8.16 - Simplified equivalent circuit for modelling impulses across an off-state valve.
C_1, C_2, R_1, R_2 Equivalent circuit elements for an impulse generator.
C'_J Thyristor junction capacitance, referred to a valve.

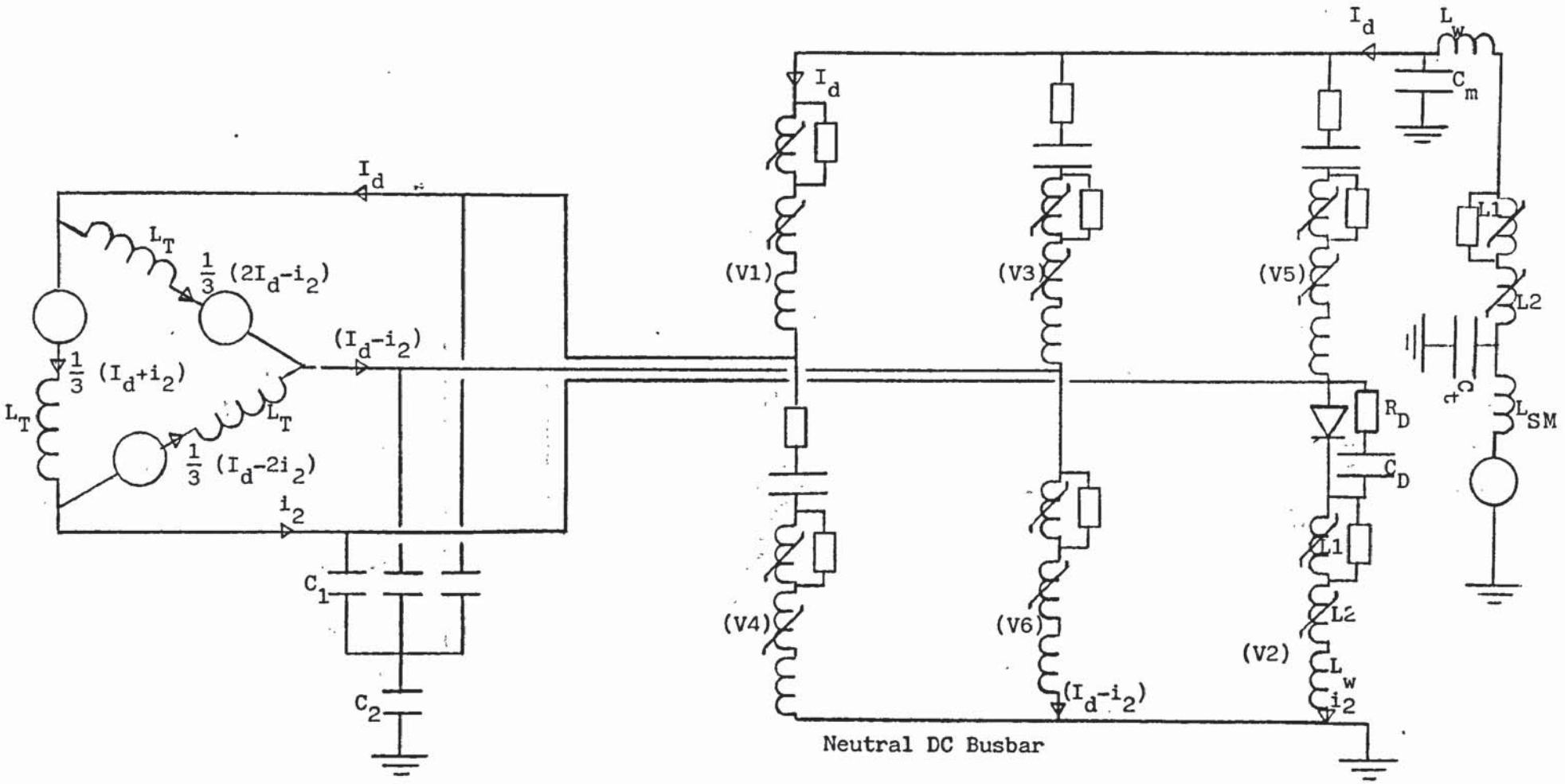

Fig.8.17 - Simplified equivalent circuit of a six-pulse bridge, used for coherent turn-on studies.
Pre-established current in valve 2 (i_2) is due for example to a switching-impulse (250/2500 μs)
C_1, C_2 Transformer electrostatic model.
(VN) Normal valve firing sequence.

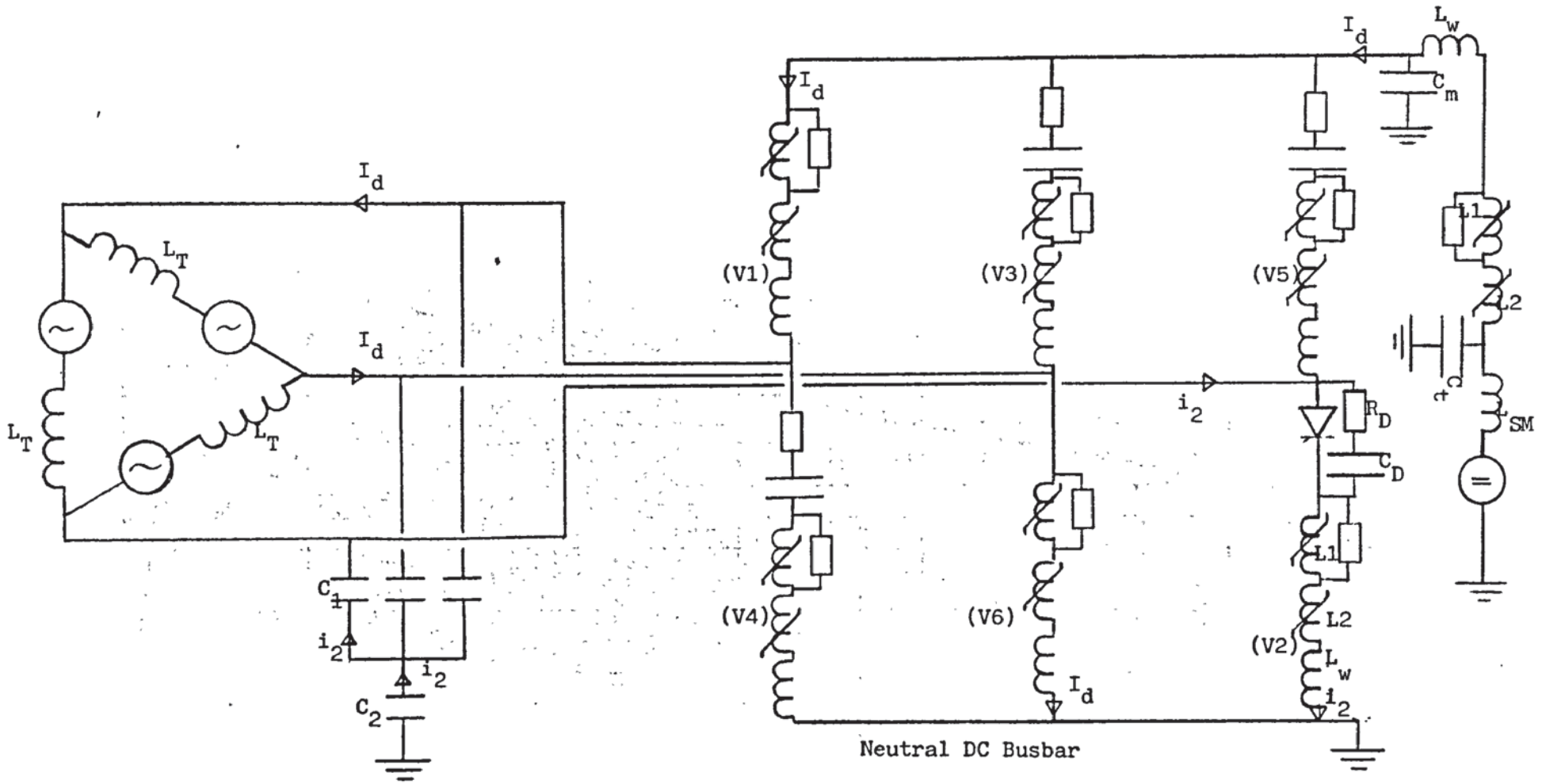

Fig.8.18 - Simplified equivalent circuit of a six-pulse bridge, used for coherent turn-on studies. Pre-established current in valve 2 (i_2) is due for example to a lightning (1.2/50μs) or front of wave (0.25/5μs) impulse.
C_1, C_2 Transformer electrostatic model.
(VN) Normal valve firing sequence.

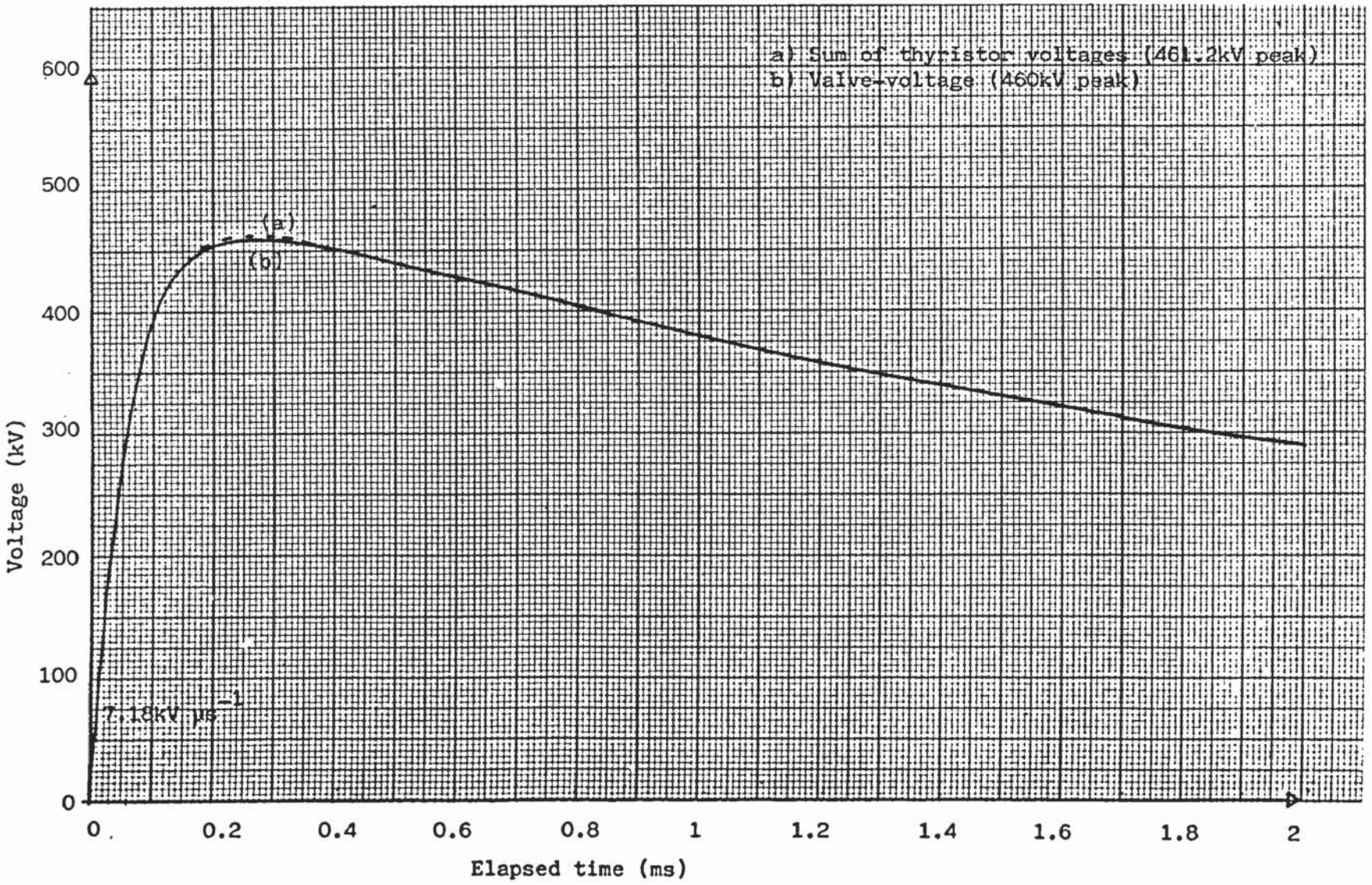

Fig.8.19 - Voltage waveforms associated with an off-state valve when a switching-impulse (250/2500 μs) is impressed across the valve.

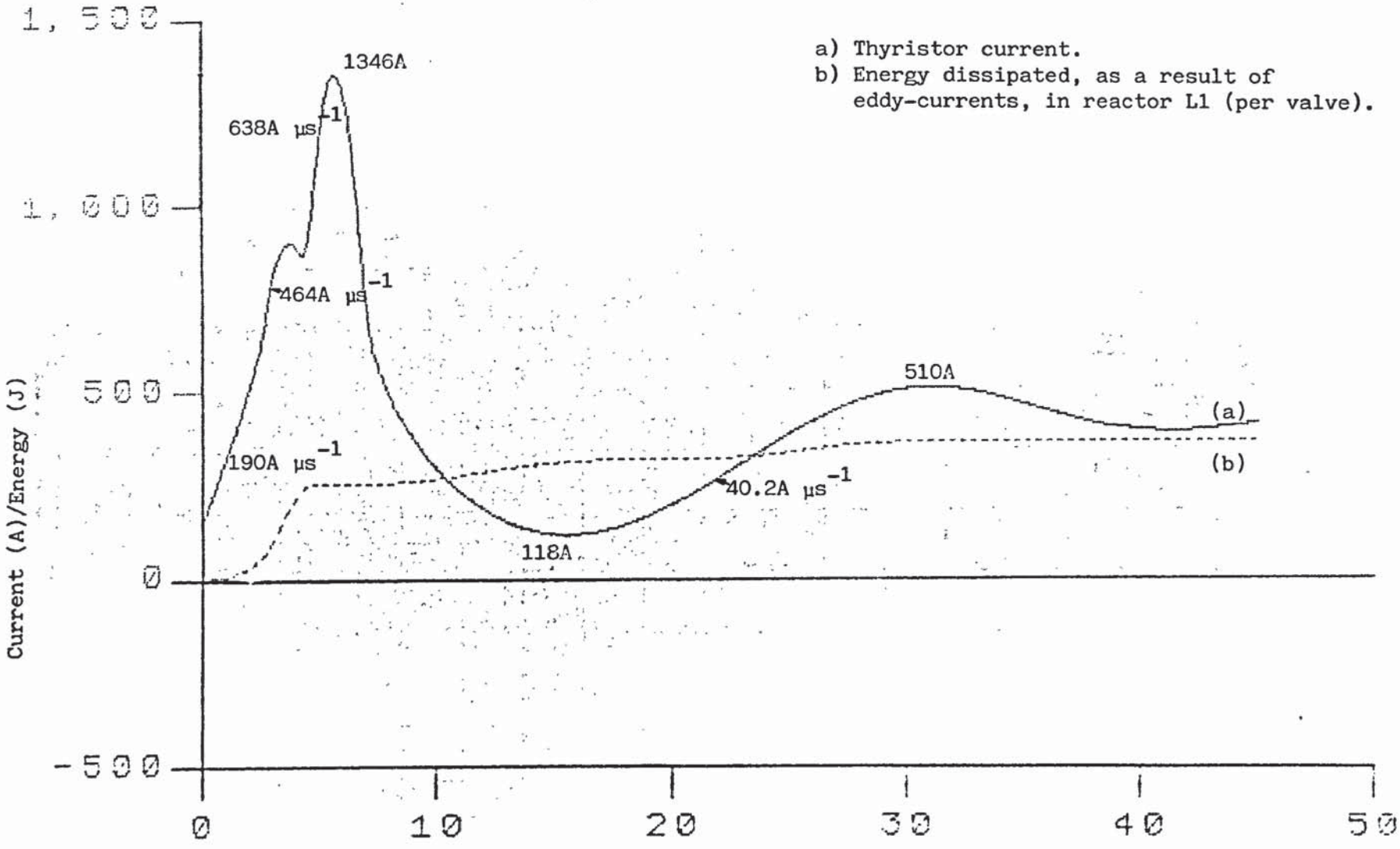

Fig.8.20 - Predicted thyristor inrush current and energy dissipation in reactor L1 for turn-on from a sum of thyristor voltages equal to 400kV.
Pre-established current in commutating valve - due to a switching-impulse (250/2500 μs).

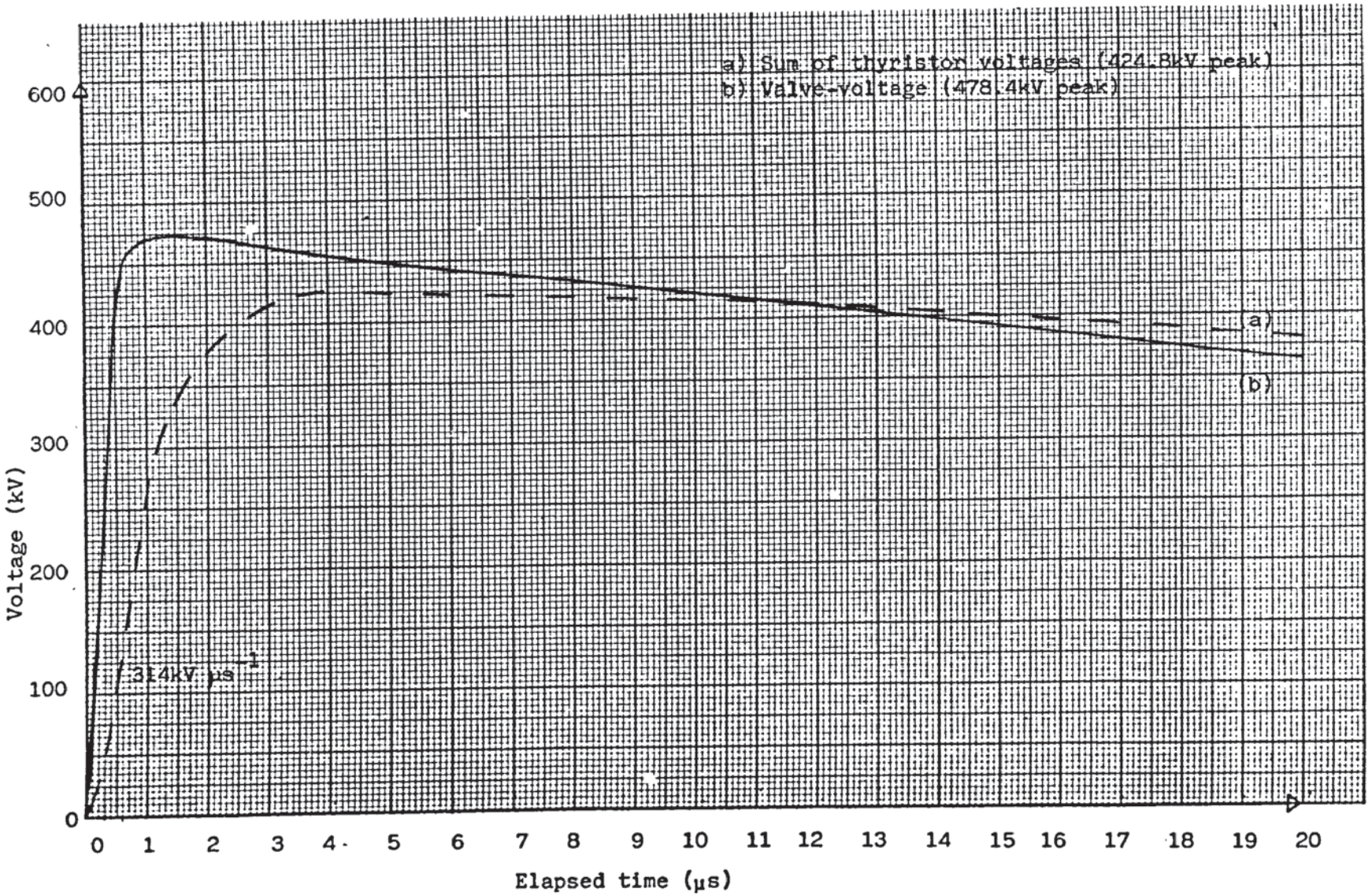

Fig.8.21 - Voltage waveforms associated with an off-state valve when a lightning-impulse (1.2/50µs) is impressed across the valve.

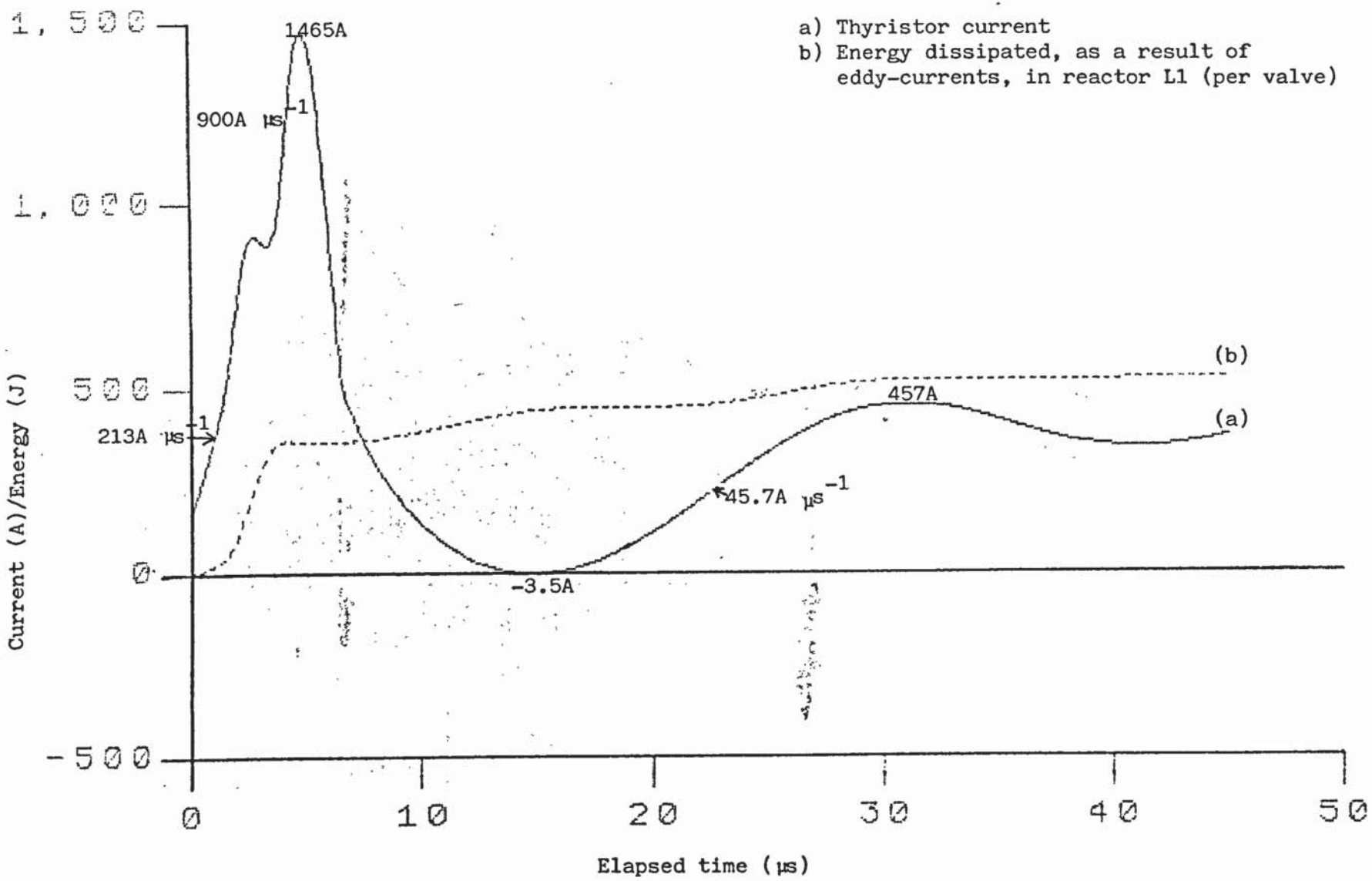

Fig.8.22 - Predicted thyristor inrush current and energy dissipation in reactor L1 for turn-on from a sum of thyristor voltages equal to 400kV. Pre-established current represented in commutating valve due to a lightning-impulse (1.2/50 μs).

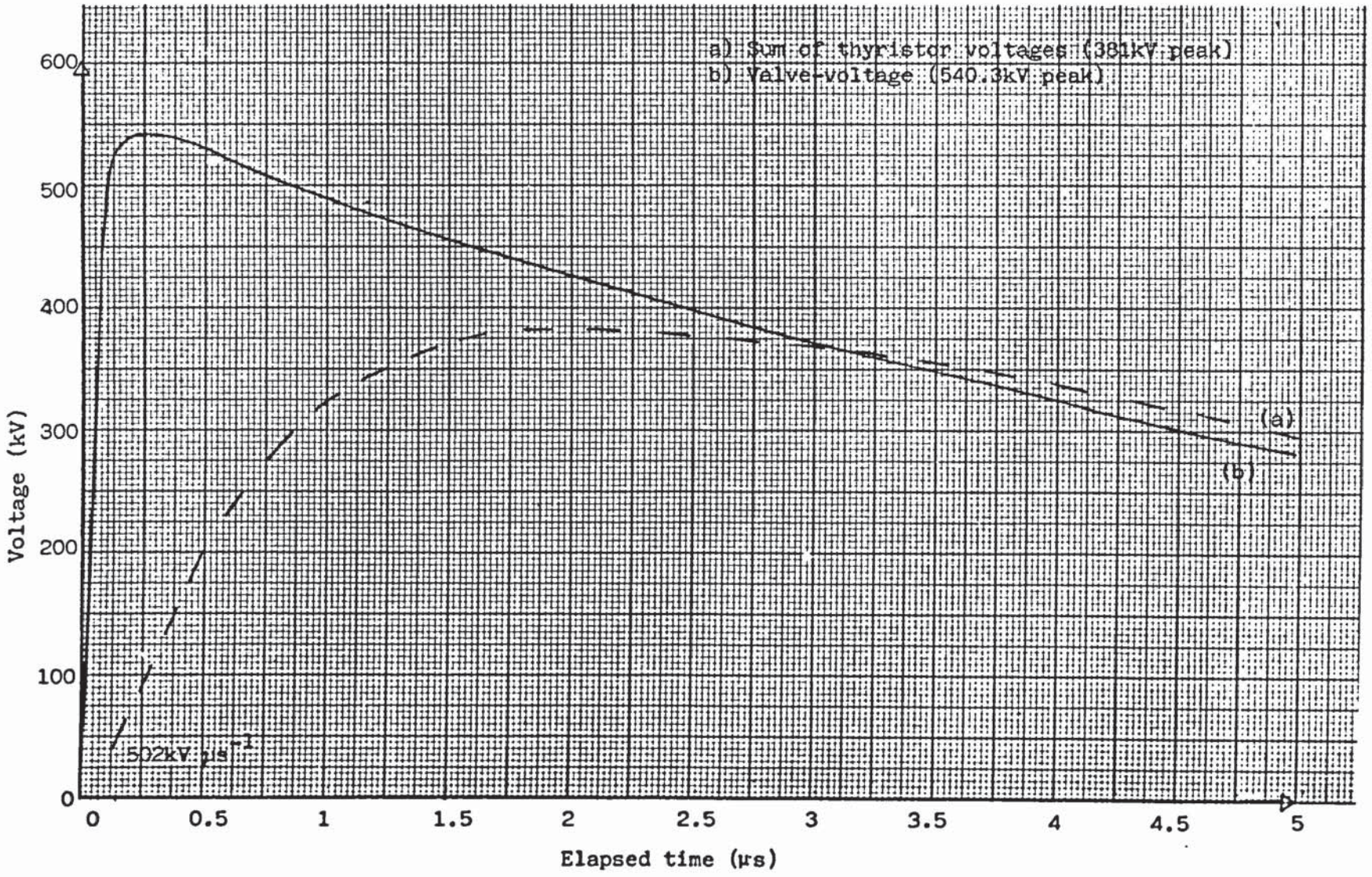

Fig.8.23 - Voltage waveforms associated with an off-state valve when a front-of-wave impulse (0.25/5 μs) is impressed across the valve.

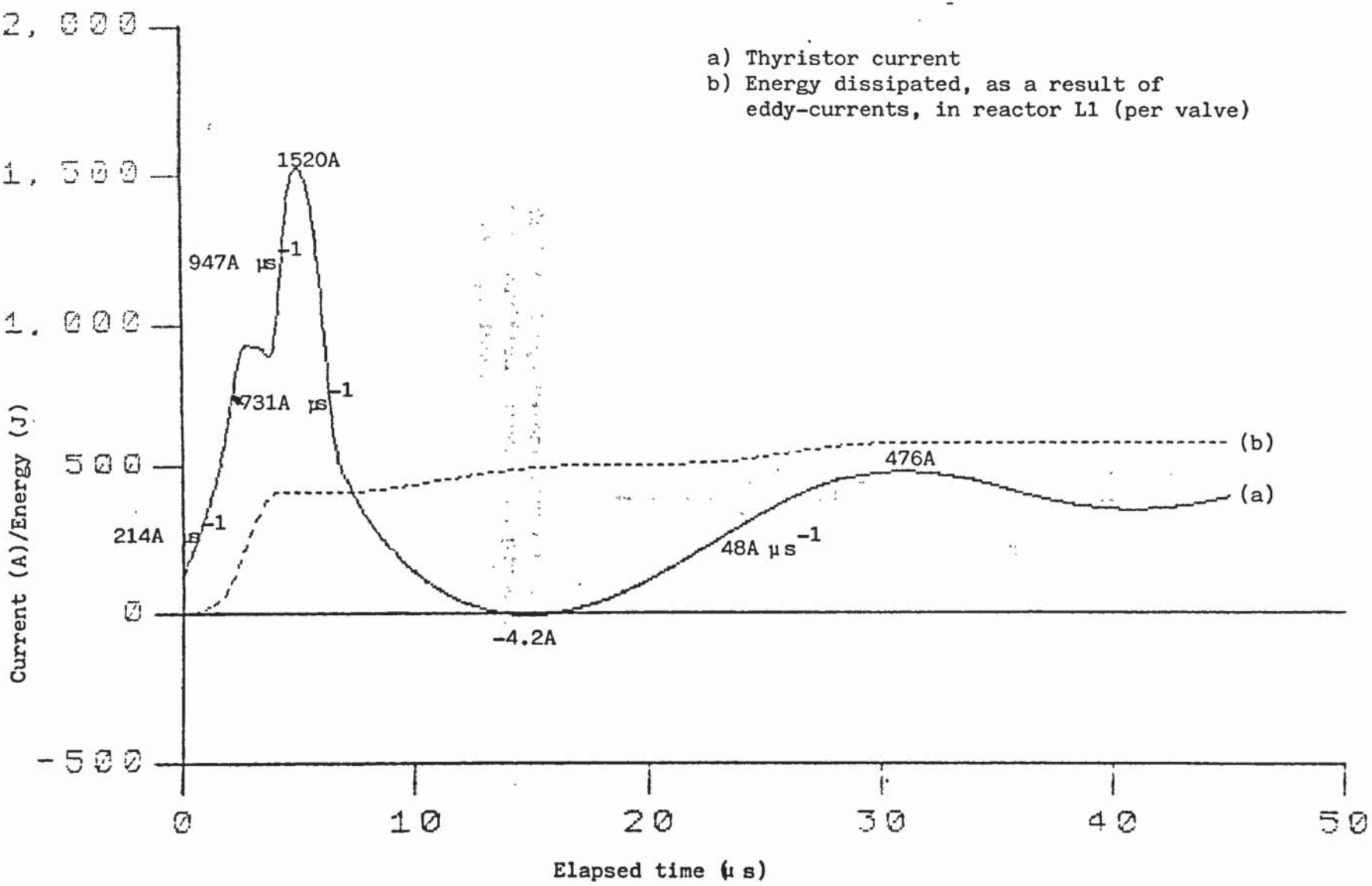

Fig.8.24 - Predicted thyristor inrush current and energy dissipation in reactor L1. Valve turn-on occurs at an elapsed time of 1μs after a front-of-wave impulse (0.25/5μs) is impressed across the off-state valve.

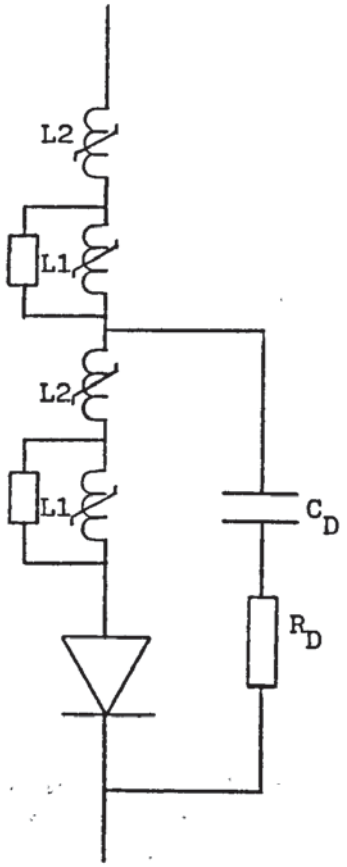

Fig.9.1 - Simplified equivalent circuit of a thyristor valve. This, modified, circuit is proposed for future investigations.

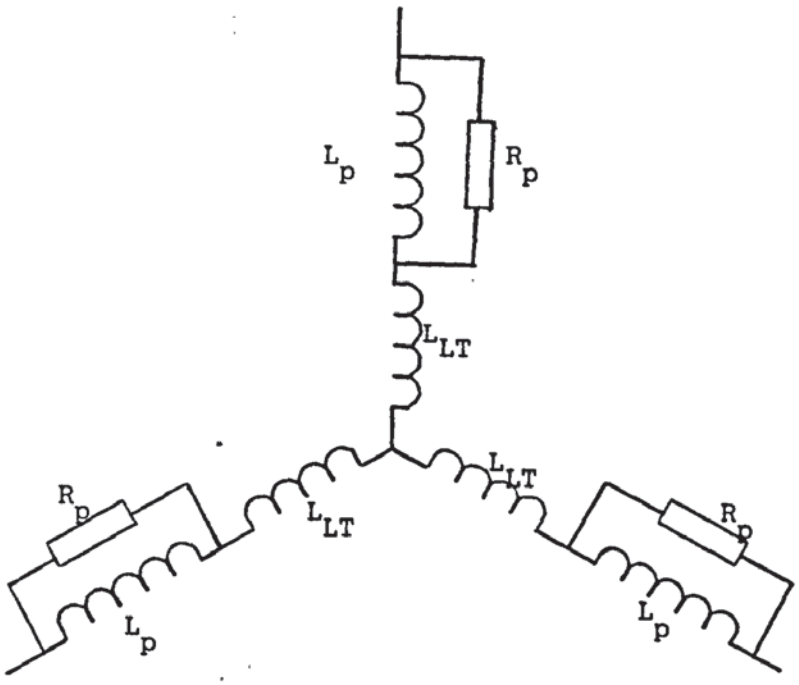

Fig.AII.1 - Single-section representation of transformer high-frequency resistance characteristic.

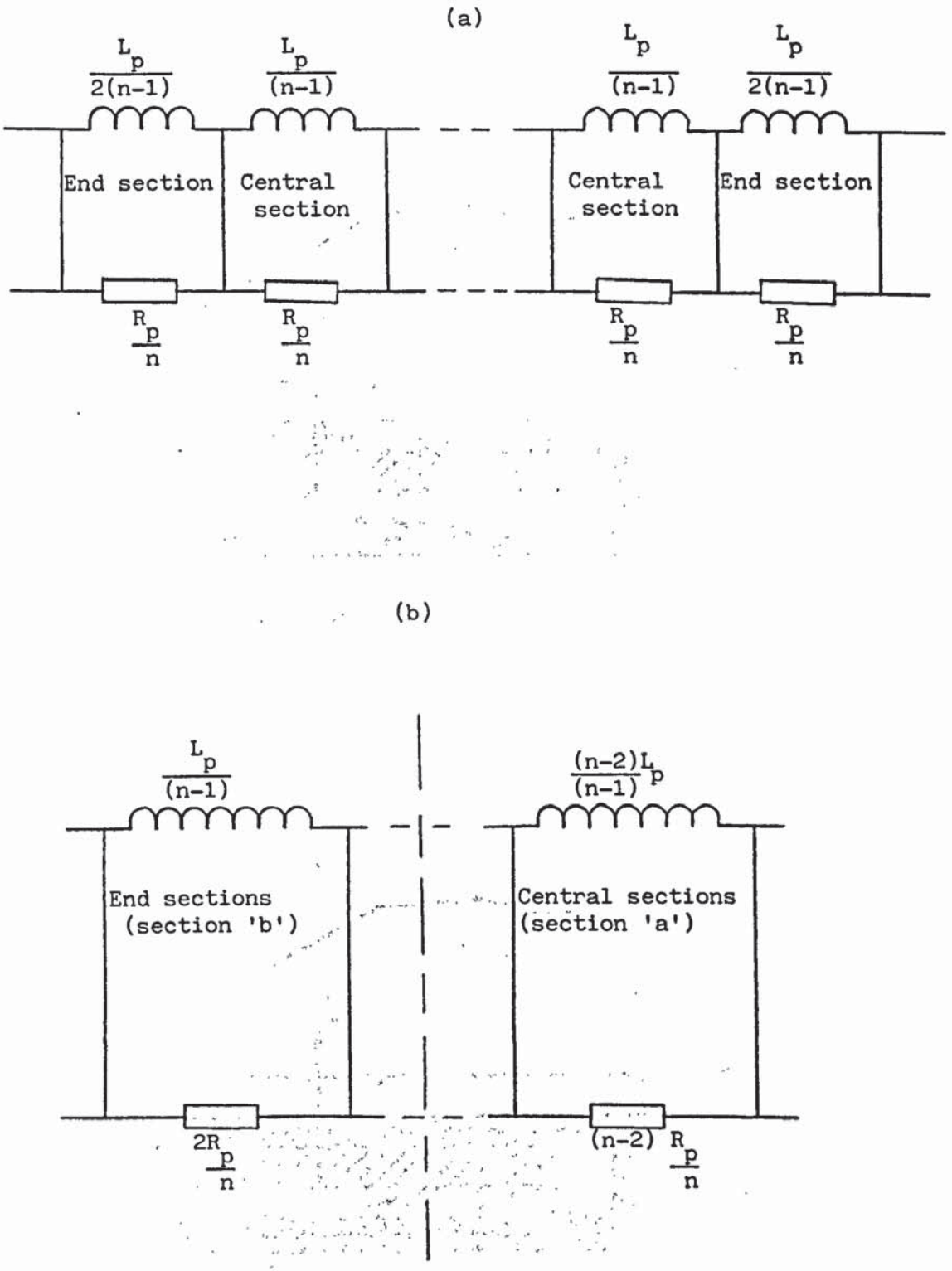

Fig.A.II.2 - n-section representation of transformer high-frequency resistance characteristic ('series' inductance is not shown).

(a) Fully distributed equivalent circuit.

(b) Lumped equivalent circuit of (a) used for evaluating the values of L_p and R_p.

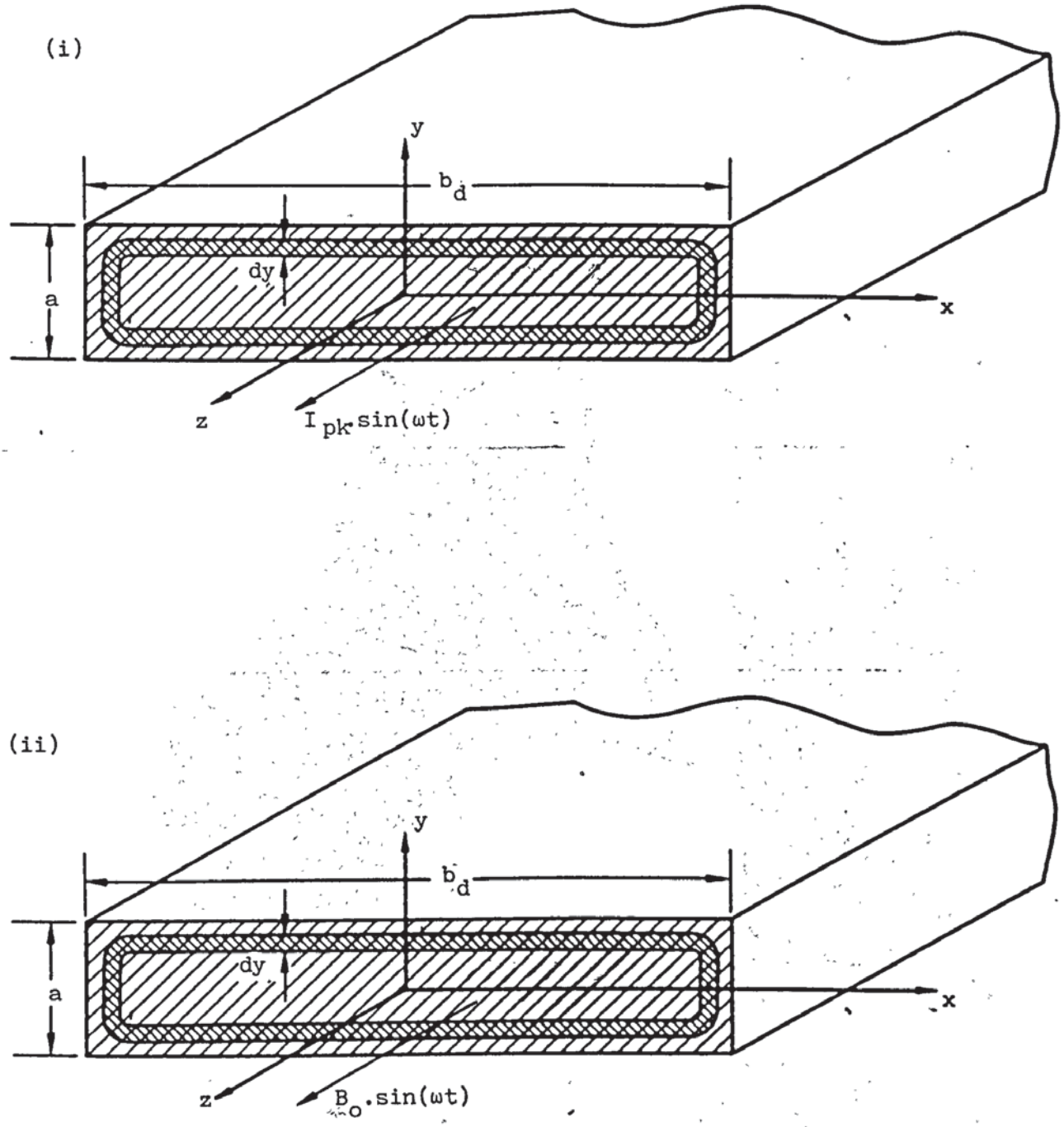

Fig.A.IV.1 - Eddy-currents induced in a thin magnetic sheet by, sinusoidal, fixed;

(i) H-field

(ii) B-field

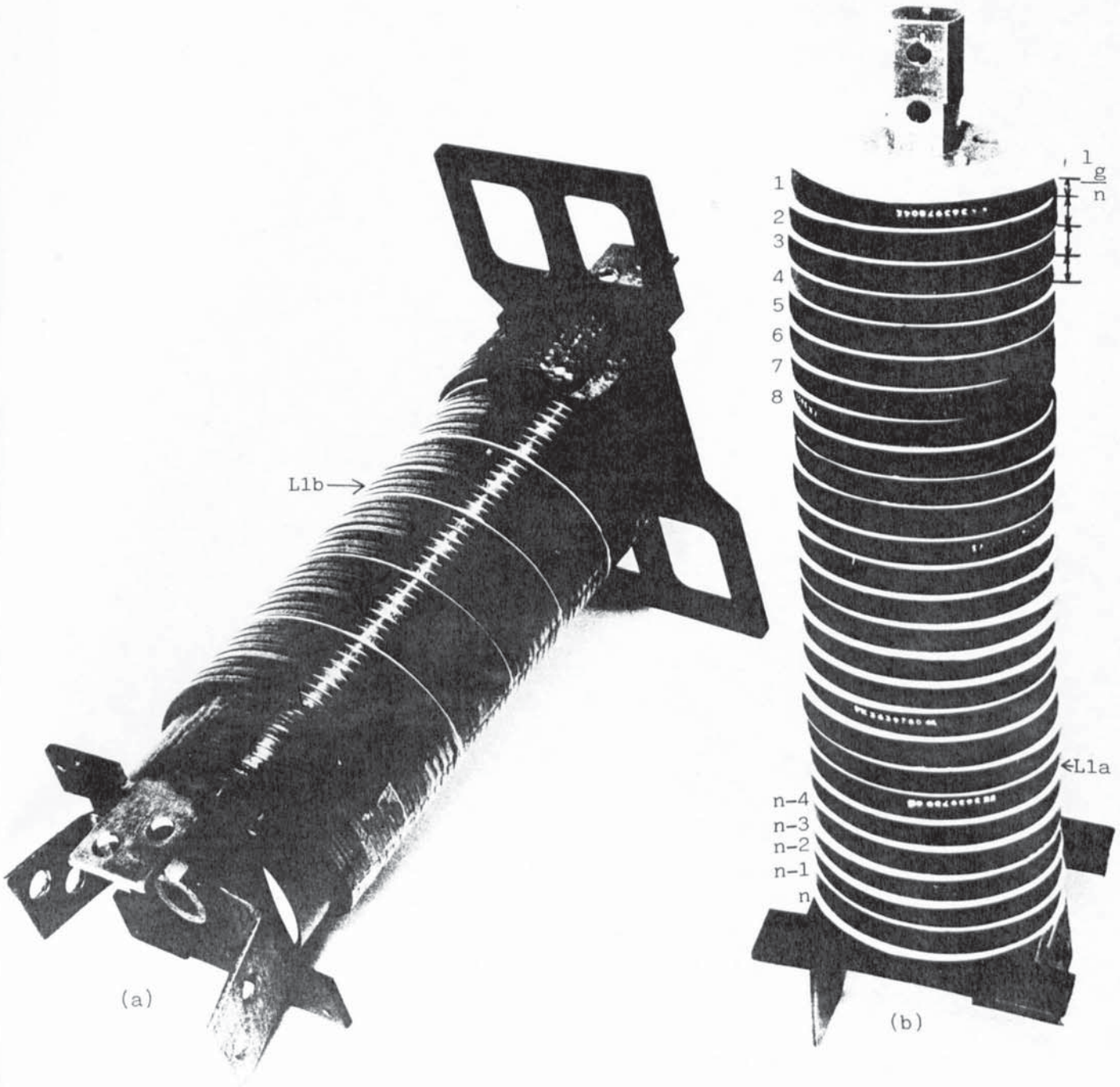

Fig.A.V.1 - One levels worth of saturating-reactor for the Sellindge converter station.

(a) Assembled reactor with a six-turn spiral (L1b)

(b) Ferrite reactor (L1a) prior to assembly of the six-turn spiral.

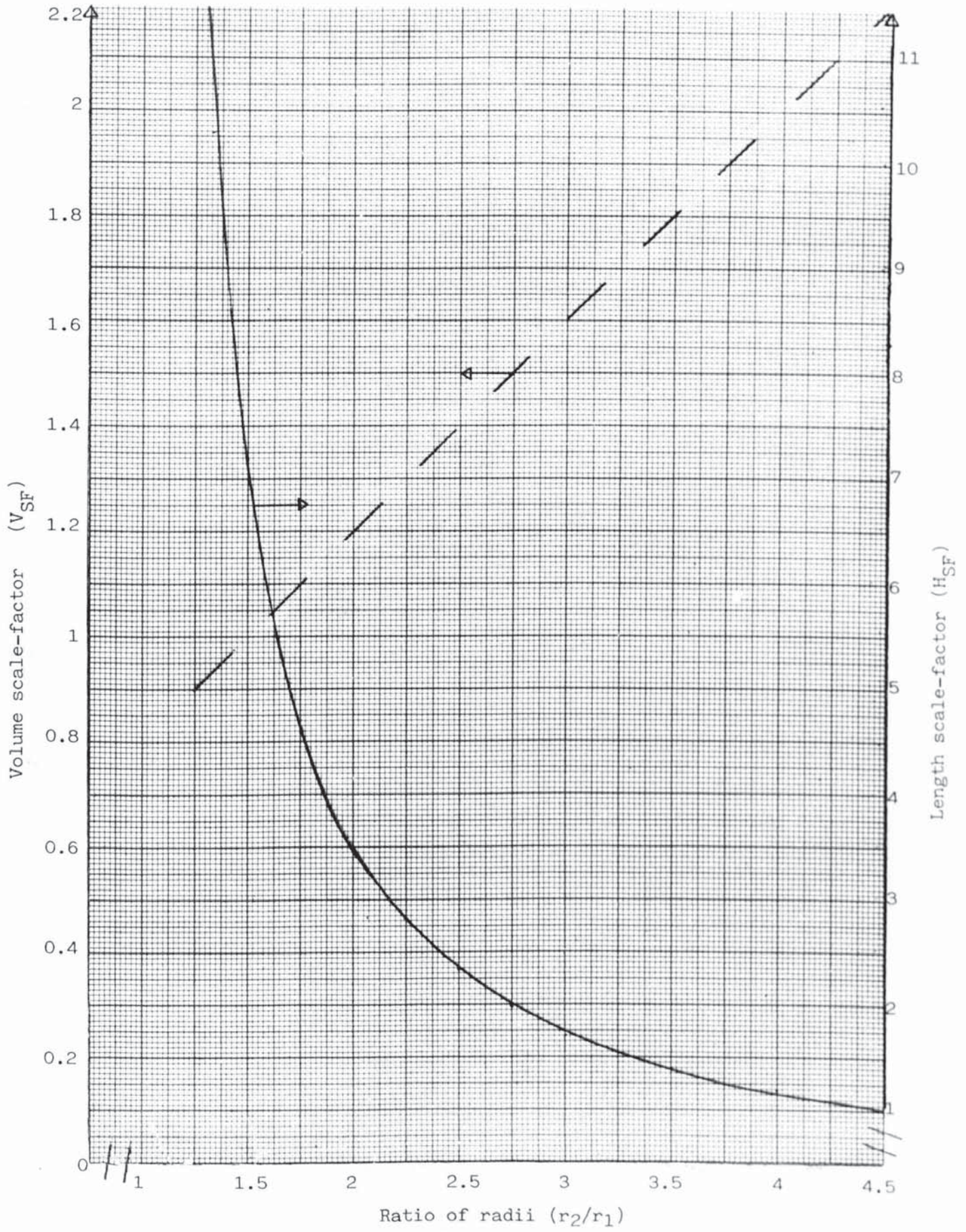

Fig.A.V.2 - Dependence of the volume scale-factor and length scale-factor upon the ratio of radii.

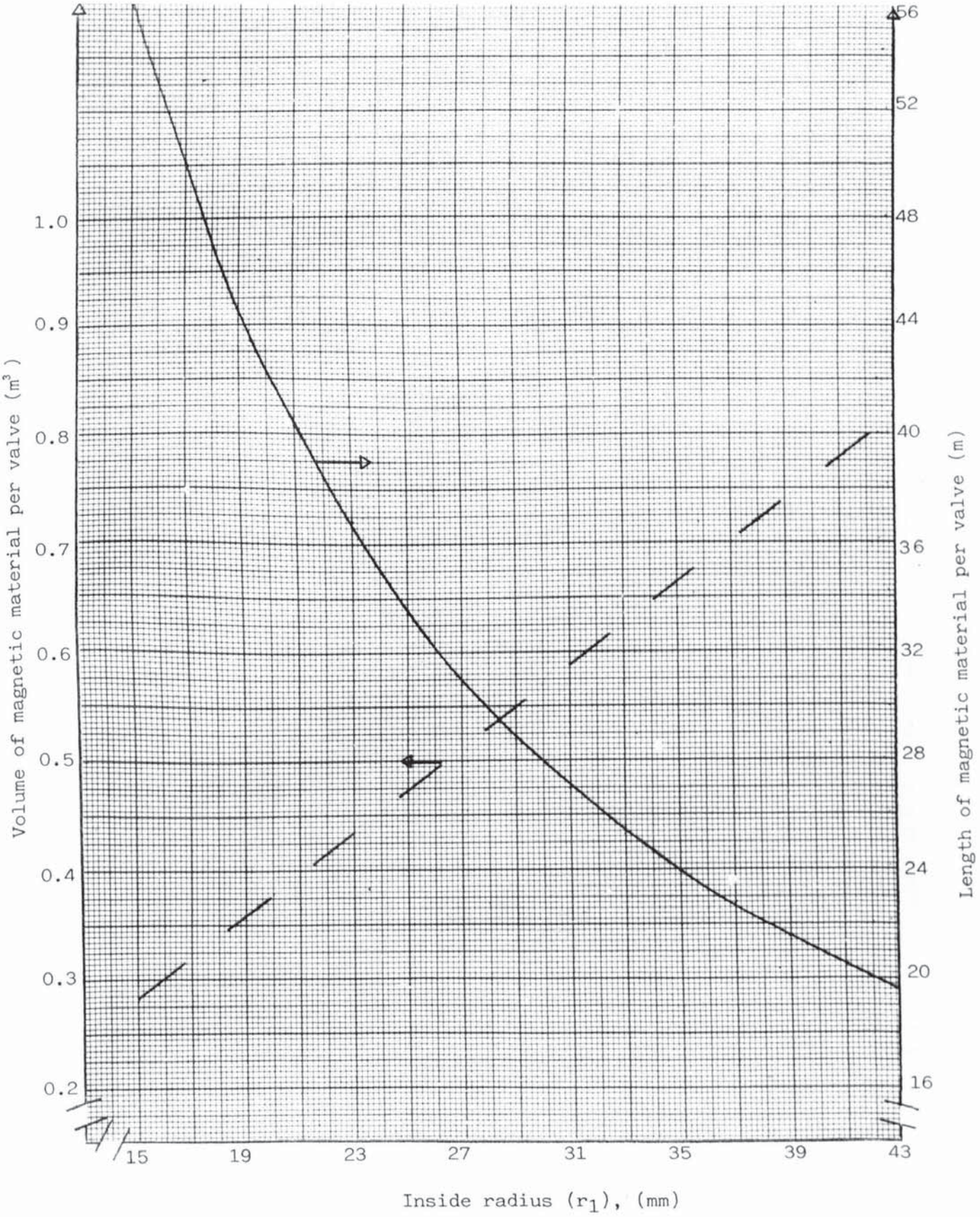

Fig.A.V.3 - Dependence of the volume and length of magnetic material upon the inside radius of the toroid (r_2/r_1 = 2.875, Ø = 1.6Wb per valve, B_{SAT} = 1.2T, 85% space-factor).

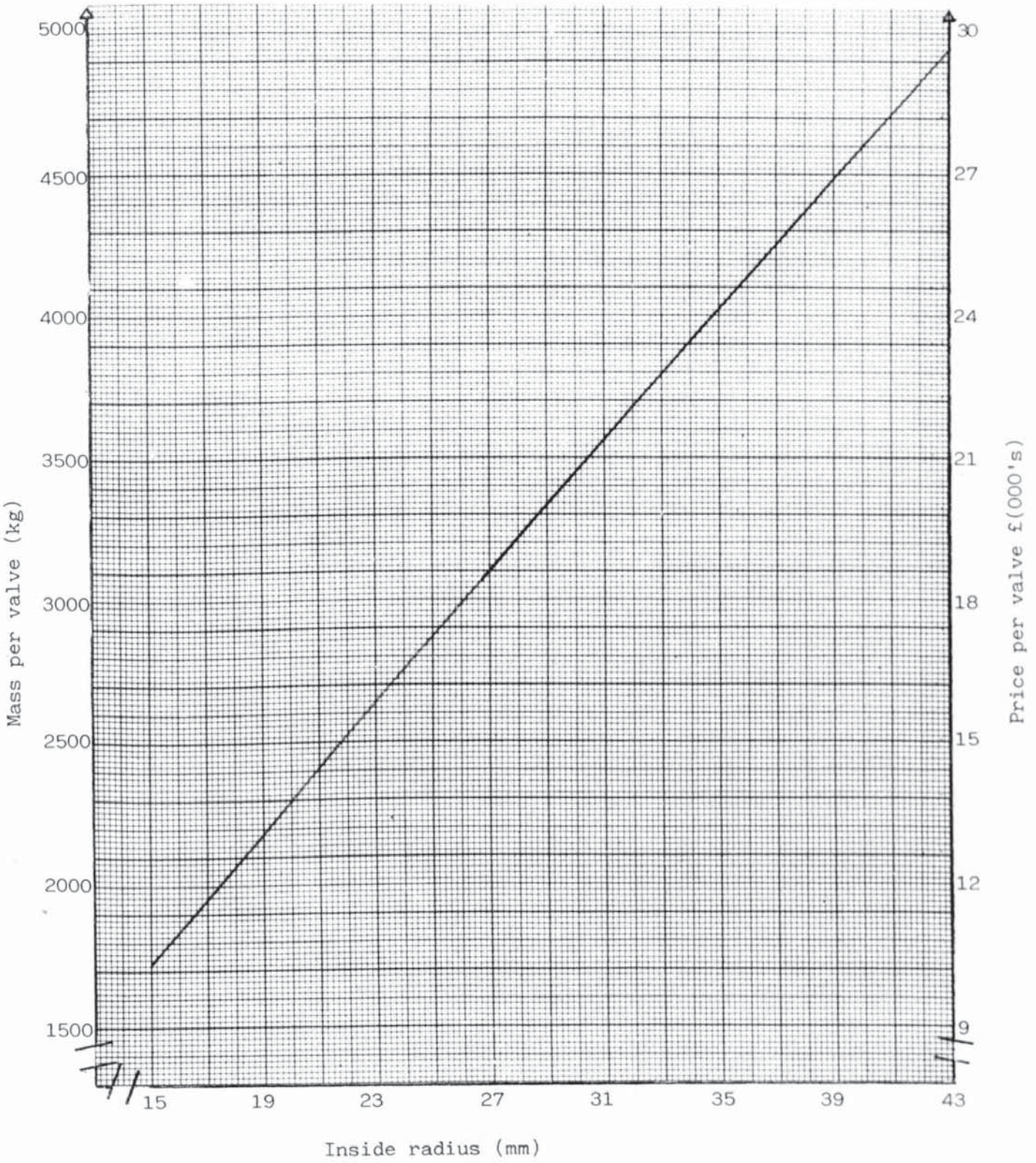

Fig.A.V.4 - Dependence of the mass and cost of magnetic material upon the inside radius of the toroid.
(r_2/r_1 = 2.875, Ø = 1.6Wb, B_{SAT} = 1.2T, 85% space-factor, p = 7.1g cc^{-3}, £6 per kg).